Contribution to Rotor Position and Speed Estimation for Synchronous Machine Drive Using High Frequency Voltage Injection : Application to EV/HEV Powertrains

Amir Messali

UNIVERSITE BRETAGNE LOIRE / MATHSTIC

CENTRALE NANTES

THESE DE DOCTORAT DE

L'ÉCOLE CENTRALE DE NANTES
COMUE UNIVERSITE BRETAGNE LOIRE

ECOLE DOCTORALE N° 601
Mathématiques et Sciences et Technologies de l'Information et de la Communication

Spécialité : Automatique, Productique et Robotique

Par **Amir MESSALI**

« Contribution to Rotor Position and Speed Estimation for Synchronous Machine Drive Using High Frequency Voltage Injection: Application to EV/HEV Powertrains »

Thèse présentée et soutenue à l'Ecole Centrale de Nantes le 22 novembre 2019
Unité de recherche : Laboratoire des Sciences du Numérique de Nantes (LS2N)

Rapporteurs avant soutenance :

Maurice FADEL	Professeur, ENSEEIHT INP Toulouse, LAPLACE
Gildas BESANÇON	Professeur, Grenoble INP, GIPSA-Lab

Composition du jury :

Président :	Xuefang LIN-SHI	Professeur, INSA Lyon, AMPERE
Examinateurs :	Philippe MARTIN	Maître de recherche, Ecole des Mines de Paris, CAS
Dir. de thèse :	Malek GHANES	Professeur, Ecole Centrale de Nantes, LS2N ECC,
Co-encadrant :	Mohamed A. HAMIDA	Ecole Centrale de Nantes, LS2N

Invité(s) :

Mohamad KOTEICH	Docteur Ingénieur, Schneider-Toshiba
Abdelkader BOUARFA	Docteur Ingénieur, Renault Guyancourt

Remerciement

Ce travail de thèse est le fruit d'une collaboration entre le laboratoire LS2N de L'école Centrale de Nantes (ECN) et le groupe automobile Renault entre Octobre 2016 et Novembre 2019. Ce travail a été realisé dans le cadre d'une Chaire Renault pour améliorer les véhicules électriques et hybrides Renault en termes de fiabilité et performance énergétique.

Je souhaite remercier très chaleureusement mes encadrants du laboratoire LS2N et de Renault, qui ont non seulement fait que ces travaux de thèse aboutissent mais qui ont aussi réussi à toucher plusieurs aspects de ma personnalité. Il serait dur sans doute de résumer en quelques mots ma reconnaissance pour tout ce qu'ils ont fait pour moi lors de ces dernières années.

Un grand merci à mon directeur de thèse Pr. Malek Ghanes et à mon co-encadrant Dr. Mohamed Assad Hamida coté ECN qui m'ont soutenu et encouragé tout le durant de ces trois ans de thèse. Je tiens à remercier mon encadrant coté Renault Dr. Mohamad Koteich, là aussi, je retiens de nombreuses qualités aussi bien techniques qu'humaines.

Je remercie Mme Xuefang Lin-Shi d'avoir eu la gentillesse d'accepter de présider le jury de soutenance de thèse. Je remercie Mr. Maurice Fadel et Mr. Gildas Besançon d'avoir accepté de juger mon travail en tant que rapporteurs. Je remercie Mr. Philippe Martin d'avoir accepté de faire partie du jury. Je remercie les membres invités Mr. Abdelkader Bouarfa et Mr. Mathias Tientcheu.

J'adresse aussi mes remerciements au Pr Jean-Pierre Barbot et Alain Glumineau pour leur conseils.

Du coté Renault, mes remerciements s'adressent d'abord à Mr. Abdelmalek Maaloum, Ahmed Ketfi-Cherif, Olivier Reyss, Edouard Nègre et Ludovic Mérienne qui m'ont fait confiance et cru en moi depuis mes tous premiers pas à Renault.

Mes remerciements s'adressent de la même façon, a tous mes collègues, qui m'ont précieusement aidé et encouragé pendant ces dernières années.

À mon dieu.

À mes parents qui me sont les plus chers au monde et à qui je dois ce que je suis et ce que je serai.

À mes soeurs et mes Frères, pour leur soutien et auxquelles je tiens à leur témoigner mon affection et mon profond attachement.

À ma future femme, pour son soutien et pour nos futures miniatures.

À toutes les personnes que j'aime et qui me sont chères.

Veuillez trouver dans ce modeste travail un humble témoignage de mon amour et de ma profonde gratitude.

J'espère avoir été digne de votre confiance et à la hauteur de vos espérances.

Contents

List of symbols

IPMSM	Interior Permanent Magnet Synchronous Motor
HF	High Frequency
PLL	Phase-Locked-Loop
MSO	Mechanical System Observer
LPF	Low Pass Filter
HPF	High Pass Filter
BPF	Band Pass Filter
SFF	Synchronous Frame Filter
$\underline{x}$	Complex notation of x
$\underline{x^*}$	Conjugated component of x
R_s	Stator resistance
L_d, L_q	dq-axis inductances
L_0, L_2	Average and differential inductances, respectively
ϕ_f	Permanent-magnet flux linkage
$\underline{\psi_s^s}$	Stator flux linkage vector presented in the stator reference frame
$\underline{v_s^s}$	Stator voltage vector presented in the stator reference frame
$\underline{i_s^s}$	Stator current vector presented in the stator reference frame
$\underline{i_s^{r*}}$	Conjugated stator current vector presented in the rotating reference frame
$\underline{i_s^m}$	Stator current vector presented in the measurement axis displaced by 45° from the the estimated reference frame $\hat{d}-\hat{q}$
$\underline{\psi_s^r}$	Stator flux linkage vector presented in the rotating reference frame
ϕ_d, ϕ_q	dq stator flux linkage presented in the rotating reference frame
i_d, i_q	Stator currents presented in the rotating reference frame
i_d^m, i_q^m	Stator currents presented in the measurement axis displaced by 45° from the the estimated reference frame $\hat{d}-\hat{q}$
$\underline{v_{sc}^{\hat{r}}}$	HF injected voltage vector presented in the estimated reference frame
V_c, ω_c	Amplitude and frequency of the HF injected voltage
$\underline{v_{sc}^s}$	HF injected voltage vector presented in the stator reference frame
$\underline{\phi_{sc}^s}$	HF flux linkage vector presented in the stator reference frame
$\underline{\phi_{sc}^{s*}}$	Conjugated HF flux linkage vector presented in the stator reference frame
$\underline{i_{sc}^s}$	HF stator current vector presented in the stator reference frame
$\underline{i_{sc}^{\hat{r}}}$	HF stator current vector presented in the estimated reference frame
$\underline{i_{s1}^s}$	Fundamental current component
$\underline{i_{sg}^s}$	The general current vector $(\underline{i_{sc}^s} + \underline{i_{s1}^s})$ presented in the stator reference frame
$\underline{i_{sh}^s}$	HF obtained current vector presented in the stator reference frame after removing the fundamental components $\hat{d}-\hat{q}$
$\underline{i_{sc}^s}$	HF obtained current vector presented in the stator reference frame after demodulation process
$\underline{i_{sc1}^{\hat{r}}}$	HF stator current vector presented in the estimated reference frame after demodulation process
$\underline{i_{scl}^{\hat{r}}}$	HF stator current vector presented in the estimated reference frame after demodulation process and signal processing
e_θ	Rotor position estimation error
I_{cp}	Magnitude of HF positive current component
I_{cn}	Magnitude of HF negative current component
Ω	Rotor mechanical speed
θ	Rotor angular position $\theta_e = p\theta$

ε	Current resulting from HF injection method, containing the information on the rotor position
ε_p	Current resulting from pulsating sine-wave HF injection, containing the information on the rotor position
ε_s	Current resulting from pulsating square-wave HF injection, containing the information on the rotor position
ε_r	Current resulting from rotating sine-wave HF injection, containing the information on the rotor position
J	Moment of inertia
K_f	Viscous friction coefficient
T_l	Load torque
T_m	Electromagnetic torque
PWM	Pulse with modulation
DAC	Digital-to-analog converter
ADC	Analog-to-digital converter

List of Figures

List of Tables

1

General Introduction

1.1 Problem statement and objectives

The thermal energy is a new source of energy which is a result of developments in the steam engine during the 18th century, it plays a very important role in the industrial revolution. This new energy source has given rise to a new means of transport, motorized: the automobile. The 19th century brought other remarkable inventions that have revolutionized the motor vehicle industry, including internal combustion engines and electric motors.

The development of EV vehicle has a long history [12, 15]. Since the invention of electric motor, EV has been around for 150 years. From simple non-chargeable to modern state of art control system, the development of electric vehicle (EV) can be classified into three stages: Early years, Midterm and Present as described in Figure 1.1.

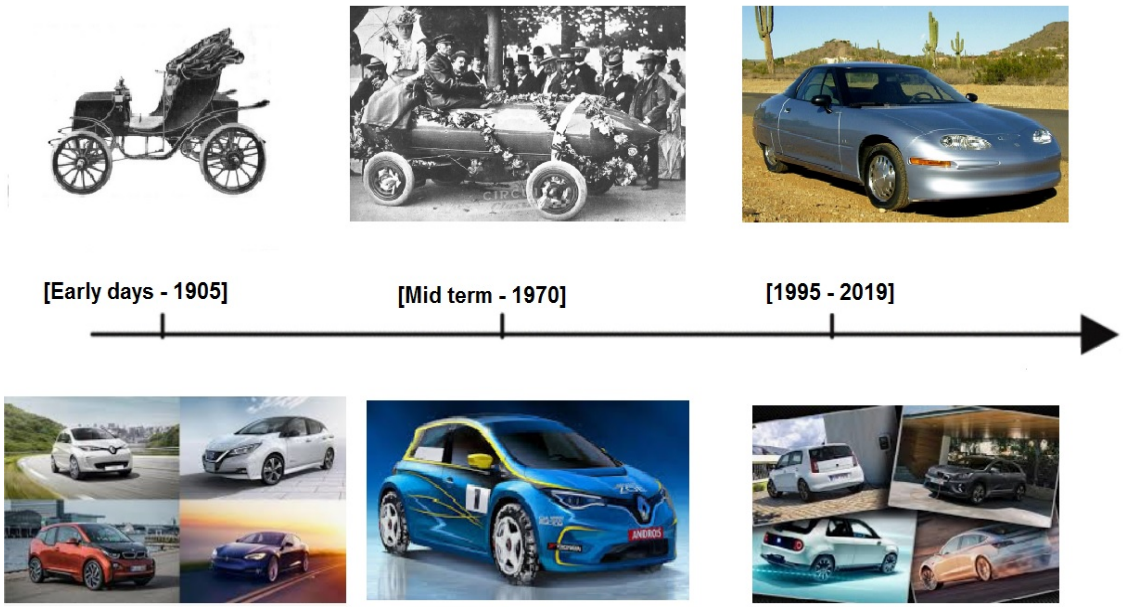

Figure 1.1: Electric vehicle time line [12]

The transport and electric traction sector, in general, is at the forefront of progress in the use of the most advanced technologies in the field of electrical engineering [16, 12]. Indeed, transport research and development activities in recent years have focused on the development of safe, affordable and environmentally friendly transport. To meet these requirements, hybrid electric (HEV) or all-electric vehicles are available [17]. These vehicles are increasingly occupying the automotive market and are trying to replace combustion-powered vehicles [18, 19, 20].

The motor vehicle is one of the most common means of transport. Generally speaking, it is composed of a structure on which a motorcycle power unit is installed. The latter consists of a motor that produces the necessary mechanical energy. The most well-known engine is the internal combustion engine [17]. The latter uses gasoline, alcohol or even a gas as an energy source. Despite poor efficiency, the advantage of this solution lies in the autonomy linked to the high mass energy of the fuel and its ease of storage. These engines are being challenged for their emissions of greenhouse gases and unhealthy particulates, as well as the use of fossil fuels that will become scarce in the coming decades [21, 22]. Pollution from combustion engines reduces air quality, especially in large cities where vehicle concentrations can be very high. An alternative solution to reduce pollution produced locally by combustion engines is the use of vehicles powered by clean energy such as EVs and HEVs. Of course, the energy cost and pollution associated with electricity production will have to be taken into account to power the electric vehicle, including recycling and waste treatment to generate electricity [15] [21].

The field of electric traction has attracted a lot of interest in recent years [12, 18] [20]. HEVs and EVs have rapidly gained ground in the global automotive market by offering high energy efficiency with significant reductions in greenhouse gas emissions at increasingly affordable prices. Many automotive suppliers are currently working on new models of HEV and EV vehicles [12] [20] . One of its main challenges is to design traction machines that meet criteria such as energy efficiency, reliability, power density, technological maturity, robustness and cost. From the point of view of industrial applications, the most common machines used in these vehicles are direct current (DC) machines, and alternating current (AC) machines: permanent magnet synchronous machines (PMSM) and asynchronous machines (AM).

The EVs uses one or more electric motors or traction motors for propulsion [15]. EVs may be powered through a collector system by electricity from off-vehicle sources, or may be self-contained with a battery, solar panels or an electric generator (like for example fuel cell) to convert fuel (hydrogen as an example) to electricity. EVs first came into existence in the mid-19th century, when electricity was among the preferred methods for motor vehicle propulsion, providing a level of comfort and ease of operation that could not be achieved by the gasoline cars of the time [22] [23]. Modern internal combustion engines (ICEs) have been the dominant propulsion method for motor vehicles for almost 100 years, but electric power has remained commonplace in other vehicle types, such as trains and smaller vehicles of all types [19] [24].

The very first prototype of an autonomous individual electric vehicle was made by a Scottish businessman, Robert Anderson in 1830 [24]. It was a cart towed by an electromagnetic engine, but it was in 1859 that the history of the electric vehicle took a decisive turn with the French Planté and its invention of the rechargeable battery with lead acid, which is used to store electricity [21] [25].

This innovation marks the beginning of the history of the electric vehicle, even though a

prototype at gasoline is realized. The two engines are then in competition. Driven by the dynamics of French inventions, English and then American, the first electric vehicle was marketed for the first time in 1884 [15] [19] [21] . The electric vehicle d efinitively acquired its letters of nobility in 1889 when Camille Jenatzy's Jamais Contente was the first vehicle to exceed 100 km/h, whose batteries accounted for more than half of the weight of the car [21] [26].

The electric vehicle experienced its development at the beginning of the 19th century even before the internal combustion vehicle. At that time, the majorities of Parisian taxis were electric and charged via a dedicated infrastructure: public charging stations or battery exchange stations (see Figure 1.2). The range of these vehicles was between 50 and 80 km/h with travel speeds of less than 40 km/h [13] [15] [21] .

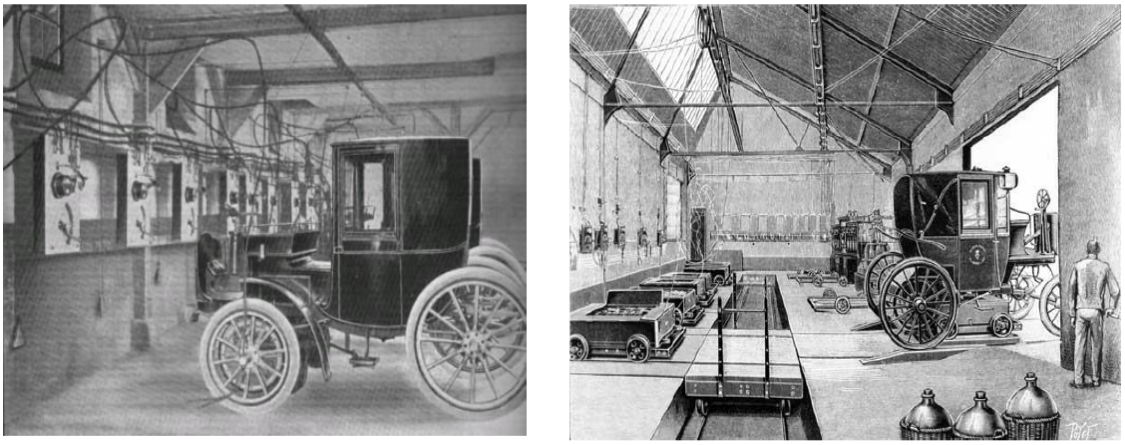

Figure 1.2: Charging stations (Left) and battery exchange station (Right) [13]

Although the first vehicle to exceed the 100 km/h threshold was a vehicle powered by two DC electric motors, gasoline vehicles predominated in the global automotive market during the 20th century. This is due to several factors, including the invention of the starter and the competitive price of the petrol vehicles. Autonomy, energy storage, recharging time and infrastructure were the main limitations for powered vehicles by electric motors.

In the 21st century, EVs saw resurgence due to technological developments, and an increased focus on renewable energy. A great deal of demand for electric vehicles developed engineers began sharing technical details for doing electric vehicle conversions. The composition of the various components of an electric vehicle has changed and these components use new technologies but still have the same operating principles. The first lead batteries have been replaced by lithium batteries [26, 27], which have the highest power densities today. DC motors have given way to AC three-phase motors, which also have higher power density, better energy efficiency and reduced maintenance. The electric converters have been adapted to drive the motors but keep the same principle which is to transfer electrical energy between the batteries motor. Today, several models of electric vehicles were developed and produced with high performances (see Figure 1.3)

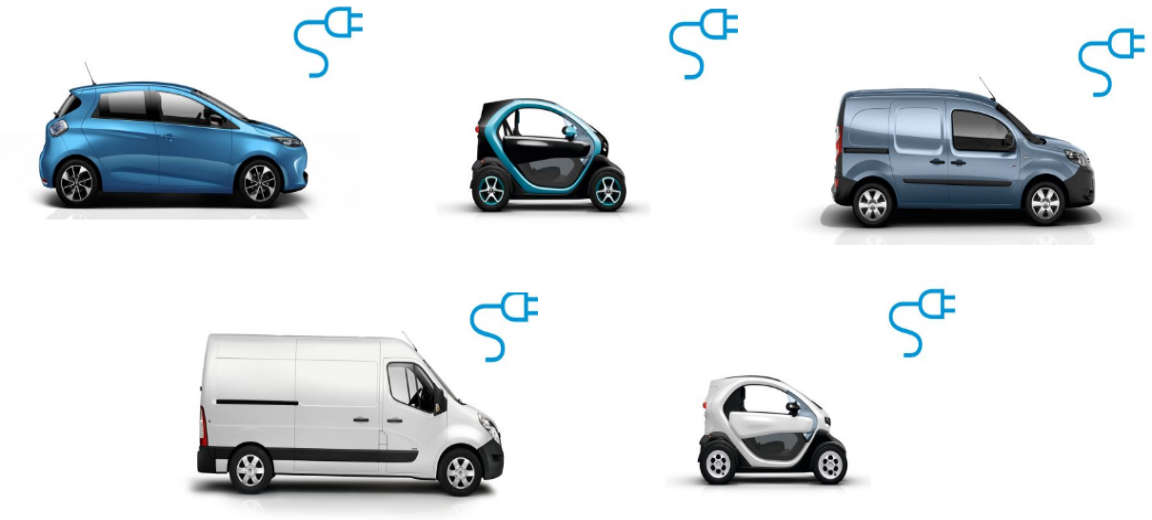

Figure 1.3: Some electric vehicles of one of car manufacturers (Renault).

Many countries support the development of EVs through subsidies, aid for the purchase or installation of bollards, urban tolls, use of bus lanes, dedicated parking spaces, etc. In Europe, in addition to the standards limiting emissions from new "EURO" vehicles (EURO 6 in 2014), manufacturers' average CO2 emissions are subject to the Corporate Average Fuel Economy (CAFE), with an ambitious target of 95 g CO2/km in 2020, which implies electrification of vehicle ranges under penalty of financial penalties [14][28, 29, 30].

In parallel with the evolution of standards, the number of large and medium series EV models has been steadily increasing since 2010, with sales growing faster than the hybrid in 1999 [12] [14]. During 2014, the global fleet of electric vehicles is estimated at around 500,000 units, with penetration rates that vary widely from one country to another. Figure 1.4 shows the penetration rate of electric vehicles for some countries. Norway has the highest number of EVs per capita [12]. The Renault-Nissan Alliance announced that it had sold 200,000 electric vehicles in 2014 [15].

Country	PEV fleet (Cum sales or registrations)	Population as of December 2013	PEV market penetration per 1,000 people (Dec 2013)	PEV market share of total new car sales in 2013	Comments
United States	172,000	320,050,716	0.53	0.62%	(a)
Japan	74,124	127,143,577	0.58	0.85%	(b)
China	38,592	1,385,566,537	0.03	0.08%	(c)
Netherlands	28,673	16,759,229	1.71	5.37%	(d)
France	28,560	64,291,280	0.44	0.65%	(e)
Norway	20,486	5,042,671	4.04	5.60%	(f)

Note: Plug-in electric vehicle fleets include only highway-capable vehicles except where noted in comments. French and Norwegian registrations do not include plug-in hybrids.

Comments: **(a)** Sales between 2008 and December 2013. Includes only plug-in electric passenger cars. **(b)** Sales since July 2009 through December 2013. Kei cars not included for market share estimate. Includes plug-in electric cars and all-electric utility vans. (c) New energy vehicle sales between 2011 and 2013. Includes a significant number of all-electric buses. **(d)** Registrations between 2009 and December 2013.Includes plug-in cars and all-electric commercial vans. **(e)** Registrations between 2010 and December 2013. Includes only all-electric cars and 11,304 utility vans. Market share is 0.49% if only all-electric cars are considered. **(f)** Registrations between 2003 and December 2013. Includes only all-electric cars, vans and over 1,500 heavy quadricycles.

Figure 1.4: World fleet of electric vehicles at the end of 2013 [14]

The development of the EV is nevertheless limited by a shorter range, a longer charging time and a higher manufacturing cost, compared to an equivalent combustion engine vehicle: in 2014, an electric vehicle such as Renault Zoé, Nissan Leaf or Volkswagen e-Golf has a range between 100 and 150 km/h with a battery of about 24 kWh for a minimum charging time of 30 minutes [15]. Use for journeys exceeding the vehicle's range is therefore more restrictive.
During the 20th century, the technology of controlling electrical machines has witnessed some remarkable developments. The formulation of the theory of the two circuits (called Park's theory), the contributions of Automatics, especially observer theory, and developments in control and power electronics have contributed to the emergence of new and more efficient techniques for the control of AC electrical machines [31], such as vector control and direct torque control. On the other hand, high-performance digital computers, high switching frequency power components and some additional sensors connected to the rotor shaft are required for advanced control of AC machines [32, 33, 34].

The reliability and operational safety of the electric powertrain are essential. Three types of defects can be commonly identified:

- Machine defects;
- Sensor faults;
- Faults in the power electronics stage.

Defects of the first type and third type will not be covered in this thesis. For the second type of defect, we are particularly interested in position sensors, which are the most vulnerable sensors to defects compared to current and voltage sensors.

In the domain of classical (FOC [35, 36, 37], Feedback linearization [38], ...) and modern (sliding modes [39, 40], backstepping [41], passivity [42], ... etc) controls of these machines, the knowledge of rotor position and speed are required, which are obtained generally by a physical sensor (encoder or resolver). However, mechanical sensors are expensive, bulky, sensitive to the environment (temperature, noise, mechanical oscillations, electromagnetic compatibility, etc.) and reduce the system reliability. The mechanical sensor can be also a sign of defects that can lead to the total loss of information or its degradation, resulting in a significant drop in performance and a malfunction of the traction chain. Taking into account all these limitations, numerous studies [43, 44, 45, 46, 47] have been carried out to remove these mechanical sensors in order to maintain the correct operation of the machine. These studies have revealed several methods of self-sensing control using software sensors. The position estimation becomes an ongoing need, namely within EVs and HEVs, either for the closed-loop self-sensing control or for fault diagnosis and safety applications.

From the above points of view, this work thesis, conducted in the framework of the Chair between CN and Renault in Guyancourt about EVs performances, addresses the problematic of self-sensing control by using HF signal injection methods. Mainly, we address the problem of position and speed estimation algorithms based HF signal injection methods that:

- Ensures stability and robustness (less dependency on machine parameters) in all speed area and torque ranges.
- Reduces the effects of delays/phase shifts, complexity and harmonics, and
- Facilitates the tuning. To solve this problem, the innovations of this work are focused on the development and design of advanced estimation techniques and improved HF signal injection methods.

By doing so, we set-up a self-sensing control strategy taking account the 3 points cited above and consequently responding to the objectives of the Chair between Renault and CN.

Today, several industrial companies (like Renault) offer an importance to self-sensing control by HF signal injection techniques. HF signal injection becomes one of the most challenging approaches present in several industrial applications. However, there is still a need to reinforce the robustness and stability of the motor operation without mechanical sensor at all speed ranges. For the problematic cited just above, this approach remains a very active field of industrial and academic research area.

The rapport presented in this thesis is part of the Renault Chair project for the improvement of EV/HEV propulsion performances. The main goal is to innovate on the control strategy of the electric motor (especially synchronous motors) for future vehicles. The main innovations are focuses on the development and design of the new self-sensing control strategy based on advanced estimation techniques to increase the performance, reliability, robustness of the control chain and reduce risk, cost and implementation complexity.

1.2 Report organization and contributions

The thesis report is organized as follows:

Chapter 2: State-of-the-art of self-sensing control of IPMSM-based electric drives: The goal of this chapter is to give a literature review of self-sensing interior PMSM (IPMSM) techniques. The objective is to the most suitable self-sensing technique to the EV traction application. Therefore, the classical and HF IPMSM modeling are firstly given. Then, the vector control of IPMSM using an encoder is introduced. A focus is given to self-sensing techniques. The main interests and limitations of each self-sensing techniques are recalled.

Chapter 3: Contribution to demodulation of high frequency voltage injection (HFVI): The objective of this chapter is to improve the classical HF signal injection techniques in terms of delays effects, cost, complexity implementation. This allows to improve the estimation chain of theses techniques and hence the self-sensing performance.

The concerned improvements depend on the HFVI nature, for this, the chapter is organized as follows. Section 3.2 introduces the pulsating square-wave improved demodulation for the self-sensing drive control. Section 3.3 focuses on contribution to demodulation process for the pulsating-sine wave strategy. An improved demodulation for the rotating wave-sine is detailed in the Section 3.4. Some results are highlighted in order to validate the optimized demodulation process under operating conditions. All these contributions allow to improve significantly the estimation process and cover an extended operating range of the machine (medium and high speeds operating modes with different torque values).

Chapter 4: Contribution to rotor position and speed tracking algorithms: This chapter is to Firstly, the chapter introduces the practical implementation issues and describes the experimental setup used to validate the proposed contributions in Section 4.35. Then, the classical tracking algorithms, associated to the HF signal injection techniques, for the rotor and speed estimation are also introduced in Section 4.35. In Sections 4.4.1, 4.4.2 and 4.4.3, the proposed self-sensing tracking algorithms of HFVI are presented to estimate the rotor position and speed in all speed operation (zero, low and high) at different torque ranges. The aim of these algorithms is to get rid of machine's electrical and mechanical parameters, to improve their tuning and compensate of position and speed estimation errors in transient modes. In the context of EV drives, another

critical issue is the torque ripples, primarily due to the accuracy of the rotor position and speed estimator. The proposed improvements in this chapter help in the minimization of these effects. The effectiveness of the claimed contributions is proved by simulation and experimental tests under a drive benchmark that is more representative of EVs/HEVs applications. A comparative study on the robustness and performances between proposed tracking observers is given in Section 4.4.4 in order to select the most appropriate observer. In Section 4.4.5, a comparative study on the robustness and performances between the selected estimation technique and the existing techniques is exhibited. Then, in Section 4.5, the selected observer is coupled with classical and improved HFVI techniques (pulsating sine-wave, pulsating square-wave and rotating sine-wive) given in the previous chapter in order to compare their performances and to choose the best HFVI from the presented techniques. The Section 4.6 focuses on comparative study between the improved pulsating sine-wave, the improved pulsating square-wave and the improved rotating sine-wave in terms of rotor position and speed estimation error, sensitivity to electrical and mechanical parameters, delays caused by filters used, noise generated by the HF of the injected signal, acoustic noise and phase shifts generated by sampling time and inverter, the number of used filters and the implementation complexity is discussed. Sections 4.7 consist in studying the accuracy of the optimized self-sensing strategy under 0% and 120% load torque (greater than the nominal torque).

Chapter 5: Conclusion and open topics: This chapter concludes the thesis report and gives the recommendations for future research.

1.3 Scientific outputs

This work has been the subject of several patents and publications:

1.3.1 Patents

– Patent PJ-18-5036, A. Messali, M. Ghanes and M. Koteich: Procédé d'estimation de la position, vitesse et accélération d'une machine électrique tournante triphasée, (Accepted in France, international extension is in progress).

– Patent PJ-18-5153, A. Messali, M. Ghanes and M. Koteich: Procédé de commande des machines électriques triphasées sans capteur de position, (Accepted in France, international extension is in progress).

– Patent PJ-19-0160, A. Messali, M. Ghanes and M. Koteich: Compensation des retards physiques générés par la chaîne calculateur-moteur-calculateur pour la démodulation du resolver (capteur de position) pour et hors contexte contrôle sans capteur, (Under review).

1.3.2 Journal papers

– A. Messali, M. Ghanes, M. Hamida, and M. Koteich *A resilient adaptive sliding mode observer for self-sensing AC machine drives based on an improved HF injection technique*, IFAC Control Engineering Practice (Accepted).

– M. Hamida, J. Deleon and A. Messali. *Observer design for nonlinear interconnected systems: experimental tests for self-sensing control of synchronous machine*, International

Journal of Advanced Manufacturing Technology. (Accepted).

– A. Messali, M. Hamida, M. Ghanes and M. Koteich. *An estimation procedure based on less filtering and robust tracking for a self-sensing control of pole salient ac machine*, IEEE Transactions on Industrial Electronics (Accepted).

– A. Messali, M. Ghanes, M. Koteich and M. Hamida. *Enhanced square wave signal injection for self-sensing AC machines with improved transient performances*, IET Electric Power Applications (Correction phase).

1.3.3 Conference papers

– A. Messali, M. Ghanes, M. Hamida and M. Koteich. *Robust adaptive sliding mode observer for self-sensing IPMSM control based on optimized HF injection method, Nonlinear Control Systems* - 11th IFAC Symposium on Nonlinear Control Systems (NOLCOS 2019), Vienna, Austria, 4-6 September 2019.

– A. Messali, M. Koteich, M. Ghanes and M. Hamida. *A robust observer of rotor position and speed for IPMSM HFI self-sensing drives*, IEEE International Conference on Sensorless Control for Electrical Drives (SLED), Helsinki, Finland, September, 13-14, 2018

– A. Messali, M. Hamida, M. Ghanes and M. Koteich. *A Novel High Frequency Signal Injection Strategy for Self-Sensing Control of Electric AC Machine Drives*, IEEE International Conference on Industrial Electronics Society (IECON), October 21-23, Washington D.C, USA, 2018.

– A. Messali, M. Hamida, M. Ghanes and M. Koteich. *A Rotor position, speed and acceleration estimation for salient-pole AC machines at all speed and torque ranges*, IEEE International Conference on Power Electronics and Drive Systems (PEDS 2019), July 09-12, Toulouse, France, 2019

– A. Messali, M. Hamida, M. Ghanes and M. Koteich. *Rotating HF signal injection method improvement based on robust phase-shift estimator for self-sensing control of IPMSM*, IEEE International Conference on Diagnostics for Electric Machines, Power Electronics and Drives (SDEMPED), August 27-29, Toulouse, France, 2019.

– A. Messali, M. Hamida, M. Ghanes and M. Koteich. *Robust phase-shift estimator for self-sensing control of PM synchronous machines*, IEEE International Conference on Sensorless Control for Electrical Drives (SLED), September 9-10, Torino, Italy, 2019.

– M. Koteich, A. Messali and S. Duarelle. *Self-sensing control of the externally-excited synchronous machine for electric vehicle traction application*, IEEE International conference on Sensorless Control for Electrical Drives (SLED), September 18-19, Catania, Italy. 2017.

2

State-of-the-art of self-sensing control of IPMSM-based electric drives

This chapter presents a brief literature review of self-sensing techniques for IPMSM drives. The objective is to the most suitable self-sensing technique to the EV traction application. Therefore, the classical and HF IPMSM modeling are firstly given. In a second phase, the vector control if IPMSM using an encoder is introduced. Then, introduction to self-sensing techniques is highlighted; the main interests and limitations of each self-sensing techniques are recalled.

2.1 Introduction

PMSMs have attracted attention for many industrial applications. They have many advantages such as high power density, high-precision positioning, high torque to inertia ratio and high efficiency. There are many reasons for this such as the development of power electronics component technology, and the emergence of digital processors with high frequency and high computing power. In addition, technology is evolving with permanent magnets on rare earths (Samarium-Cobalt and Neodymium-Iron-Boron). In addition, the advantages of IPMSMs are their high efficiency, a high speed, a clean environment and a long-lasting operation. The fact that not using mechanical collectors or sliding contacts allows them to work in the most difficult environments and to have a low maintenance cost. The first concept of vector control of these machines was proposed by K. Hasse in 1969 and F. Blaschke in 1972 [48, 49]. Vector control is also called field oriented control, and uses a rotating frame dq-axis aligned to the rotor flux to control the torque and field independently through rotor flux orientation. Vector control has been used on AC machines such as induction motors and permanent magnet motors. Vector control utilizes the motor shaft mounted encoder to obtain the flux position for field orientation and closed-loop motor control. However, the encoders in many industrial applications have several disadvantages. They increase cost, reduce reliability, increase machine size, need installation, and are susceptible to noise interference. Therefore, the self-sensing control of AC machine without encoder has attracted considerable research over recent years. The first self-sensing control of an induction motor was proposed by Joetten and Maeder in 1983 [50]. The rotor frequency observer/ forms an inner control loop, as part of the drive control system [51]. With the development of the self-sensing approach, a signal processing technique is used as a speed

or position observer/estimator. The observer/estimator for speed and position is based on the fundamental mathematical models of the machine. The estimation is obtained from the motor back-EMF. The observer/ shows good performance in the higher speed range and fails at very low or zero speed [51]. The magnitude of back-EMF is very small at low speed that has a low signal-to-noise ratio, which is made worse by the nonlinear effects of the power converter. The observer/ estimator structure used in fundamental mathematical model estimation techniques also strongly depends on the machine parameters, which can be changed due to heating and saturation[52]. The fundamental model based self-sensing technique does not produce good results if the machine has un-modeled nonlinearities and disturbances [53]. Therefore, other approaches to self-sensing control techniques have been introduced using motor saliency-based techniques to estimate rotor position and speed. The high frequency injection techniques are currently the main trend of research on the self-sensing control at low or zero speed. In this chapter, the classical and HF IPMSM modeling are given, the research for self-sensing control of AC machines is reviewed. The fundamental model based techniques are recalled. The saliency based techniques are also presented. Finally, the classical tracking algorithm needed for the estimation chain, including a mechanical system observer (MSO) and a phase locked loop (PLL), will be presented.

2.2 IPMSM Modeling

The permanent magnet AC machine attracts attention in many industrial, commercial and transportation applications due to its advantages [54]. They are becoming more and more popular, attractive and competitive with other motors. The synchronous motor can be very useful in many applications, as

- Domestic equipment (washing machine),
- Information technology equipment (DVD drives),
- Power tools, toys, vision systems and their equipment,
- Medical and health care equipment (dentist's milling cutter),
- Servomotors,
- Robotic applications,
- Electricity generation,
- The propulsion of electric vehicles,
- The submarine Propulsion,
- Machine tools,
- The application of wind turbine energy.

The term synchronous machine includes all machines whose rotational speed of the rotor is equal to the rotational speed of the stator rotating field [54]. To obtain a such operation, the rotor magnetic field is generated either by magnets (PMSM) or by an excitation circuit (externally-excited synchronous machine (EESM)). The stator phases are connected to a sinusoidal three phase voltage source (a,b,c) (see Figure 2.1). The superposition of the three magnetic fluxes created by the three phase windings of the stator produces a sinusoidal flux rotating at the frequency of the voltage source. This rotating magnetic flux interacts with the rotor flux in the air gap separating the stator from the rotor and creates an electromagnetic force leading to the rotation of the rotor. The value of the motor speed corresponds then to the frequency of the motor voltage. Permanent magnets have the advantage of eliminate brushes and rotor losses, as well as the need for a source to provide the excitation current.

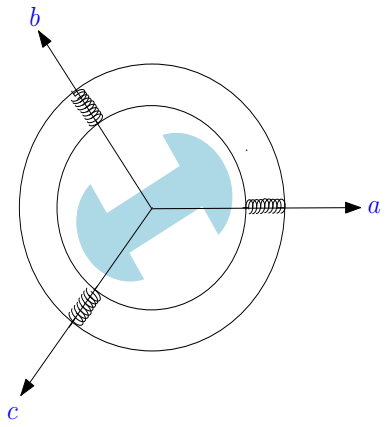

Figure 2.1: Three IPMSM (a,b,c) phases

There are two main types of PMSMs: the surface mounted permanent magnet motor also called SPMSM [55] which has attached magnets to the surface of the rotor; the interior permanent magnet motor also called called IPMSM [55] which has buried magnets inside the rotor. An IPMSM has stronger mechanical strength than SPMSM because the magnets of SPMSM need to be fixed on the surface of the rotor. From magnetic point of view, the SPMSM rotor is symmetric while the IPMSM rotor is asymmetric. Hence, the SPMSM stator inductances do not vary with the rotor position [56]. By contrast, the IPMSM inductances values change according to the rotor position [57] and create a geometric saliency which is an important feature for low speed control. The IPMSM can be classified according to the shape of the electromotive force [54] [58]: sinusoidal and trapezoidal. In particular, IPMSM with sinusoidal f.e.m. are classified into two groups categories according to the position of the magnets

- Smooth poles (Figure 2.2-Left).
- Salient poles (Figure 2.2-Right).

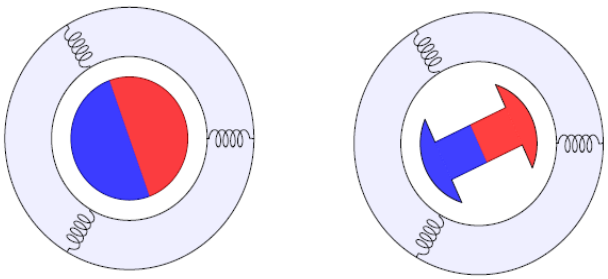

Figure 2.2: Smooth (Left) and salient (Right) poles

The study of the behavior of IPMSM is difficult and necessary task, first and foremost, a good knowledge of its dynamic model in order to properly predict its behavior, by means of simulation, in the different operating modes envisaged. The modeling of a PMSM is identical to that of a conventional synchronous machine except that the DC excitation attached to the rotor is replaced by the flux of the magnet. So, the model is derived from the classical model of synchronous machine [54] [59, 60]. In this study, the machine consists of a stator and a rotor with a symmetrical constitution with p pairs of poles. Stator windings are most often connected in a star configuration to isolated neutral. The rotor excitation is created by permanent magnets at the rotor. In order to simplify machine modeling, the usual assumptions given in the most references are adopted [59, 60, 61, 62, 63]

- The stator winding resistances are constant

- The damping effect on the rotor is neglected,
- The magnetic characteristic is linear (no saturation),
- The spatial amplitude of the PM flux linkage is constant,
- Hysteresis phenomena, temperature effect, skin effect and Foucault's currents are neglected.

These assumptions provide a simplified model for both control and observer synthesis. In order to discuss the different aspects of self-sensing control, a basic understanding of different machine models is needed. The following section describes the classical and the HF model of the IPMSM. In the first subsection, the classical model of the IPMSM is derived in different frame, then, the HF model of the machine, which is needed for HF signal injection techniques is given. In each part,the voltage-flux and flux-current models are introduced.

2.2.1 Classical IPMSM models

IPMSM are physical systems governed by electrical, magnetic, mechanical, thermal, acoustic and other phenomena. In the context of torque or speed control of these machines, only electromagnetic and electromechanical phenomena are relevant for the implementation of a simplified and a representative model. These phenomena can be described by laws of physics such as Maxwell's equations (for the electromagnetic part) and Laplace's force and Newton's second law (for the electromechanical part) [54] [61] [64]. The modeling of electrical machines for their control requires the consideration of some simplifying assumptions, and is based on 3 types of equations

- Magnetic equations: Ampere's theorem describes the flux as a function of the currents that run through the windings.
- Electrical equations: Ohm's law generalized with Faraday's law describe the relationship between voltages and currents.
- Mechanical equations: Newton's second law describes the speed variation of the machine shaft as a function of torque (resulting from Laplace force).

Despite the consideration of simplifying assumptions, the equations of AC machine remain highly nonlinear, which makes it very difficult to analyze the machine's behavior, especially in transient conditions. To facilitate the analysis of the transient and permanent regimes of IPMSM machines and as well as their control, the theory of the 2 circuits (Park's) (see Section 2.2.1.1) has been introduced; it is a series of mathematical transformations that simplify the machine model by keeping the physical aspect of the quantities transformed. In this chapter, we present the physical laws and mathematical tools useful for modeling IPMSM machines. Machine modeling details are given in [51] [64, 65] .

2.2.1.1 Theory of the two circuits

The three-phase synchronous machine model is strongly coupled. In order to facilitate the study of electrical machines, engineers and researchers of the early 20th century (Blondel, Park, Doherty, Nickle, Concordia, Clarke and others) proposed mathematical transformations that maintain the physical aspect of the variables. Their results now allow us to better analyze the behaviour of AC machines, especially in transient conditions. The most interesting contribution was published by Park in the years 1929 [66] and 1933 [67]. It consists in modeling the synchronous machine with two windings (circuits) in two-phase rotating phases linked to the rotor. Later, this theory was generalized, for the study of transient regimes of all AC machines, through the work of Concordia [68], Stanley [69], Kron [63] [70] and others. In the 1970s, Blaschke proposed to apply this theory to the control of three-phase machines [48], which opened

a new strategy in the theory of speed drives variable. The basic idea of the theory of the two circuits is based on the fact that, for any multi-phase AC machine, the operating principle is the same: the rotor interacts with the rotating magnetic field created by the stator to generate a torque that allows the rotor to start rotating. It is therefore necessary to represent the rotating variables (field and magnetic flux, subsequently electrical current and voltage) as vectors in an orthonormal reference frame. This marker can be linked to the stator (α,β) or to the rotating frame (d,q) as shown in Figure 2.3. Mathematically, the transition from a fixed polyphase reference frame to a two-phase reference frame is done by projecting the resultant of the desired variable (flux, current, etc.) on a 2 axis system. Then, the passage of a two-phase reference mark to another is done by a rotation $P(\theta)$, where θ is the angle between the two frames

$$P(\theta) = \begin{bmatrix} \cos(\theta) & -\sin(\theta) \\ \sin(\theta) & \cos(\theta) \end{bmatrix} \tag{2.1}$$

The set of variable changes that transforms the polyphase system into a rotating two-phase is called Park transformation. In this paragraph, one can deal with the case of three-phase machines, which are the most widespread AC machines. The passage of the winding system (X_{abc}) to a fixed two-phase system ($X_{\alpha,\beta}$) is possible through the relationship (Figure 2.3) transformation

$$\begin{bmatrix} x_\alpha \\ x_\beta \end{bmatrix} = (\frac{2}{3})^n \begin{bmatrix} 1 & -\frac{1}{2} & -\frac{1}{2} \\ 0 & \frac{\sqrt{3}}{2} & -\frac{\sqrt{3}}{2} \end{bmatrix} \begin{bmatrix} x_a \\ x_b \\ x_c \end{bmatrix}. \tag{2.2}$$

Depending on the value of n, there are two main types of three-phase to two-phase transformation

– Clarke transformation, noted C_{32}, for n = 1

$$x_{ab} = C_{32} x_{abc} = (\frac{2}{3}) \begin{bmatrix} 1 & -\frac{1}{2} & -\frac{1}{2} \\ 0 & \frac{\sqrt{(3)}}{2} & -\frac{\sqrt{(3)}}{2} \end{bmatrix}. \tag{2.3}$$

It keeps the amplitude of the transformed quantities but not the power nor the torque (one must multiply by the coefficient 3/2).

– Concordia transformation, noted T_{32}, for n = 0.5

$$x_{ab} = T_{32} x_{abc} = (\frac{2}{3})^{\frac{1}{2}} \begin{bmatrix} 1 & -\frac{1}{2} & -\frac{1}{2} \\ 0 & \frac{\sqrt{3}}{2} & -\frac{\sqrt{3}}{2} \end{bmatrix}. \tag{2.4}$$

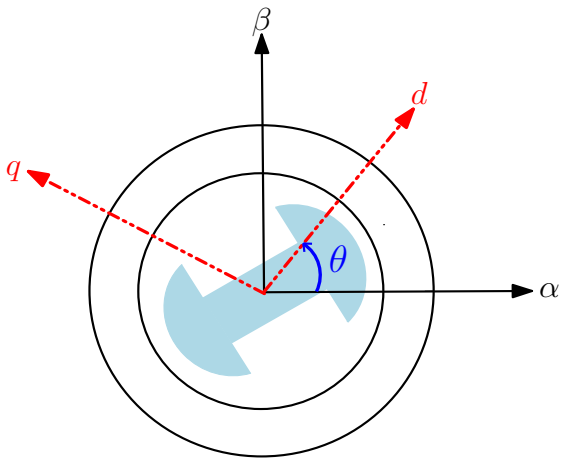

Figure 2.3: The Park transform

It keeps the power but not the amplitude of the transformed quantities. Properties and advantages of transformation matrices are given in [66, 67, 68]. The IPMSM can be described by two

models, voltage-flux and flux-current model, for each one, the components will be presented on two references frames (stationary and rotating reference frames).

2.2.1.2 Voltage−Flux models

Using Ohm's Law, the stator voltage-flux model is described stator reference frame (in a fixed two-phase system (α,β)) as follows

$$\underline{v_s^s} = R_s \underline{i_s^s} + \frac{d\underline{\psi_s^s}}{dt} \tag{2.5}$$

with $\underline{v_s^s}$, $\underline{i_s^s}$, $\underline{\psi_s^s}$ and R_s are the complex stator voltage, complex stator current and flux expressed in the stator reference frame and the stator resistance, respectively.
This model can be expressed under matrix notation as follows

$$\begin{bmatrix} v_\alpha \\ v_\beta \end{bmatrix} = R_s \begin{bmatrix} i_\alpha \\ i_\beta \end{bmatrix} + \frac{d}{dt} \begin{bmatrix} \psi_\alpha \\ \psi_\beta \end{bmatrix}. \tag{2.6}$$

Based on the Park transformation (2.1) and on Equation (2.5), the voltage-flux model expressed in the rotating reference frame is given as follows

$$\underline{v_s}^r = R_s \underline{i_s^r} + \frac{d\underline{\psi}^r_s}{dt} + j\omega \underline{\psi_s}^r \tag{2.7}$$

with $\underline{v_s^r}$, $\underline{i_s^r}$, $\underline{\psi_s^r}$ and ω are the complex stator voltage, complex stator current and flux expressed in the rotor reference frame and the electrical speed, respectively.
This model can be expressed under matrix notation as follows

$$\begin{bmatrix} v_d \\ v_q \end{bmatrix} = \begin{bmatrix} R_s & 0 \\ 0 & R_s \end{bmatrix} \begin{bmatrix} i_d \\ i_q \end{bmatrix} + \begin{bmatrix} s & -\omega \\ \omega & s \end{bmatrix} \begin{bmatrix} \psi_d \\ \psi_q \end{bmatrix}. \tag{2.8}$$

2.2.1.3 Flux−Current models

The magnetic flux in the rotating frame is given by

$$\underline{\psi_s}^r = \psi_d + j\psi_q \tag{2.9}$$

where,

$$\psi_d = L_d i_d + \psi_m, \quad \psi_q = L_q i_q \tag{2.10}$$

with L_d, L_q are $d-q$ axes inductances, respectively and ψ_m is the permanent magnet flux. By replacing Equation (2.10) in Equation (2.9), the following expression is obtained

$$\underline{\psi_s}^r = L_0 \underline{i_s}^r + L_2 \underline{i_s}^{r*} + \psi_m \tag{2.11}$$

where,

$$L_0 = \frac{L_d + L_q}{2} \tag{2.12}$$

is the average inductance and

$$L_2 = \frac{L_d - L_q}{2} \tag{2.13}$$

is the differential inductance.
Based on the Park transformation (2.1) and on Equation (2.11), the stator flux-current model expressed in stator reference frame is given as follows

$$\underline{\psi_s}^s = L_0 \underline{i_s}^s + L_2 \underline{i_s}^{s*} e^{j2\theta} + \psi_m e^{j\theta}. \tag{2.14}$$

Under matrix notation, the stator flux-current model expressed in the stator reference frame as follows

$$\begin{bmatrix} \psi_\alpha \\ \psi_\beta \end{bmatrix} = \begin{bmatrix} L_0 + L_2\cos(2\theta) & L_2\sin(2\theta) \\ \sin(2\theta) & L_0 - L_2\cos(2\theta) \end{bmatrix} \begin{bmatrix} i_\alpha \\ i_\beta \end{bmatrix} + \psi_m \begin{bmatrix} \cos(\theta) \\ \sin(\theta) \end{bmatrix}. \tag{2.15}$$

Based on the inverse of Equation (2.15), the stator current expressed in the stator reference frame by using matrix the notation is given as follows

$$\begin{bmatrix} i_\alpha \\ i_\beta \end{bmatrix} = \frac{1}{{L_0}^2 - {L_2}^2} \begin{bmatrix} L_0 - L_2\cos(2\theta) & -L_2\sin(2\theta) \\ -L_2\sin(2\theta) & L_0 + L_2\cos(2\theta) \end{bmatrix} [\begin{bmatrix} \psi_\alpha \\ \psi_\beta \end{bmatrix} + \psi_m \begin{bmatrix} \cos(\theta) \\ \sin(\theta) \end{bmatrix}]. \tag{2.16}$$

By using the complex notation, Equation (2.16) becomes

$$\underline{i_s}^s = \frac{1}{{L_0}^2 - {L_2}^2} [L_0 \underline{\psi_s}^s - L_2 \underline{\psi_s}^{s*} e^{j2\theta} - \psi_m e^{j\theta}]. \tag{2.17}$$

2.2.2 HF IPMSM models

In order to apply the self-sensing control using the HF injected voltage, the HF machine model should be studied.

2.2.2.1 Assumptions

The following assumptions are regarded to build the HF IPMSM model [71, 72, 73].
- The impedance of the machine is dominated by self-inductance ($R_s < j\omega_c L_s$), it means that the influence of the stator resistance is neglected.
- Because the angular speed of the injected high frequency voltage is much larger than the rotor angular speed, it is assumed that the permanent magnet linkage is much smaller than the magnet linkage of the stator current and can be neglected [73].
- In the rotor reference frame, the two axis (dq) being magnetically decoupled.
- The rotating Back-EMF is neglected.
- The cross saturation effect are neglected.

Base on previous assumptions, the HF voltage-flux and HF flux introduced hereafter.

2.2.2.2 HF voltage−flux models

By considering above assumptions and Equation (2.5), the HF stator voltage-flux model is

$$\underline{v_s}^s \simeq \frac{d\underline{\psi_s}^s}{dt}. \tag{2.18}$$

2.2.2.3 HF flux−current models

By considering above assumptions and Equation (2.11), the HF stator flux-current model is described as follows

$$\underline{\psi_s}^s = L_0 \underline{i_s}^s + L_2 \underline{i_s}^{s*} e^{j2\theta}. \tag{2.19}$$

From Equation (2.17), the HF current expression is given by

$$\underline{i_s}^s = \frac{1}{{L_0}^2 - {L_2}^2}(L_0 \underline{\psi_s}^s - L_2 \underline{\psi_s}^{s*} e^{j2\theta}). \tag{2.20}$$

Then, by using the complex notation, the HF stator current expressed in stator reference frame is expressed as follows

$$\begin{bmatrix} i_\alpha \\ i_\beta \end{bmatrix} = \frac{1}{{L_0}^2 - {L_2}^2} \begin{bmatrix} L_0 - L_2\cos(2\theta) & -L_2\sin(2\theta) \\ -L_2\sin(2\theta) & L_0 + L_2\cos(2\theta) \end{bmatrix} \begin{bmatrix} \psi_\alpha \\ \psi_\beta \end{bmatrix}. \tag{2.21}$$

2.3 Vector control of IPMSM using an encoder

The principle of vector control is very known in the literature [48, 49] [54] [61][74, 75]. A variety of implementation techniques has now been developed [61] [76] [77], these techniques can be broadly classified into two groups [49] [54]: Direct vector control and indirect vector control. Indirect control requires a high resolution position sensor, such as an encoder or a resolver, to determine the rotor flux position. Direct vector control determines the magnitude and position of rotor flux vector by direct flux measurement or by a computation based on terminal conditions [74]. Vector control requires implementation using a microprocessor for the signal processing and coordinate transformation. All the signal processing required in a high-performance AC servo drive can be executed by a single microprocessor [74]. Vector control is based on Park transformation (see Section 2.2.1.1) [78, 79]. The implementation of vector control requires information about the magnitude and position of the flux vector. Vector control acts in a field-coordinate system using two constants as input references for stator currents and voltages. They are the torque producing current i_q and the field producing current i_d. Vector control structure deals with instantaneous electrical quantities. This makes the control more accurate in every working operation such as steady-state and transient modes [78]. The vector control of a PMSM is based on controlling the rotor flux and torque independently. For a PMSM, this is achieved by aligning the d-axis with the axes of the magnet. This can be derived from a shaft mounted position encoder, or through self-sensing means. The two stator currents i_d and i_q control the flux and torque, respectively. The currents command i_d and i_q in the rotating frame are compared with their feedback generated respectively from Concordia and Park transformations (see Section 2.2.1.1) to create an error signal. At this point, this control structure shows an interesting advantage: it can be used to control either synchronous or induction machines by varying the flux command and correctly obtaining the rotor flux position [78]. In a PMSM, the rotor flux is determined by the magnets which have the fixed values. Therefore, the reference current i_{d-req} is usually set to zero. The current error signals pass through a PI controller to produce the reference voltage v_d and v_q. These two voltage components are transformed into a three phase voltage reference using respectively the Park inverse and the Concordia inverse transformations.

2.4 Introduction to self-sensing techniques

The classical (FOC, Feedback Linearization, ...) and modern (sliding modes, backstepping, high gain, passivity, ... etc) controls of synchronous machines require the knowledge of rotor position and speed, which are obtained generally by a physical sensor (encoder or resolver). However, mechanical sensors are expensive, bulky, sensitive to the environment (temperature, noise, mechanical oscillations, electromagnetic compatibility, etc.) and reduce the system

reliability. Taking into account all these limitations, numerous studies [43, 44, 45, 46, 47] have been carried out to remove these mechanical sensors in order to maintain the correct operation of the machine. These studies have revealed several techniques of self-sensing control using software sensors. The classification of self-sensing techniques is often made based on their feasibility and performances according to the operating speed. At medium and high speeds, model based techniques, generally exploit the estimated back-EMF. Conversely, at standstill and low-speeds, the system becomes unobservable and the back electromotive force (EMF) amplitude is too low to be exploited [80, 81]. Such limitations can be overcome with saliency-based techniques which are very interesting in this case, since they take advantage of the machine anisotropy [82, 83]. As for the soft computing technique, they can be used independently on the speed range, since they rather depend on a relevant choice of the input data (also called features), which leads to the estimation of the motor position/speed. In this chapter, each of these techniques is briefly described. Then, an in-depth understanding of saliency-based self-sensing techniques are provided. In the last decades, researchers have implemented various self-sensing schemes. As shown in Figure 2.4, position estimators can be broadly classified into three main categories

- Model-based techniques.
- Saliency-based techniques.
- Soft computing based technique (artificial intelligence based techniques).

This section presents a brief literature review used for self-sensing IPMSM drives. The objective is to select the self-sensing technique most suited to the EV traction application.

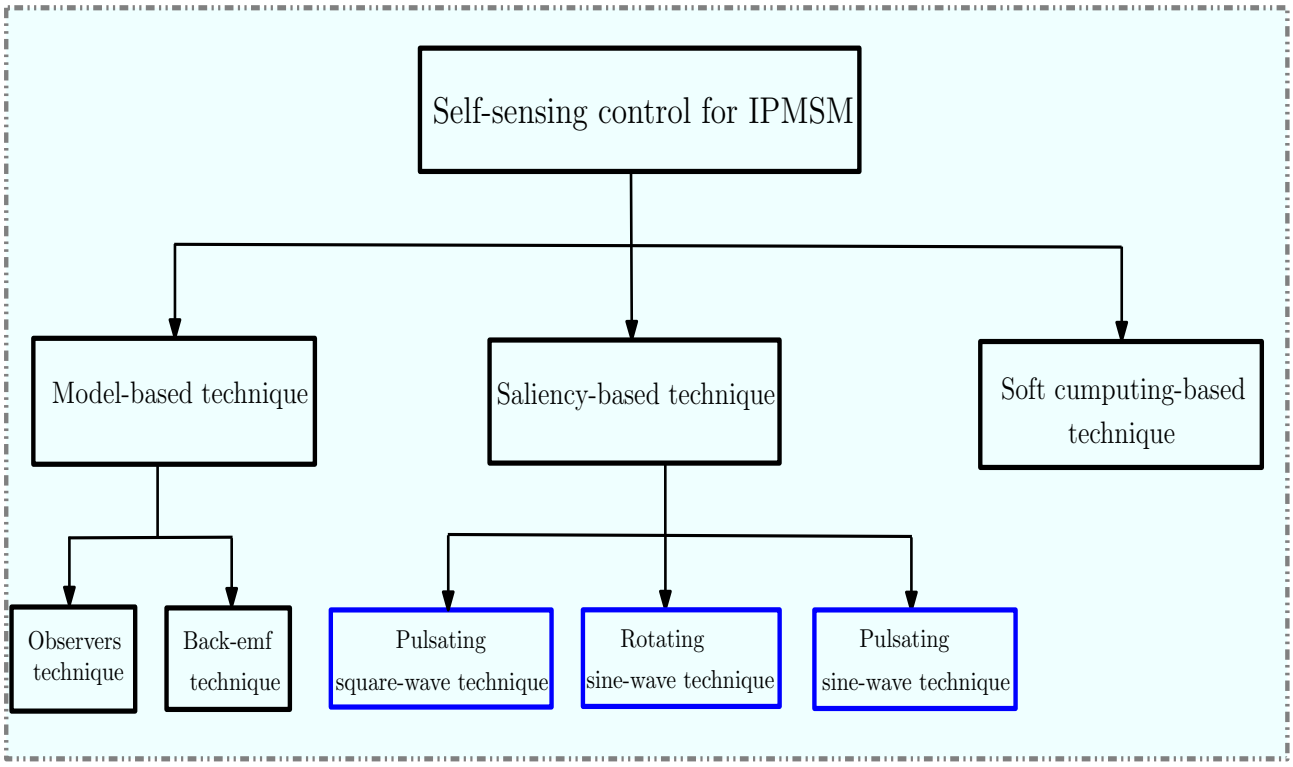

Figure 2.4: Self-sensing control techniques

2.5 Self-sensing control based on the fundamental mathematical model

The objective of this section is to discuss the basic structures and classification of model based techniques [45] [84, 85], their advantages and disadvantages. The model-based technique relies on the estimation of back-EMF or flux linkage according to the fundamental model, which contains the rotor position information. The fundamental mathematical based self-sensing techniques have the simplest realization; but, they are parameter dependent and generally fail at zero and low speed [86] . At zero and low speed, the rotor flux and speed signals are difficult to observe due to the low back-EMF voltage. In [80, 81, 87], the rotor flux and speed become unobservable from the models which use stator currents and voltages at zero and low speed (when stator voltage is reduced to a small value). During motor operation, parameters assumed constant actually vary as the flux level or temperature changes, which causes variations of the rotor time-constant and the stator resistance as well as inductances due to the saturation of magnetic characteristics and magnet flux variation. The online identification of parameters or an adaptive controller has to be implemented for a good estimation. Alternatively, the saliency tracking techniques are introduced as the non-model based techniques for position estimation. These techniques are applicable for self-sensing control at zero and low speeds. In the sequel, firstly model based techniques will be briefly recalled. Then the non-model based techniques will be discussed as well as the saliency tracking techniques.

2.5.1 Observer based techniques

The state observer models were the first technique proposed to estimate the rotor position and speed of the IPMSM (see for instance [46, 47] [88, 89, 90]). The state observer estimates the internal variables of a real system from the measurements of input and output signals if only if the system is observable [91]. Typically, the state observer is a computer-implemented mathematical model, which can be used for flux estimation in self-sensing control of IPMSM drives. Also note that observers should be faster than the system they observe, but also slow enough to suppress noise and other kinds of disturbances [44]. Two observation approaches can be distinguished: the deterministic approach and the stochastic approach. The first one consists in using deterministic observers which lean on the system model without considering measurement noises and modeling errors. One can cite the Luenberger observer or the Extended Luenberger observer [92] usually used for nonlinear systems [85] [93, 94, 95, 96, 97]. Also under this heading, other self-sensing techniques can be used for the rotor and speed estimation. One can cite [98, 99], a full-order adaptive flux observers [80, 81, 87], a model reference adaptive system [43, 44], high gain observers [100, 101, 102] and sliding mode observers [103, 104]. The second approach is based on stochastic observers such as Kalman filter for linear systems and Extended Kalman filter (EKF) for nonlinear systems [85] [105, 106, 107, 108].

2.5.2 Back-EMF based techniques

The flux linkage estimators and back-emf estimators are based on the voltage model of the IPMSM (see Section 2.2.1). This approach consists in extracting the back-EMF from the implemented machine electrical Equations [109, 110]. In this way, the primary estimated quantities are the back-emf and the stator flux linkage. The estimates contain the rotor position and speed information [64] [111, 112]. This information can be calculated directly from flux and Back-EMF estimates or obtained with a suitable tracking algorithm like the phase locked-loop

(PLL) (see Section 4.3) , these techniques have been widely developed in the past decades [113, 114, 115].

2.6 Saliency-based techniques

Due to the problem at zero speed estimation for the first category described in Section 2.5 which is based on the model-based techniques of the machine [80, 81] [113, 114], the fundamental component model technique relies on the position and velocity dependency of the back-EMF of the motor. These techniques present a general problem at standstill, the back-EMF is zero amplitude when the machine rotates at low speed, so we can not distinguish between the real component of the Back-EMF and noise signal. During the ten last years, extensive research has been carried out to develop estimators where model-based techniques are avoided. To overcome the observability problem of IPMSM at zero/low speed encountered when techniques, of first category are used, where the current is the only available variable for measurement, a HF signal is injected to the motor at low speed [90] [116]. Hence, the rotor position can be estimated using the geometric saliency. In this section, the principle of HF injection techniques are applied to estimate the rotor position of IPMSM [117]. For this purpose, firstly, the state of the art of estimation with HF voltage injection is given. Then, the steps to recover the position by means of these techniques are detailed. In recent decades, saliency-based estimators have been extensively developed to allow and improve the low-speed operation capability [82, 83] [118]. So that, the start-up of the machine can be ensured in a closed-loop and in the desired direction, since the initial position can be estimated. Unlike model-based techniques which would fail due to lack of valuable signals (insufficient back-EMF amplitude), saliency-based self-sensing techniques avail from the anisotropic property of the machine, which is independent of the speed. As a consequence, such techniques are expected to be reliable and suited to zero/low-speeds. Basically, the idea behind saliency-based self-sensing estimation can be explained by the fact that the machine winding inductance is function of the rotor position due to saliency, and then the rotor position can be deduced from the inductance variation [119]. According to the type and the duration of the injected signal, saliency-based self-sensing techniques can be in turn, classified into four major groups: Rotating wave sine-wave signal injection [120, 121, 122] pulsating sine-wave signal injection [123, 124, 125, 126, 127], pulsating square-wave signal injection [128, 129, 130, 131] and other HF injection technique (inherent PWM excitation with no additional injection [132] and INFORM [45] [133]). Here, the most popular techniques related to each of these groups are presented.

2.6.1 Rotating sine-wave injection techniques

Rotating (also called revolving) HF carrier injection for position/speed estimation has been introduced by Professor R.D. Lorenz (University of Madison). In this paragraph, a brief history about the evolution of this technique over the years is provided. During the 90-ties, researchers of Madison University have made considerable strides in this field, particularly on induction machines [121, 122], linear induction machines [122], permanent magnet synchronous machines [45], Switched reluctance motors and universal motors. Later, other universities (Wuppertal, Nottingham Aster, Bradley, Cilia, Teske , etc..) have kept making the history of this technique by also proposing a self-sensing oriented design of electrical machines. In early stage trials, both rotating current and voltage vectors were evaluated [134]. Later, the voltage-based injection was preferred since the current-based one actually needs very high bandwidths for the current regulators, even larger than the carrier frequency. This technique was proposed by Lorenz to remedy to problem at low and zero speed. It is based on adding a circle carrier voltage in order

to extract the position information [135], this technique was successfully tested on a PMSM by Wang and Lorenz in 2000 [71] and many scientists. Since, this technique is widely used for self-sensing control of all AC machines. Basically, a constant amplitude voltage vector rotating with a high frequency (usually ranging between 500 Hz and 2.5 kHz) is superimposed to the fundamental voltage vector in the stationary frame α,β. As a consequence, a rotating HF current vector arises, superimposed to the fundamental current vector. The measured HF current vector contains information of the rotor position that can be extracted using signal processing and demodulation process detailed below. On the other hand, the fundamental current is used as a feedback for the current controllers after filtering the injected HF currents. The mathematical principle is given below.

2.6.1.1 Injected rotating sine-wave voltage

This voltage injection technique is often called "α,β" injection because the rotating voltage signal is applied in the stationary frame (α,β). The voltage signal with constant voltage amplitude rotating at the injected high frequency can be represented as

$$\underline{v_{sc}^{s}} = V_c e^{j(\omega_c t-\frac{\pi}{2})} = V_c \begin{bmatrix} \sin(\omega_c t) \\ -\cos(\omega_c t) \end{bmatrix} \tag{2.22}$$

where V_c and ω_c are respectively the magnitude and the carrier frequency of the injected signal. Figure 2.5 shows the rotating voltage vector that is applied in the stator reference frame.

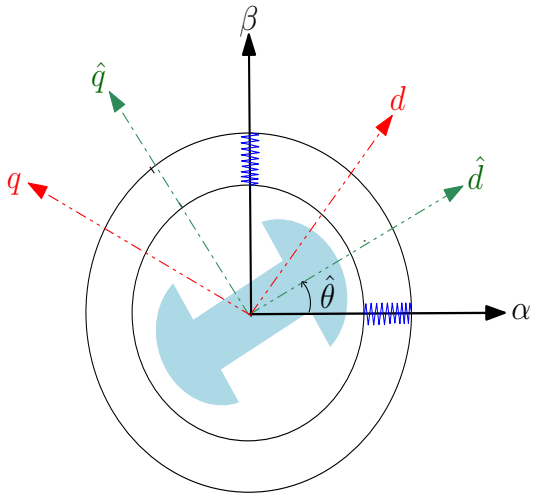

Figure 2.5: Rotating HFVI technique in the stationary reference frame

2.6.1.2 HF Flux-current resulting from the injected voltage

The stator flux generated by the high frequency signal injection can be obtained by integrating the injected stator voltage given in Equation (2.22)

$$\underline{\psi_{sc}^{s}} = \int V_c e^{j(\omega_c t-\frac{\pi}{2})} dt = \frac{V_c}{j\omega_c} e^{j(\omega_c t-\frac{\pi}{2})} = \frac{V_c}{\omega_c} e^{j(\omega_c t-\pi)}. \tag{2.23}$$

From Equations (2.23) and (2.20), the HF stator current is obtained

$$\underline{i_{sc}^{s}} = \frac{V_c}{\omega_c(L_0{}^2 - L_2{}^2)} (L_0 e^{j(w_c t-\pi)} - L_2 e^{j(2\theta-w_c t+\pi)}). \tag{2.24}$$

The general current expression is given by

$$\underline{i^s_{sg}} = \frac{V_c}{\omega_c(L_0^2 - L_2^2)}(L_0 e^{j(w_c t - \pi)} - L_2 e^{j(2\theta - w_c t + \pi)}) + i^s_{s1} \tag{2.25}$$

where,

$$I_{cp} = \frac{L_0 V_c}{\omega_c(L_0^2 - L_2^2)} \tag{2.26}$$

$$I_{cn} = \frac{L_2 V_c}{\omega_c(L_0^2 - L_2^2)} \tag{2.27}$$

and i^s_{s1} are respectively the magnitude of the positive component, the negative component and the fundamental component of the stator current. From Equation (2.25), it can be seen that only the negative current component $I_{cn}e^{j(2\theta - w_c t + \pi)}$ contains the saliency information located in the IPMS machine rotor. In order to extract the saliency information, it is necessary to use some signal processing techniques that will be detailed in the following part.

2.6.1.3 Signal processing and demodulation: extraction of the rotor position estimation error

In order to support the extraction of the saliency information, contained in the phase of the negative sequence component of the carrier signal current, the positive sequence and the fundamental current signal must be filtered off. For this purpose, several techniques are proposed in the literature review [59] [136, 137]. One of these approaches is based on BPF (band pass filter) to remove the fundamental component, then an heterodyne process followed by LPF (low pass filter) is used to extract only the the negative sequence that contains the error position information. This approach [137, 138] is shown in Figure 2.6.

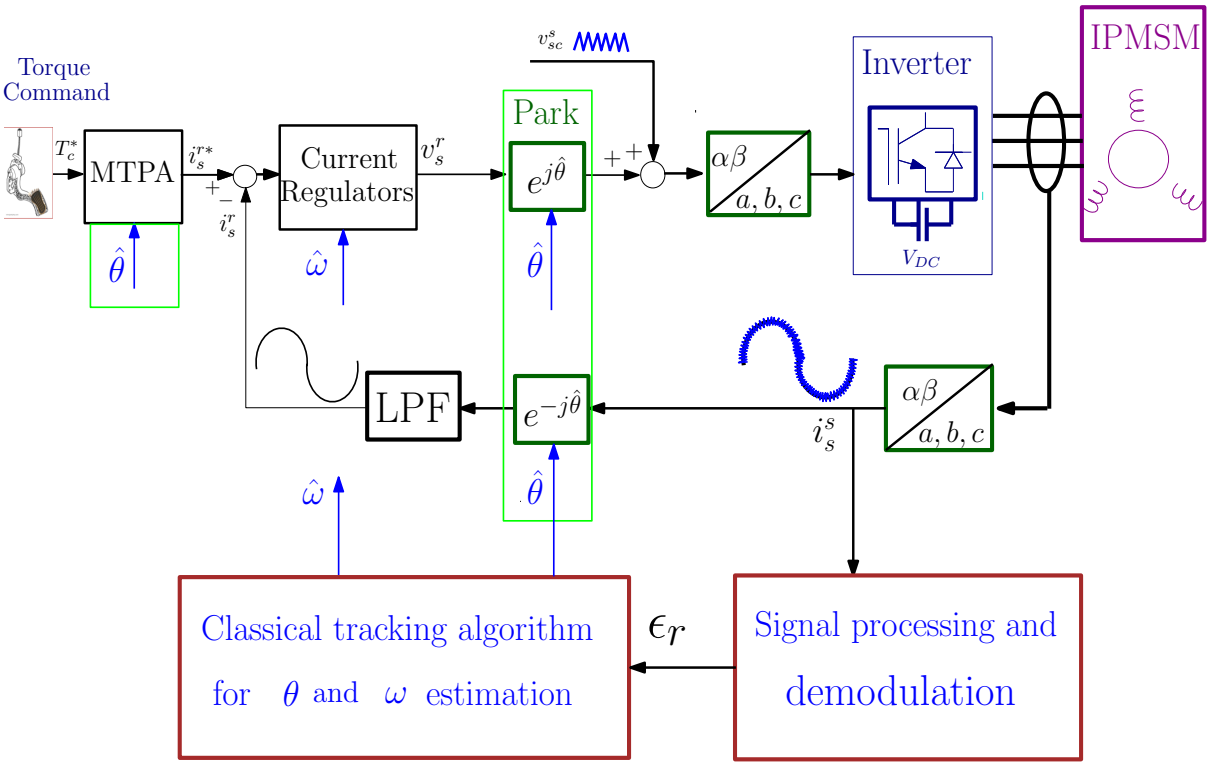

Figure 2.6: General bloc for the rotating sine-wave HFVI technique

In order to separate the HF current components from the fundamental stator currant component, a heterodyne demodulation technique is proposed [122]. The bloc signal processing and demodulation include two steps. The first is based on using the BPF in order to extract only the HF, followed by an heterodyne process to demodulate the spatial saliency with the high frequency modulated in the negative sequence component. Whereas, the second step is made of the LPF to recover the rotor position error estimation component as shown in the Figure 2.7.

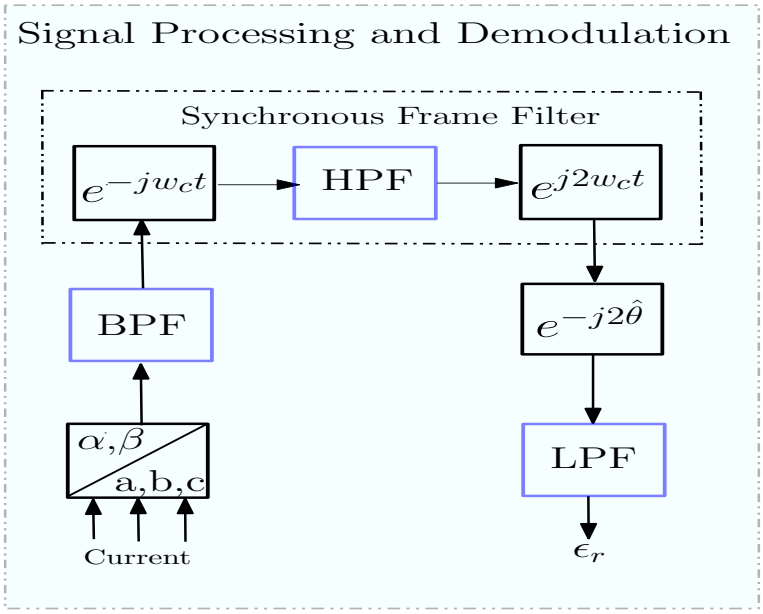

Figure 2.7: Rotating signal processing and demodulation Process for the rotor position estimation error extraction

Several techniques have been proposed in the literature [121, 122] to remove the fundamental current component $\underline{i_{s1}}^s$. One of these approaches is based on BPF. Consequently Equation (2.25) becomes

$$\underline{i^s_{sh}} = I_{cp}e^{j(\omega_c t-\pi)} - I_{cn}e^{j(2\theta-\omega_c t+\pi)}. \tag{2.28}$$

Then, the obtained HF current $\underline{i^s_{sh}}$ in the second step is used by a synchronous frame filter [1] (SFF) [139, 65]. It is being widely known and applied for self-sensing control chain. This operation requires two rotations($e^{-j\omega_c t}$ and $e^{j2\omega_c t}$) and a HPF (see Figure 2.7) allows to filter off the positive components, one can deduce

$$\underline{i^{\hat{r}}_{sc}} = SFF(\underline{i^{\hat{r}}_{sh}}) = -I_{cn}e^{j2\theta}. \tag{2.29}$$

In order to recover the rotor position estimation error, Equation (2.29) is multiplied by $e^{j2\hat{\theta}}$. One get

$$\underline{i^{\hat{r}}_{sc1}} = \underline{i^{\hat{r}}_{sc}}e^{j2\hat{\theta}} = -I_{cn}e^{j2(\theta-\hat{\theta})}. \tag{2.30}$$

By using a LPF, Equation (2.29) becomes

$$\underline{i^{\hat{r}}_{scfil}} = LPF(\underline{i^{\hat{r}}_{sc1}}) = -I_{cn}e^{j(2(\theta-\hat{\theta}))} = -I_{cn}\begin{bmatrix}\cos(2(\theta-\hat{\theta}))\\ \sin(2(\theta-\hat{\theta}))\end{bmatrix}. \tag{2.31}$$

1. $e^{2j\omega_c t}[HPF(i^s_{sh} * e^{-j(\omega_c t)})]$.

The position estimation error expression can be deduced as follows

$$\varepsilon_r = Im(\underline{i^{\hat{r}}_{scfil}}) = -I_{cn}\sin(2e_\theta) \tag{2.32}$$

where

$$e_\theta = \theta - \hat{\theta}. \tag{2.33}$$

Is the rotor position estimation error.
If $e_\theta \simeq 0$, (2.32) becomes

$$\varepsilon_r = -2I_{cn}e_\theta. \tag{2.34}$$

Assumption 2.6.1. *This technique is valid as long as the position error $e_\theta \simeq 0$. All the classical tracking observer (see Section 4.3) are based on the following hypothesis $e_\theta \simeq 0$. This hypothesis reduces the tolerated error range and makes the stability very local. Moreover, it requires an initial rotor position.*

This estimation error ε_r (2.34) is used as an information by classical tracking algorithms for the rotor position and speed estimation. These algorithms are recalled in Section 4.3. The main drawback of this demodulation process is related to the rotor position processing from the measured currents. This operation requires two filters and two rotations. Moreover, the rotating sine-wave technique is based on the following hypothesis $e_\theta \simeq 0$ (Assumption 2.6.1). This technique depends on the accuracy knowledge of the gain I_{cn} which depends on the inductance machine parameters (2.27) that vary according to several phenomenon (saturation, magnet flux and so on). Moreover, the presence of the inverter and the sampling time produce delays and phase shift on the estimation chain which affect strongly the estimated quantities.

2.6.2 Pulsating sine-wave injection technique

Similarly, the pulsating sine-wave (also called alternating) HF injection technique takes advantage of saliencies present in the machine to extract the rotor position. Over the years, this technique has also been widely developed due to its inherent advantages (compared to the rotating vector injection technique), such as being less computational intensive, having a faster dynamic response, and an intrinsic cancellation of the filter lags during signal processing [135]. Here, a brief overview of the progress registered on this technique is also given. Classically, a HF voltage is injected in one axis of the estimated (d,q) reference frame (whether the estimated d-axis or q-axis). The current response, is then evaluated in orthogonal directions relative to the injected signal direction [140]. In 1998, Corley and Lorenz applied the pulsating HF voltage injection in the estimated q-axis on an IPMSM [126]. The response in the d-axis current is amplitude-modulated by the rotor position and is first multiplied by a sine wave at the same frequency as the carrier, then applied to proper filters, which allow obtaining the position error. Later works have demonstrated that the q-axis injection is a major source of torque ripples for IPMSM, as it directly reports to the machine electromagnetic torque [126]. Conversely, the d-axis injection has been tested for IPMSM, PMSM, IM and SRM machines with promising results and reported in a number of successful research works [124, 125]. Last but not least, pulsating HF injection vector can be regarded as the superposition of two rotating carrier vectors with opposite rotating directions [127].

2.6.2.1 Injected pulsating sine-wave voltage

The injection of an alternating HF voltage on the d-axis is selected. An alternating voltage is superimposed on the stator voltage reference in the estimated rotor reference frame (Figure 2.8).

Since high frequencies are considered, the back-emf and the resistive voltage drop are omitted, giving

$$v_{sc}^{\hat{r}} = -V_c \sin(\omega_c t) \begin{bmatrix} 1 \\ 0 \end{bmatrix} \tag{2.35}$$

where V_c and ω_c are the magnitude and the carrier frequency of the injected signal, respectively.

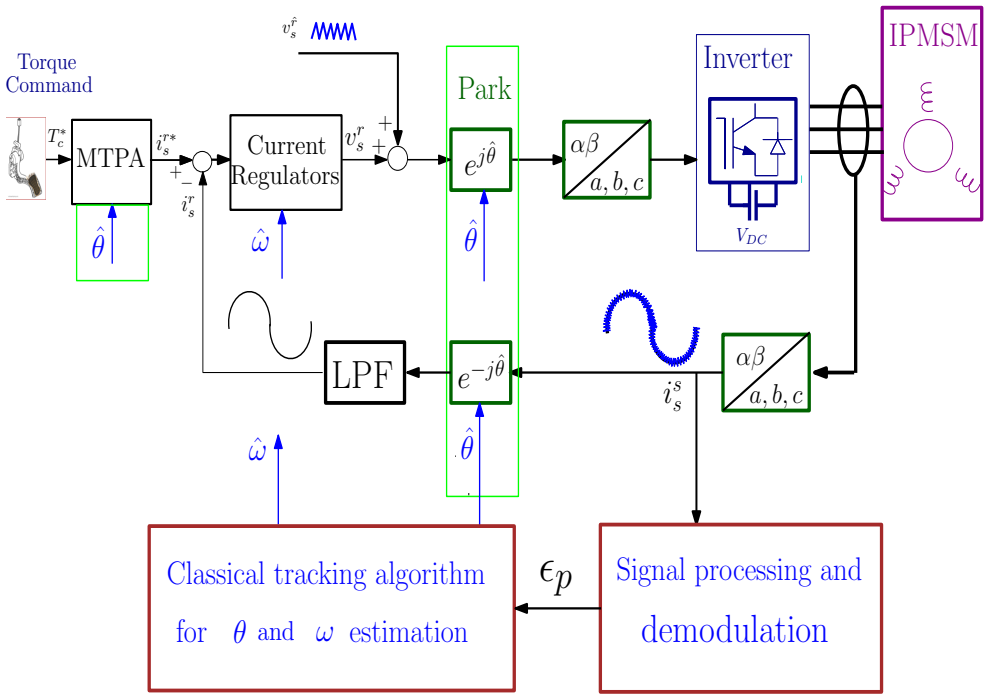

Figure 2.8: General bloc for pulsating sine-wave HFVI technique

The injected pulsating voltage vector in the estimated reference frame is shown in Figure 2.9.

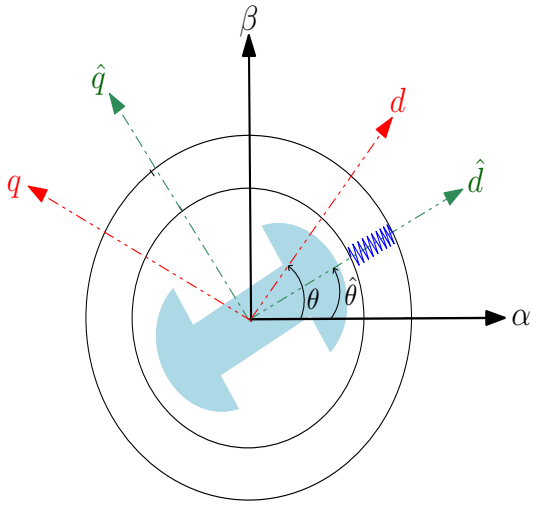

Figure 2.9: Pulsating sine-wave HFVI technique in the estimated reference frame

By using Park transform, the expression of the HF injected voltage in the stator reference frame is given by

$$v_{sc}^{s} = -V_c \sin(\omega_c t) e^{j\hat{\theta}}. \tag{2.36}$$

2.6.2.2 HF Flux-current resulting from the injected voltage

By integrating the injected stator voltage given in Equation (2.36), the following HF stator flux expression is obtained

$$\underline{\psi^s_{sc}} = \int -V_c \sin(\omega_c t) e^{j\hat{\theta}} dt = \frac{V_c}{\omega_c} \cos(\omega_c t) e^{j\hat{\theta}}. \tag{2.37}$$

The HF stator current expression can be obtained by combining Equations (2.37) and (2.20)

$$\underline{i^s_{sc}} = \frac{V_c}{\omega_c (L_0{}^2 - L_2{}^2)} (L_0 e^{j\hat{\theta}} - L_2 e^{j(2\theta - \hat{\theta})}) \cos(\omega_c t). \tag{2.38}$$

By taking the fundamental current component i^s_{s1} into account, the general stator current $\underline{i^s_{sg}}$ can be expressed as

$$\underline{i^s_{sg}} = I_{cp} \cos(\omega_c t) e^{j\hat{\theta}} - I_{cn} \cos(\omega_c t) e^{j(2\theta - \hat{\theta})} + i^s_{s1} \tag{2.39}$$

where, I_{cp} given by Equation (2.27), I_{cp} given by Equation (2.26) and i^s_{s1} are the magnitude of the HF positive component, HF negative component of the stator current and the fundamental current component, respectively.
In order to make appear the position information on the current spectrum, where all positive and negative frequencies are required, Equation (2.39) is rewritten as follows

$$\underline{i^s_{sg}} = \frac{I_{cp}}{2} [e^{j(\omega_c t + \hat{\theta})} + e^{j(-\omega_c t + \hat{\theta})}] - \frac{I_{cn}}{2} [e^{j(\omega_c t + 2\theta - \hat{\theta})} + e^{j(-\omega_c t + 2\theta - \hat{\theta})}] + i^s_{s1}.$$

Figure 2.10 gives an illustration of the spectral content of the $\alpha\beta$ currents.

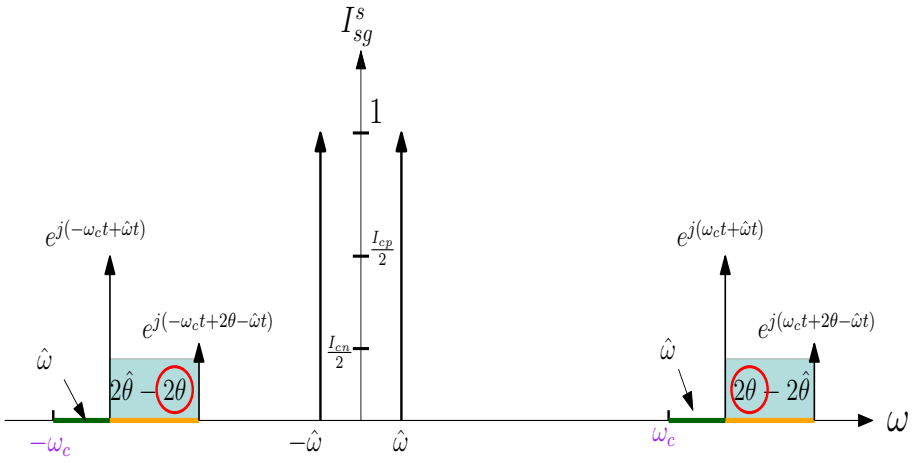

Figure 2.10: Spectral representation of $\alpha\beta$ currents for the pulsating sine-wave HFVI

From the previous equation and Figure 2.10, the same conclusion as the rotating one can be deduced; it is noticed that only the negative frequency component $I_{cn} e^{j2(\theta - \hat{\theta})} \sin(w_c t)$ contains the information of the saliency location of the IPMSM, whereas, the positive component represents a perturbation component, it is necessary to use some signal processing techniques which will be detailed in the following parts in order to extract only the saliency information.

2.6.2.3 Signal processing and demodulation: extraction of the rotor position estimation error

To make the extraction easier for the spatial information, contained in the negative sequence component, it is possible to filter the positive sequence and the fundamental current signal. For

this purpose, several techniques are proposed in the literature [141, 142]. One of such techniques is based on BPF to remove the fundamental component, then a heterodyne process followed by a LPF is used to extract only the rotor position estimation error information contained in the negative sequence, as shown in Figure 2.11

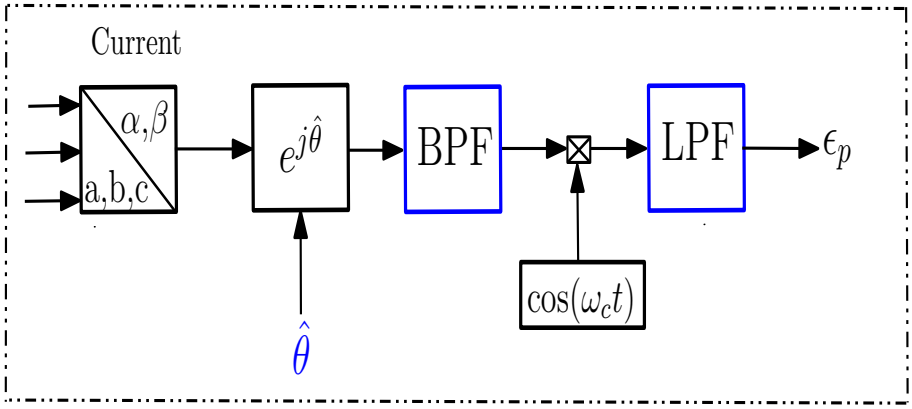

Figure 2.11: Signal processing and demodulation for the HF pulsating sine-wave technique

Several techniques have been proposed in the literature [142] to remove the fundamental current component $\underline{i_{s1}}^s$ for the pulsating sine-wave technique. One of these approaches is based on BPF. Consequently Equation (2.39) becomes

$$\underline{i_{sh}^s} = I_{cp}\cos(\omega_c t)e^{j\hat{\theta}} - I_{cn}\cos(\omega_c t)e^{j(2\theta-\hat{\theta})}. \tag{2.40}$$

Then, the obtained HF current in the second step is multiplied by $e^{-j\hat{\theta}}$, one has

$$\underline{i_{sc}^{\hat{r}}} = \underline{i_{sh}^{\hat{r}}}\, e^{-j\hat{\theta}} = I_{cp}\cos(\omega_c t) - I_{cn}\cos(\omega_c t)e^{j(2(\theta-\hat{\theta}))}. \tag{2.41}$$

To avoid the effect of the positive term given as $I_{cp}\cos(\omega_c t)$, only the imaginary part of Equation (2.41) is taken as follows

$$\underline{i_{sc1}^{\hat{r}}} = Im(\underline{i_{sc}^{\hat{r}}}) = -I_{cn}\sin(2(\theta-\hat{\theta})\cos(\omega_c t). \tag{2.42}$$

In order to separate the rotor position information from the HF career $\cos(\omega_c t)$, Equation (2.42) is multiplied by $\cos(\omega_c t)$, one can deduce

$$\begin{aligned} \underline{i_{scl}^{\hat{r}}} &= \underline{i_{sc1}^{\hat{r}}}\cos(\omega_c t) = -I_{cn}\sin(2(\theta-\hat{\theta})\cos^2(\omega_c t) \\ &= \frac{-I_{cn}}{2}\sin(2(\theta-\hat{\theta})[1+\cos(2\omega_c t)]. \end{aligned} \tag{2.43}$$

The position estimation error expression is then extracted by using a LPF

$$\varepsilon_p = LPF(\underline{i_{scl}^{\hat{r}}}) = \frac{-I_{cn}}{2}\sin(2e_\theta) \tag{2.44}$$

where e_θ given by Equation (2.33) is the rotor position estimation error.
If $e_\theta \simeq 0$, Equation (2.44) becomes

$$\varepsilon_p = -2I_{cn}e_\theta. \tag{2.45}$$

Similarly to the rotating sine-wave HF voltage injection technique (see Assumption 2.6.1), This technique is valid as long as the position error $e_\theta \simeq 0$. This hypothesis reduces the tolerated error range and makes the stability very local. Moreover, it requires an initial rotor position.

2.6.2.4 Other demodulation techniques

Ha et al. (2003) and Sung-Ki-sul (1999) [143] proposed another types of demodulation with the pulsating sine-wave signal injection for IPMSM. The idea is to compare the HF current at two orthogonal axes that are displaced by 45°from the estimated reference frame $\hat{d}-\hat{q}$. For this case, the current expression must be recovered in the measurement axis, that offsets by $(\hat{\theta}-\frac{\pi}{4})$ from the stator reference frame. The current in the measurement axis is computed by

$$\underline{i}_s^m = \underline{i}_{sh}^s e^{-j(\hat{\theta}-\frac{\pi}{4})} \tag{2.46}$$

where $\underline{i}_{sh}^s$ is given by Equation (2.40).
By exploiting Equations (2.46) and (2.40), the current expression obtained in the measured $\underline{i}_s^m$ frame is

$$\underline{i_s}^m = \frac{V_c}{(L_o^2-L_2^2)}(L_0 e^{j\frac{\pi}{4}} - L_2 e^{j(2e_\theta-\frac{\pi}{4})})\cos(\omega_c t). \tag{2.47}$$

By using the complex notation, Equation (2.47) reads

$$\begin{bmatrix} i_d^m \\ i_q^m \end{bmatrix} = \begin{bmatrix} I_{cp}\frac{\sqrt{2}}{2} - I_{cn}\cos(2e_\theta+\frac{\pi}{4}) \\ I_{cp}\frac{\sqrt{2}}{2} - I_{cn}\sin(2e_\theta+\frac{\pi}{4}) \end{bmatrix}\cos(\omega_c t). \tag{2.48}$$

By using the following trigonometric formulas

$$\begin{aligned} \cos(a+b) &= \cos(a)\cos(b) - \sin(a)\sin(b) \\ \sin(a+b) &= \sin(a)\cos(b) + \cos(a)\sin(b), \end{aligned} \tag{2.49}$$

the current expression obtained is

$$i_s^m = \begin{bmatrix} i_d^m \\ i_q^m \end{bmatrix} = \begin{bmatrix} I_{cp}\frac{\sqrt{2}}{2} - \frac{\sqrt{2}}{2}I_{cn}[\cos(2e_\theta) - \sin(2e_\theta)] \\ I_{cp}\frac{\sqrt{2}}{2} - I_{cn}\frac{\sqrt{2}}{2}[\sin(2e_\theta) + \cos(2e_\theta)] \end{bmatrix}\cos(\omega_c t). \tag{2.50}$$

Several techniques have been proposed in the literature to extract the rotor position estimation error [59] [143]. The rotor position estimation error is extracted as the difference between the squares of the components of the current i_d^m and i_q^m as follows

$$\varepsilon_p = LPF(|i_q^m|^2 - |i_d^m|^2). \tag{2.51}$$

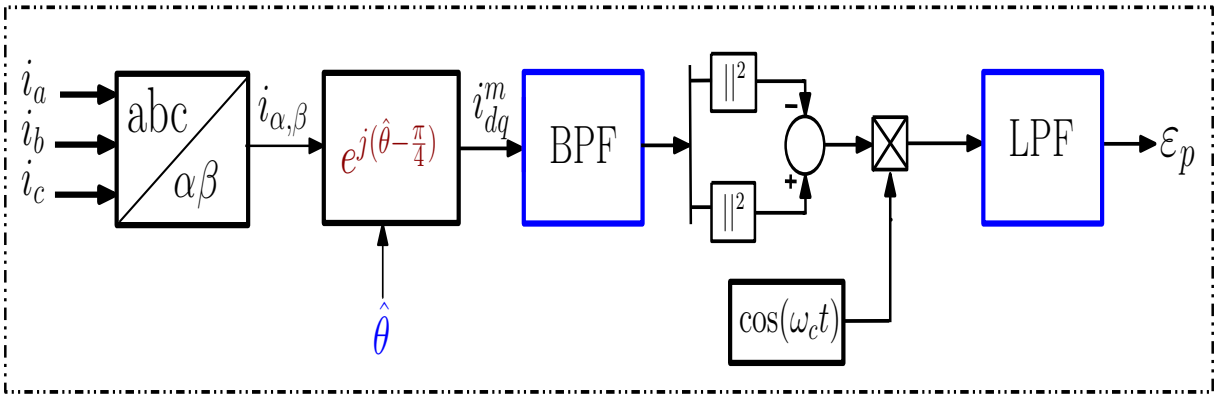

Figure 2.12: Pulsation sine-wave HF injection : signal processing and demodulation with a measurement axis offsets 45 °from the injected (estimated) axis

The resulting rotor position estimation error is

$$\varepsilon_p \approx \frac{(L_q - L_d)V_c^2}{8L_d^2 L_q^2 \omega_c^2}[2(L_d + L_q)\sin(2e_\theta) - 2(L_d - L_q)\sin(4e_\theta)]. \tag{2.52}$$

If $e_\theta \approx 0$, then, Equation (2.52) can be written as

$$\varepsilon_p \approx -2k_c e_\theta \tag{2.53}$$

where,

$$k_c = \frac{4(L_q - L_d)(3L_q - L_d)V_c^2}{8L_d^2 L_q^2}. \tag{2.54}$$

Another technique for rotor position estimation error extraction is proposed by Seung-Ki-Sul in [59] (see Figure 2.13). It consists on computing ε_p as a difference between absolute of i_{dh}^m and absolute of i_{qh}^m

$$\varepsilon_p = |i_d^m|^2 - |i_q^m|^2 = LPF(i_d^m \cos(w_c t))^2 + LPF(i_d^m \sin(w_c t))^2 - LPF(i_q^m \cos(w_c t))^2 - LPF(i_q^m \sin(w_c t))^2. \tag{2.55}$$

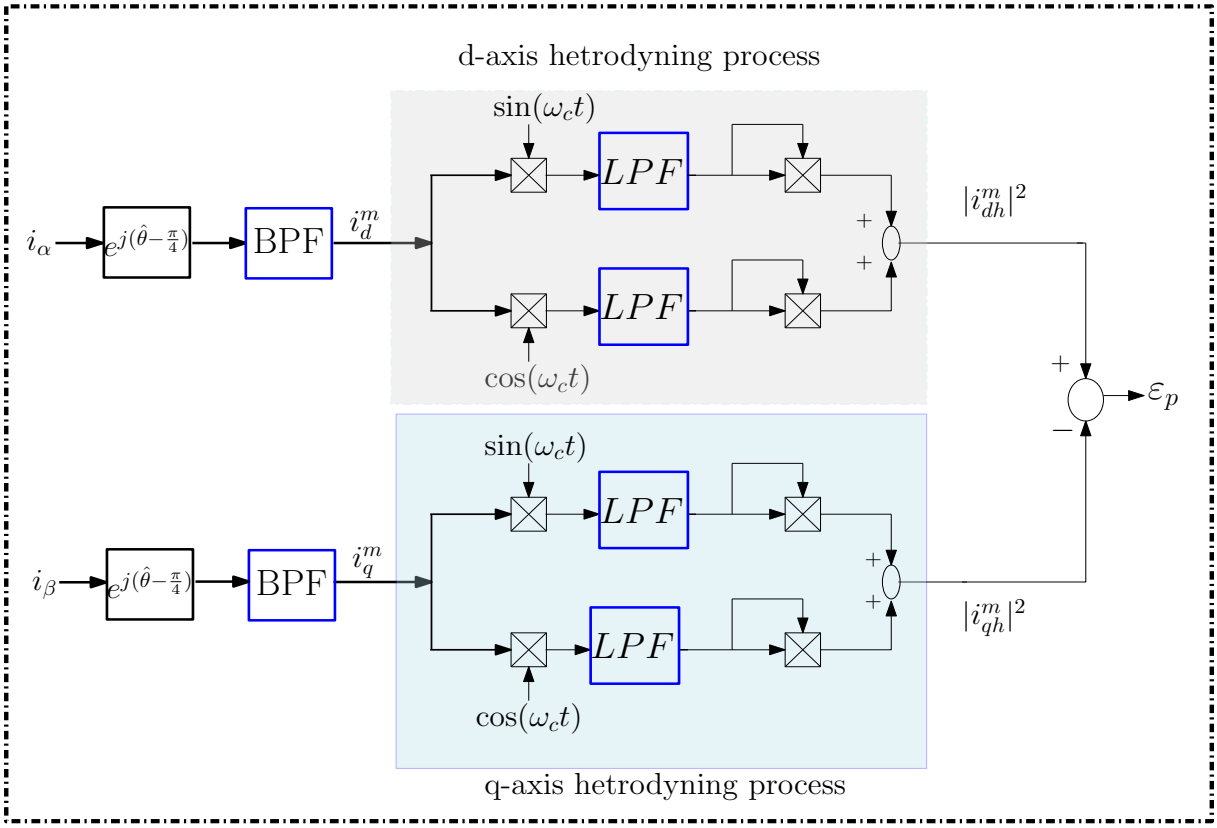

Figure 2.13: Pulsating sine-wave HFVI technique signal processing and demodulation process

The rotor position estimation error can be expressed as

$$\varepsilon_p \approx \frac{V_c^2}{4\omega_c^2 L_d L_q}\{-2\omega_c^2 L_0 L_2 + (\omega_c L_2)^2\}\sin(2e_\theta). \tag{2.56}$$

If $e_\theta \approx 0$, the, the rotor position estimation error expression (2.56) can be written as

$$\varepsilon_p = 2k_e e_\theta \tag{2.57}$$

where,

$$k_e = \frac{V_c^2}{4\omega_c^2 L_d L_q}\{-2\omega_c^2 L_0 L_2 + (\omega_c L_2)^2\}. \tag{2.58}$$

The rotor position expression of Equations (2.45), (2.53) or (2.57) that is resulting from the demodulation process, will be used as an information in a classical tracking algorithms, which ensures the rotor position and speed estimation. These algorithm are the subject of Section 4.3. The main drawback of this demodulation process is related to the rotor position processing from the measured currents. This operation requires two filters. Moreover, the assumption 2.6.1 is valid for this technique as well as the limitations with to I_{cn}. It requires an initial rotor position. Moreover, this technique depends on the accuracy knowledge of the gain I_{cn} which depends on the inductance machine parameters that vary according to several phenomenon, the presence of the inverter and the sampling time produce delays and phase shift on the estimation chain that affect strongly the estimated quantities.

2.6.3 Pulsating square-wave injection techniques

It is worth noting that rotating and pulsating HF sinusoidal carrier signal injection-based self-sensing technique have been very popular since they first appeared. Although they have simple physical principles and low implementation cost, the limited dynamic bandwidth of the system due to the signal demodulation process represents a major drawback. Alternatively, the square-wave signal injection technique proposed in [130, 131], which injects a rectangular waveform rather than a sinusoidal waveform, has been recognized for its higher dynamics and also for eliminating the requirement of LPF for signal demodulation [128, 129]. In order to overcome the factors limiting the bandwidth of the observer, the square-wave injection algorithm is applied so as the carrier frequency is usually increased to its maximum i.e. the switching frequency. This modification has also an effect on the way the demodulation is implemented [128]. Here again, as for the pulsating sine-wave type, the pulsating square-wave HF signal is injected in the estimated d-q frame. So that, the self-sensing dynamic performance is claimed to be remarkably enhanced. In [144, 145], an effective solution with the integration of pulsating square-wave injection and current control loop is proposed for the self-sensing control of a SPMSM. without the use of filters, it is reported that the synchronization between the PWM, the current control and the carrier injection provides a satisfactory separation between the fundamental and the carrier current components. Besides, this technique is much less sensitive to the machine geometry than sinusoidal carrier signal injection-based technique. However, one of the serious limitations of the pulsating square-wave injection technique is the number of samples used to recover the position information. Actually, the number of samples depends on the sampling time, which is usually too small to produce a good signal-to noise ratio, thus a good position estimation quality. As stated in [146], pulsating square-wave-based demodulation techniques allow no more than two points per period of the injected signal to be sampled. Moreover, the counterpart of the pulsating square-wave injected voltage is that it generates non negligible acoustic noise and requires sensitive current sensors. All high frequency estimators presented previously are similar in the use of LPFs in order to get the position error expression. However, these LPFs degrade self-sensing control performances severely because of the inherent time delay of LPFs. To enhance the performance, the delay should be minimized or removed. This technique relies on higher frequency square-wave type voltage injection. As a result, the error signal can be calculated without any LPF, this means it will be no time delay. Hence, the position estimation

performance can be enhanced remarkably. As a consequence, bandwidths of current, speed and position controllers can be highly increased compared to those by the conventional pulsating and rotating sine-wave type voltage injection technique.
The pulsating square-wave voltage technique is a recent technique. Several possible pulsating square-wave type voltages are considered in the literature as shown in Figure. 2.14. However, for convenience of the explanation, the injected voltage used in this work (which is described by the Equation (2.61)) is shown in Figure. 2.14-(1).

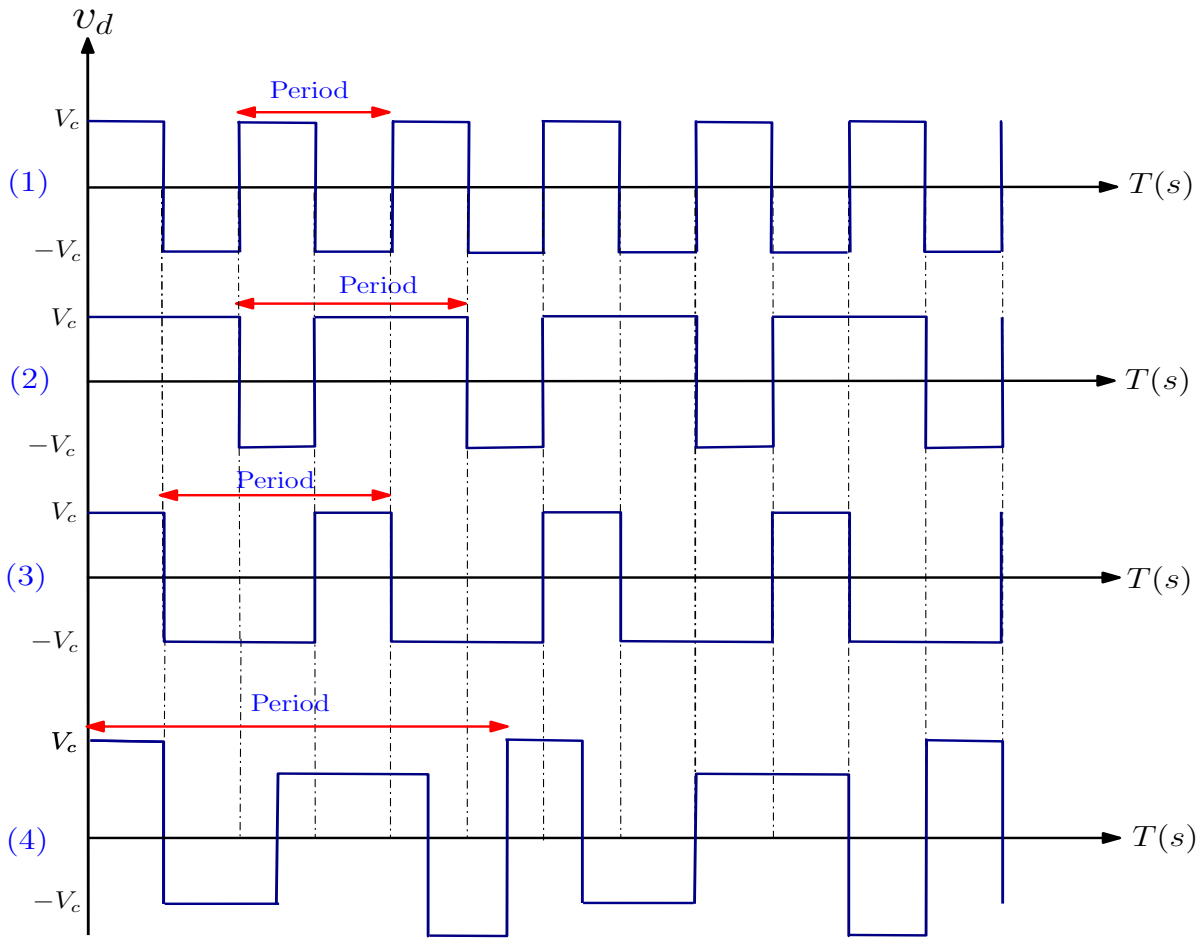

Figure 2.14: Different form for the pulsating square-wave injected voltage

The dynamic of the equation (2.19) is obtained by using Taylor's theorem first derivative as

$$\underline{\Delta\psi}_s^s = L_0\underline{\Delta i}_s^s + L_2\underline{\Delta i}_s^{s*}e^{j2\theta}. \tag{2.59}$$

From (2.59), the current variation dynamic equation is deduced

$$\underline{\Delta i}_s^s = \frac{1}{{L_0}^2 - {L_2}^2}(L_0\underline{\Delta\psi}_s^s - L_2\underline{\Delta\psi}_s^{s*}e^{j2\theta}). \tag{2.60}$$

2.6.3.1 Injected pulsating square-wave voltage

In this part, the HF injected voltage signal is applied in a fixed direction, and added to the d axis output voltage. The square-wave voltage vector in the estimated $(\hat{d}-\hat{q})$ frame (see Figure. 2.15) can be expressed as

$$v_s^{\hat{r}} = \begin{bmatrix} v_{\hat{d}} \\ v_{\hat{q}} \end{bmatrix} = V_c(-1)^k \begin{bmatrix} 1 \\ 0 \end{bmatrix} \tag{2.61}$$

where V_c is the magnitude of the injected voltage and k is the index of PWM cycles.

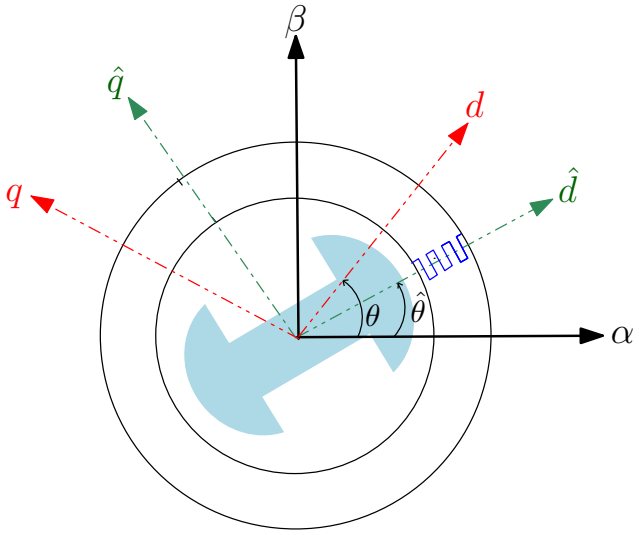

Figure 2.15: Pulsating square-wave HFVI technique

Figure. 2.16 describes the general principal of the pulsating square-wave HF voltage injection technique for the self-sensing control of IPMSM.

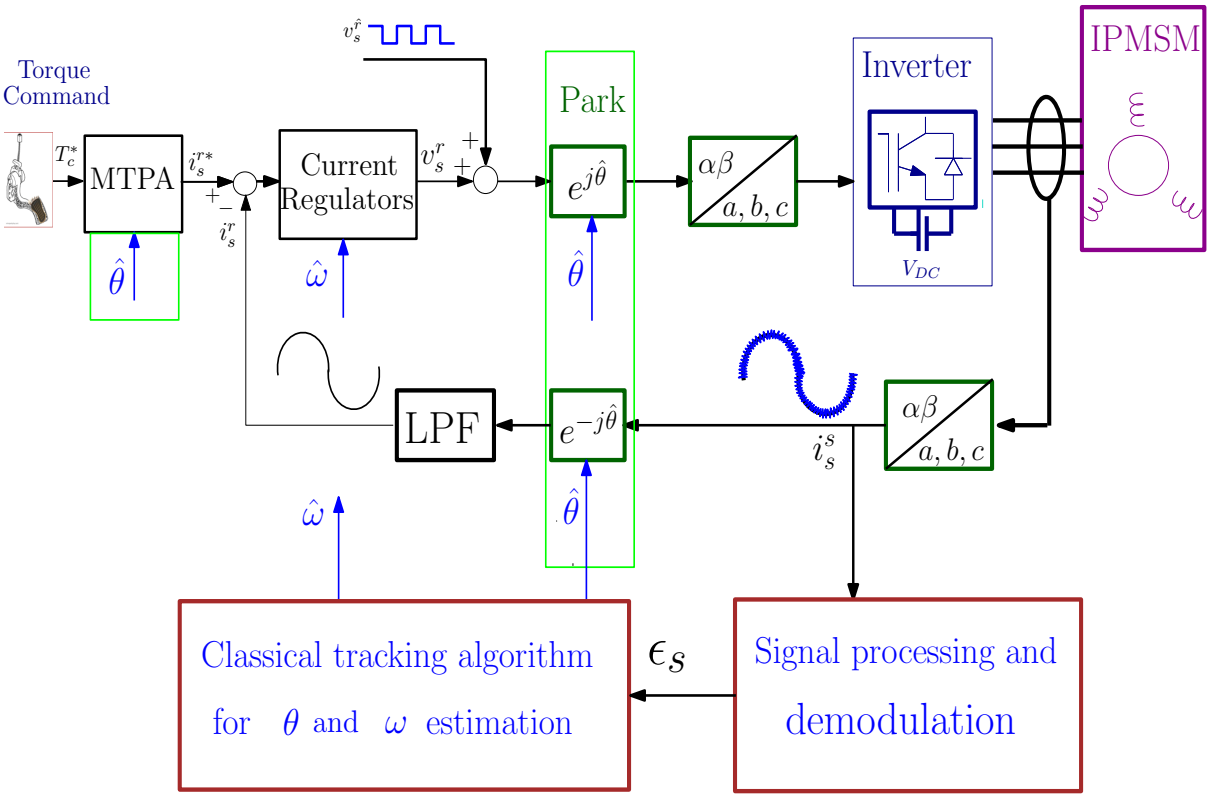

Figure 2.16: General scheme of the pulsating square-wave HFVI technique

From (2.61), the HF injected voltage in the stator reference frame is given

$$v_s^s = V_c(-1)^k e^{j\hat{\theta}}. \tag{2.62}$$

2.6.3.2 HF Flux-current resulting from the injected voltage

The HF stator flux generated by the HF voltage signal injection can be obtained by using equations (2.18) and (2.62)

$$\underline{\Delta\psi_s^s} = V_c(-1)^k \Delta T e^{j\hat{\theta}}. \tag{2.63}$$

From (2.63) and (2.60) and by taking into account the fundamental current component i_{s1}^s, the general stator current can be expressed as follows

$$\underline{\Delta i_{sg}^s} = \frac{V_c(-1)^k \Delta T}{(L_0{}^2 - L_2{}^2)}(L_0 e^{j\hat{\theta}} - L_2 e^{j(2\theta-\hat{\theta})}) + i_{s1}^s. \tag{2.64}$$

The deduced general current in the estimated reference frame is expressed by

$$\underline{\Delta i_s^s} = I_{cp} e^{j\hat{\theta}} - I_{cn} e^{j(2\theta-\hat{\theta})} + i_{s1}^s. \tag{2.65}$$

where

$$I_{cp} = \frac{L_0 V_c(-1)^k \Delta T}{(L_0{}^2 - L_2{}^2)} = \frac{(L_d + L_q) V_c(-1)^k \Delta T}{2 L_d L_q} \tag{2.66}$$

$$I_{cn} = \frac{L_2 V_c(-1)^k \Delta T}{(L_0{}^2 - L_2{}^2)} = \frac{(L_d - L_q) V_c(-1)^k \Delta T}{2 L_d L_q} \tag{2.67}$$

and i_{s1}^s are the magnitude of the HF positive component, the HF negative components and the fundamental component of the stator current, respectively.
From (2.65), it can be seen that only the HF negative current component $\frac{V_c(-1)^k \Delta T L_2}{(L_0{}^2 - L_2{}^2)} e^{j(2\theta-\hat{\theta})}$ contains the rotor position information of the IPMSM.

2.6.3.3 Signal processing and demodulation: extraction of the rotor position estimation error

Several techniques of pulsating square-wave demodulation technique are proposed in the literature [129] [142] to support the extraction of the rotor position information, contained in the phase of the negative sequence component of the carrier signal current. One of these approaches is based on BPF to remove the fundamental current component $\underline{i_{s1}}^s$ [147, 148], then an heterodyning process is adopted (see Figure. 2.17) as it will be detailed in this section. By applying the BPF to Equation (2.65), consequently Equation (2.65) becomes

$$\underline{\Delta i_{sh}^s} = I_{cp} e^{j\hat{\theta}} - I_{cn} e^{j(2\theta-\hat{\theta})}. \tag{2.68}$$

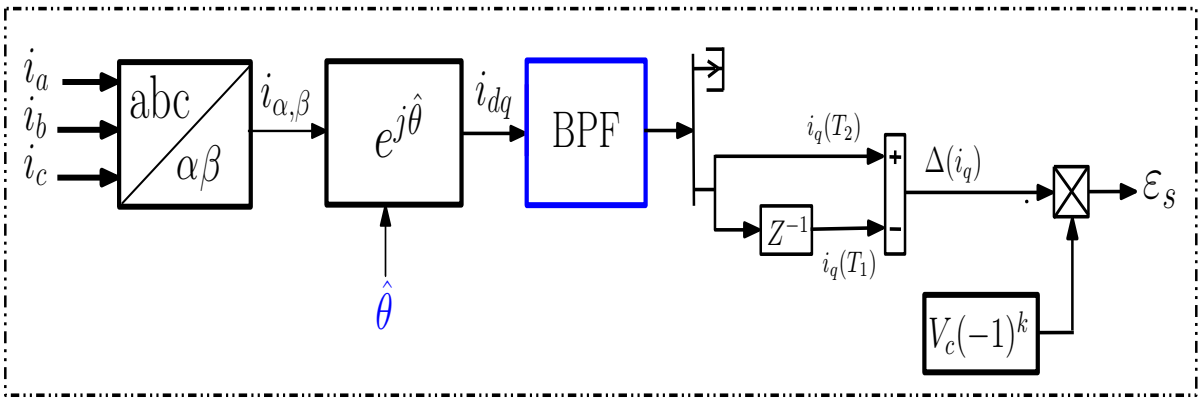

Figure 2.17: Pulsating square-wave HFVI technique signal processing and demodulation process

Then, the obtained HF current in the second step is multiplied by $e^{-j\hat{\theta}}$, one can deduce

$$\underline{\Delta i_{sc}^{\hat{r}}} = \underline{\Delta i_{sh}^{s}} e^{-j\hat{\theta}} = I_{cp} \begin{bmatrix} 1 \\ 0 \end{bmatrix} - I_{cn} e^{2je_\theta}. \tag{2.69}$$

where e_θ is defined in (2.33).
In order to avoid the effect of the positive term given as I_{cp}, only the imaginary part of Equation (2.69) is taken as follows

$$\underline{\Delta i_{scl}^{\hat{r}}} = Im(\underline{\Delta i_{sc}^{\hat{r}}}) = -I_{cn} \sin(2e_\theta). \tag{2.70}$$

To ensure the positivity of the gain I_{cn} and to get the rotor position estimation error expression (see Figure. 2.17), the equation (2.70) multiplied by $V_c(-1)^k$, (2.70) becomes

$$\varepsilon_s = \underline{\Delta i_{scl}^{\hat{r}}} V_c(-1)^k = -I_{cn-s} \sin(2(e_\theta). \tag{2.71}$$

where

$$I_{cn-s} = \frac{(L_d - L_q)[V_c(-1)^k]^2 \Delta T \sqrt{2}}{2L_d L_q} \tag{2.72}$$

If $e_\theta \simeq 0$, (2.71) becomes

$$\varepsilon_s = -I_{cn-s}\, e_\theta. \tag{2.73}$$

The rotor position estimation error ε_s described by Equation (2.73) is injected as an information in a classical tracking algorithm, which ensures the rotor position and speed estimation. These algorithm are recalled in Section 4.3. The main drawback of this demodulation process is related to the rotor position processing from the measured currents. This operation requires BPF (see Figure. 2.17). Moreover, the pulsating square-wave technique is based on the following hypothesis $e_\theta \simeq 0$ (Similarity to the Assumption 2.6.1).

2.6.4 Others HFVI techniques

In this section, another saliency based technique scheme is introduced which uses the transient motor current response [45] [133]. The position dependent saliency can be obtained due to rotor slotting effect for PMSM or main magnetic flux saturation for PMSM. The first technique for voltage vector excitation is the Indirect Flux detection by On-line Reactance Measurement (INFORM) technique [149] . The INFORM technique is based on real time inductance measurements using specific test pulses. The second technique uses the PWM switching vector changes to integrate the transient excitations into the fundamental PWM waveform. The estimation can be achieved by measuring the current derivatives associated with each switching vector. For both techniques, the position estimation can be achieved, because the PWM voltage vector causes a change in stator current which is limited by the leakage inductance, which varies as a function of position. The position estimation can also be achieved by tracking the leakage inductance variations induced by the saturation saliency.

2.6.4.1 INFORM technique

The INFORM technique is the first technique to achieve the saliency tracking by using active voltage test vectors [45] [150]. Typically the INFORM technique, which stands for " Indirect Flux detection by On-line Reactance Measurements" has been introduced by Schroedl in 1993 [150, 151]. The basic idea is to measure the current response, resulting from the applied voltage vectors during the PWM switching period. This technique has been investigated by many

researchers [51] [152] due to its improved low speed or standstill operation. Some researchers [153] use the INFORM technique to link with model based techniques so that the sensorless operations can be achieved over the full speed range. It is based on applying an impulse voltage vector to the machine u and then process the current transient response $\frac{dI}{dt}$. The progress in power electronics and micro-controllers has allowed the on line realization of these principles. The corresponding INFORM reactance, which contains the desired rotor position information, can be then be expressed as

$$x_{inform} = \frac{u}{\frac{dI}{dt}}. \tag{2.74}$$

However, some drawbacks have to be mentioned. The major problem for the standard INFORM technique is the introduced current disturbance due to the transient voltage vectors. Moreover, there is a need of additional di/dt sensors as well as an increased calculation power of the used numeric target (DSP, uC...), which is most of the times, already operated at full capacity in industrial applications [149].

2.6.4.2 PWM excitation without additional injection

The fundamental PWM excitation technique is a scheme proposed by Gao [50]. This scheme is based on the voltage vector excitation, which employs vectors from the normal PWM to achieve the excitation for di/dt measurement. This scheme can be used with sine-wave PWM modulation (SPWM) or space vector PWM (SVPWM) with various sampling techniques. The current transients are measured to establish the position vectors. The fundamental PWM excitation has the advantage over the INFORM technique in terms of the current ripples and acoustic noise and does not require the injection of an additional voltage. But it is not suitable for industrial use because it needs a high current sampling frequency. The inverter caused high frequency switching oscillations in the stator currents always appear within every PWM period. It should be possible to measure the current transient response introduced by the inherent PWM, so as to extract the saliency position information [45] [154]. By this way, some classic problems generally encountered with signal injection techniques can be avoided, i.e. additional current ripple, higher switching loss [45] [155]. In this way, no modification is required in the PWM, even at zero voltage, and the injected signal does not interact with the current controller. The response to the injected signal is obtained by a simple current derivative sensor. The carrier is provided by the already existing alternations of the zero vectors (111) and (000) in the standard space vector PWM. This carrier has the same frequency as switching. Consequently, the position estimation has a fast dynamic and no additional audible noise is produced. Because the excitation signal is in the zero sequence, it also does not interact with the current controller. In the literature, other combinations of the measured current derivative in response to specific voltage vectors can be found [140, 50, 156]. Despite the aforementioned advantages, common to all these techniques is that they require some additional hardware, comprising an LC filter, current derivative sensors, and two additional A/D converter inputs obviously, this is unwelcome in the context of industrial applications, where cost-electiveness is quite substantial.

2.7 Soft computing-based techniques

Soft computing-based self-sensing (Artificial intelligence-based techniques (AI)) algorithms have been developed since the 90-ties. Among the interesting strengths of these techniques, one can state that in contrast to other conventional techniques previously described, they do not require a physical model of the machine. Thus, they can approximate any function, regardless of its linearity and they particularly prove to be advantageous when datasets are available for

learning. The implementation of soft computing based algorithms has firstly started with vector controlled motor drives [84] [157, 158]. It was believed that such approaches help reducing the tuning efforts associated with the controllers and obtain improved results. Most of them, also had an industrial interest since they do not require excessive memory and high computational cost. A number of research papers based on using artificial intelligence techniques for the control of electric drives [157] [159, 160, 161, 162, 163, 164]. Then, their first application for the specific self-sensing applications appeared with speed controllers [158] [160]. Indeed, they have been used either as an adaptive model associated to the MRAS observer to solve the discretization instability problem in field-weakening, or to replace a PI-based speed controller. AI-based techniques have also been used for position estimation purposes [160] [162] to ensure the full sensorless operation. In contrast to model-based conventional schemes, AI-based position estimators allow avoiding the direct use of a speed-dependent mathematical model of the machine. AI-based techniques can be classified into four main categories:

- Neural networks-based position estimation [158] [160].
- Fuzzy logic-based position estimation [161, 162].
- Neuro fuzzy-based position estimation [164].
- Machine learning-based position estimation [163].

2.8 Conclusion

The major aspects on the rotor position and speed estimation of IPMSM have been reviewed comprehensively in this chapter. As well known the classical (FOC, feedback linearization,) and modern (sliding modes, backstepping, high gain, passivity, etc) controls of synchronous machines need an accurate position estimate in order to make the transforms to rotor reference frame. The three principle categories for self-sensing control of AC machines presented in the literature are summarized in this chapter. The fundamental mathematical based self-sensing techniques are very effective at high speed ranges and have the simplest realization. However, the drawbacks are that they are dependent on the machine parameters and generally fail at zero and low speeds. As alternative to the model based category, saliency based category is represented as a good candidate to achieve the self-sensing task. Techniques of this category are known by their less physical model-dependency, less-demanding in terms of tuning efforts and overcome the observability problem of IPMSM at zero and low speeds encountered. Despite these advantages, saliency based techniques still depend on the accurate knowledge of the machine inductances and mechanical parameters. The techniques of this category are very effective at zero and low speeds by they require filters in the estimation chain that affects the estimated quantities and increase the cost and implementation complexity.

The saliency based category is adopted in this work for the rotor position and speed estimation. Some improvements on the estimation chain are introduced in Chapters 3 and 4 in terms of filtering, parameters (inductance, inertia and friction) sensitivity, and delays taking into account the specific requirements of the EV application.

3

Contribution to demodulation of high frequency voltage injection (HFVI)

3.1 Introduction

Position estimation is an ongoing need, namely within EVs and HEVs, either for the closed-loop self-sensing control, or for fault diagnosis and safety applications. This is particularly critical at zero and low-speeds for the model-based self-sensing method. To take up these challenges, HF signal injection-based self-sensing techniques have been adopted in this work given their robustness and their suitability to the highly solicited salient-pole PM synchronous motors.

HFVI techniques exploit some machine properties that are not reproduced by the machine fundamental model. The HFVI techniques is persistently superimposed on the fundamental excitation. This interfers with the machine saliency and results in a position-dependent carrier signal.

As stated in the state of the art, these techniques have been studied by different researchers mainly R.D Lorenz [165] and J. Holtz [166] together with their research staff. Later, they have been widely developed and improved by a number of interesting research works [167, 168, 169, 170, 171, 172]. Bianchi, Bolgnagni and Seung–Ki Sul [59] [173] have addressed the problem from a different angle, by proposing a self-sensing-oriented-design of the PMSM. Thanks to its recognized robustness through these previous works, the HFVI techniques have been applied within the framework of this study. These techniques are classified according to the nature of the signal injection and to the choice of the injected frame, three main signal injection techniques can be find in the literature: Rotating sine-wave technique [121, 122], pulsating square-wave [130, 131] and pulsating sine-wave techniques [124, 125] [127]. All these techniques involve HPF/SFF and LPFs in the demodulation process part that can cause a number of adverse effects, like

- Generation of delays in the process of position/speed estimation,
- increase the cost and the complexity of implementation,
- necessity of injecting a very high frequency voltage signal in order to ensure frequency separation with the fundamental one,
- increase the estimation chain tuning complexity.

One of the problems that arises from the depicted self-sensing approach is the carrier recovery at the demodulation side. The drive system can in fact introduces an unknown delay and phase shifts in the HF signals which can hardly be analytically predicted. A wrong phase shift of the demodulation signal with respect to the useful one can in fact lead to a reduction of the amplitude of the error signals from which the rotor position information is extracted. This reduces the signal-to-noise ratio of the demodulation scheme leading to poor accuracy of the estimates or, in the worst case, to the impossibility of extracting the rotor position . This implies that the actual phase of superimposed HF signals has to be known, but this is not true in practical implementations. In fact, the inverter nonlinearity effects (dead time, T_{on}, T_{off},...) [174], the use of HPF/SFF [146], sampling time, current sensors and LPFs [175] are considered the main delays and phase shifts sources in the case of the HFVI approach. These delays sources reflect uncertainties in the demodulated signal. Then a suitable carrier recovery algorithm is needed for a correct demodulation of the HF current components. According to the problem statement mentioned above and to what it is proposed in the literature, the main contributions of this chapter are to

- Reduce the number of filters (HPF/SFF and LPF) (Step 1 and Step 3 in Figures. 3.1) and harmonics (Step 1) in the estimation process which improve the estimation process in terms of delays, cost and complexity of the implementations,
- estimate the phase shift related to the effects of inverter, HPF/SFF, sampling time, current sensors sensitivity and delays generated by the use of LPF (Step 2 in Figure 2),
- reclaim a new position estimation error,
- get over the knowledge of electrical and mechanical machine parameters on the self-sensing control of IPMSM (Step 3 in Figure 3.1).

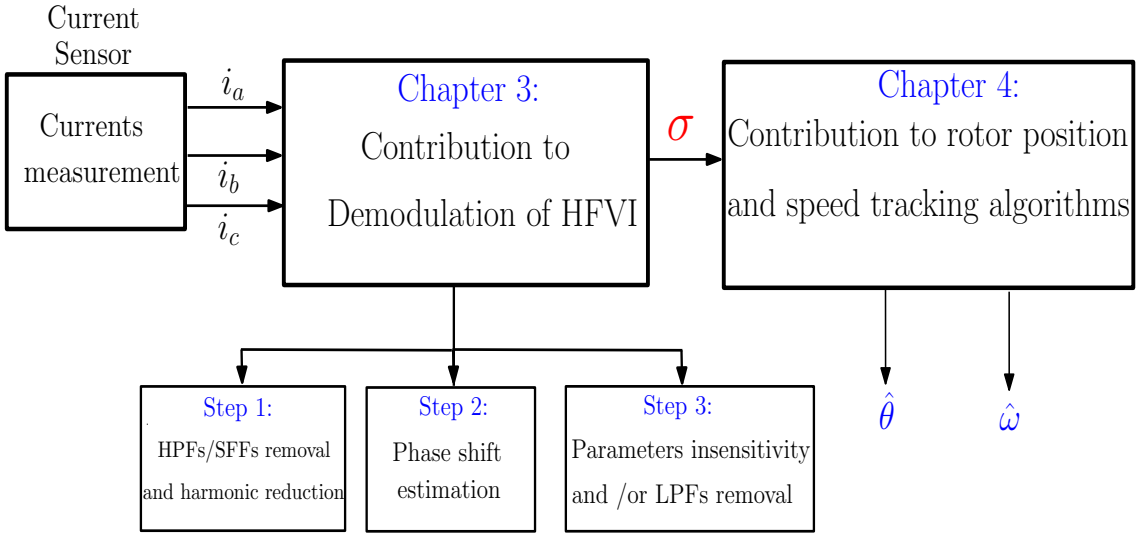

Figure 3.1: Proposed contributions with different steps

These contributions [7] [2] allow to improve significantly the estimation process and cover an extended operating range of the machine (medium and high speeds operating modes with different torque values). Moreover, The proposed improvements in this chapter help for reducing the effects of delays sources as well as the cost and implementation in order to improve the estimation chain and thus increase the self-sensing control performance. To introduce the contributions, three HFVI techniques are selected (as it is shown in Section 4.25). Section 3.2 introduces the pulsating square-wave demodulation improvements for the self-sensing drive control, (Step 1 and Step 3 in Figure 3.1). As the pulsating square-wave technique consist of injecting a voltage with very HF, the phase shift and delays effects on the estimation process is

neglected, which explain why the Step 2 is not needed in this case. Section 3.3 is dedicated to contributions of the demodulation process with the pulsating sine-wave strategy, where the three steps of Figure 3.1 are requested. The demodulation improvements for the self-sensing rotating sine-wave strategy is detailed in the Section 3.4, where the three steps of Figure 3.1 are needed. Some results are highlighted in order to validate the improvements of the demodulation process of each self-sensing HFVI techniques.

3.2 Pulsating square-wave voltage injection

Through the HFVI self-sensing techniques can detect the rotor position in any operating condition, there are still several issues: delays caused by the demodulation process and used filters, the dependency of the machine parameters, additional losses associated with the injected signal and the limited bandwidth of both the tracking observer and the control. This section introduces the improvement on the demodulation process for the pulsating square-wave voltage injection. The classical pulsating square-wave HFVI technique is developed for self-sensing control of AC machines. Compared with other classical techniques like rotating sine-wave, pulsating sine-wave, INFORM...etc, this technique offers numerous advantages

- Low pass filters are removed in the estimation chain, which allows to improve the rotor position and speed estimation and reduce the cost and implementation complexity.
- Thanks to the high injected frequency, the injected signal frequency is well separated from the fundamental signal frequency.
- Bandwidths of both the tracking observer and the regulator are increased.
- The stator resistance and the back EMF effects due to the too high injected frequency are reduced.

All these advantages lead to better modulation effect and an improvement in the output harmonics. The induced HF current due to the reduction of harmonics can be more accurate for estimating the rotor position and speed of the machine. In addition, a pulsating square-wave voltage is selected as the excitation signal to minimize the influence of LPF delays on the position estimation error which leads to reduce the cost and implementation complexity. However, pulsating square-wave HFVI technique generates non negligible acoustic noise, requires sensitive current sensors and generates harmonics on the rotor position and speed estimation [130] [148].

3.2.1 Pulsating square-wave demodulation process improvements for the position error extraction [1, 2]

According to Equation (3.7), the rotor position information is included in the envelope of the HF-induced current. Adopting a HPF is a feasible method to extract the HF-induced current. However, when the load is changed abruptly, the fundamental component of the induced current will change as well to balance the load torque, producing a loaded HF component. As a result, it may reduces the accuracy of the estimated position in the transient. Numerous demodulation process have been proposed in the literature [147, 148] [176]. In these works, HPF/BPF are used in order to remove the fundamental component. However, these filters can cause a number of adverse effects like

- Generation of delays in the process of position/speed estimation.
- Increase the cost and implementation complexity.

3.2.1.1 Injected square-wave voltage

The pulsating square-wave voltage injection technique is briefly recalled in this section in order to introduce the contributions to demodulation process. The dynamic of the Equation (2.19) is obtained by using Taylor's theorem first derivative as

$$\underline{\Delta\psi}_s^s = L_0\underline{\Delta i}_s^s + L_2\underline{\Delta i}_s^{s*}e^{j2\theta}. \tag{3.1}$$

From Equation (3.1), the current variation dynamic equation is deduced

$$\underline{\Delta i}_s^s = \frac{1}{{L_0}^2 - {L_2}^2}(L_0\underline{\Delta\psi}_s^s - L_2\underline{\Delta\psi}_s^{s*}e^{j2\theta}). \tag{3.2}$$

In this part, the HF injected voltage is applied in a fixed direction, and added to the d axis output voltage. The square-wave voltage vector in the estimated $(\hat{d}\hat{q})$ frame (see Figure 3.2) is expressed as

$$v_s^{\hat{r}} = \begin{bmatrix} v_{\hat{d}} \\ v_{\hat{q}} \end{bmatrix} = V_c(-1)^k \begin{bmatrix} 1 \\ 0 \end{bmatrix} \tag{3.3}$$

where V_c is the magnitude of the injected voltage and k is the index of PWM cycles.

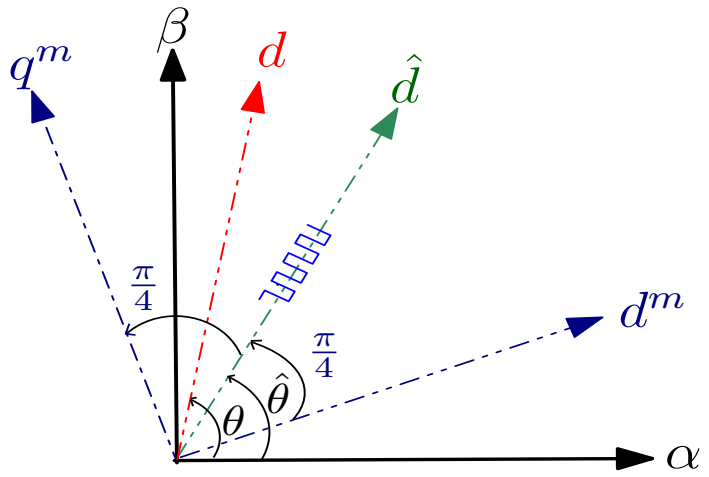

Figure 3.2: Pulsating square-wave HFVI technique with a measurement of the current shifted by $\frac{\pi}{4}$ from the estimated frame

Figure 3.3 represents the pulsating square-wave voltage signal that is applied in the estimated reference frame.

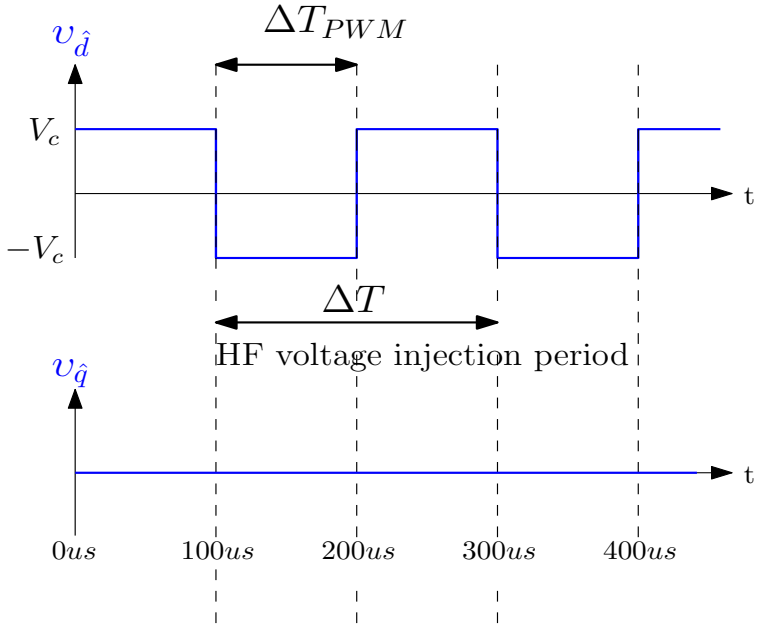

Figure 3.3: pulsating square-wave HFVI vector

From Equation (3.3), the HF injected voltage in the stator reference frame is expressed

$$v_s^s = V_c(-1)^k e^{j\hat{\theta}}. \tag{3.4}$$

3.2.1.2 HF Flux-current resulting from the injected voltage

The HF stator flux generated by the HF voltage signal injection can be obtained by integrating Equation (3.4) as follows

$$\underline{\Delta\psi_s^s} = V_c(-1)^k \Delta T e^{j\hat{\theta}}. \tag{3.5}$$

From (3.5) and (3.2), the HF stator current is expressed by

$$\underline{\Delta i_s^s} = \frac{V_c(-1)^k \Delta T}{({L_0}^2 - {L_2}^2)}(L_0 e^{j\hat{\theta}} - L_2 e^{j(2\theta-\hat{\theta})}). \tag{3.6}$$

The general current expression is given by

$$\underline{\Delta i_s^s} = \frac{V_c(-1)^k \Delta T}{({L_0}^2 - {L_2}^2)}(L_0 e^{j\hat{\theta}} - L_2 e^{j(2\theta-\hat{\theta})}) + \delta e^{j\hat{\theta}} \tag{3.7}$$

where, δ is the HF noise, that can be due to current sensors, inverter and un-modeled phenomena. From Equation (3.7), it can be seen that only the HF negative current component $\frac{V_c(-1)^k \Delta T L_2}{({L_0}^2-{L_2}^2)} e^{j(2\theta-\hat{\theta})}$ contains the rotor position information of the IPMSM.
In next sections, The proposed improvements to the demodulation process of the pulsating square-wave technique are introduced.

3.2.1.3 Step 1: HPF removal for pulsating square-wave HFVI

In this part, a new demodulation process is proposed to get over the adverse effects mentioned previously and increase the control performance. These assets improve the estimation chain regarding to the influence of the induced HF harmonics and the HPF delays. By doing so, the cost and implementation complexity will be reduced.

The HF current expression in the reference frame shifted by $\frac{\pi}{4}$ with respect to the injection frame is given

$$\underline{\Delta i_s^m} = I_{cp} e^{j\frac{\pi}{4}} - I_{cn} e^{j(2e_\theta + \frac{\pi}{4})} + \delta e^{j\frac{\pi}{4}} \tag{3.8}$$

where, I_{cp} given by Equation (2.66) and I_{cp} given by Equation (2.67) are the magnitude of the HF positive and the HF negative components of the stator current respectively.
Equation (3.8) can be rewritten as follows

$$\begin{bmatrix} \Delta i_d^m \\ \Delta i_q^m \end{bmatrix} = \begin{bmatrix} I_{cp}\frac{\sqrt{2}}{2} - I_{cn}\cos[2e_\theta + \frac{\pi}{4}] \\ I_{cp}\frac{\sqrt{2}}{2} - I_{cn}\sin[2e_\theta + \frac{\pi}{4}] \end{bmatrix} + \begin{bmatrix} \delta\frac{\sqrt{2}}{2} \\ \delta\frac{\sqrt{2}}{2} \end{bmatrix}. \tag{3.9}$$

By using the following trigonometric formulas given

$$\cos(a+b) = \cos(a)\cos(b) - \sin(a)\sin(b) \tag{3.10}$$

$$\sin(a+b) = \sin(a)\cos(b) + \cos(a)\sin(b) \tag{3.11}$$

Equation (3.9) can be rewritten as

$$\begin{bmatrix} \Delta i_d^m \\ \Delta i_q^m \end{bmatrix} = \begin{bmatrix} I_{cp}\frac{\sqrt{2}}{2} - I_{cn}\frac{\sqrt{2}}{2}[\cos(2e_\theta) - \sin(2e_\theta)] \\ I_{cp}\frac{\sqrt{2}}{2} - I_{cn}\frac{\sqrt{2}}{2}[\cos(2e_\theta) + \sin(2e_\theta)] \end{bmatrix} + \begin{bmatrix} \delta\frac{\sqrt{2}}{2} \\ \delta\frac{\sqrt{2}}{2} \end{bmatrix}. \tag{3.12}$$

Several techniques to extract e_θ are proposed in literature [130, 131] [147]. In this work, the estimation position error expression is deduced by computing the current difference quantities $\Delta i_q^m - \Delta i_d^m$ (see Figure 3.4)

$$\begin{aligned} \varepsilon &= \Delta i_q^m - \Delta i_d^m \\ &= -I_{cn}\sqrt{2}\sin[2e_\theta] \end{aligned} \tag{3.13}$$

where

$$\Delta i_d^m = (1 - z^{-1}) i_d^m \tag{3.14}$$

and

$$\Delta i_q^m = (1 - z^{-1}) i_q^m. \tag{3.15}$$

From Equations (3.14) and (3.15), the fundamental current and all DC components are canceled (this operation has the same behavior as numeric HP filter usually used in the literature) which proves the non-necessity of using HP/BP filters.

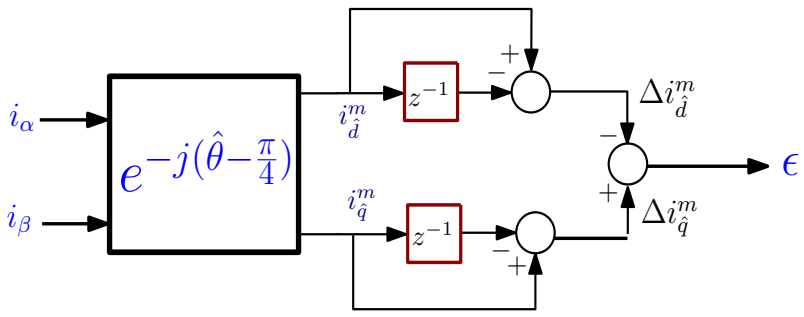

Figure 3.4: Block-diagram of the proposed demodulation with a measurement of the current shifted by $\frac{\pi}{4}$ from the estimated frame

From Equation (3.13), it can be seen that the position estimation error expression is independent of the HF noise δ.
As a conclusion, the proposed demodulation process introduced in this part doesn't involve HP/BP filters and is robust with respect to some additional HF-DC noises. Thanks to these properties, performance of the estimation process is improved, as it will be illustrated by simulations and experimental results in Chapter 4.
To ensure the positivity of the injected voltage, the Equation (3.13) multiplied by $(v_{\hat{d}})$ becomes

$$\begin{aligned} \varepsilon_s &= v_{\hat{d}}\varepsilon \\ &= v_{\hat{d}}(\Delta i_q^m - \Delta i_d^m) \\ &= -V_c(-1)^k I_{cn}\sqrt{2}\sin(2e_\theta). \end{aligned} \tag{3.16}$$

(3.17)

Finally, ε_s that represent the stator current resulting from the HF voltage injection, contains the information of the rotor position and can be expressed as

$$\varepsilon_s = -I_{cn-s}\sin(2e_\theta), \tag{3.18}$$

where,

$$I_{cn-s} = \frac{(L_d - L_q)[V_c(-1)^k]^2 \Delta T\sqrt{2}}{2L_d L_q}. \tag{3.19}$$

The above developed demodulation process based on pulsating square-wave voltage injection technique is summarized in Figure 3.5. In this figure, the block "Robust estimation of θ and ω and α" will be the subject of the chapter 4.

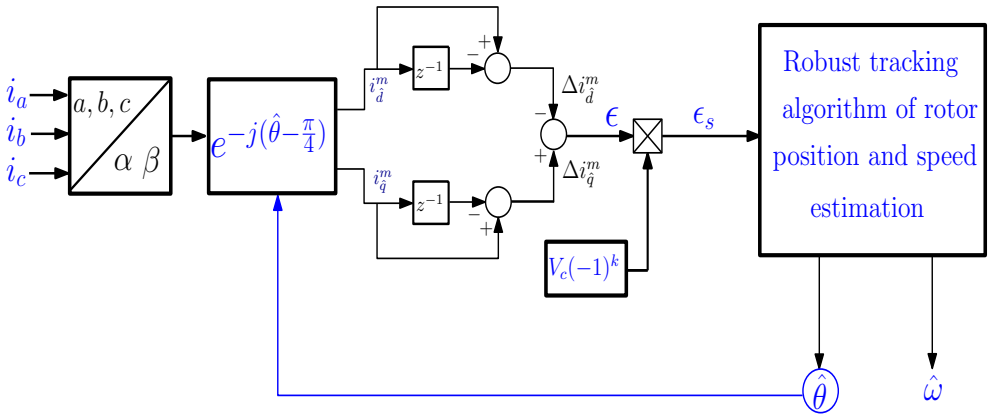

Figure 3.5: Scheme of the proposed demodulation of pulsating square-wave injection method

3.2.1.4 Step 3: Parameters insensitivity and new rotor position estimation error extraction for pulsating square-wave HFVI

As mentioned on the literatures, existing tracking algorithms (as it is shown in Section 4.3) are used to estimate the rotor position/speed based on the error expression given in (3.18). However, this error expression depends on the knowledge of the current negative sequence I_{cn-s} defined in Equation (3.19). As I_{cn-s} depends both on machine parameters (inductances L_d, L_q and injected signal characteristics (magnitude V_c and frequency $\frac{1}{\Delta T}$), all these tracking algorithms are sensitive to I_{cn-s} variations (due to the magnetic saturation) and not adapted to high speed variations (sensitive to the acceleration). Moreover, these parameters vary significantly according to several unknown factors. The rotor position/speed estimation in all speed/torque ranges

independently of machine parameters (inductances, inertia...) and HF characteristics (magnitude and frequency) is still an open problem. The proposed strategy describes a new method for the rotor position estimation extraction error. This error is used as an input for the proposed tracking algorithms which will be detailed in Chapter 4.
The proposed estimation error extraction allows to

- Avoid the knowledge of the gain I_{cn-s} and have free machine parameters estimation strategy.
- Have a new simple estimation error information.
- Replace the classical tracking algorithms by a new robust tracking observer.
- Extend the error range on the position estimation.

To overcome the I_{cn-s} dependency, the proposed strategy consists in using only the sign of the position estimation error instead of using the position error ε_s defined in Equation (3.18)

$$\sigma_s = sign(\varepsilon_s) = sign(I_{cn-s}\sin(2e_\theta)) \tag{3.20}$$

when $e_\theta \in [-\frac{\pi}{2};\frac{\pi}{2}]$,

$$\sigma_s = sign(I_{cn-s})sign(e_\theta). \tag{3.21}$$

For all salient pole machine, $I_{cn-s} > 0$ because $L_q > L_d$ and $[V_c(-1)^k]^2\Delta T > 0$, consequently (3.20) becomes

$$\sigma_s = sign(e_\theta) \tag{3.22}$$

where $sign(e_\theta)$ is the signum function [177] of the form

$$sign(e_\theta): \begin{cases} 1 \quad \text{if} \quad e_\theta > 0 \\ -1 \quad \text{if} \quad e_\theta < 0 \\ \in [-1,1] \quad \text{if} \quad e_\theta = 0. \end{cases}$$

Assumption 3.2.1. *The proposed technique is valid as long as the position error e_θ belong to $[-\frac{\pi}{2};\frac{\pi}{2}]$ (see Figure 3.6). This includes situations when the motor suddenly gets blocked, or slows down due to some unpredictable circumstances, or when the initial rotor position is wrong.*

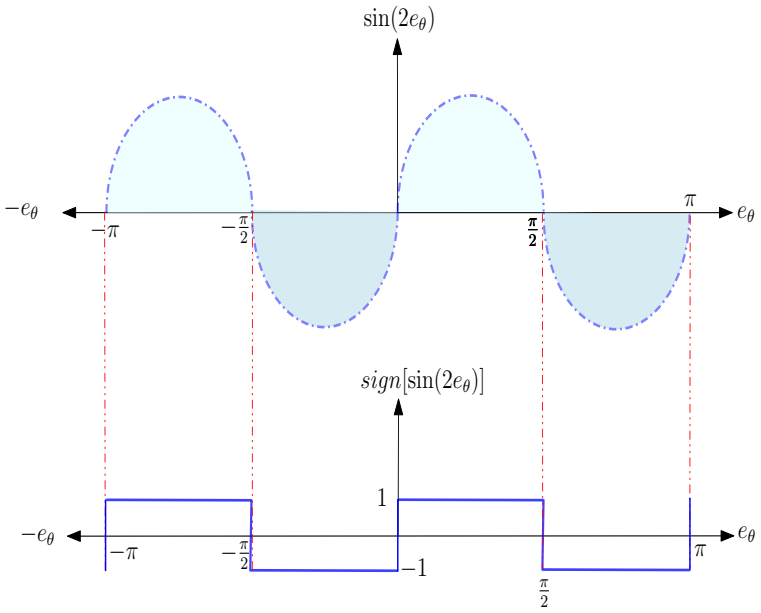

Figure 3.6: The position error tolerated for the correct estimation

Moreover, all the existing tracking algorithms are valid if and only if the hypothesis 2.6.1 (in the Chapter 2) is verified. This fact reduces the tolerated error range and makes the stability very local Moreover, it requires an initial rotor position algorithm [173] [178].

It can be argued that Equation (3.22) doesn't depend on machine parameters (L_d, L_q, ...) and injected signal characteristics (V_c, $\frac{1}{\Delta T}$). This estimation error σ_s (3.22) is used instead of ε_s as an information in a new robust tracking algorithm which is introduced in Chapter 4.

In the next section, the contributions to pulsating sine-wave demodulation process are introduced.

3.3 Pulsating sine-wave voltage injection

As well as the pulsating square-wave carrier injection, the pulsating carrier signal injection-based self-sensing techniques have also been well developed thanks to their inherent advantages, such as being less computational intensive and presenting small filter lags and simple demodulation scheme during signal processing [147, 148]. This section introduces the improvement demodulation process of the pulsating sine-wave HFVI technique for the self-sensing drive applications.

3.3.1 Pulsating sine-wave demodulation process improvements for the error extraction [3, 4, 5]

In this section, a new robust demodulation strategy is proposed for a self-sensing IPMSM drives . It allows to cover an extended operating range of the machine (medium and high speeds operating modes with different torque values) and reduce the delays and phase shift in the estimation precess. As a consequence, the cost and implementation complexity will be reduced in the estimation chain. According to the problem statement and to what it is proposed in the literature (see Section 2.6.2), the original contributions of the dedicated estimation strategy are to

- Remove the technological barriers related to the use of LPF that are located at steps 3 in Figure 3.1.
- remove the technological barriers related to the use of HPF/SFF that are located at steps 1 in Figure 3.1.
- estimate the phase shift related to the use of HPF/SFF, inverter effects, the sampling time, current sensors sensitivity and delays generated by the use of LPFs (located at Step 2 in Figure 3.1).
- get a position estimation error with reduced harmonics and independently from the knowledge of machine parameters (Step 3).

3.3.1.1 Injected pulsating sine-wave voltage

This technique will be briefly recalled in this section in order to introduce the contributions to the demodulation process. The pulsating sine-wave technique exploited in this part consists in injecting a HF voltage into the estimated $\hat{d}$ axis as illustrated in Figure 3.7, which can be expressed as

$$v_s^{\hat{r}} = -V_c \sin(\omega_c t) \begin{bmatrix} 1 \\ 0 \end{bmatrix} \tag{3.23}$$

where V_c and ω_c are the magnitude and the carrier frequency of the injected signal, respectively. The injected pulsating voltage vector in the estimated reference frame is shown in Figure 3.7.

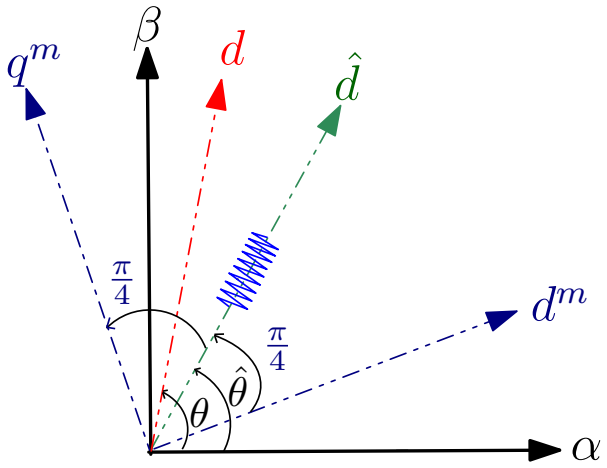

Figure 3.7: Pulsating sine-wave HFVI technique with a $\frac{\pi}{4}$ shift on the current measurement

By using Park transform, the expression of the HF injected voltage in the stator reference frame is given by

$$v_s^s = -V_c \sin(\omega_c t) e^{j\hat{\theta}}. \tag{3.24}$$

3.3.1.2 HF Flux-current resulting from the injected voltage

By integrating the injected stator voltage given in Equation (3.24), the following HF stator flux expression is obtained

$$\underline{\psi_s}^s = \int -V_c \sin(\omega_c t) e^{j\hat{\theta}} dt = \frac{V_c}{\omega_c} \cos(\omega_c t) e^{j\hat{\theta}}. \tag{3.25}$$

The HF stator current expression can be obtained by combining Equations (3.25) and (2.20)

$$\underline{i_s}^s = \frac{V_c}{\omega_c (L_0{}^2 - L_2{}^2)} (L_0 e^{j\hat{\theta}} - L_2 e^{j(2\theta - \hat{\theta})}) \cos(\omega_c t). \tag{3.26}$$

Where, I_{cp} given by Equation (2.27) and I_{cp} given by Equation (2.26) are respectively the HF positive and negative current components. By taking the fundamental current component i_{s1}^s into account, the general stator current can be expressed as

$$\underline{i_s}^s = I_{cp} \cos(\omega_c t) e^{j\hat{\theta}} - I_{cn} \cos(\omega_c t) e^{j(2\theta - \hat{\theta})} + i_{s1}^s \tag{3.27}$$

In the sequel, the proposed contributions to demodulation improvements of the pulsating sine-wave are introduced.

3.3.1.3 Step 1: HPF removal for pulsating sine-wave HFVI

This step focuses on HPF removal which is used in signal processing and demodulation part. Adopting a HPF is a feasible method to extract the HF-induced current. The fundamental component of the induced current is always changing. This fundamental component must be effectively separated from the injection HF component. Numerous heterodyning processes have been proposed in the literature in order to remove the fundamental component by using HPF/BPF [141, 142]. However, these filters cause a number of adverse effects like

- Generation of delays in the process of position/speed estimation.
- Increase the cost and implementation complexity.

The general current expression is given by

$$\underline{i_s}^s = I_{cp}\cos(\omega_c t)e^{j\hat{\theta}} - I_{cn}\cos(\omega_c t)e^{j(2\theta-\hat{\theta})} + i_{s1}^s. \tag{3.28}$$

In this section, an improved method is proposed to remove the fundamental current component i_{s1}^s by using its reference i_{s-ref}^s.

$$\underline{i_s}^s = I_{cp}\cos(\omega_c t)e^{j\hat{\theta}} - I_{cn}\cos(\omega_c t)e^{j(2\theta-\hat{\theta})} + i_{s1}^s - i_{s-ref}^s + \delta e^{-j\hat{\theta}} \tag{3.29}$$

where δ represents some HF current components which can be due to the inverter frequency, current sensors, etc.
The control performance suppose to be achieved even in the transient mode. The demodulation process proposed in this step improves performance and simplifies the real time implementation of the estimation process. It also allows to get over the drawbacks due of using HPF/BPF. These assets improve the demodulation process and the estimation chain regarding the induced HF harmonics quality and the influence of HPF delays on the position estimation error, which reduces the cost and implementation complexity. The injection frame and the measurement one are shown in Figure 3.7. The current expression in the reference frame (d^m q^m) shifted by $\frac{\pi}{4}$ with respect to the injection frame is given by

$$\underline{i_s}^m = I_{cp}\cos(\omega_c t)e^{j\frac{\pi}{4}} - I_{cn}\cos(\omega_c t)e^{j(2\theta-2\hat{\theta}+\frac{\pi}{4})} + \delta\, e^{j(\frac{\pi}{4})}. \tag{3.30}$$

In matrix notation, Equation (3.30) can be written as follows

$$\begin{bmatrix} i_d^m \\ i_q^m \end{bmatrix} = \begin{bmatrix} I_{cp}\frac{\sqrt{2}}{2} - I_{cn}\frac{\sqrt{2}}{2}[\cos(2e_\theta) - \sin(2e_\theta)) \\ I_{cp}\frac{\sqrt{2}}{2} - I_{cn}\frac{\sqrt{2}}{2}[\cos(2e_\theta) + \sin(2e_\theta)) \end{bmatrix} \cos(\omega_c t) + \begin{bmatrix} \delta\frac{\sqrt{2}}{2} \\ \delta\frac{\sqrt{2}}{2} \end{bmatrix}.$$

The position estimation error expression can be deduced by computing the difference of current quantities $i_q^m - i_d^m$

$$\begin{aligned} \rho &= i_q^m - i_d^m \\ &= -I_{cn}\sqrt{2}\sin(2e_\theta)\cos(\omega_c t). \end{aligned} \tag{3.31}$$

The proposed demodulation introduced in (3.31) can reduce some harmonics δ and remove the effect of the term $I_{cp}\frac{\sqrt{2}}{2}\cos(\omega_c t)$ on the rotor position estimation error that improves the robustness and the accuracy of the estimation.
From Equations (3.29) and (3.31), the fundamental current and some of DC/HF components are canceled which proves the non-necessity of using HP/BP filters. As conclusion, the proposed demodulation process introduced in this section does not involve HPF/BPF and is robust with respect to any additional HF-DC noise. Thanks to these properties, performance of the estimation process are improved, as it will be illustrated by experimental results in the next Chapter 4.
The first step of the part 1 in Figure 3.1 is summarized in Figure .3.8.

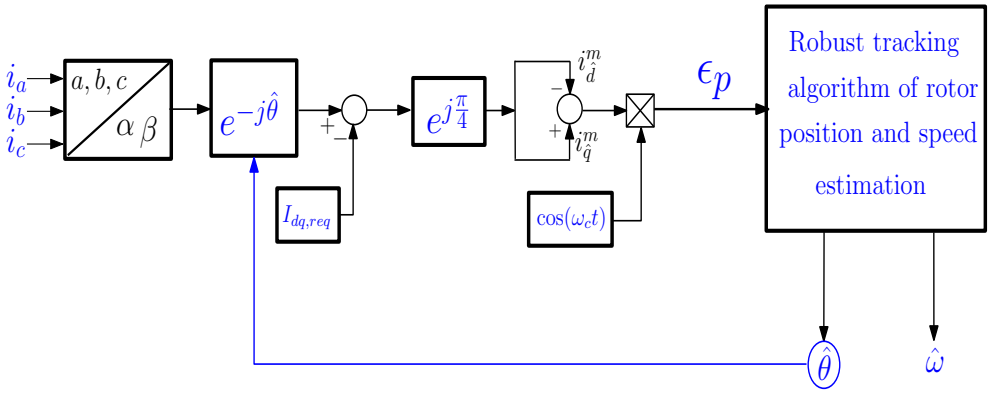

Figure 3.8: Block-diagram of the proposed demodulation with a measurement of the current shifted by $\frac{\pi}{4}$ from the estimated frame

3.3.1.4 Step 2-A: Numerical phase shift controlled oscillator estimation (NPCO) for pulsating sine-wave HFVI

The use of HPF/SFF produces a phase shift $\phi_{HBF/SFF}$ at the carrier $(\cos(\omega_c t + \phi_{HPF}))$. Moreover, inverter effects (dead time, T_{on}, T_{off},...), sampling time, current sensors and LPFs cause significant delays and phase shift that are not easily predictable. Then, a carrier recovery algorithm is needed for a correct demodulation of the high frequency current components. A more representative expression for HF current containing the position estimation error ρ, should consider the above cited phenomena shown in Figure 3.9.
The HF current resulting from the HFVI (3.31) could be expressed as

$$\rho = A\cos(\omega_c t + \phi_m) \tag{3.32}$$

where

$$A = -I_{cn}\sqrt{2}\sin(2e_\theta)) \tag{3.33}$$

and ϕ_m is an unknown phase shift due to previously cited phenomena (ϕ_{HPF}, ϕ_{LPF}, $\phi_{Inverter}$ and $\phi_{sampling\ time}$, etc.) on the HF carrier signal, which can be seen on the Equation (3.32).

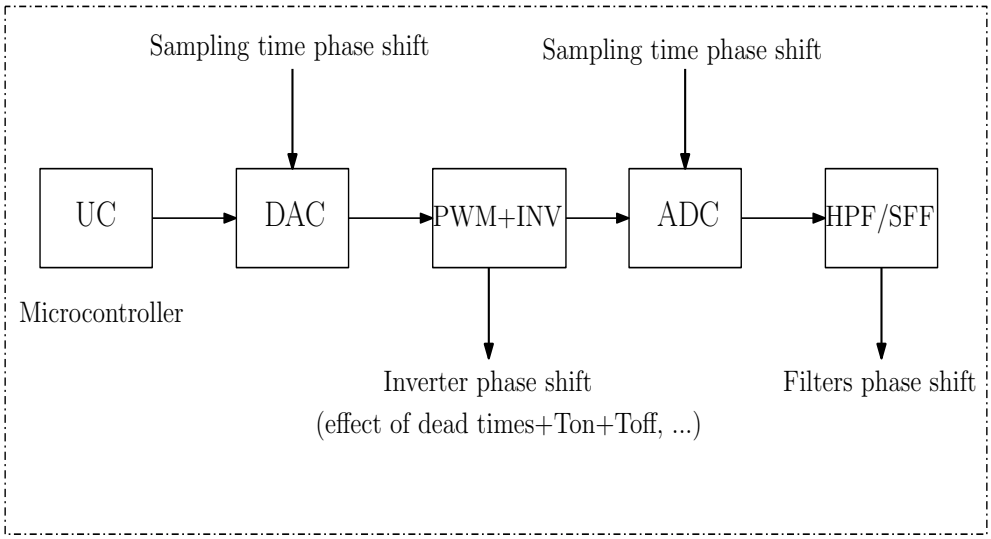

Figure 3.9: Signal phase shift generation sources

To estimate the phase shift, Equation (3.32) is multiplied by $\sin(\omega_c t + \hat{\phi}_m)$, which leads to

$$\begin{aligned}\rho * \sin(\omega_c t + \hat{\phi}_m) &= A\cos(\omega_c t + \phi_m) * \sin(\omega_c t + \hat{\phi}_m) \\ &= \frac{A}{2}[\sin(2\omega_c t + \phi_m + \hat{\phi}_m) + \sin(\phi_m - \hat{\phi}_m)].\end{aligned} \tag{3.34}$$

By applying a LPF to Equation (3.34), the expression of λ is obtained

$$\lambda = LPF[\rho * \sin(\omega_c t + \hat{\phi}_m)] = \frac{A}{2}[\sin(\phi_m - \hat{\phi}_m)]. \tag{3.35}$$

The expression of λ is used as an input for the phase shift tracking observer (PSTO) to estimate the ϕ_m

$$PLL(\frac{A}{2}[\sin(\phi_m - \hat{\phi}_m)]) = \hat{\phi}_m. \tag{3.36}$$

The Figure 3.10 details the NPCO design.

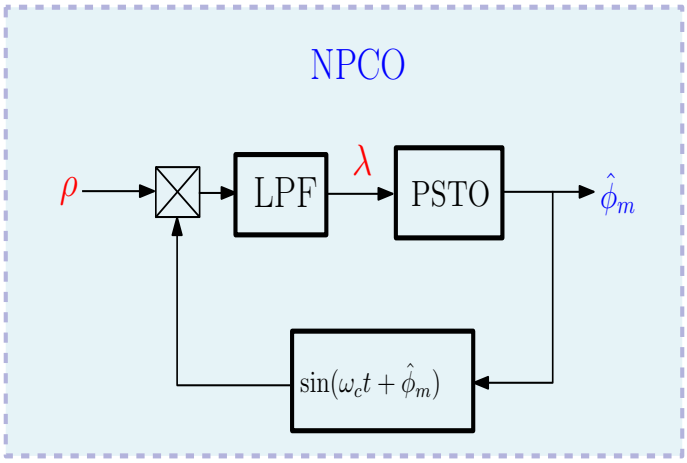

Figure 3.10: NPCO design

3.3.1.5 Phase shift tracking observer:

The phase-locked loop (PLL) is used as a PSTO (see Figure 3.11) to estimate the phase shift ϕ_m, its design is given by

$$\begin{aligned}\dot{\hat{\eta}} &= K_\eta \lambda \\ \dot{\hat{\phi}}_m &= \hat{\eta} + K_{\phi_m}\lambda\end{aligned} \tag{3.37}$$

Gains K_η and K_{ϕ_m} are chosen according to the stability analysis given in [179].

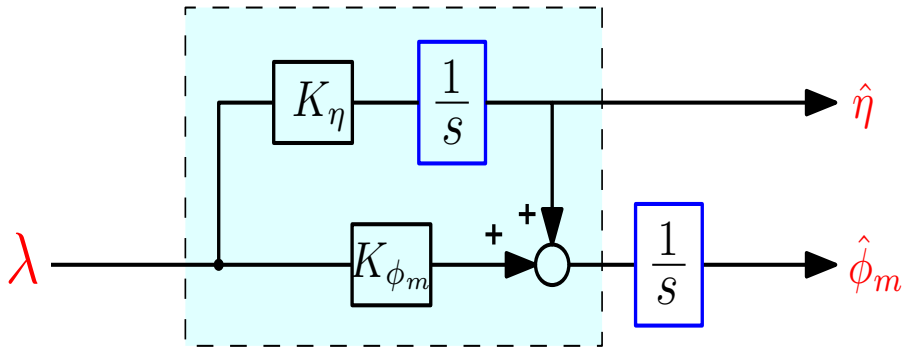

Figure 3.11: PSTO design to phase shift tracking

Existing phase shift estimation algorithms (NPCO,...) are based on numerous hypothesis, the amplitude A given in Equation (3.33) of Equation (3.32) is considered constant [174, 175]. Note that A depends on electrical machine parameters (L_d, L_q), HF signal characteristics and the invariance of the term $\sin(2e_\theta)$. In this step, a robust estimation approach (without considering assumptions) of the carrier signal phase, which is needed for the demodulation process is presented, to get over the above mentioned limitations.

3.3.1.6 Step 2-2: Robust numerical phase shift controlled oscillator estimation (RNPCO) for pulsating sine-wave HFVI

In this section, a robust estimation approach of the carrier signal phase needed for the demodulation process is presented. This approach doesn't depend on machine parameters (gain A) which are uncertain and vary according to several factors (temperature, speed and applied torque), HF characteristics of the the injected signal and invariance of the term $\sin(2e_\theta)$.
The current difference quantity could be expressed in the form

$$\rho = -I_{cn}\sin(2e_\theta)\cos(\omega_c t + \phi_m). \tag{3.38}$$

To extract the phase shift ϕ_m localized in Equation (3.38), the terms I_{cn}, $\sin(2e_\theta)$ and $\cos(\omega_c t)$ should be removed. By multiplying the estimation error of equation (3.38) by $\sin(\omega_c t + \hat{\phi}_m)$, (3.38) reads

$$\begin{aligned}\rho_m = \rho * \sin(\omega_c t + \hat{\phi}_m) &= -I_{cn}\sin(2e_\theta)\cos(\omega_c t + \phi_m)\sin(\omega_c t + \hat{\phi}_m) \\ &= \frac{-I_{cn}}{2}\sin(2e_\theta))[\sin(2\omega_c t + \phi_m + \hat{\phi}_m) + \sin(\phi_m - \hat{\phi}_m)].\end{aligned} \tag{3.39}$$

By applying a LPF to Equation (3.39), ones has

$$LPF[\rho_m] = \frac{-I_{cn}}{2}\sin(2e_\theta))[\sin(\phi_m - \hat{\phi}_m)]. \tag{3.40}$$

To get the expression λ, which contains the phase shift error, independently of the parameters A, one propose in this step to use the sign of Equation (3.40) as follows

$$\lambda = sign(LPF[\rho_m]). \tag{3.41}$$

$$\lambda = sign(\frac{-I_{cn}}{2})sign(\sin(2e_\theta)sign([\sin(\phi_m - \hat{\phi}_m)]). \tag{3.42}$$

For all salient pole AC machines, $sign(\frac{-Icn}{2}) > 0$ because $L_q > L_d$, $V_c > 0$ and $\omega_c > 0$, consequently Equation (3.42) becomes

$$\lambda = sign(\sin(2e_\theta)sign([\sin(\phi_m - \hat{\phi}_m)]). \tag{3.43}$$

To extract the phase shift ϕ_m, the Equation (3.43) is multiplied by $sign(\sin(2(\theta - \hat{\theta})))$, the method to obtain the term $sign(\sin(2e_\theta))$ (see Figure (3.12)) will be given in Section 3.3.1.10), one can obtain

$$\lambda_{sign} = \lambda * sign(\sin(2e_\theta)). \tag{3.44}$$

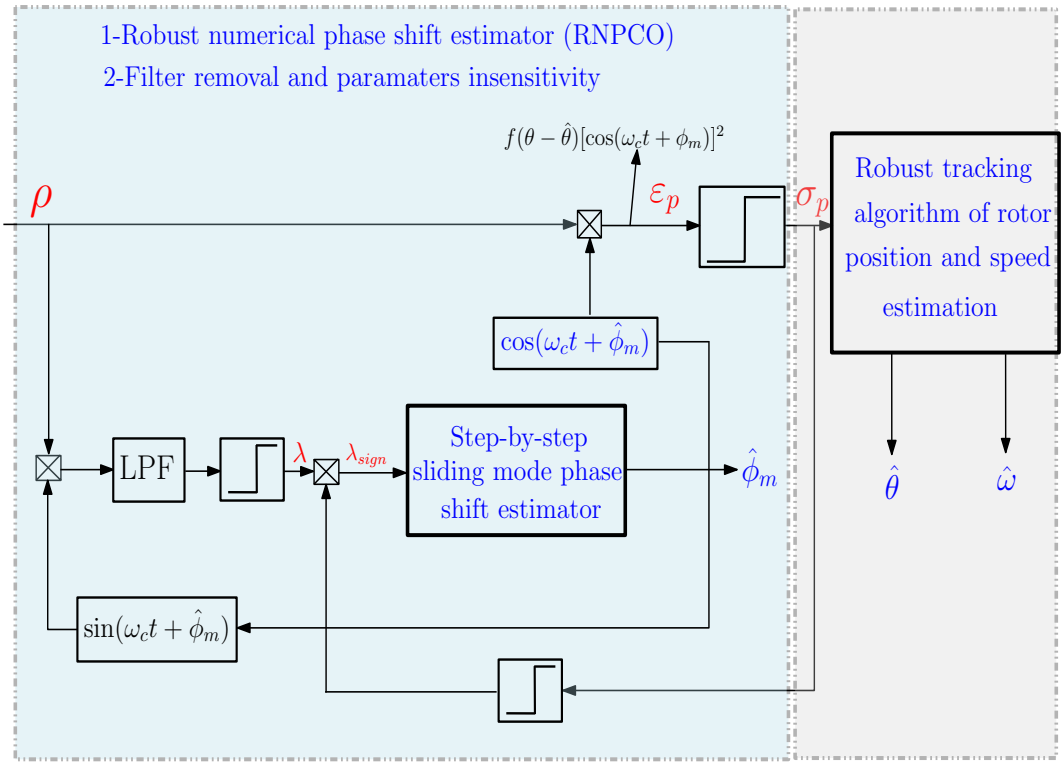

Figure 3.12: General scheme of the proposed phase shift estimation

Then, Equation (3.44) becomes

$$\lambda_{sign} = sign(\sin(2e_\theta))^2 sign([\sin(\phi_m - \hat{\phi}_m)]). \tag{3.45}$$

It is known that $sign(\sin(2e_\theta))^2 = 1$, then Equation (3.45) is written as

$$\lambda_{sign} = sign([\sin(\phi_m - \hat{\phi}_m)]). \tag{3.46}$$

The sign of the phase shift estimation error (3.46) is used as an information in a new tracking algorithm, which has a in finite time convergence. This algorithm, which is the subject of the next part, aims to estimate the phase shift and its time derivative (to have a good estimation even if the phase shift has a dynamic) without knowing machine parameter's, rotor position estimation error $\sin(2e_\theta)$ and HF signal characteristics.
For all $e_\phi \in [-\pi;\pi]$, λ_{sign} in Equation (3.46) becomes

$$\lambda_{sign} = sign(e_\phi) \tag{3.47}$$

where $sign(e_\phi)$ is the signum function [177] of the form

$$sign(e_\phi): \begin{cases} 1 \quad \text{if} \quad e_\phi > 0 \\ -1 \quad \text{if} \quad e_\phi < 0 \\ \in [-1,1] \quad \text{if} \quad e_\phi = 0 \end{cases}$$

and

$$e_\phi = \phi_m - \hat{\phi}_m. \tag{3.48}$$

Assumption 3.3.1. *The proposed technique is valid as long as the phase shift error belong to* $e_\phi \in [-\pi;\pi]$ *(see Figure 3.13).*

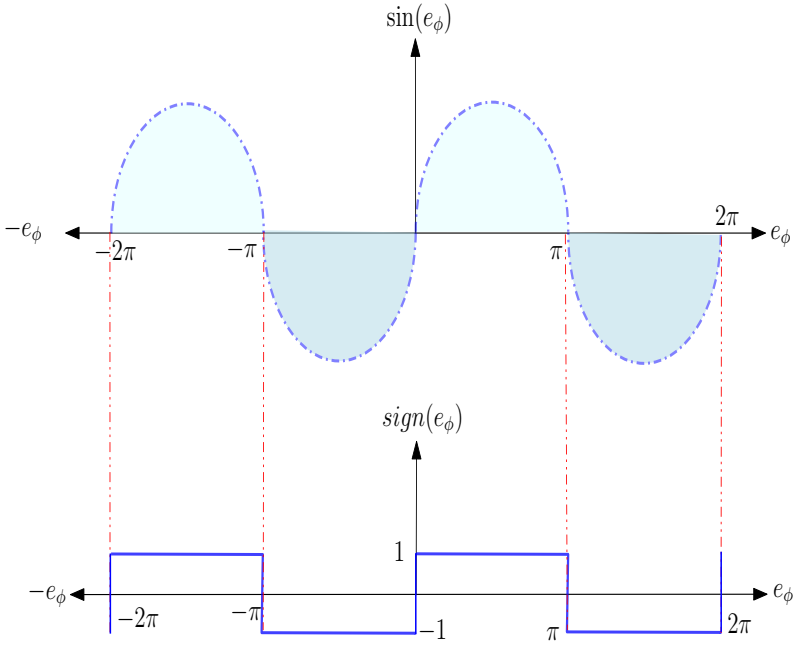

Figure 3.13: The relation between the proposed phase shift estimation error and the classical error

It can be argued that Equation (3.47) doesn't depend on machine parameters (L_d, L_q), the position estimation error ($\sin(2e_\theta)$) and injected signal characteristics (V_c, ω_c).

3.3.1.7 Step-by-step robust estimation of phase shifts

Only the sign of the phase shift estimation error is required to estimate the phase shift and its time derivative by the proposed (3.49)-(3.50) finite time step-by-step sliding mode observer.

$$\dot{\hat{\phi}}_m = \hat{\mu}_m + K_\phi \lambda_{sign} \tag{3.49}$$

$$\dot{\hat{\mu}}_m = E_\phi K_\mu sign(\bar{\mu}_m - \hat{\mu}_m) \tag{3.50}$$

where,

$$\bar{\mu}_m = \hat{\mu}_m + K_\phi (\lambda_{sign})_{filtred} \tag{3.51}$$

$$E_{\phi_m} : \begin{cases} 1 & \text{if} \quad g(k) = 0 \\ 0 & \text{if} \quad g(k) \neq 0, \end{cases}$$

and, $g(k) = |\sum_{k=1}^{2} \lambda_{sign}(k)| + |\sum_{k=2}^{3} \lambda_{sign}(k)| + |\sum_{k=3}^{4} \lambda_{sign}(k)|$ with $\lambda_{sign}[k]$ (see Figure 3.14) is the discrete form of the temporal function $\lambda_{sign}(t)$, k is the delay of one time step by one control period in the discrete domain. The gains (K_ϕ, K_μ) are chosen according to the stability analysis and given in Section 3.3.1.8.

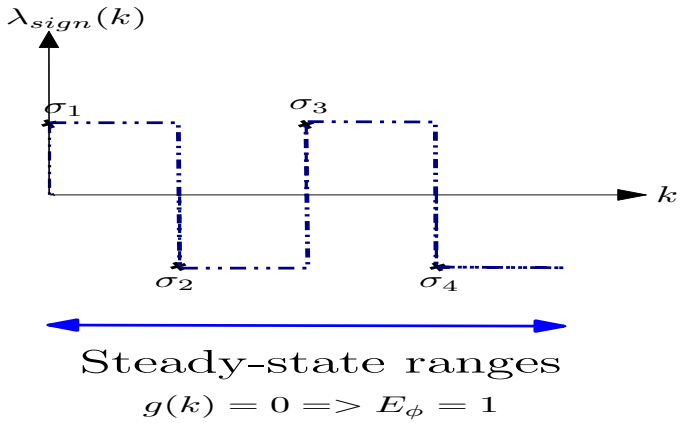

Figure 3.14: The chattering function

Remark 3.1. *The function $g(k)$ is introduced to detect the chattering phenomenon, because as mentioned before only the sign of the phase-shift estimation error is available as an information for the observer.*

3.3.1.8 Stability analysis based on the sign propagation

The stability analysis of the step-by-step sliding mode observer for phase shift and its dynamic estimation is given in this section.
The mechanical double integrator system of the phase shift and its time derivative dynamic estimation which is used to design the observer (4.66)-(4.67) is given by

$$\dot{\phi}_m = \mu_m \tag{3.52}$$

$$\dot{\mu}_m = 0. \tag{3.53}$$

Consider (3.54)–(3.55) the phase shift and its time derivative dynamic estimation errors between observer (3.49)-(3.50) and system (3.52)–(3.53)

$$e_\phi = \phi_m - \hat{\phi}_m \tag{3.54}$$

$$e_\mu = \mu_m - \hat{\mu}_m \tag{3.55}$$

whose dynamics are given by

$$\dot{e}_\phi = e_\mu - K_\phi \lambda_{sign} \tag{3.56}$$

$$\dot{e}_\mu = -E_\phi K_\mu sign(\bar{\mu}_m - \hat{\mu}_m). \tag{3.57}$$

Theorem 3.3.1. *For any bounded $K_\phi > max(|e_\mu|)$ and $K_\mu > 0$, the , the observers (3.49)-(3.50) ensures the finite-time convergence of phase shift and its time derivative dynamic estimation errors (3.57)-(3.56) to zero.*

Proof: Let K_ϕ and K_μ satisfying theorem conditions. Firstly, the stability of the phase shift error dynamics (3.57) is analyzed. Considering the nonempty manifold $S = \{e_\phi \setminus e_\phi = 0\}$ and the following candidate Lyapunov function V_ϕ

$$V_\phi = \frac{1}{2} e_\phi^2. \tag{3.58}$$

One proves the attractivity of S as follows

$$\begin{aligned} \dot{V}_\phi &= e_\phi \dot{e}_\phi \\ &= e_\phi (e_\mu - K_\phi sign(e_\phi)) \\ &= e_\phi e_\mu - e_\phi K_\phi sign(e_\phi) \\ &\leq |e_\phi||e_\mu| - K_\phi |e_\phi|. \end{aligned} \tag{3.59}$$

Let be

$$K_c = -|e_\mu| + K_\phi. \tag{3.60}$$

As $K_\phi > max(|e_\mu|)$, $K_c > 0$.
Then, Equation (3.59) can be written as

$$\dot{V}_\phi \leq -K_c |e_\phi| \tag{3.61}$$

which verifies the inequality $\dot{V}_\phi < 0$. It implies that the phase shift estimation error e_ϕ (3.54) converges to zero in finite-time $t_1 > 0$.
Then $\forall\, t \geq t_1$, one has

$$\dot{e}_\phi = e_\phi = 0. \tag{3.62}$$

This implies that the sliding condition for (3.54) is achieved thus $E_\phi = 1$.
By using (3.62) in (3.56), one can deduce

$$e_\mu = K_\phi sign(e_\phi). \tag{3.63}$$

Therefore, $\forall\, t \geq t_1$, the observer output $\bar{\mu}_m$ defined in (3.51) is equal to μ_m ($\bar{\mu}_m = \mu_m$) .
In the same manner, the stability of (3.57) can be proved. Consider the following candidate Lyapunov function

$$V_\mu = \frac{1}{2} e_\mu^2. \tag{3.64}$$

The time derivative of (3.64) is given as follows

$$\begin{aligned} \dot{V}_\mu &= e_\mu \dot{e}_\mu \\ &= -E_\phi K_\mu e_\mu sign(\bar{\mu}_m - \hat{\mu}_m). \end{aligned} \tag{3.65}$$

With $\bar{\mu}_m = \mu_m$ and $E_\phi = 1$, (3.65) becomes

$$\begin{aligned} \dot{V}_\mu &= -K_\mu e_\mu sign(e_\mu) \\ &\leq -K_\mu |e_\mu| \end{aligned} \tag{3.66}$$

where $K_\mu > 0$
Then, (3.66) can be written as

$$\dot{V}_\mu < 0. \tag{3.67}$$

This proves the finite time convergence of the time derivative of phase shift estimation error e_μ (3.55) to zero in $t_2 > t_1$.
Equations (3.61) and (3.67) prove the stability of the proposed observer (3.49)–(3.50).

3.3.1.9 Comparative study between NPCO and RNPCO

This part consists of studying the robustness of the RNPCO and comparing it with the classical NPCO by considering many criteria. For the first evaluation, the NPCO algorithm is tested in nominal case, where the gain (A) given by Equation (3.33) is considered constant. For this evaluation, two tests have been effectuated, with and without consider the variation of the phase shift. When the phase shift is considered constant as it is shown in Figure 3.15, the NPCO converges slowly to the real phase shift and generates a transient error that can affects the estimated rotor position and speed. Then, when the dynamic of the phase shift is considered (see Figure 3.16), the NPCO generates an important transient estimation error. This proves that the NPCO is very sensitive to the phase shift variations. The second evaluation focuses on the robustness of the NPCO with respect to the variation of the gain A given by Equation (3.33). In the literature [174, 175], the gain A is always considered constant which is not the case in reality. This gain varies according to the magnetic saturation (inductances variation) and the rotor position estimation error variations. For that, an arbitrary profile for the gain A is adopted (arbitrary profile of L_d, L_q and arbitrary variations of the term $\sin(2e_\theta)$). When this profile is considered in simulation, the NPCO diverges immediately. The proposed RNPCO algorithm is tested with respect to the considered gain (A) profile and the phase shift dynamic. The obtained results illustrated by Figure 3.17 show that the proposed RNPCO algorithm gives a good estimation of the phase shift against the gain A variations and the dynamic of the phase shift. The robustness comparative study between the proposed algorithm RNPCO and the classical algorithm is summarized in Table 3.1.

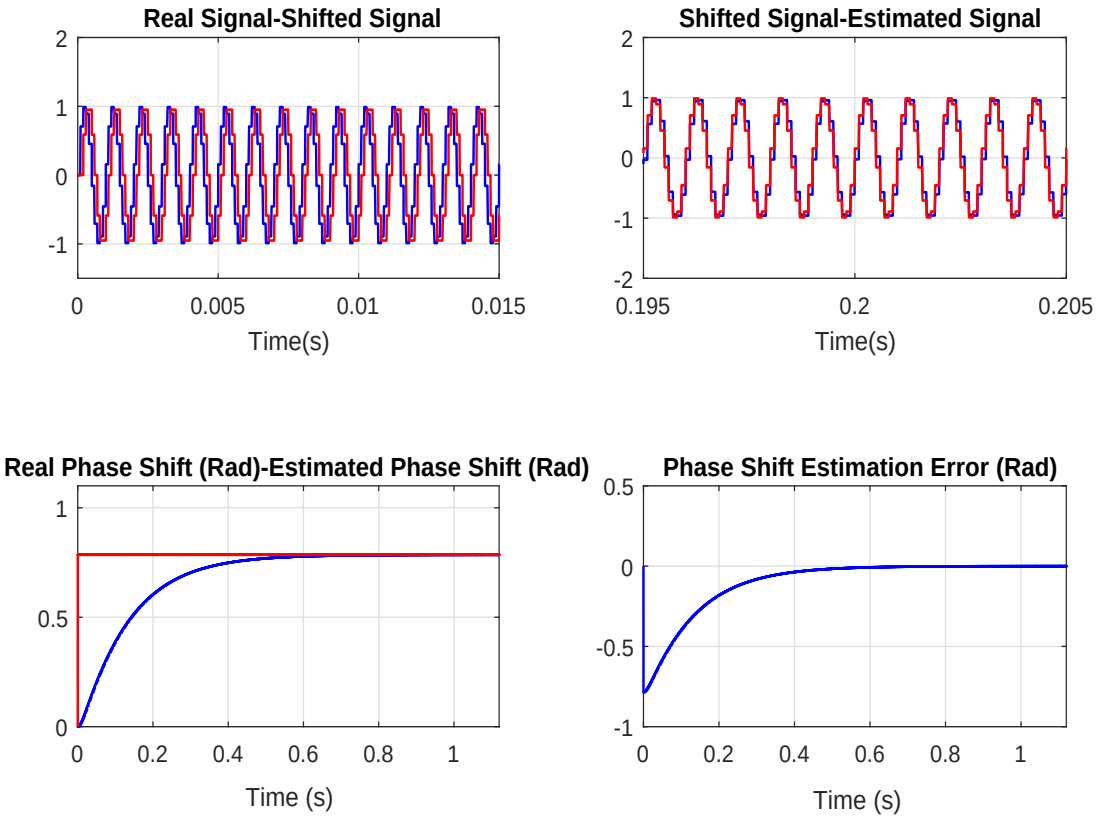

Figure 3.15: NPCO simulation results under a nominal case (without any parameters variation)

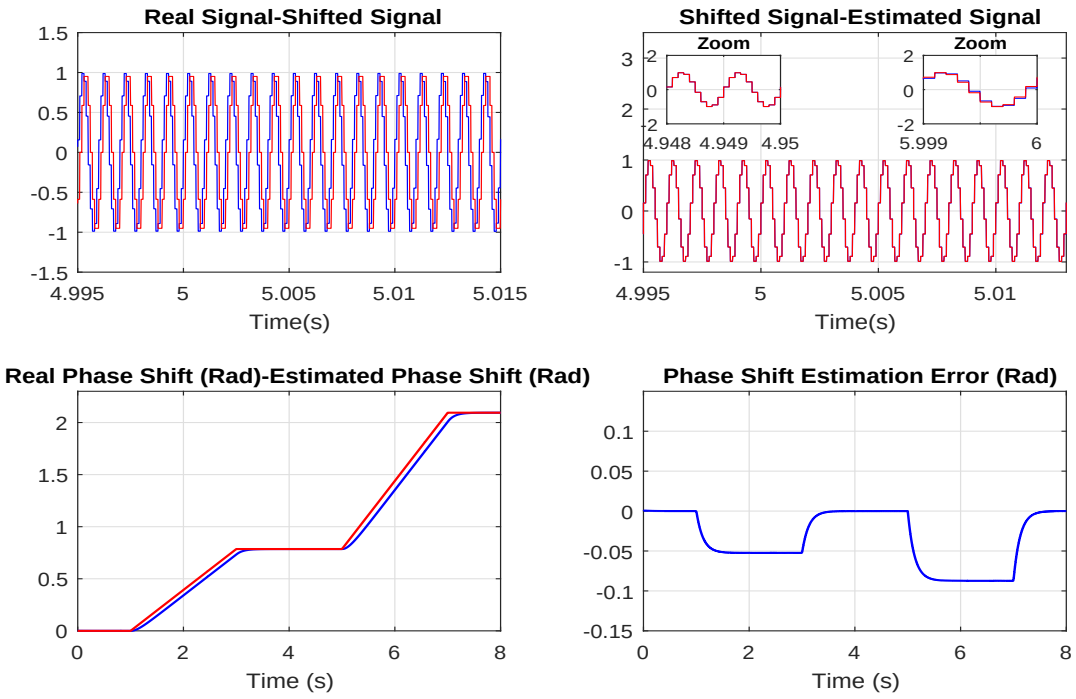

Figure 3.16: NPCO simulation results under only phase shift variation (without any parameters variation)

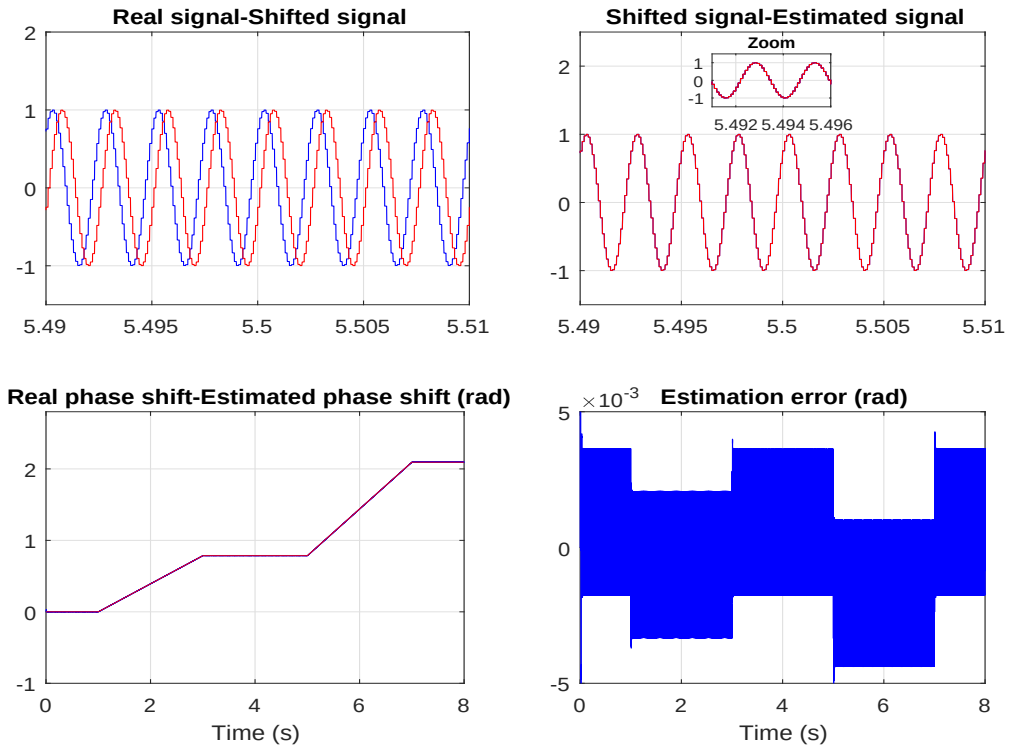

Figure 3.17: RNPCO simulation results under parameter variation, phase shift variations and the rotor position estimation error

Table 3.1: Summary of the comparative study between the RNPCO and the NPCO

Robustness vs \ Phase-shift observers	Proposed RNPCO	Classical NPCO
Phase shift dynamics	***	*
Parameter variations	Insensitive	Very sensitive
Position estimation errors	***	*

This comparative study confirms that the developed strategy offers a significant and attractive improvement compared to the previous techniques.

Parameters Tuning

- RNPCO: Parameters K_ϕ, K_μ, K_c, are chosen according to the stability analysis given previously in Section 3.3.1.8. Their values are given in Table 3.2.
- NPCO: Parameters K_η and K_{ϕ_m} are chosen according to the stability analysis given in Section 3.3.1.5. Their values are given in Table 3.2.

Table 3.2: Parameters tuning of RNPCO and NPCO for the phase shift estimation.

K_ϕ, K_μ, K_c	50, 8, 2
K_η, K_{ϕ_m}	30, 750

3.3.1.10 Step 3: Parameters insensitivity, LPFs removal and the new rotor position estimation extraction for pulsating sine-wave HFVI

As detailed in Section 3.2.1.4, several tracking algorithms are based on error expression given in Equation (3.31) to estimate the rotor position and speed. However, this error expression requires accurate knowledge of the current negative sequence I_{cn} defined in Equation (2.27) which depends both on machine parameters and HF signal characteristics. These tracking algorithms suffer from the I_{cn} variations and they are not adapted to high speed variations (sensitive to the acceleration). Moreover, in the estimation process of HFVI techniques, LPFs [141][180] (first,... or forth order) are used to recover the rotor position estimation error. This step focus on LPFs removal to separate the high frequency component from the low frequency one and to get over the dependency on electrical machine parameters (inductances).

The principle is described as follows. The expression ρ (3.31) obtained in Step 1 is multiplied by $\cos(\omega_c t + \hat{\phi}_m)$, where ϕ_m in Equation (3.31) is replaced by $\hat{\phi}_m$ and $\hat{\phi}_m$ is the estimated phase shift obtained in Step 2.

$$\varepsilon_p = \rho * \cos(\omega_c t + \hat{\phi}_m) = -I_{cn} \sin(2e_\theta)[\cos(\omega_c t) + \hat{\phi}_m]^2. \tag{3.68}$$

In the literature [180, 181], the term $[\cos(\omega_c t) + \hat{\phi}_m]^2$ is always removed by using LPFs and I_{cn} function of machine inductances and HF injected signal characteristics is considered as a constant gain, which is not a strong assumption. In this part, an new approach is proposed to remove LPFs and to avoid inductances knowledge requirement. As it is mentioned in Section 3.2.1.4, It is known that $[\cos(\omega_c t) + \hat{\phi}_m]^2 \geqslant 0$. Also, for all salient pole machines, $-I_{cn} > 0$ because $L_q > L_d$, $V_c > 0$ and $\omega_c > 0$. Consequently the sign of Equation (3.68) σ_p is defined

$$\sigma_p = sign(\varepsilon_p) = sign(\sin(2e_\theta)). \tag{3.69}$$

For all $e_\theta \in [-\frac{\pi}{2};\frac{\pi}{2}]$, σ in (3.69) becomes

$$\sigma_p = sign(e_\theta) \tag{3.70}$$

where $sign(e_\theta)$ is the signum function [177] of the form

$$sign(e_\theta): \begin{cases} 1 \quad \text{if} \quad e_\theta > 0 \\ -1 \quad \text{if} \quad e_\theta < 0 \\ \in [-1,1] \quad \text{if} \quad e_\theta = 0. \end{cases}$$

From (3.70), it is confirmed that the HF component can be removed without using LPF and it can be seen that the new rotor position estimation error σ_p is no longer dependent on machine parameters (L_d, L_q) and injected signal characteristics (V_c, ω_c).

Assumption 3.3.2. *The proposed technique is valid as long as the position error e_θ belong to $[-\frac{\pi}{2};\frac{\pi}{2}]$ (see Figure 3.6). This includes situations when the motor suddenly gets blocked, or slows down due to some unpredictable circumstances, or when the initial rotor position is wrong. so we suppose that $e_\theta \in [-\frac{\pi}{2};\frac{\pi}{2}]$.*

This estimation error σ_p (3.70) is used instead of ε_p as an information in a new tracking algorithm, which has a finite time convergence. This algorithm is the subject of the Chapter 4. In the next section, contributions to demodulation process of the rotating sine-wave injected voltage will be given.

3.4 Rotating sine-wave voltage injection

In this section, a robust rotating wave demodulation strategy is proposed for a self-sensing IPMSM drives. As for the two above self-sensing techniques (pulsating square-wave and sine-wave), this strategy allows to reduce the effects of delays and phase shift and consequently the cost and implementation complexity of the estimation chain. All these assets permit to cover an extended operating range of the machine and improve the self-sensing control of IPMSM.

3.4.1 Rotating sine-wave demodulation process improvements for the error extraction [6]

In this part, an improved demodulation strategy is proposed for a rotating sine wave self-sensing IPMSM drives in order to cover an extended operating range of the machine, reduce the cost and implementation complexity and optimize the estimation precess regarding delays and phase shifts generated by filters, the inverter and sampling time. The proposed contributions for this technique are to

- reduce the filters number, which allows to improve the self-sensing control in terms of delays, cost and implementation complexity.
- estimate the phase shift related to the use of HPF/SFF, inverter effects, sampling time, current sensors sensitivity.
- extract a new position estimation error with reduced harmonics and independently from the knowledge of machine parameters.

3.4.1.1 Rotating sine-wave injected voltage

In this part, the HF injected voltage signal is used, both in two fixed direction, and added to the α,β axes output voltage. The carrier signal in the stator (see Figure 2.5) frame can be expressed as

$$\underline{v_c}^s = V_c e^{j(\omega_c t - \frac{\pi}{2})} = V_c \begin{bmatrix} \sin(\omega_c t) \\ -\cos(\omega_c t) \end{bmatrix}. \tag{3.71}$$

where V_c and ω_c are respectively the magnitude and the carrier frequency of the injected signal.

3.4.1.2 Flux-current resulting from the injected voltage

The stator flux generated by the HF signal injection can be obtained by integrating the injected stator voltage given in Equation (3.71)

$$\underline{\psi_s}^s = \int V_c e^{j(\omega_c t - \frac{\pi}{2})} dt = \frac{V_c}{j\omega_c} e^{j(\omega_c t - \frac{\pi}{2})} = \frac{V_c}{\omega_c} e^{j(\omega_c t - \pi)}. \tag{3.72}$$

From Equations (3.72) and (2.20), the high frequency stator current is expressed by

$$\underline{i_s}^s = \frac{V_c}{\omega_c(L_0{}^2 - L_2{}^2)}(L_0 e^{j(w_c t - \pi)} - L_2 e^{j(2\theta - w_c t + \pi)}). \tag{3.73}$$

The general current expression is given by

$$\underline{i_s}^s = \frac{V_c}{\omega_c(L_0^2 - L_2^2)}(L_0 e^{j(w_c t - \pi)} - L_2 e^{j(2\theta - w_c t + \pi)} + i_{s1}^s \tag{3.74}$$

where,

$$I_{cp} = \frac{L_0 V_c}{\omega_c(L_0^2 - L_2^2)} \tag{3.75}$$

$$I_{cn} = \frac{L_2 V_c}{\omega_c(L_0^2 - L_2^2)} \tag{3.76}$$

and i_{s1}^s are respectively the magnitude of the positive component, the negative component and the fundamental component of the stator current. From Equation (3.74), it can be seen that only the negative current component $I_{cn}e^{j(2\theta - w_c t + \pi)}$ contains the saliency information located in the IPMSM.

3.4.1.3 Step 1: HPF removal for rotating sine-wave HFVI

In the literature [141, 142], the term i_{s1}^s is generally removed by using HPF. This step focus on HPFs removal by using its reference $i_{s,ref}^s$. The control performance supposed to be achieved even in the transient mode. Consequently Equations (3.74) reads

$$\underline{i_{s,HF}^s} = \frac{V_c}{\omega_c(L_0^2 - L_2^2)}(L_0 e^{j(w_c t - \pi)} - L_2 e^{j(2\theta - w_c t + \pi)}. \tag{3.77}$$

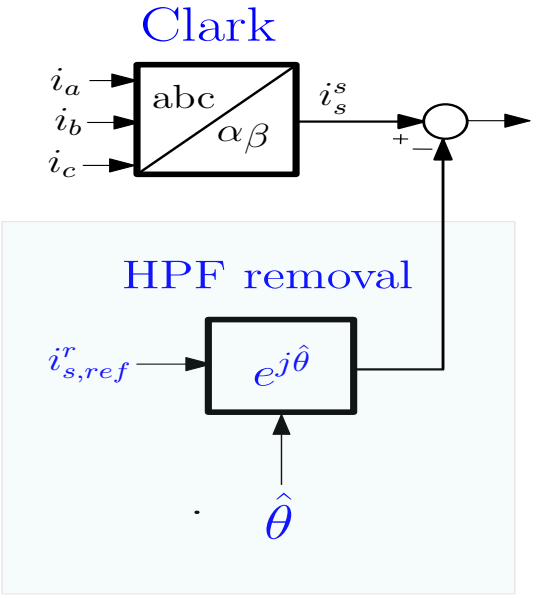

Figure 3.18: HPF removal

3.4.1.4 Step 2: Robust phase shift estimator (RPSE) for rotating sine-wave HFVI

The use of filters produces a phase shift $\phi_{HBF/SFF}$ at the carrier $e^{j(2\theta - w_c t)}$. Moreover, the effects of inverter nonlinearities (dead time, T_{on}, T_{off},...), sampling time, current sensors cause significant delays and phase shift on the rotor position estimation that are not easily predictable. Then, a phase shift estimation algorithm is needed for a correct demodulation in order to improve the rotor position and speed estimation. By taking into account the phase shift in the HF current, the Equation (3.77) can be written

$$\underline{i}_{s,HF}^s = \frac{V_c}{\omega_c(L_0^2 - L_2^2)}(L_0 e^{j(w_c t + \phi_m - \pi)} - L_2 e^{j(2\theta - w_c t + \phi_m + \pi)}. \tag{3.78}$$

and ϕ_m is an unknown phase shift due to previously cited phenomenas (ϕ_{HPF}, ϕ_{LPFs}, $\phi_{Inverter}$ and $\phi_{sampling\ time}$,) on the HF carrier signal, which can be seen on the rotor position estimation error. In this part, a robust phase shift estimator (RPSE) is developed for the rotating sine-wave in order to estimate the phase shift and its time derivative due to the phenomenas cited Figure 3.9. To estimate the phase shift ϕ_m, the expression of $\underline{i}_{s,HF}^s$ given in Equation (3.78) is multiplied by $e^{j(\omega_c t + \pi)}$, which leads to

$$\underline{i_{sc}}^s = \underline{i}_{s,HF}^s e^{j(\omega_c t + \pi)} = \frac{V_c}{\omega_c(L_0^2 - L_2^2)}(L_0 e^{j(2w_c t + \phi_m)} - L_2 e^{j(2\theta + \phi_m + 2\pi)}. \tag{3.79}$$

By applying a HPF to Equation (3.79), one can obtain

$$\underline{i}_{sc,fil}^s = HPF(\underline{i_{sc}}^s) = \frac{V_c}{\omega_c(L_0^2 - L_2^2)}(L_0 e^{j(2w_c t + \phi_m)}). \tag{3.80}$$

$$\underline{i}_{s,\phi}^s = \underline{i}_{sc,fil}^s e^{j(\hat{\phi}_m - 2w_c t)} = \frac{V_c}{\omega_c(L_0^2 - L_2^2)}(L_0 e^{j(\phi_m - \hat{\phi}_m)}). \tag{3.81}$$

The last step consists to use the sign of the imaginary part of (3.81), this allows to

$$\varepsilon_\phi = sign(Im(\underline{i}_{s,\phi}^s)) = sign(I_{cp} sin(e_\phi)) \tag{3.82}$$

where, $e_\phi = \phi_m - \hat{\phi}_m$. It is known that, $I_{cp} > 0$ because $L_q + L_d > 0$, $V_c > 0$ and $\omega_c > 0$. Consequently the sign of imaginary part of (3.82) ε_ϕ is defined

$$\varepsilon_\phi = sign(Im(\underline{i}^s_{s,\phi})) = sign(sin(e_\phi)). \tag{3.83}$$

The Figure 3.19 presents the implementation of RPSE developed in this part.

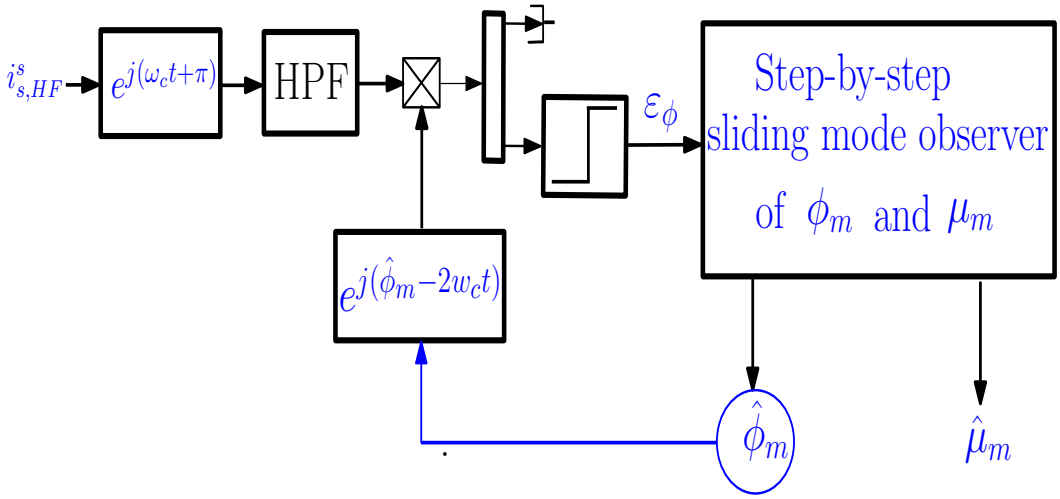

Figure 3.19: RPSE design

For all $e_\phi \in [-\pi;\pi]$, ε_ϕ in (3.83) becomes

$$\varepsilon_\phi = sign(e_\phi) \tag{3.84}$$

where $sign(e_\phi)$ is the signum function [177] of the form

$$sign(e_\phi) : \begin{cases} 1 \quad \text{if} \quad e_\phi > 0 \\ -1 \quad \text{if} \quad e_\phi < 0 \\ \in [-1,1] \quad \text{if} \quad e_\phi = 0. \end{cases}$$

Assumption 3.4.1. *The proposed technique is valid as long as the phase shift error belong to* $\Delta\phi_m \in [-\pi;\pi]$ *(see Figure 3.13).*

The new phase shift estimation error (3.84) is used as an information in a new tracking algorithm, step-by-step which has a in finite time convergence. This algorithm, which is the subject of the next section, aims to estimate the phase shift and its time derivative without knowing machine parameters and HF signal characteristics.

3.4.1.5 Step-by-step sliding mode phase-shift estimator

It can be argued that Equation (3.84) doesn't depend on machine parameters (L_d, L_q), the position estimation error ($\sin(2e_\theta)$) and injected signal characteristics (V_c, ω_c). Only the sign of the phase shift estimation error is required to estimate the phase shift and its time derivative by the proposed (3.85)-(3.86) finite time step-by-step sliding mode observer.

$$\dot{\hat{\phi}}_m = \hat{\mu}_m + K_\phi \varepsilon_\phi \tag{3.85}$$

$$\dot{\hat{\mu}}_m = E_\phi K_\mu sign(\bar{\mu}_m - \hat{\mu}_m) \tag{3.86}$$

where,

$$\bar{\mu}_m = \hat{\mu}_m + K_\phi(\varepsilon_\phi)_{filtred} \tag{3.87}$$

$$E_{\phi_m} : \begin{cases} 1 & \text{if} \quad g(k) = 0 \\ 0 & \text{if} \quad g(k) \neq 0, \end{cases}$$

and, $g(k) = \sum_{k=1}^{4} \varepsilon_\phi(k)$ with $\varepsilon_\phi[k]$ (see Figure 3.14) is the discrete form of the temporal function $\varepsilon_\phi(t)$, k is the delay of one time step by one control period in the discrete domain.

Remark 3.2. *The function $g(k)$ is introduced to detect the chattering phenomenon, because as mentioned before only the sign of the phase shift error is available as an information for the observer.*

3.4.1.6 Stability analysis of the RPSE

The stability analysis of the step-by-step sliding mode observer for phase shift and its dynamic estimation is given in Section 3.3.1.8.

3.4.1.7 Robusteness study of robust phase shift estimator (RPSE)

This part consists of studying the robustness of the RPSE by considering many criteria. For this evaluation, the RPSE algorithm is tested by considering the variation of the gain I_{cp} given by Equation (3.75). Two tests have been effectuated, with and without consider the dynamic variation of the phase shift. From the obtained simulation results given in Figure 3.20, the RPSE converges quickly to the real phase shift in the two cases. This proves that the RPSE is very robust to the phase-shift and the machine inductances variations.

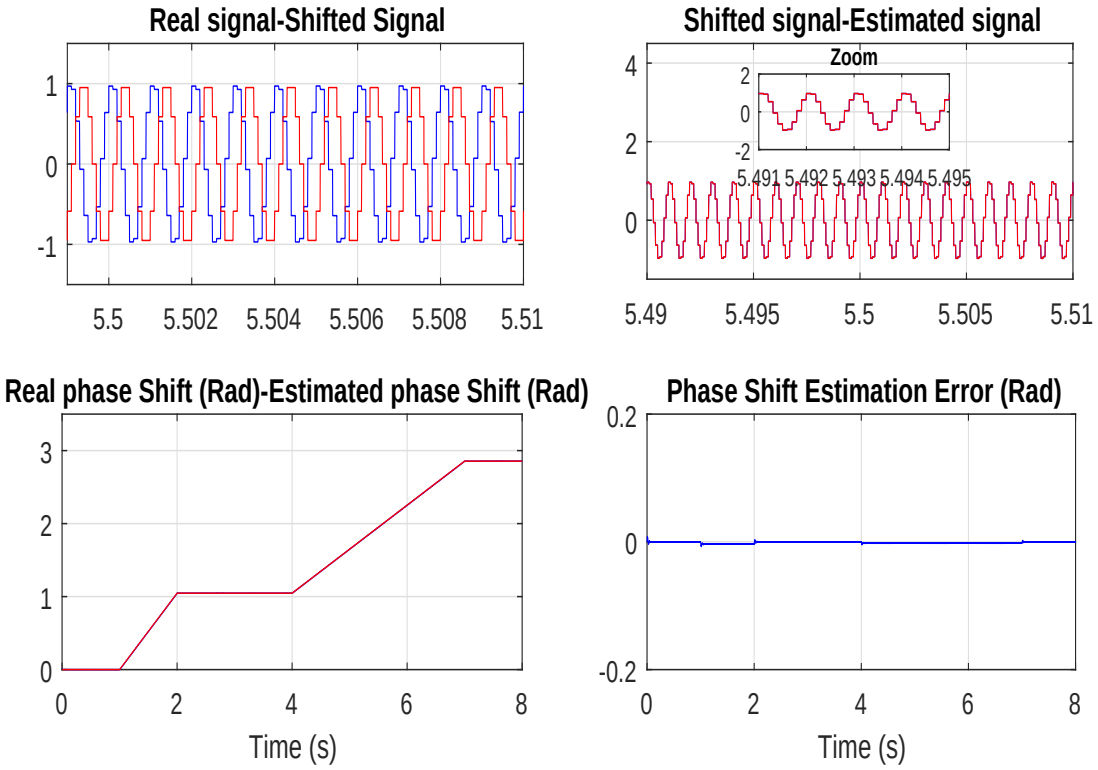

Figure 3.20: simulation results of the RPSE

3.4.1.8 Step 3: Parameters insensitivity and new rotor position estimation error extraction for rotating sine-wave HFVI

In this section a new rotor position estimation error extraction is proposed. Supposing that phase-shift is available, and by multiplying Equation (3.77) by $e^{j(-\omega_c t-\pi-\hat{\phi}_m)}$, one can obtain

$$\underline{i}_{sp}^{s} = \underline{i}_{s,HF}{}^{s} e^{j(-\omega_c t-\pi-\hat{\phi}_m)} = \frac{V_c}{\omega_c(L_0^2-L_2^2)}(L_0 e^{j2\pi} - L_2 e^{j(2\omega_c t+2\theta)} \tag{3.88}$$

where, $\hat{\phi}_m$ is the estimated phase shift obtained by the RPSE.
By applying a HPF to Equation (3.88), one can deduce

$$\underline{i}_{sp\_fil}^{s} = HPF(\underline{i}_{sp}{}^{s}) = -I_{cn} e^{j(2\omega_c t+2\theta)}. \tag{3.89}$$

To remove the HF component from the carrier current in order to extract the rotor position estimation error, Equation (3.89) is multiplied by $e^{j(2\hat{\theta}-2\omega_c t)}$

$$\underline{i}_{s,p}^{s} = \underline{i}_{sp\_fil}^{s} e^{j(2\hat{\theta}-2\omega_c t)} = -I_{cn} e^{j2(\theta-\hat{\theta})}. \tag{3.90}$$

The final rotor position estimation error expression ε is deduce as follows

$$\varepsilon_r = LPF(Im(\underline{i}_{s,p}^{s})) = -I_{cn} sin(2e_\theta). \tag{3.91}$$

where, $\hat{\theta}$ is the estimated rotor position obtained by the robust tracking algorithm given in Chapter 4.
As detailed in Section 3.2.1.4, the term I_{cn} function of machine inductances and HF injected signal characteristics is considered as a constant gain, which is not a strong assumption. In this part, a new approach to avoid inductances knowledge requirement is proposed. It is known that, for all salient pole machines, $-I_{cn} > 0$ because $L_q > L_d$, $V_c > 0$ and $\omega_c > 0$. Consequently the sign of imaginary part of Equation (3.92) σ_r is defined

$$\sigma_r = sign(\varepsilon_r) = sign(sin(2e_\theta)) \tag{3.92}$$

where, $e_\theta = \theta - \hat{\theta}$.
For all $e_\theta \in [-\frac{\pi}{2}; \frac{\pi}{2}]$, σ in (3.92) becomes

$$\sigma_r = sign(e_\theta) \tag{3.93}$$

where $sign(e_\theta)$ is the signum function [177] of the form

$$sign(e_\theta): \begin{cases} 1 \quad \text{if} \quad e_\theta > 0 \\ -1 \quad \text{if} \quad e_\theta < 0 \\ \in [-1,1] \quad \text{if} \quad e_\theta = 0. \end{cases}$$

From Equation (3.93), it is confirmed that the new rotor position estimation error σ_r is no longer dependent on machine parameters (L_d, L_q) and injected signal characteristics (V_c, ω_c).

Assumption 3.4.2. *The proposed technique is valid as long as the position error belong to* $e_\theta \in [-\frac{\pi}{2}; \frac{\pi}{2}]$ *(see Figure 3.6). This includes situations when the motor suddenly gets blocked, or slows down due to some unpredictable circumstances, or when the initial rotor position is wrong.*

This estimation error σ_r (3.93) is used instead of ε_r (3.91) as an information in a new robust tracking algorithm for the self-sensing control of IPMSM which will be given in Chapter 4.

3.5 Conclusion

In this chapter, some contributions have been introduced to improve the existing HFVI techniques. Some contributions can be used for all HFVI techniques, whereas, the others depend on the used injection method. A new strategy is proposed in this chapter to reduce the number of used filters to extract the rotor position estimation error. Hence, the cost and implementation complexity are reduced and filters effect (phase shift and delays) is avoided on the estimation process.

Moreover, robust phase shift estimators are introduced for the pulsating sine-wave and the rotating sine-wave HFVI techniques to estimate delays and phase shifts generated by the inverter non linearity (dead time, T_{off}, T_{on}..etc) used filters (HPF/SFF and LPF) and sampling time (DAC and ADC), the estimator aims to improve the rotor position and speed estimation process.

Furthermore, a new demodulation process is introduced in this chapter for the pulsating square-wave HFVI. The improved technique is insensitive to the electrical and mechanical machine parameters and does not use any filter to extract the rotor position estimation error. These advantages make it a good candidate for self-sensing control of IPMSM. However, this technique generates non negligible acoustic noise and requires sensitive current sensors. To get over the drawbacks of using machine parameters to estimate the rotor position and speed of IPMSM, new rotor position estimation error was extracted is this chapter. These estimation errors (σ_s, σ_p are σ_r) given respectively in (3.22), (3.70) or (3.93) are independent of machine parameters and injected signal characteristics. However, as only the sign of rotor position estimation error is available, the classical tracking algorithms cannot estimate the rotor position and speed, that prompted us to propose new tracking algorithms adapted with new situation. These algorithms are the subject of the next chapter where a novel concept based on sliding mode methodology is introduced. These algorithms aims at

- Estimating the rotor position and speed of AC electrical machines without knowing machine parameters.
- Estimating the acceleration that compensate the speed error in the acceleration phase, i.e. improve the position/speed estimation.
- Robustifying the estimation even in the case of magnetic saturation.
- Extending the error ranges on the position estimation which avoid the estimation of initial rotor position while $e_\theta \in [-\frac{\pi}{2}\,;\frac{\pi}{2}]$.

4

Contribution to rotor position and speed tracking algorithms

This chapter presents the second main contribution of this thesis work from the side of the tracking algorithms of HFVI, intended for zero, low and high speeds operation at different torque ranges. It deals with the analysis and the compensation of position estimation errors, especially those linked to the machine's electrical and mechanical parameters and tuning of the self-sensing algorithm. In the context of EV drives, another critical issue is the torque ripples, primarily due to the accuracy of the rotor position and speed estimation. The proposed improvements in this chapter help in the reduction of these effects. The effectiveness of the claimed contributions is proved by simulation and experimental tests under a drive benchmark which is representative of EV/HEV applications.

4.1 Introduction

As mentioned in the state-of-the-art (Chapter 2), self-sensing control techniques of IPMSM can be classified into three principle categories: model-based methods [157] [159, 160, 161, 162, 163, 164], saliency-based methods [120, 121, 122, 123, 124, 125, 126, 127] and soft-computing methods [157] [159, 160, 161, 162, 163, 164]. Due to the observability problem, model-based methods are only used at medium and high speed ranges. Moreover they are sensitive to parameter variations and unmodeled dynamics. To overcome these limitations, researchers have resorted to the second category which is based on the machine saliency. Compared to the others categories, these techniques offer attractive advantages such as the robustness of the position and speed estimation when the machine is running at low speed (including zero velocity). However, they are still dependent on the knowledge of certain parameters like machine inductances and mechanical parameters [7] [2]. Moreover, these techniques are often validated only over a reduced operating range of the machine, namely the low speed operation. Furthermore, the machine magnetic saturation due to high speed and high torque affects strongly the rotor position/speed estimation process. Several models have been proposed in the literature [45] to deal with the magnetic saturation effects and machine parameters variations. These studies, which take into account an approximate magnetic saturation models [51] are not sufficiently adequate because they are based on numerous assumptions and they depend on machine parameters. As the developed HF

signal injection-based self-sensing control is aimed to ensure critical applications within the EV operation, a high level of performances is requested and the main sources of position estimation errors should be analyzed and efficiently compensated. The main contribution here is then to identify the most impactful of these sources, analyze their effects and propose algorithms and procedures to compensate them. Among these sources and critical problem in the self-sensing context is its dependency of machine parameters, which reduces the robustness of estimators, affects the estimation process. It is regarded as one of the main obstacles to self-sensing industrialization. In literature, several tracking algorithms (phase locked-loop [182], mechanical system observer [183],...) are used to estimate the rotor position and speed of IPMSM based on the extracted rotor position estimation error. The main problem of using these tracking algorithms in self-sensing applications is their dependency on electrical and mechanical parameters that are uncertain and can vary significantly according to several unpredictable effects such as the applied load torque, temperature variations, magnetic circuit saturation, weight, road type and tires quality in automotive applications. Moreover, these algorithms are sensitive to acceleration effects (transient modes). All these barriers affect strongly the performance of the self-sensing control of AC machines. Prompted by this knowledge, this chapter proceeds as follows: In Section 4.3, the classical tracking algorithms used in HFVI for the rotor and speed estimation are recalled. The proposed sliding mode observers used as tracking algorithms for the rotor position and speed estimation are introduced in Sections 4.4.1, 4.4.2 and 4.4.3, respectively. The stability of the proposed sliding mode observers is proven in both transient and steady-state modes. The proposed algorithms coupled with the classical pulsating sine-wave HFVI are tested experimentally showing good performances. A comparative study between the proposed sliding mode observer is conducted in Section 4.4.4 to choose the most appropriate one regarding to acceleration effects and chattering phenomena. Then, a comparative study is performed between the selected A adaptive step-by-step sliding mode observer and the classical tracking algorithms in Section 4.4.5. This comparative study shows the superiority of the selected algorithm in terms of sensitivity to machine parameters and robustness against acceleration effects. Sections 4.5.1, 4.5.2 and 4.5.3 focus on the validation of the selected tracking algorithm without and with demodulation improvements given in Chapter 3 for pulsating sine-wave, pulsating square-wave and rotating sine-wave HF injection techniques. The robustness comparative study between the improved pulsating-sine wave, the improved pulsating sine-wave and the improved rotating-sine wave is discussed in Section 4.6, this study is conducted according to the effect of

- Rotor position and speed estimation error,
- delays caused by filters used, noise generated by the HF of the injected signal,
- acoustic noise and phase shifts generated by sampling time and inverter,
- number of used filters and the implementation complexity.

This section ends by selecting an appropriate self-sensing HF injection technique among the three techniques. The Section 4.7 consist in studying the accuracy of the selected appropriate self-sensing strategy under 0% and 120% step load torque (greater than the nominal torque). The test is performed at zero and high speed in order to check the robustness and efficiency of the selected strategy in critical hard situation.

4.2 Test Bench (http://www2.irccyn.ec-nantes.fr/BancEssai/)

This study takes place in the context of the fully electric vehicle application, where innovative and cost-effective technologies are very welcome. To propose suitable solutions, two prototype IPMSMs tested on a rated power experimental setup are used. This is all the more important that the developed control design should satisfy the specifications dictated by the typical speed-torque EV cycle. Then to perform a robust closed-loop self-sensing operation, an accurate estimation of the rotor position information along the targeted operating area should be provided. At the same

time, it is mandatory to maintain the system efficiency and stability. The test bench (see Figure 4.1-4.2) is made up of a rated 3 kW target IPMSM with an incremental coder as position sensor which is only used for the comparison purpose. A dSPACE board DSP1103 is used to carry out the real time algorithm. The converter is composed of a three-phase IGBT power module from SEMIKRON, a DC-link voltage sensor and protection circuits. IPMSM parameters are shown in Table 4.1. The switching frequency is set to 10 kHz and the sampling period is chosen to be 10^{-4} s. The DC voltage is set to 400 V.

Table 4.1: Motor parameters

Speed	2100 RPM	Torque	$9Nm$
J	7.3 10^{-3} $kg.m^2$	Φ_f	0.33 Wb
R_s	1.4 Ω	L_d	5.7 mH
p	3	L_q	9.9 mH

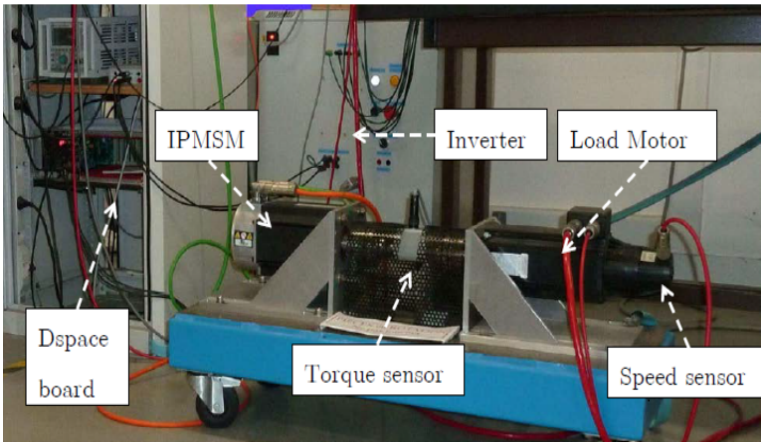

Figure 4.1: Experimental test bench

Figure 4.2: More details of Experimental test bench

In order to evaluate the performance and the effectiveness of the proposed strategy in realistic situation, a representative cycle of drive benchmark shown in Figure 4.3 is considered and the applied torque is shown. These profiles are defined by industrials for automotive applications. It

Table 4.2: Parameters of the control system and characteristics of the HFVI techniques

Inverter switching Frequency	10 kHz	Pulsating sine-wave HF characteristics	$V_c = 10\,V$, $f_c = 1$ kHz
DC bus voltage	400 V	Sampling period	$10^{-4}\,s$
Pulsating square-wave HF characteristics	10 V, 5Khz	Rotating sine-wave HF characteristics	$V_c = 10\,V$, $f_c = 1$ kHz

should be noted that the control that is used is a current control as shown in Figure 2.6. This control is used as a field oriented control where the dq axis current commands i_s^{r*} is imposed by the torque command, the speed control is applied to the load motor (the road profile). The objective is to test the motor in different possible speed/torque ranges. At the beginning, the IPMSM is operated at zero speed and maximum torque which represents a difficult test in automotive applications. From 3.2 s to 4 s, the developed self-sensing strategy is evaluated in nominal speed with nominal torque. Then, the motor is operated in zero speed without torque from 4.9 s to 5.5 s, which allows to evaluate the performance of the developed strategy in critical observability area. The gain I_{cn} defined in Equation (2.27) is a function of the machine inductances, which can vary significantly depending on the operation conditions (temperature variations, magnetic circuit saturation,...) and on injected signal characteristics. As pointed out earlier, the developed self-sensing strategy is independent from machine parameters (mainly inductances and mechanical time-constant mismatches). To highlight this independence, an arbitrary I_{cn} profile (Figure 4.4) and an arbitrary mechanical time-constant (Figure 4.5) are defined.
For simulation tests (to be closer to the realistic situation) a white noise with a magnitude of 0.8 A is added to current measurements. Characteristics of selected HF voltage injection methods (pulsating sine-wave, rotating sine-wave and pulsating square-wave) are given in Table 4.2.

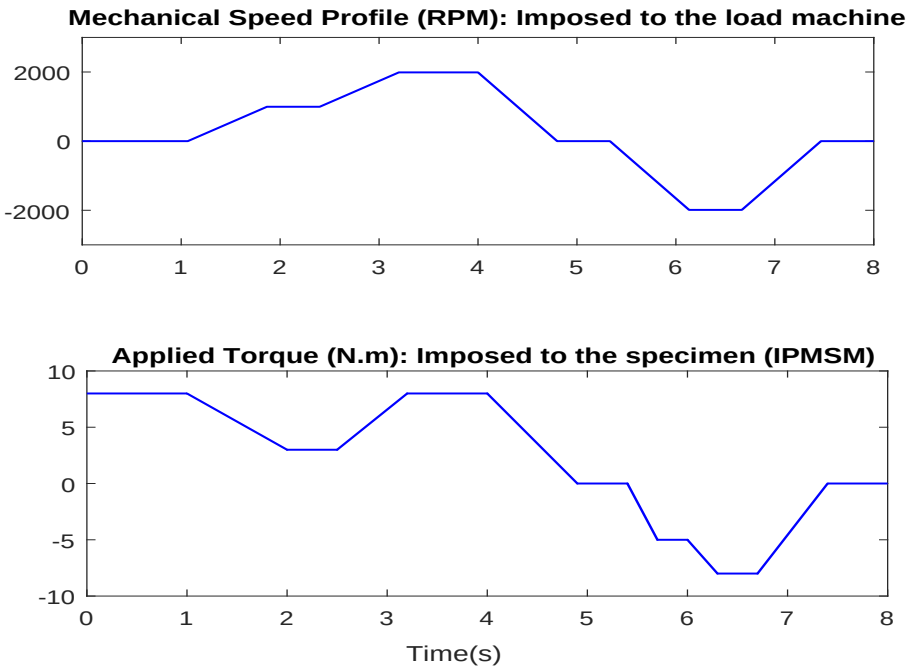

Figure 4.3: Drive benchmark cycle

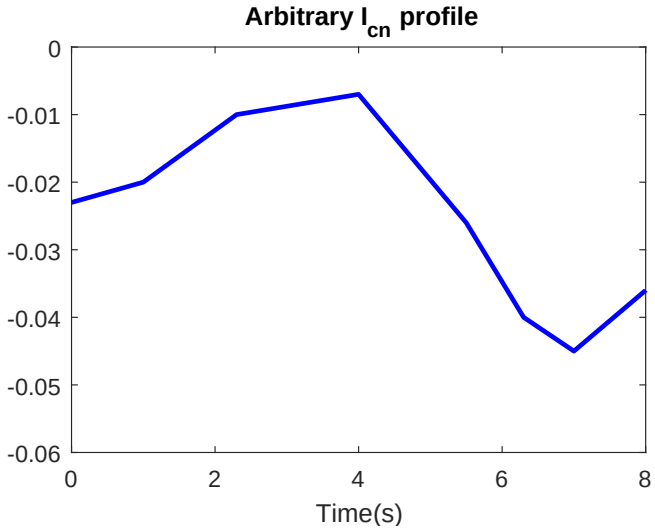

Figure 4.4: Arbitrary I_{cn} profile

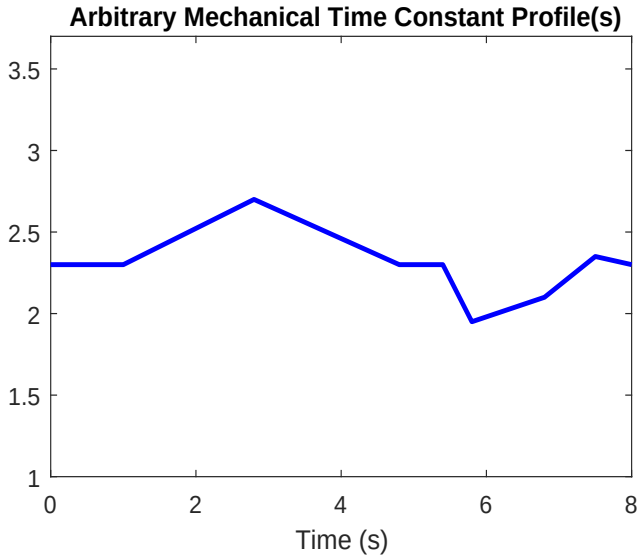

Figure 4.5: Arbitrary mechanical time constant

4.3 Existing tracking algorithms

Numerous tracking algorithms (inverse of tangent [138], the phase locked-loop (PLL) [179] [182], and the mechanical tracking observers (MSO) [183, 184, 185]) can be applied directly after obtaining the rotor position estimation error expression given in Equation (3.68) (in case of the pulsating sine-wave HFVI technique) or in Equation (3.91) (in case of the rotating sine-wave HFVI technique) or in Equation (3.18) (in case of the pulsating square-wave HFVI technique) for every estimation methods in order to minimize the rotor position error. PLLs and MSO are the principle tracking observers used in the literature to estimate the rotor position and speed based on the extracted rotor position estimation. The MSO is the most robust towards measurement noise and less sensitive to the speed variation, however, it requires accurate knowledge of mechanical parameter (Inertia J, frictions K_f) and the load torque T_l. The PLLs can replace the MSO with no need for mechanical parametric knowledge, but it is not well adapted to the variation of the

speed (sensitive to the acceleration). In this section, an overview of theses tracking observers is described.
Several expressions of ε can be obtained. All of them can be presented as a function of the rotor position estimation error defined in Equation (2.33)

$$\varepsilon = f(e_\theta). \tag{4.1}$$

where ε is the current resulting from HFVI technique after the signal processing and demodulation and $e_\theta = \theta - \hat{\theta}$ is the rotor position estimation error.

In the self-sensing control field and as it has been presented in the above sections, ε can be written in the following form [186]

$$\varepsilon = I_{cn} \sin(m(e_\theta)) \tag{4.2}$$

where $I_{cn} = f(L_d, L_q, V_c, \omega_c)$ is an application-specific gain parameter and $m = 2$.
If the rotor position estimation error is considered to be small, ie, $e_\theta \approx 0$, (4.2) can be written as

$$\varepsilon \approx 2 I_{cn} e_\theta. \tag{4.3}$$

4.3.1 Phase-locked loop (PLL) structure in self-sensing control of IPMSM

A PLL, proposed by [179] and studied in [182] [187, 188] is a feedback system that includes a voltage-controlled oscillator (VCO), phase detector (PD), and a LPF. Its purpose is to force the VCO to replicate and track the frequency and phase of the input when in lock. It consists of a control system allowing one oscillator to track with another. It is possible to have a phase offset between input and output, but when locked, the frequency must exactly be tracked. All part of the PLL have an objective on the input signal, the PD produces an error signal that is proportional to the phase error, i.e. to the difference between the phases of input and output signals. The LPF is characterized by a transfer function, it removes the noise and unwanted PD output and determines the dynamics of the PLL. The VCO generates a sinusoidal signal. The PLL observer is one of the principal tracking algorithm used to overcome problems of frequency estimation with periodic signal. It is studied in details in [179] [182]. Using this approach, the speed is considered to be slowly varying with respect to the position ((4.4)-(4.5))

$$\dot{\omega} = 0 \tag{4.4}$$

$$\dot{\theta} = \omega. \tag{4.5}$$

4.3.1.1 Linear PLL design

Based on Equation (4.3), the rotor position and speed estimates can be driven to their true value by the following algorithm

$$\dot{\hat{\omega}} = K_\omega \varepsilon \tag{4.6}$$

$$\dot{\hat{\theta}} = \hat{\omega} + K_\theta \varepsilon. \tag{4.7}$$

By using the expression of ε given in (4.3), (4.6) and (4.7) can be written as

$$\dot{\hat{\omega}} = K_{\omega,p} e_\theta \tag{4.8}$$

$$\dot{\hat{\theta}} = \hat{\omega} + K_{\theta,p} e_\theta. \tag{4.9}$$

where $K_{\omega,p} = 2I_{cn}K_\omega$ and $K_{\theta,p} = 2I_{cn}K_\theta$. Gains ($K_{\theta,p}$ $K_{\omega,p}$) can be tuned by poles placement of a characteristic polynomial system in left half-plane [179] as shown in next part. The PLL observer is illustrated in Figure 4.6

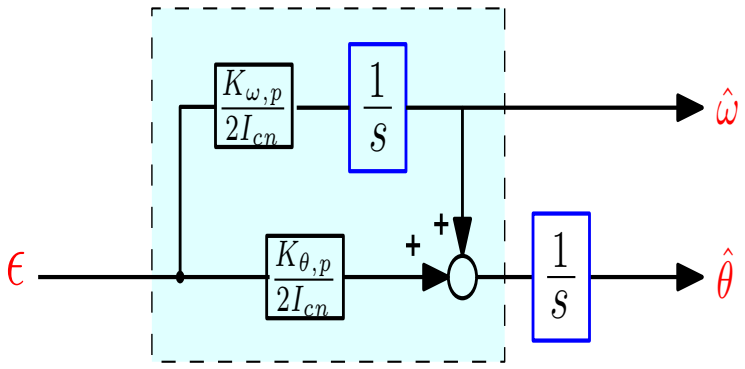

Figure 4.6: PLL design

4.3.1.2 Tuning of linear PLL Estimator

In the frequency (Laplace) domain, the relation between the input and outputs signal are given

$$\hat{\theta} = \frac{1}{s}(\hat{\omega} + K_{\theta,p}(e_\theta)) \tag{4.10}$$

$$\hat{\omega} = \frac{1}{s} K_{\omega,p} e_\theta. \tag{4.11}$$

The transfers function of the linear PLL observer can be written as

$$\frac{\hat{\theta}(s)}{\theta(s)} = \frac{K_{\omega,p}}{s^2 + K_{\theta,p}s + K_{\omega,p}} \tag{4.12}$$

$$\frac{\hat{\omega}(s)}{\theta(s)} = \frac{K_{\theta,p}s + K_{\omega,p}}{s^2 + K_{\theta,p}s + K_{\omega,p}}. \tag{4.13}$$

The characteristic polynomial deduced is

$$D(s) = s^2 + K_{\theta,p}s + K_{\omega,p}. \tag{4.14}$$

Let $-p_1$ and $-p_2$ be the complex poles of the system located in the stable plane (left half), then the characteristic polynomial of theses poles is

$$D(s) = (s+p_1)(s+p_2) = s^2 + (p_1+p_2)s + p_1p_2. \tag{4.15}$$

Therefore, the PLL linear parameter gains can be tuned to

$$K_{\theta,p} = p_1 + p_2 \tag{4.16}$$

$$K_{\omega,p} = p_1p_2. \tag{4.17}$$

One choice is to place both poles at $-p$, where p is a positive constant, to avoid oscillations

$$K_{\theta,p} = 2p \tag{4.18}$$

$$K_{\omega,p} = p^2. \tag{4.19}$$

Nevertheless, complex conjugated poles can be set in order to improve the dynamics of the observer, by shaping a well damped oscillating response. In this case, the denominator can be written with the following form

$$D(s) = s^2 + 2\zeta\omega_n s + \omega_n^2 \tag{4.20}$$

where ω_n is the bandwidth of the observer and ζ defines the damping ratio. In this case, the PLL parameter gains can be tuned to

$$K_{\theta,p} = 2\zeta\omega_n \tag{4.21}$$

$$K_{\omega,p} = \omega_n^2. \tag{4.22}$$

According to this analysis, the PLL parameters $K_{\theta,p}$ and $K_{\omega,p}$ are chosen according to Table 4.3

Table 4.3: PLL parameters tuning for the self-sensing control.

$K_{\theta,p}$, $K_{\omega,p}$	30, 750

4.3.1.3 Tuning of nonlinear PLL observer

In the case where the rotor position estimation error signal is a non linear function (4.2), the PLL observer becomes a non linear observer where it's dynamic is given by

$$\dot{\hat{\theta}} = \hat{\omega} - K_{\theta,1}\sin(2e_\theta) \tag{4.23}$$

$$\dot{\hat{\omega}} = -K_{\omega,1}\sin(2e_\theta), \tag{4.24}$$

where $K_{\omega,1} = K_\omega I_{cn}$ and $K_{\theta,1} = K_\theta I_{cn}$.
Consider (4.25)–(4.26) the rotor position estimation errors between observer (4.24)–(4.23) and system (4.4)–(4.5)

$$e_\theta = \theta - \hat{\theta} \tag{4.25}$$

$$e_\omega = \omega - \hat{\omega}. \tag{4.26}$$

whose dynamics are given by

$$\dot{e}_\theta = e_\omega - K_{\theta,1}\sin(2e_\theta) \tag{4.27}$$

$$\dot{e}_\omega = -K_{\omega,1}\sin(2e_\theta). \tag{4.28}$$

Theorem 4.3.1. *For any bounded $K_{\omega,1} > 0$ and $K_{\theta,1} > 0$ the rotor position and speed observers given by equations (4.23) and (4.24), respectively are asymptotically stable [179].*

Proof: Let $K_{\omega,1}$ and $K_{\theta,1}$ satisfying theorem conditions. The stability of the rotor position and speed estimation error dynamics (4.27) and (4.28) is analyzed. Considering the following candidate Lyapunov function $V(e_\omega, e_\theta)$

$$V(e_\omega, e_\theta) = \beta e_\omega^2 + \alpha(1 - \cos(2e_\theta)) \tag{4.29}$$

where, α and β are both positive constants, then the Lyapunov function $V(e_\omega, e_\theta) > 0$ for $e_\omega \neq 0$ and $e_\theta \neq \pi n$. Furthermore $V(0, \pi n) = 0$. One proves the attractivity of V as follows

$$\dot{V} = -2K_{\omega,1}\beta e_\omega \sin(2e_\theta) + 2\alpha\sin(2e_\theta)[e_\omega - K_{\theta,1}\sin(2e_\theta)]. \tag{4.30}$$

Then, it can be written as

$$\dot{V} = -2K_{\omega,1}\beta e_\omega \sin(2e_\theta) + 2\alpha \sin(2e_\theta)e_\omega - K_{\theta,1}2\alpha[\sin(2e_\theta)]^2. \tag{4.31}$$

To get a negative time derivative Lyapunov function, let's take: $\beta = 1$ and $\alpha = K_{\omega,1}$, then the previous equation becomes

$$\dot{V} = -K_{\theta,1}K_{\omega,1}[\sin(2e_\theta)]^2 \leq 0. \tag{4.32}$$

$\dot{V}$ is negative if $K_{\theta,1}$ and $K_{\omega,1}$ have the same sign. So V chosen is a Lyapunov function. When, $\dot{V} = 0 \Longrightarrow \sin[2e_\theta]^2 = 0 \Longrightarrow e_\theta = \pi n \Longrightarrow e_\omega = 0$, According to LaSalle's invariance principle, the rotor position an speed estimation are asymptotically stable.

4.3.2 Mechanical system observer (MSO) structure in self-sensing control of IPMSM

This observer proposed by [165] and studied in [183, 184, 185] is based on the mechanical system model shown in Figure 4.7. The expression of position error can be used as an input of MSO, if mechanical parameters of the machine are well known, which is not the case in reality. The tuning of MSO is detailed in [183] [189]. In addition, the mechanical observer can incorporate the load torque as a feed-forward term to improve dynamic response. The MSO is a closed loop PID controller combined with the mechanical parameters of the system. The PID controller is derived from the machine parameter such as inertia and frictions. The dynamic properties of the mechanical observer are defined by its mechanical coefficients K_p K_i and K_d. The advantage of using a PID controller is that the estimation noise is reduced because its transfer function acts as a LPF and the quality of estimation is improved. The torque is added as a feed forward input to the mechanical observer and this provides zero lag and the estimation error can be effectively minimized to zero [165]. The mechanical behavior is governed by the Newton's second law as follows

$$J\frac{d\omega}{dt} + K_f\omega = T_m - T_l. \tag{4.33}$$

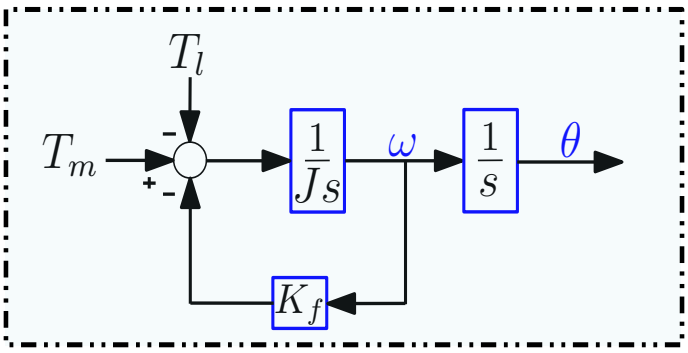

Figure 4.7: Mechanical system model

4.3.2.1 Mechanical system model analysis

The mechanical system of the motor system can be represented as shown in Figure 4.7. The variation of the disturbance load torque can be considered as zero. The state equation of the mechanical system can be written as

$$\dot{x} = A\,x + B\,u, \quad y = c\,x, \tag{4.34}$$

where,

$$x = [\theta \quad \omega \quad T_l]^T \qquad u = T_m \qquad y = \theta, \tag{4.35}$$

and

$$A = \begin{bmatrix} 0 & 1 & 0 \\ 0 & -\frac{K_f}{J} & -\frac{1}{J} \\ 0 & 0 & 0 \end{bmatrix}, \qquad B = [0 \quad \frac{1}{J} \quad 0]^T, \qquad C = [1 \quad 0 \quad 0]. \tag{4.36}$$

4.3.2.2 Observability analysis

The mechanical system is observable since the following observability matrix is full rank

$$Ob = \begin{bmatrix} C \\ CA \\ CA^2 \end{bmatrix} = \begin{bmatrix} 1 & 0 & 0 \\ 0 & 1 & 0 \\ 0 & -\frac{K_f}{J} & -1/J \end{bmatrix}. \tag{4.37}$$

4.3.2.3 Mechanical Observer Design

The MSO is described by the following equations

$$\dot{\hat{\theta}} = \hat{\omega} + K_\theta \varepsilon \tag{4.38}$$

$$\dot{\hat{\omega}} = \frac{1}{J}[T_m - \hat{T}_l - K_f \hat{\omega}] + K_\omega \varepsilon \tag{4.39}$$

$$\dot{\hat{T}}_l = K_T \varepsilon. \tag{4.40}$$

By using the expression of ε given in Equation (4.3), (4.38)-(4.40) can be written as

$$\dot{\hat{\theta}} = \hat{\omega} + K_{\theta,2} e_\theta \tag{4.41}$$

$$\dot{\hat{\omega}} = \frac{1}{J}[T_m - \hat{T}_l - K_f \hat{\omega}] + K_{\omega,2} e_\theta \tag{4.42}$$

$$\dot{\hat{T}}_l = K_{T,2} e_\theta. \tag{4.43}$$

where, K_θ, K_ω and K_T are the observer gains, $K_{\theta,2} = 2I_{cn}K_\theta$, $K_{\omega,2} = 2I_{cn}K_\omega$ and $K_{T,2} = 2I_{cn}K_T$. Gains $(K_{\theta,2}, K_{\omega,2}, K_{T,2})$ are identify in such a way as to render the characteristic polynomial stable [183], These parameters describe the parameters of the PID regulator as shown in Figure (4.8).

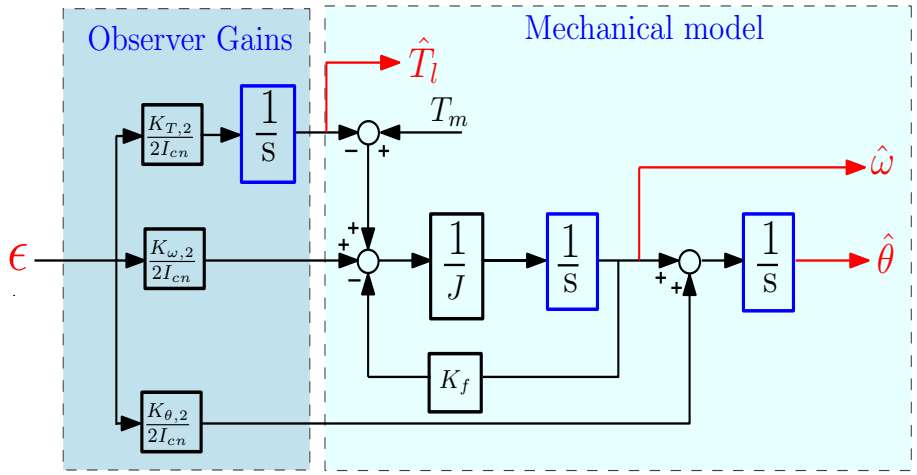

Figure 4.8: MSO design

Suppose that $K_f \approxeq 0$, then, in the frequency (Laplace) domain, the relation between the input and outputs signal are

$$\frac{\hat{\theta}(s)}{\theta(s)} = \frac{K_{\theta,2}s^2 + K_{\omega,2}s - \frac{K_{T,2}}{J}}{s^3 + K_{\theta,2}s^2 + K_{\omega,2}s - \frac{K_{T,2}}{J}} \tag{4.44}$$

$$\frac{\hat{\omega}(s)}{\theta(s)} = \frac{K_{\omega,2}s^2 - \frac{K_{T,2}}{J}s}{s^3 + K_{\theta,2}s^2 + K_{\omega,2}s - \frac{K_{T,2}}{J}} \tag{4.45}$$

$$\frac{\hat{T}_l(s)}{\theta(s)} = \frac{K_{T,2}s^2}{s^3 + K_{\theta,2}s^2 + K_{\omega,2}s - \frac{K_{T,2}}{J}} \quad . \tag{4.46}$$

The characteristic polynomial deduced is

$$D(s) = s^3 + K_{\theta,2}s^2 + K_{\omega,2}s - \frac{K_{T,2}}{J}. \tag{4.47}$$

4.3.2.4 Stability analysis

By applying Routh criteria, the transfer function of MSO is stable if its characteristic polynomial is Hurwitz, this can be seen as

$$a_n > 0 \qquad \forall n \tag{4.48}$$

$$a_1 a_2 > a_0\, a_1 \tag{4.49}$$

where a_n for $n = 1, 2...$, are the coefficient of the characteristic polynomial, which gives

$$K_{\theta,2} > 0 \tag{4.50}$$

$$K_{\omega,2} > 0 \tag{4.51}$$

$$K_{T,2} < 0 \tag{4.52}$$

$$K_{\omega,2}K_{\theta,2} < \frac{|K_{T,2}|}{J}. \tag{4.53}$$

4.3.2.5 Tuning of the MSO

The observer is stable if the denominator is Hurwitz. Denoting the characteristic polynomial equation as $D(s)$ given as

$$D(s) = s^3 + K_{\theta,2}s^2 + K_{\omega,2}s - \frac{K_{T,2}}{J}. \tag{4.54}$$

The desired characteristic polynomial is

$$D(s) = (s + r_1)(s + r_2)(s + r_3) \tag{4.55}$$

where r_1, r_2 and r_3 are desired poles that could be placed in the stable plan (left half). Then, one gets

$$D(s) = s^3 + (r_1 r_2 + r_2 r_3 + r_3 r_1)s^2 + (r_1 + r_2 + r_3)s + r_1 r_2 r_3. \tag{4.56}$$

Therefore the gains of the MSO can be tuned to

$$K_{\theta,2} = r_1 + r_2 + r_3, \tag{4.57}$$

$$K_{\omega,2} = r_1 r_2 + r_2 r_3 + r_1 r_3, \tag{4.58}$$

$$K_{T,2} = -J r_1 r_2 r_3. \tag{4.59}$$

The observer can be seen as a PID controller for the mechanical system model, the controller gains are

$$K_p = J K_\omega = J(r_1 r_2 + r_2 r_3 + r_1 r_3) \tag{4.60}$$

$$K_i = -K_{T,2} = J r_1 r_2 r_3 \tag{4.61}$$

$$K_d = K_{\theta,2} = r_1 + r_2 + r_3. \tag{4.62}$$

According to this stability analysis, parameters $K_{\theta,2}$, $K_{\omega,2}$, $K_{T,2}$ are chosen with respect to Table 4.4.

Table 4.4: Parameters tuning of MSO the self-sensing control.

K_θ, K_ω, K_T	250, 110, 50

4.4 Proposed algorithms

Existing tracking algorithms (the inverse of tangent [138], the PLL [179] [182], and the mechanical observer [183, 184, 185]) are used to estimate the rotor position/speed based on the rotor position error ε (ε_s or ε_p or ε_r) given respectively in Equations (3.18), 3.68) or (3.91). However, this error expression depends on the knowledge of the current negative sequence I_{cn} defined in (3.19). As I_{cn} depends both on machine parameters (inductances L_d, L_q in (2.13)) and injected signal characteristics (magnitude V_c and frequency ω_c in (3.19)), all these tracking algorithms are sensitive to I_{cn} variations (due to the magnetic saturation). Moreover, the mechanical observer requires the good knowledge of mechanical parameters (Inertia J, frictions K_f...) and the load torque, these parameters vary significantly according to several unknown factors. PLLs are also not adapted to high speed variations (sensitive to the machine acceleration). The rotor position/speed estimation in all speed/torque ranges and independently of machine parameters (inductances, inertia...) and injected signal characteristics (magnitude and frequency) is still an open problem. The proposed strategy describes a new method for the rotor estimation extraction error. This sign of the rotor estimation error σ (σ_s or σ_p or σ_r) given respectively in (3.22), (3.70) or (3.93) is used instead of ε (ε_s, ε_p or ε_r) as an information in a new tracking algorithm, which has a finite-time convergence. This algorithm, which is the subject of this chapter, aims at

- Estimating the rotor position, speed and acceleration of AC electrical machines without knowing machine parameters. This allows to robustify the estimation even in the case of magnetic saturation.
- Estimating the acceleration. This allows to compensate the speed error in the acceleration phase, and consequently to improve the position/speed estimation in transient modes.
- Extending the error ranges on the position estimation, which avoids the estimation of initial rotor position while $e_\theta \in [-\frac{\pi}{2}; \frac{\pi}{2}]$.
- Improving the estimation process by considering the gains adaptation in both transient and steady-sate modes. This allows to reduce chattering effects.

The novelty of the proposed strategy [7] [2] consists in using only the sign of the position error in the correction term of the estimation algorithm, instead of using the position error ε defined in Equation (3.31)

$$\sigma = sign(-I_{cn} sin(2e_\theta)) = sign(-I_{cn}) sign(sin(2e_\theta)). \tag{4.63}$$

In general case $-I_{cn} > 0$ because $L_q > L_d$, then (4.63) can be written as follows

$$\sigma = sign(sin(2e_\theta)). \tag{4.64}$$

For all $e_\theta \in [-\frac{\pi}{2}; \frac{\pi}{2}]$, σ in (4.64) becomes

$$\sigma = sign(e_\theta). \tag{4.65}$$

where $sign(e_\theta)$ is the signum function [177] of the form

$$sign(e_\theta) : \begin{cases} 1 \quad \text{if} \quad e_\theta > 0 \\ -1 \quad \text{if} \quad e_\theta < 0 \\ \in [-1,1] \quad \text{if} \quad e_\theta = 0 \end{cases}$$

The proposed technique is valid as long as the position error belong to $e_\theta \in [-\frac{\pi}{2}; \frac{\pi}{2}]$. This includes situations when the motor suddenly gets blocked, or slows down due to some unpredictable circumstances, or when the initial rotor position is wrong (see Figure 3.6).
This chapter presented a novel approach for tracking algorithms associated to HFVI technique in order to estimate the rotor position of self-sensing AC salient pole machines.
The main benefit of this approach is to use only the sign of the rotor position estimation error as known information instead of the rotor position estimation error used by the classical tracking algorithms. By having only the sign of the rotor position estimation error as known information, the first order sliding mode observer is the natural solution to estimate the rotor position.
From this point of view, this chapter proposed some improved alternative tracking algorithms based first-order sliding mode methodology. Among them the step-by-step sliding mode observer with constant and adaptive gains.

4.4.1 Sliding mode observer (SMO) for the rotor and speed estimation [7, 8]

The control and observation strategy based on sliding mode control is known for its strong robustness against parametric uncertainties and external disturbances [190, 191, 192, 193, 194, 195, 196]. The SMO methodology is first proposed by Slotine and Walcott in the middle of 1980s [191]. Since then, the SMO technique has been widely investigated by researchers in control engineering and applied to the state estimations [191], parameter monitoring [190], fault detections and reconstruction of input fault signals [195] for many industrial systems. It has been noted that, in most recent industrial applications, the sliding observer methodology has been extensively adopted to develop the online estimation software with the excellent performance against uncertainties and disturbances [197]. Owing to the strong robustness property, SMOs are particularly suitable for the industrial systems with complex nonlinearities and large uncertain dynamics [198].
In this section, a robust SMO (tracking algorithm) for speed and position estimation of AC drive motors (not limited to IPMSM) is presented including its design, analysis, applications and its implementations. The algorithm is based on first SMO since only the sign of the rotor position estimation error (4.65) is available for measurement and it is shown ideally to be globally stable with a finite-time convergence. The algorithm can be also used in other applications like for

example frequency and position estimation of electrical grids. This estimation error σ (4.65) is used instead of ε given in (3.18), 3.68) or (3.91) as an information in a new tracking algorithm, which has a finite-time convergence and it doesn't depend on any electrical and mechanical machine parameters (L_d, L_q, J, K_f, ...) and injected signal characteristics (V_c, ω_c).

4.4.1.1 Observer design

Only the sign of the position error is required to estimate the rotor position/speed of IPMSM by the proposed (4.66)-(4.67) SMO

$$\dot{\hat{\omega}} = K_\omega \sigma \tag{4.66}$$
$$\dot{\hat{\theta}} = \hat{\omega} + K_\theta \sigma \tag{4.67}$$

where θ and ω are respectively the position and the speed, and σ is defined in equation (4.65). $K_\theta > 0$ and $K_\omega > 0$ are constant gains. The implementation of the proposed SMO for the self-sensing control of AC drive machine is shown in Figure 4.9.

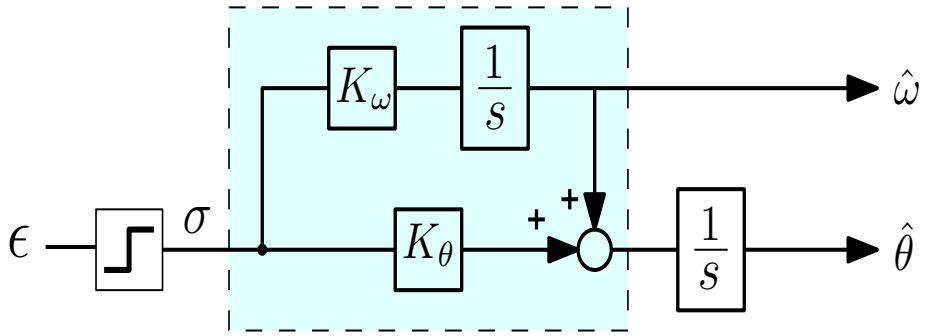

Figure 4.9: SMO design

The mechanical double integrator system of position/speed which is used to design the observer (4.66)-(4.67) is given by

$$\dot{\omega} = 0 \tag{4.68}$$
$$\dot{\theta} = \omega. \tag{4.69}$$

4.4.1.2 Stability analysis

Let be (4.70)-(4.71) the position and the speed estimation errors between system (4.68)-(4.69) and observer (4.66)-(4.67)

$$e_\omega = \omega - \hat{\omega} \tag{4.70}$$
$$e_\theta = e_\theta \tag{4.71}$$

whose dynamics are given by

$$\dot{e}_\omega = -K_\omega \sigma \tag{4.72}$$
$$\dot{e}_\theta = e_\omega - K_\theta \sigma. \tag{4.73}$$

Theorem 4.4.1. *Consider the speed ω slowly variable. Then, (4.66)-(4.67) is a finite-time observer of (4.68)-(4.69) for $K_\omega > 0$ and $K_\theta > max(|e_\omega|)$. Moreover, the convergence to zero of position and speed estimation errors (4.72)-(4.73) is ensured in finite-time.*

Proof: The first step is to analyze the stability of the position estimation error dynamic (4.73). For that let consider the following candidate Lyapunov function V_θ

$$V_\theta = \frac{1}{2}e_\theta^2 \tag{4.74}$$

whose derivative reads

$$\begin{aligned} \dot{V}_\theta &= e_\theta \dot{e}_\theta = e_\theta(e_\omega - K_\theta sign(e_\theta)) \\ &= e_\theta e_\omega - e_\theta K_\theta sign(e_\theta) \leqslant |e_\theta||e_\omega| - K_\theta|e_\theta| \end{aligned} \tag{4.75}$$

Le be

$$K_1 = -|e_\omega| + K_\theta > 0 \tag{4.76}$$

then (4.75) can be written as

$$\dot{V}_\theta \leq -K_1|e_\theta| \tag{4.77}$$

which implies that the position estimation error e_θ (4.71) converges to zero in finite-time $t_1 > 0$ and for all $t \geq t_1$, one has

$$\dot{e}_\theta = e_\theta = 0. \tag{4.78}$$

Expression (4.78) means that the sliding condition is reached. Right now, by using condition (4.78) ($\dot{e}_\theta = 0$) in (4.73), one has

$$e_\omega = K_\theta sign(e_\theta). \tag{4.79}$$

It can be seen from (4.76) that $K_\theta > 0$, one can deduce

$$sign(e_\omega) = sign(e_\theta) \tag{4.80}$$

Therefore, one call the equation (4.80) as the "sign propagation rule".
Similarly, the stability of the speed estimation error dynamic (4.72) can be analyzed. Let us define the following candidate Lyapunov function

$$V_\omega = \frac{1}{2}e_\omega^2 \tag{4.81}$$

By taking into account (4.80) in (4.72), the time derivative of (4.81) is given by

$$\dot{V}_\omega = e_\omega \dot{e}_\omega = -K_\omega e_\omega sign(e_\omega) \tag{4.82}$$

that becomes

$$\dot{V}_\omega \leq -K_\omega|e_\omega| \tag{4.83}$$

where K_ω is a positive constant. This implies that the speed estimation error e_ω converges to zero in finite-time $t_2 > t_1$ for all $t \geq t_2$.
From (4.83) and (4.77), the finite-time convergence of the proposed SMO (4.66)-(4.67) is obtained. This ends the proof.

4.4.1.3 Parameters tuning

– Parameters K_θ and K_ω are chosen according to the previous stability in order to ensure the convergence of the first SMO. Their values for the next section are given in Table 4.5. K_θ should dominate the speed maximum error and K_ω should be positive.

Table 4.5: Parameters tuning of for the self-sensing control.

K_θ, K_ω	250, 110

4.4.1.4 Results of the proposed SMO coupled with the classical pulsating sine-wave HFVI

Experimental results (Figure 4.10) of the SMO coupled with the pulsating sine-wave HFVI show the evolution of following quantities: the measured and the estimated mechanical speeds, the mechanical speed estimation error, the measured and the estimated electrical positions and the electrical position estimation error. It can be seen that

- Convenient rotor position and speed estimation results are obtained in all speed/torque ranges even in difficult situations mentioned on the cycle of drive benchmark.
- A transient position and speed estimation error is shown, this error is due to the acceleration that is not considered and the phase shift generated by several sources such as filters, inverter, DAC and ADC.
- A chattering effect that can be seen on both rotor position and speed estimation error is generated by the sign function and the HF signal injection. The chattering is reduced by the forth order LPF used, this later, generates delays on the estimation process.

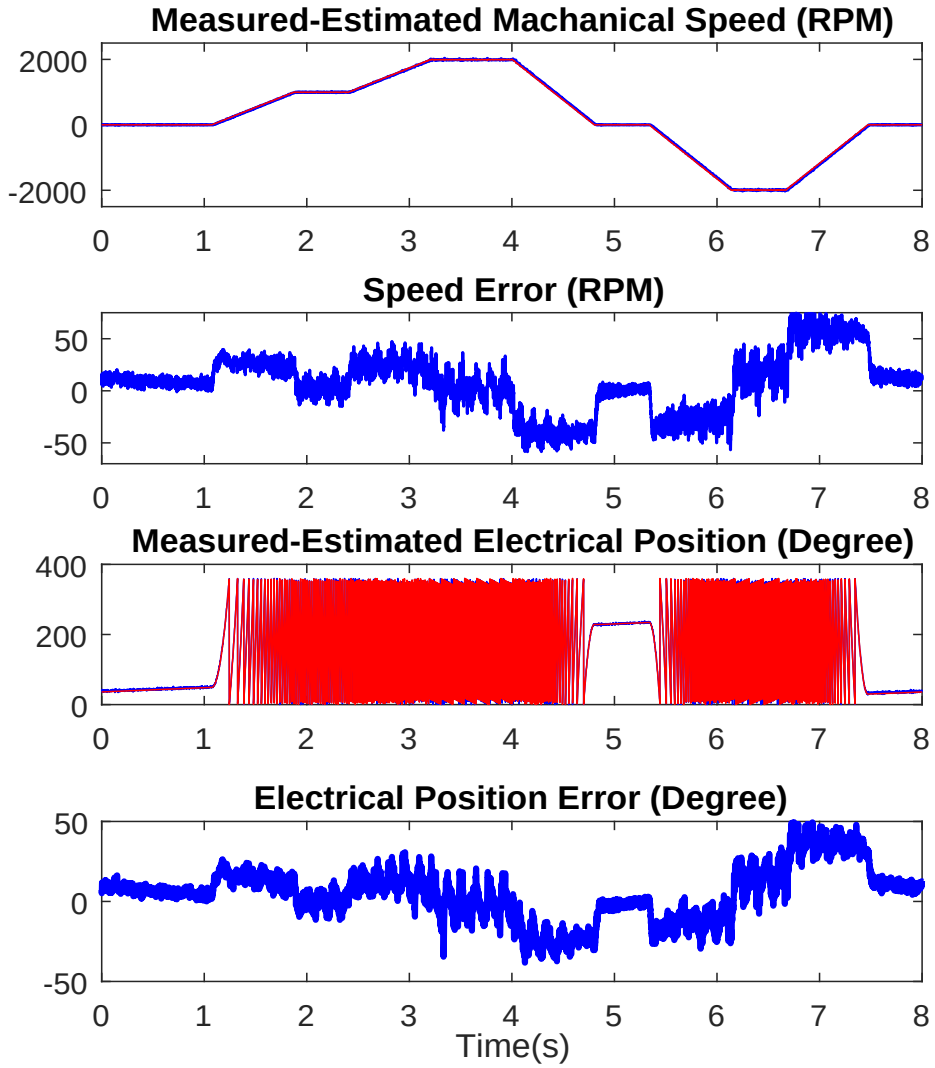

Figure 4.10: Experimental Results of the proposed SMO coupled with the classical pulsating sine-wave HFVI

As a conclusion, acceptable results are obtained in experiments (Figure 4.10) at different speed/torque ranges. Despite advantages of this strategy, it has some limitations mentioned above (the machine acceleration not taken into account, chattering phenomenon and phase shifts

on the estimated quantities). In the next section, an improved SMO is proposed to remedy the mentioned limitations.

4.4.2 Step-by-step sliding mode observer (S-B-S SMO) for the rotor position, speed and acceleration estimation [9, 10]

A robust and finite-time exact differentiator based on the step-by-step sliding mode observer [199] was introduced and applied in this section. Note that the machine acceleration is estimated to compensate the rotor position and speed estimation errors in transient modes and to improve performance compared to traditional techniques. The S-B-S SMO consists of the gradual convergence of the observation error to zero [200]. At each step of the algorithm, the sliding corrective term is applied, which is only a function of the states known at this step in order to obtain, after a finite-time, a convergence of some other observation error components to zero. This kind of S-B-S SMO is very useful and was developed for many reasons as

- to work with reduced observation error dynamics,
- to obtain a step-by-step design,
- to ensure a finite-time convergence for all observables states,
- to design, under some conditions, an observer for nonsmooth systems, and
- to ensure a robustness under parameter variations, if the condition (dual of the well-known matching condition) is verified.

The function σ (4.65) is used by the S-B-S SMO to estimate the position, speed and the acceleration of the IPMSM without knowing machine parameters and to achieve the tuning of position, speed and acceleration observer gains in a decoupled manner.

4.4.2.1 Observer design

Based on the sign of rotor position estimation error (4.65), finite-time S-B-S SMO (4.84)-(4.86) is proposed to estimate the rotor position, speed and acceleration of IPMSM.

$$\dot{\hat{\theta}} = \hat{\omega} + K_\theta \sigma \tag{4.84}$$

$$\dot{\hat{\omega}} = (\hat{\alpha} + E_1 K_\omega sign(\bar{\omega} - \hat{\omega})) \tag{4.85}$$

$$\dot{\hat{\alpha}} = E_2 (K_\alpha sign(\bar{\alpha} - \hat{\alpha})) \tag{4.86}$$

where,

$$\bar{\omega} = \hat{\omega} + K_\theta (\sigma)_{filtred} \tag{4.87}$$

$$\bar{\alpha} = \hat{\alpha} + K_\omega sign(\bar{\omega} - \hat{\omega}) \tag{4.88}$$

$$E_1 : \begin{cases} 1 & \text{if} \quad g(k) = 0 \\ 0 & \text{if} \quad g(k) \neq 0, \end{cases} \tag{4.89}$$

$$E_2 : \begin{cases} 1 & \text{if} \quad E_1 = 1 \quad \text{and} \quad \bar{\omega} - \hat{\omega} = 0 \\ 0 & \text{if} \quad \text{whereas}, \end{cases} \tag{4.90}$$

and

$$g(k) = |\sum_{k=1}^{2} \sigma(k)| + |\sum_{k=2}^{3} \sigma(k)| + |\sum_{k=3}^{4} \sigma(k)| \tag{4.91}$$

shown in Figure 4.11 with $\sigma[k]$ is the discrete form of the temporal function $\sigma[t]$, k is the delay of one time step by one control period in the discrete domain.

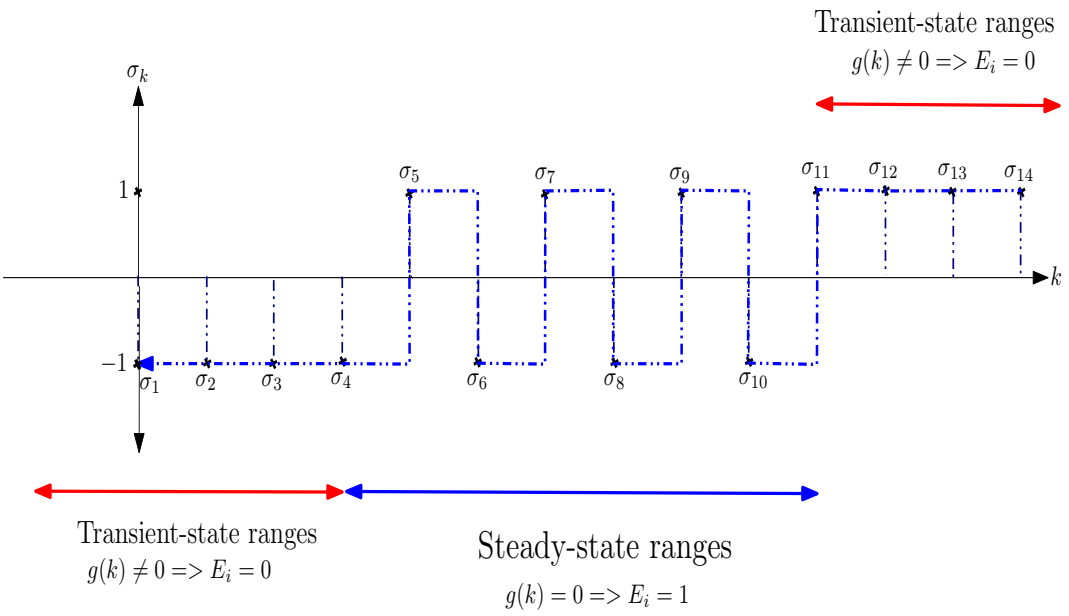

Figure 4.11: Chattering detector

Remark 4.1. *The function $g(k)$ is introduced to detect the chattering phenomena (steady-state ranges) in order to validate the estimation of the observer first step and then go to the next step. The next estimation step is validated only if the first step has converged. This allows to use the estimation variable of the first step as a virtual measurement to estimate the variable of the next step, and so on. The reason is to detect the chattering phenomenon. When $g(k) = 0$, the function $\sigma(k)$ changed the sign twice, which is the mark for the finite-time convergence of the rotor position estimation error for $t > t_1$. This means that the steady-state behavior of the position estimation is reached. At this moment t_1, E_1 takes the value 1 allowing to attack the second step. If for example this upper bound of summation is chosen less than 4, the periodicity of $g(k)$ is not established and the position estimation step is still in transient mode.*

The proposed virtual system for the observer design (4.84)–(4.86) is given as follows

$$\dot{\theta} = \omega \tag{4.92}$$
$$\dot{\omega} = \alpha \tag{4.93}$$
$$\dot{\alpha} = 0. \tag{4.94}$$

Remark 4.2. *Usually, in the literature, the rotor speed is considered constant (as done in the design of observer (4.66)-(4.67)), leading to decreased estimation performance in transients. When dynamics of rotor speed are taken into account, mechanical parameters must be well known. The proposed virtual system (4.92)–(4.94) makes it possible to overcome limitations of accurate knowledge of mechanical parameters. Additionally, the constant speed assumption is not needed by taking into account the acceleration of the machine in the estimation process. All these assets allow to improve the rotor position and speed estimation in transients modes.*

4.4.2.2 Stability analysis

Consider (4.95) –(4.97) the position, the speed and the acceleration estimation errors between observer (4.84)–(4.86) and system (4.92)–(4.94)

$$e_\theta = \theta - \hat{\theta} \tag{4.95}$$

$$e_\omega = \omega - \hat{\omega} \tag{4.96}$$

$$e_\alpha = \alpha - \hat{\alpha} \tag{4.97}$$

whose dynamics are given by

$$\dot{e}_\theta = e_\omega - K_\theta \sigma \tag{4.98}$$

$$\dot{e}_\omega = e_\alpha - E_1(K_\omega sign(\bar{\omega} - \hat{\omega})) \tag{4.99}$$

$$\dot{e}_\alpha = -E_2(K_\alpha sign(\bar{\alpha} - \hat{\alpha})). \tag{4.100}$$

Theorem 4.4.2. *Consider the acceleration α slowly variable. Then, for any bounded $K_\theta > max(|e_\omega|)$, $K_\omega > max(|e_\alpha|)$ and $K_\alpha > 0$, (4.84)-(4.86) is a finite-time observer of (4.92)-(4.94), where E_1 (4.89) and E_2 (4.90) are defined according to the function $g(k)$ (4.91). Moreover the position, speed and acceleration estimation errors converge to zero step-by-step and in finite-time.*

proof: Let K_θ, K_ω and K_α satisfying theorem conditions. Firstly, the stability of the position estimation error dynamics (4.98) is analyzed. Considering the nonempty manifold $S = \{e_\theta \setminus e_\theta = 0\}$ and the following candidate Lyapunov function V_θ

$$V_\theta = \frac{1}{2} e_\theta^2. \tag{4.101}$$

One proves the attractivity of S as follows

$$\begin{aligned} \dot{V}_\theta &= e_\theta \dot{e}_\theta \\ &= e_\theta(e_\omega - K_\theta sign(e_\theta)) \\ &= e_\theta e_\omega - e_\theta K_\theta sign(e_\theta) \\ &\leq |e_\theta||e_\omega| - K_\theta |e_\theta|. \end{aligned} \tag{4.102}$$

Let be

$$K_1 = -|e_\omega| + K_\theta. \tag{4.103}$$

As $K_\theta > max(|e_\omega|)$, $K_1 > 0$
then, (4.102) can be written as

$$\dot{V}_\theta \leq -K_1 |e_\theta| \tag{4.104}$$

which verifies the inequality $\dot{V}_\theta < 0$. It implies that the position estimation error e_θ (4.95) converges to zero in finite-time $t_1 > 0$.
Then $\forall\, t \geq t_1$, one has

$$\dot{e}_\theta = e_\theta = 0. \tag{4.105}$$

This implies that the sliding condition for (4.95) is achieved thus $E_1 = 1$.

$$e_\omega = K_\theta sign(e_\theta). \tag{4.106}$$

Therefore, $\forall\, t \geq t_1$, the observer output $\bar{\omega}$ defined in (4.87) is equal to ω $(\bar{\omega} = \omega)$.
In the same manner, the stability of (4.99) can be proven. Consider the following candidate Lyapunov function

$$V_\omega = \frac{1}{2} e_\omega^2. \tag{4.107}$$

The time derivative of (4.107) is given as follows

$$\begin{aligned} \dot{V}_\omega &= e_\omega \dot{e}_\omega \\ &= e_\omega(e_\alpha - E_1 K_\omega sign(\bar{\omega} - \hat{\omega})). \end{aligned} \tag{4.108}$$

With $\bar{\omega} = \omega$ and $E_1 = 1$, (4.108) becomes

$$\begin{aligned} \dot{V}_\omega &= e_\omega e_\alpha - e_\omega K_\omega sign(e_\omega) \\ &\leq |e_\omega||e_\alpha| - K_\omega |e_\omega| \end{aligned} \tag{4.109}$$

$$K_2 = -|e_\alpha| + K_\omega. \tag{4.110}$$

From theorem conditions $K_\omega > max(|e_\alpha|)$, $K_2 > 0$
then, (4.109) can be written as

$$\dot{V}_\omega \leq -K_2 |e_\omega|. \tag{4.111}$$

This proves the finite-time convergence of the speed estimation error e_ω (4.96) to zero in $t_2 > t_1$.
Then, $\forall\, t \geq t_2$, one has

$$\dot{e}_\omega = e_\omega = 0. \tag{4.112}$$

This implies that the sliding condition for (4.112) is achieved thus $E_2 = 1$. Therefore, $\forall\, t \geq t_2$, the observer output $\bar{\alpha}$ defined in (4.88) is equal to α ($\bar{\alpha} = \alpha$).
In the same manner, the stability of (4.100) can be proven. Let V_α be the candidate Lyapunov function

$$V_\alpha = \frac{1}{2} e_\alpha^2. \tag{4.113}$$

The time derivative of (4.113) is

$$\begin{aligned} \dot{V}_\alpha &= e_\alpha \dot{e}_\alpha \\ &= -e_\alpha K_\alpha sign(\bar{\alpha} - \hat{\alpha}). \end{aligned} \tag{4.114}$$

As $\bar{\alpha} = \alpha$ and $E_2 = 1$, (4.114) reads

$$\dot{V}_\alpha \leq -K_\alpha |e_\alpha|. \tag{4.115}$$

where K_α is a positive constant, this proves the convergence of e_α (4.97) to zero in finite-time $t \geq t_3$, $t_3 > t_2 > t_1$.

Equations (4.104), (4.111) and (4.115), prove the stability of S-B-S SMO in finite-time.

4.4.2.3 Parameters tuning

– According to the stability analysis, parameters K_θ, K_ω and K_α are chosen to dominate the upper bounds of speed and acceleration errors (4.96)-(4.97). This allows to ensure the finite-time stability of (4.98)-(4.100) step-by-step. Their values are given in Table 4.6. They are used in the next section.

Table 4.6: Parameters tuning of S-B-S SMO for the self-sensing control.

K_θ, K_ω, K_α	250, 110, 90

4.4.2.4 Experimental results of S-B-S SMO estimation strategy

In this section, the investigation of machine parameters effect, filters, the inverter, sensitivity of current sensors sensitivity and chattering effects on self-sensing control performances is accomplished. These effects on position estimation accuracy have been verified by lab experiments. This test has been realized to confirm that the proposed self-sensing strategy is affected by above cited effects. The experimental result shown in Figure 4.12 are obtained by coupling the classical pulsating sine-wave HF voltage injection method with S-B-S SMO without demodulation improvements as for the SMO but without 4 order LPF used to reduce the chattering effects.

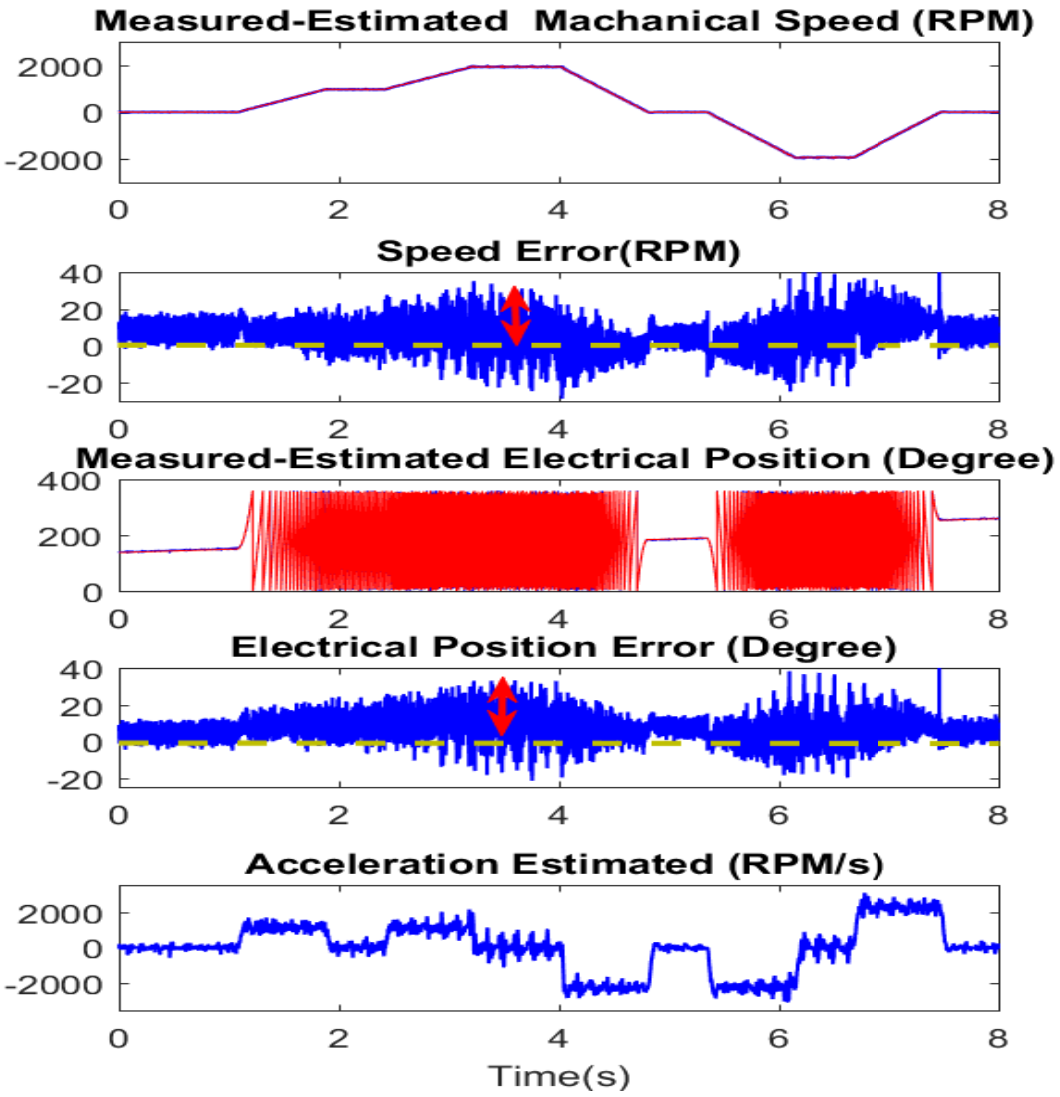

Figure 4.12: Experimental results of classical pulsating sine-wave coupled with S-B-S SMO

It can be shown from experimental results (Figure 4.12) that

- An improved rotor position and speed estimation results are obtained with respect to the SMO presented previously.
- The acceleration is well estimated, this enables to get an enhanced rotor position and speed estimation even in acceleration modes (transients modes).
- The electrical position estimation error is not really centered around zero, a position shifts can be noticed. This shift is generated by the filters of classical pulsating sine-wave HFVI

technique used, inverter and sampling time. The position estimation error is noisy which is caused by the sign function used (chattering effects), the highest noise peak does not exceed a threshold of 25 degrees.
- The mechanical speed estimation error is not centered around zero, a speed shift can be noticed. This is due to the filters used, inverter and sampling time. The speed error is noisy which is caused by the sign function used (chattering effects), the highest noise peak does not exceed a threshold of 30RPM.
- An important phase shift can be seen on both rotor position and speed estimation, which is caused by several factors such as the inverter, filters, DAC and ADC...etc.

The improvements, proposed in steps 1, 2 and 3 of chapter 3, Section 3.3.1, with respect to filters, inverter, sampling-time, and so on, will be investigated later in Section 4.5.2.
The results obtained with S-B-S SMO can be filtered with a 4 order LPF to reduce chattering effects. However, this situation increase cost and complexity and may generates delays, this is why the next part consists in proposing a new solution to improve the rotor position and speed estimation in terms of chattering.

4.4.3 Adaptive S-B-S SMO (A-S-B-S SMO) for the rotor position, speed and acceleration estimation [5, 11] [10]

An ideal sliding mode does not exist in practice since it would imply that the control commutes at an infinite frequency. In the presence of switching imperfections, such as switching time delays and small time constants in the actuators, the discontinuity in the feedback control produces a particular dynamic behavior in the vicinity of the surface, which is commonly referred to as chattering. This phenomenon is a drawback as, even if it is filtered at the output of the process, it may excite unmodeled high frequency modes, which degrades the performance of the system and may even lead to instability, the chattering effects may bring less influence on the performance of sliding observers due to its numerical implementation. Chattering also leads to high wear of moving mechanical parts and high heat losses in electrical power circuits. That is why many procedures have been designed to reduce or eliminate this chattering [201]. Using high order LPFs is one of the most techniques to reduce it's effects, however, it suffers from the following drawback, the tuning set, increase the cost and implementation complexity and it generates delays and phase shift on the estimation chain. In this section, a new method to reduce the chattering effect will be given.

4.4.3.1 Observer design

Based on the sign of rotor position estimation error (4.63), finite-time A-S-B-S SMO (4.116)–(4.120) is proposed to estimate the rotor position, speed and acceleration of IPMSM.

$$\dot{\hat{\theta}} = \hat{\omega} + [K_{\theta_{max}} - E_1\ f_1]\sigma \tag{4.116}$$

$$f_1 = K_{\theta_{max}} - K_{\theta_{min}} - (K_{\theta_{min1}} - K_{\theta_{min}})\frac{|\hat{\omega}|}{\omega_{max}} \tag{4.117}$$

$$\dot{\hat{\omega}} = \hat{\alpha} + E_1[K_{\omega_{max}} - E_2\ f_2]sign(\bar{\omega} - \hat{\omega}) \tag{4.118}$$

$$f_2 = K_{\omega_{max}} - K_{\omega_{min}} - (K_{\omega_{min1}} - K_{\omega_{min}})\frac{|\hat{\alpha}|}{\alpha_{max}} \tag{4.119}$$

$$\dot{\hat{\alpha}} = E_2 K_\alpha sign(\bar{\alpha} - \hat{\alpha}) \tag{4.120}$$

where,

$$\bar{\omega} = \hat{\omega} + K_{\theta_{max}} sign(e_\theta) \tag{4.121}$$

$$\bar{\alpha} = \hat{\alpha} + K_\alpha sign(\bar{\omega} - \hat{\omega}) \tag{4.122}$$

$$E_1 : \begin{cases} 1 & \text{if} \quad g(k) = 0 \\ 0 & \text{if} \quad \text{whereas,} \end{cases} \tag{4.123}$$

$$E_2 : \begin{cases} 1 & \text{if} \quad E_1 = 1 \quad \text{and} \quad \bar{\omega} - \hat{\omega} = 0 \\ 0 & \text{if} \quad \text{whereas.} \end{cases} \tag{4.124}$$

The stability analysis for the proposed adaptive step-by-step sliding observer for the rotor position, speed and the acceleration estimation will be detailed in Section 4.4.3.2 for both transient and steady state ranges for all rotor position, speed and acceleration states. To ensure the stability between intermediate modes (transient and steady-state modes), a new chattering detector is developed (see Figure 4.13) and given as follows

$$g(k) = \ |\sigma(k) + \sigma(k-1)| + |\sigma(k-1) + \sigma(k-2)| \tag{4.125}$$

where $\sigma(k) = sign(e_\theta(k))$ is shown in Figure 4.11 and it is the discrete form of the temporal function $\sigma[t]$, k is the delay of one time step by one control period in the discrete domain.

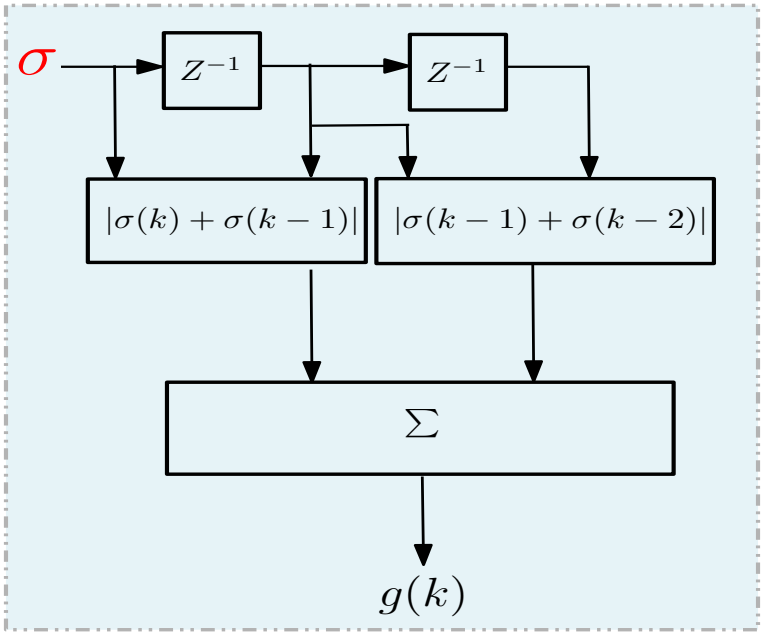

Figure 4.13: Chattering detector $g(k)$ implementation

Remark 4.3. *The function $g(k)$ is introduced to detect the chattering phenomenon, because as mentioned before only the sign of the position error is available as a known information for the observer. More precisely, at the beginning the observer is supposed to be in transient, then $E_1 = 0$, in this case maximum observer gains are applied. When the value of σ changes twice during three sampling times, $g(k) = 0$ which gives $E_1 = 1$ the observer is in steady state. In this case the applied gains are less than the maximum ones in order to reduce the chattering. The passage from steady state to transient can be detected when σ doesn't change value after one sampling time, then $g(k) \neq 0$ which gives $E_1 = 0$. In this case maximum observer gains are applied.*

4.4.3.2 Stability analysis

The proposed virtual system for the observer design (4.116)–(4.120) is given by (4.92)–(4.94). Consider (4.126)-(4.127)-(4.128) the position, the speed and the acceleration estimation errors between observer (4.116)–(4.120) and system (4.92)–(4.94)

$$e_\theta = \theta - \hat{\theta} \tag{4.126}$$

$$e_\omega = \omega - \hat{\omega} \tag{4.127}$$

$$e_\alpha = \alpha - \hat{\alpha}, \tag{4.128}$$

whose dynamics are given by

$$\dot{e}_\theta = e_\omega - [K_{\theta_{max}} - E_1\ f_1] sign(e_\theta) \tag{4.129}$$

$$\dot{e}_\omega = e_\alpha - E_1[K_{\omega_{max}} - E_2\ f_2] sign(\bar{\omega} - \hat{\omega}) \tag{4.130}$$

$$\dot{e}_\alpha = -E_2 K_\alpha sign(\bar{\alpha} - \hat{\alpha}). \tag{4.131}$$

Theorem 4.4.3. *Consider system (4.129)–(4.131) where E_1 (4.123) and E_2 (4.124) are defined according to the function $g(k)$ (4.125). Then, $\forall\ K_{\theta_{max}} = 2\ \omega_{max} > max\{|e_\omega|\}$, $K_{\omega_{max}} = 2\ \alpha_{max} > max\{|e_\alpha|\}$, $K_\alpha > 0$, $K_{\theta_{min}} = \omega_{max} > max\{|\omega|\}$, $K_{\omega_{min}} = \alpha_{max} > max\{|\alpha|\}$, $K_{\theta_{min1}} > 0$ and $K_{\omega_{min1}} > 0$, system (4.129)–(4.131) converge to zero in finite-time, where $max\{|\omega|\}$, $max\{|e_\omega|\}$, $max\{|\alpha|\}$ and $max\{|e_\alpha|\}$ are the upper bounds of speed, acceleration, speed estimation error (4.127) and acceleration estimation error (4.128).*

proof: Let $K_{\theta_{max}}$, $K_{\omega_{max}}$, K_α, $K_{\theta_{min}}$, $K_{\omega_{min}}$, $K_{\theta_{min1}}$ and $K_{\omega_{min1}}$ satisfying theorem conditions. Firstly, the stability of the position estimation error dynamic (4.129) is analyzed. Considering the nonempty manifold $S = \{e_\theta / e_\theta = 0\}$ and the following candidate Lyapunov function V_θ

$$V_\theta = \frac{1}{2} e_\theta^2. \tag{4.132}$$

One proves the attractivity of S as follows

$$\begin{aligned} \dot{V}_\theta &= e_\theta \dot{e}_\theta \\ &= e_\theta (e_\omega - [K_{\theta_{max}} - E_1\ f_1] sign(e_\theta)) \\ &= e_\theta e_\omega - e_\theta [K_{\theta_{max}} - E_1 f_1] sign(e_\theta) \\ &\leq |e_\theta||e_\omega| - [K_{\theta_{max}} - E_1\ f_1]|e_\theta|. \end{aligned} \tag{4.133}$$

Position transient ranges: In transient ranges, $E_1 = 0$, the equation (4.133) can be written

$$\dot{V}_\theta \leq |e_\theta||e_\omega| - K_{\theta_{max}}|e_\theta|. \tag{4.134}$$

Let be $K_1 = -|e_\omega| + K_{\theta_{max}}$, as $K_{\theta_{max}} = 2\omega_{max} > max(|e_\omega|)$, $K_1 > 0$, then (4.134) becomes

$$\dot{V}_\theta \leq -K_1|e_\theta|. \tag{4.135}$$

Position steady state ranges: In steady state, the sliding condition for (4.126) is achieved thus $E_1 = 1$, then

$$\dot{e}_\theta = e_\theta = 0. \tag{4.136}$$

By using (4.136) in (4.129), one can deduce

$$e_\omega = [K_{\theta_{max}} - f_1] sign(e_\theta). \tag{4.137}$$

Therefore, $\forall\, t \geq t_1$, the observer output $\bar{\omega}$ defined in (4.121) is equal to ω ($\bar{\omega} = \omega$), and $E_1 = 1$, for that, an adaptive rotor position gain estimation can be chosen to verify (4.138)

$$\dot{V}_\theta \leq |e_\theta||e_\omega| - [K_{\theta_{max}} - f_1]|e_\theta|. \tag{4.138}$$

By replacing f_1 defined in (4.117), (4.138) becomes

$$\dot{V}_\theta \leq |e_\theta||e_\omega| - [K_{\theta_{min}} + (K_{\theta_{min1}} - K_{\theta_{min}})\frac{|\hat{\omega}|}{\omega_{max}}]|e_\theta|. \tag{4.139}$$

If $\hat{\omega} = 0$, by replacing this condition in (4.139), one can obtain

$$\dot{V}_\theta \leq |e_\theta||\omega| - K_{\theta_{min}}|e_\theta|. \tag{4.140}$$

Set $K'_1 = -|\omega| + K_{\theta_{min}}$. From theorem conditions $K_{\theta_{min}} > \omega_{max}$, $K'_1 > 0$, then one has

$$\dot{V}_\theta \leq -K'_1|e_\theta|. \tag{4.141}$$

If $\hat{\omega} = \omega_{max}$ and $|e_\omega| \approx 0$, by replacing this condition into (4.139), one can obtain

$$\dot{V}_\theta \leq -K_{\theta_{min1}}|e_\theta|. \tag{4.142}$$

From theorem conditions, the gain $K_{\theta_{min1}}$ is chosen to verify $K_{\theta_{min1}} > 0$ and sufficiently small to reduce the chattering effect. Inequalities (4.135), (4.141) and (4.142) prove the finite-time convergence of the position estimation error e_θ to zero in transient/steady state position ranges for $t_1 > 0$. Figure 4.14 shows the adaptive gain K_θ with respect to the estimated speed. On this Figure it can be seen that, the position gain takes its maximum value $2\omega_{max}$ in transient modes. When the motor is operated in steady state ranges, the position gain varies between $K_{\theta_{min}}$ and $K_{\theta_{min1}}$ according to the estimated speed value.

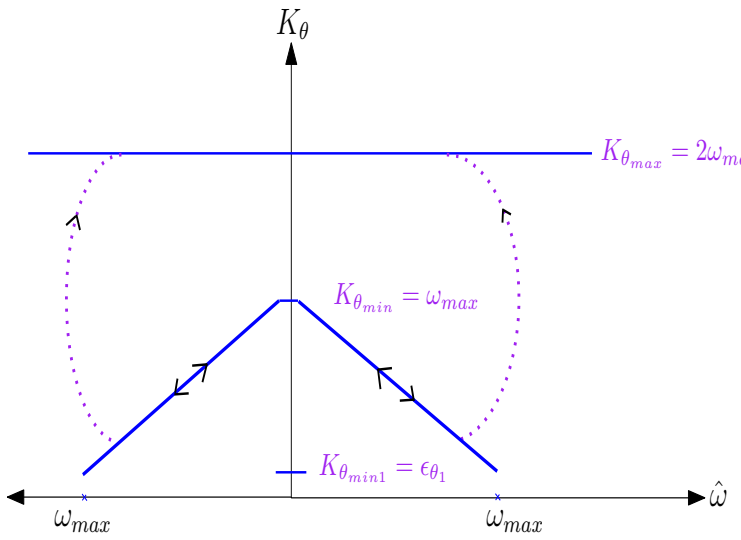

Figure 4.14: Adaptive position gain in different estimated speed ranges

In steady rotor position state, $\forall\, t \geq t_1$, the observer output $\bar{\omega}$ defined in (4.121) is equal to ω ($\bar{\omega} = \omega$), as one have $[K_{\theta_{max}} - E_1\ f_1] > 0$) and $E_1 = 1$. In the same manner, the stability of (4.130) can be proved.
Consider the following candidate Lyapunov function

$$V_\omega = \frac{1}{2}e_\omega^2. \tag{4.143}$$

The time derivative of (4.143) is given as follows

$$\begin{aligned} \dot{V}_\omega &= e_\omega \dot{e}_\omega \\ &= e_\omega (e_\alpha - E_1 [K_{\omega_{max}} - E_2\ f_2] sign(\bar{\omega} - \hat{\omega})). \end{aligned} \tag{4.144}$$

With $\bar{\omega} = \omega$ and $E_1 = 1$, (4.144) reads

$$\begin{aligned} \dot{V}_\omega &= e_\omega e_\alpha - e_\omega [K_{\omega_{max}} - E_2\ f_2] sign(e_\omega) \\ &\leq |e_\omega||e_\alpha| - [K_{\omega_{max}} - E_2\ f_2]|e_\omega|. \end{aligned} \tag{4.145}$$

Speed transient ranges: In transient ranges, $E_2 = 0$, the equation (4.145) can be written

$$\dot{V}_\omega \leq |e_\omega||e_\alpha| - K_{\omega_{max}}|e_\omega|. \tag{4.146}$$

Let be $K_2 = -|e_\alpha| + K_{\omega_{max}}$. Then from theorem conditions $K_{\omega_{max}} > max(|e_\alpha|)$, $K_2 > 0$, and (4.146) becomes

$$\dot{V}_\omega \leq -K_2|e_\omega|. \tag{4.147}$$

Speed steady state ranges: In steady state, the sliding condition for (4.127) is achieved thus $E_2 = 1$, then,

$$\dot{e}_\omega = e_\omega = 0. \tag{4.148}$$

By replacing (4.148) in (4.130), one can deduce

$$e_\alpha = [K_{\omega_{max}} - \ f_2] sign(e_\omega). \tag{4.149}$$

Therefore, $\forall\ t \geq t_2 > t_1$, the observer output $\bar{\alpha}$ defined in (4.122) is equal to α ($\bar{\alpha} = \alpha$), $sign(e_\omega) = sign(e_\alpha)$ and $E_2 = 1$. For that, an adaptive rotor speed gain estimation can be chosen to verify the following equation

$$\dot{V}_\omega \leq |e_\omega||e_\alpha| - [K_{\omega_{max}} - \ f_2]|e_\omega|. \tag{4.150}$$

By replacing f_2 defined in (4.119), (4.150) goes with

$$\dot{V}_\omega \leq |e_\omega||e_\alpha| - [K_{\omega_{min}} + (K_{\omega_{min1}} - K_{\omega_{min}}) \frac{|\hat{\alpha}|}{\alpha_{max}}]|e_\omega|. \tag{4.151}$$

If $\hat{\alpha} = 0$, by replacing this condition in (4.151), one can obtain

$$\dot{V}_\omega \leq |e_\omega||\alpha| - K_{\omega_{min}}|e_\omega|. \tag{4.152}$$

Set $K'_2 = -\alpha_{max} + K_{\omega_{min}}$. Then, from theorem conditions $K_{\omega_{min}} > \alpha_{max}$, $K'_2 > 0$, one has

$$\dot{V}_\omega \leq -K'_2|e_\omega|. \tag{4.153}$$

If $\hat{\alpha} = \alpha_{max}$ and $|e_\alpha| \approx 0$, by replacing these conditions into (4.151), one can obtain

$$\dot{V}_\omega \leq -K_{\omega_{min1}}|e_\omega|. \tag{4.154}$$

From theorem conditions, the gain $K_{\omega_{min1}}$ is chosen to verify $K_{\omega_{min1}} > 0$ and sufficiently small to reduce the chattering effect. From inequalities (4.147), (4.153) and (4.154), the finite-time convergence of the speed estimation error e_ω to zero is proved in transient/steady state ranges for $t_2 > t_1$. Figure 4.15 shows the adaptive gain K_θ with respect to the estimated speed. On this Figure it can be seen that, the position gain takes its maximum value $2\omega_{max}$ in transient

modes. When the motor is operated in steady state ranges, the speed gain varies between $K_{\omega_{min}}$ and $K_{\omega_{min1}}$ according to the estimated acceleration value.

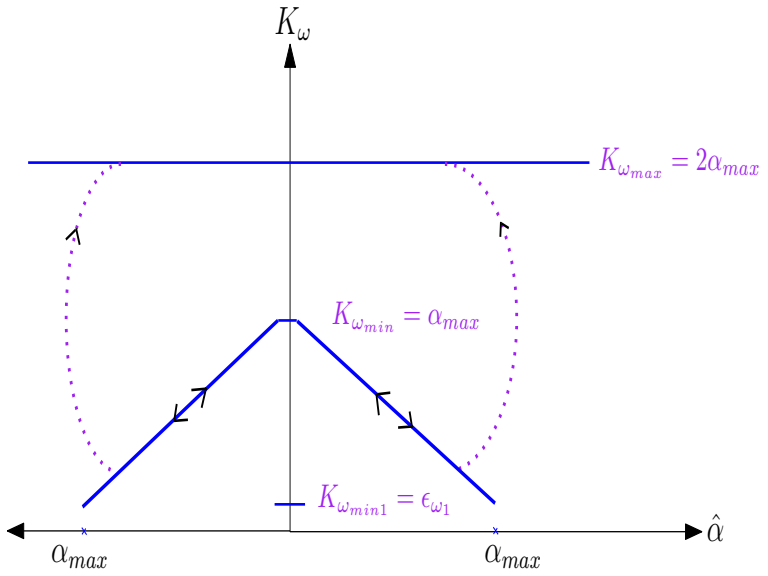

Figure 4.15: Adaptive speed gain in different estimated acceleration ranges

In steady speed state, $\forall\ t \geq t_2 > t_1$, the observer output $\bar{\alpha}$ defined in (4.122) is equal to α ($\bar{\alpha} = \alpha$), as one have $[K_{\omega_{max}} - E_2\ f_2] > 0$) and $E_2 = 1$. In the same manner, the stability of (4.131) can be proven. Let V_α be the candidate Lyapunov function

$$V_\alpha = \frac{1}{2} e_\alpha^2. \tag{4.155}$$

The time derivative of (4.155) is

$$\begin{aligned} \dot{V}_\alpha &= e_\alpha \dot{e}_\alpha \\ &= e_\alpha(-E_2 K_\alpha sign(\bar{\alpha} - \hat{\alpha})). \end{aligned} \tag{4.156}$$

As $\bar{\alpha} = \alpha$ and $E_2 = 1$, (4.156) reads

$$\begin{aligned} \dot{V}_\alpha &= -e_\alpha K_\alpha sign(e_\alpha) \\ &\leq -K_\alpha |e_\alpha|. \end{aligned} \tag{4.157}$$

From theorem conditions $K_\alpha > 0$. This proves the finite-time convergence of the acceleration estimation error e_α to zero in $t_3 > t_2$.

4.4.3.3 Parameters tuning

– Parameters $K_{\theta_{max}}$, $K_{\omega_{max}}$, K_α, $K_{\theta_{min}}$,$K_{\omega_{min}}$, $K_{\theta_{min1}}$ ($\varepsilon_{\theta 1}$) and $K_{\omega_{min1}}$ ($\varepsilon_{\omega 1}$) are chosen according to the stability analysis given in previous section in order to ensure the finite-time convergence of the observer in both transient/steady state modes. their values are given in Table 4.7.

Table 4.7: Parameters tuning of A-S-B-S SMO for the self-sensing control.

$K_{\theta_{max}}$, $K_{\omega_{max}}$, K_{α}	250, 110, 90
$K_{\theta_{min1}}$ and $K_{\omega_{min1}}$	5
$K_{\theta_{min}}$,$K_{\omega_{min}}$	110, 280

4.4.3.4 Results of the proposed A-S-B-S SMO coupled with the classical pulsating sine-wave HFVI

The obtained experimental results shown in Figure 4.16 are achieved by using the new A-S-B-S SMO. The described test is adopted as a solution to improve the position estimation accuracy in critical operation region and reduce the acting of the chattering phenomenas in steady-sate mode. These experiments tests are realized by coupled the classical pulsating sine-wave technique with the A-S-B-S SMO given in Section 4.4.3.

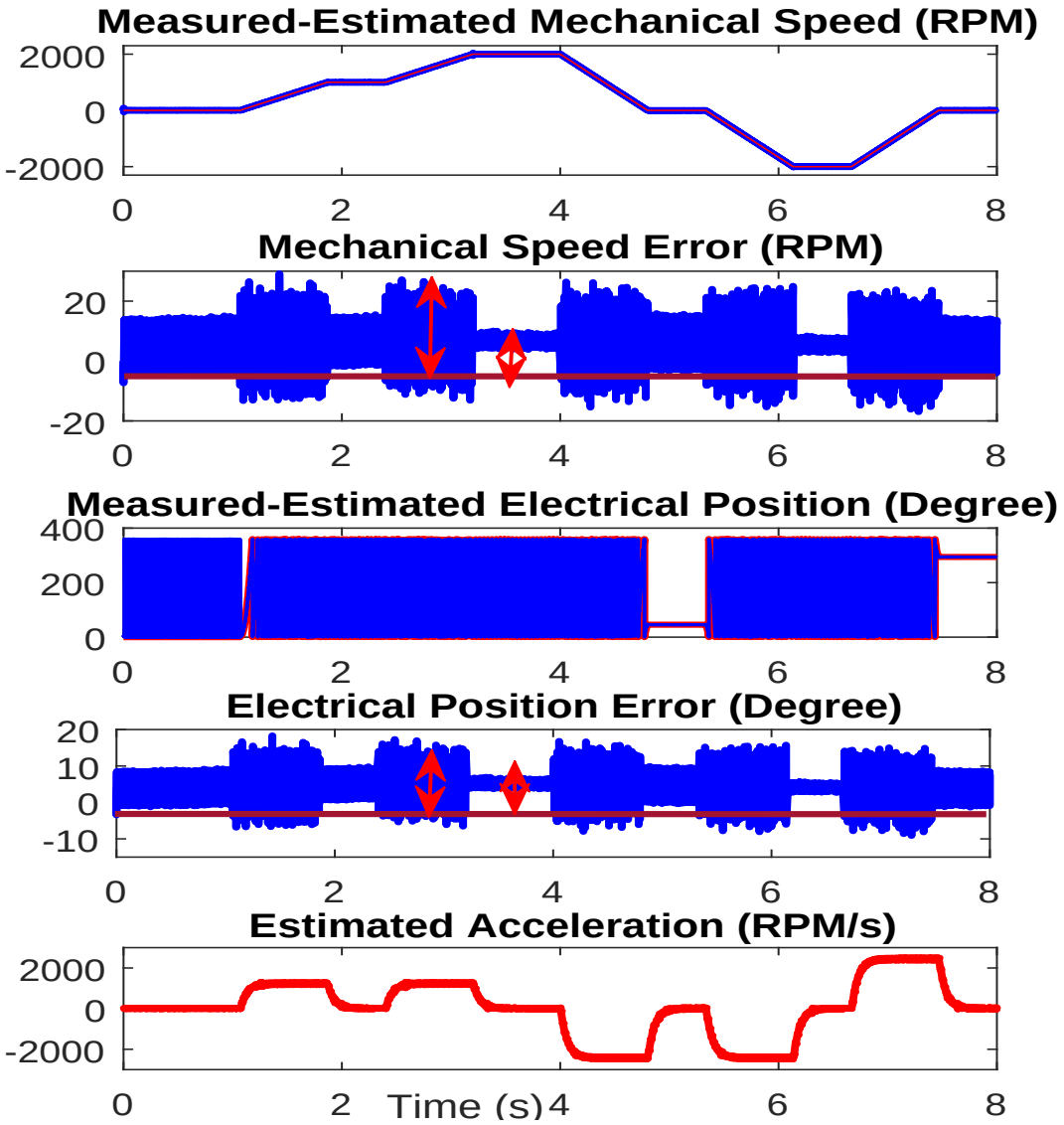

Figure 4.16: Experimental results of classical pulsating sine-wave coupled with the A-S-B-S SMO

It can be seen, from the obtained experimental results (Figure 4.16), that in addition to the advantages of the S-B-S SMO, the A-S-B-S SMO results show that

- A well improved rotor position and speed estimation results are obtained in all speed/torque ranges.
- The electrical position estimation error is very small, however, it is not centered around zero, the highest noise peak does not exceed a threshold of 7 at steady-sate.
- The mechanical speed estimation error is very small, however, it is not centered around zero, the highest noise peak does not exceed a threshold of 15*RPM* at steady-sate.
- The chattering effect is reduced compared to the previous techniques.

As a conclusion, well improved rotor position and speed estimation results are obtained at different speed/torque ranges, which confirms the accuracy and the performances of the A-S-B-S SMO compared to the S-B-S SMO. These results confirm that the improved estimation strategy offers a significant and attractive improvement compared to the previous methods.

4.4.4 Comparative study between the proposed tracking observers

In this part, a comparative study in term of robustness and performances is summarized in Table 4.8, between the proposed tracking observers: SMO given in Section 4.4.1, S-B-S SMO given in Section 4.4.2 and A-S-B-S SMO given in Section 4.4.3. This comparative study is based on the following criteria: Robustness with respect to machine acceleration, delays generated by filters, inverter and sampling time, maximal transient and steady-sate rotor position estimation error and speed estimation error, chattering effects, machine's parameters and implementation complexity.
The general robustness comparative study between improved tracking algorithms given in this chapter is summarized in the Table 4.8.

Table 4.8: Summary of the comparative study between the proposed tracking algorithms

Criterions \ Proposed Observers	SMO	S-B-S SMO	A-S-B-S SMO
Machine acceleration	Sensitive	Insensitive	Insensitive
Delays generated by filters, inverter and sampling time	Very sensitive	Very sensitive	Very sensitive
Maximal transient rotor position estimation error (Degree)	60	25	15
Maximal steady-sate rotor position estimation error (Degree)	30	18	6
Maximal transient speed estimation error (RPM)	30	25	15
Maximal steady-state speed estimation error (RPM)	20	18	10
Chattering effects	Very sensitive	Very sensitive	Less sensitive
Machine's parameters	Independent	Independent	Independent
Implementation complexity	***	**	*

4.4.5 Comparative study between the proposed sliding mode tracking observer and the classical tracking

In this part, a comparative study in terms of robustness and performances between the proposed estimation technique (A-S-B-s SMO) selected in Section 4.4.4 and the existing techniques introduced in Section 4.3 (the PLL and the MSO) is exhibited. The A-S-B-S-SMO, the PLL and the MSO, both are evaluated in simulation and experimentally with and without considering the inductance variations.

In simulation test, the inductances variations on I_{cn} (Figure 4.4) and variations on the mechanical constant time (inertia and viscous coefficient) (Figure 4.5) are considered to prove that the proposed method doesn't depend on electrical and mechanical parameters.

The obtained results of the proposed A-S-B-S-SMO (Figure 4.17) shown that the considered I_{cn} (Figures 4.4) and mechanical constant time profiles (Figure 4.5) don't affect the rotor position and speed estimation, which confirm the theoretical study given below.

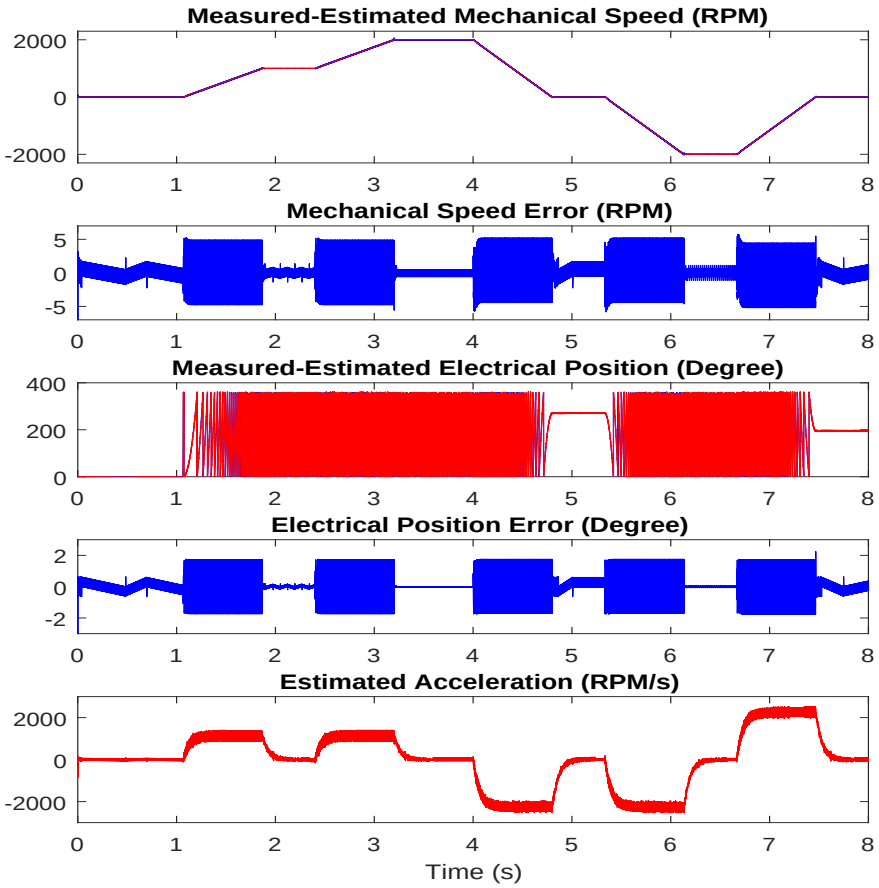

Figure 4.17: Simulations results of the proposed A S-B-S SMO coupled with the improved pulsating sine-wave HFVI

On the obtained PLL simulations (Figure 4.20) and experimental results (Figure 4.21), important transient estimation errors can be seen in the rotor position and speed estimation. Once the I_{cn} profile is considered (see Figure 4.4), the PLL algorithm diverges immediately except if one adapt the gain I_{cn} in experiments as it shown in Figure 4.21. In this case, important errors can be noticed in both rotor position and speed estimation. These results highlight that this method is very sensitive to acceleration effects and parameters (inductances) variations.

The robustness of MSO is tested with respect to mechanical time constant variation (due to the inertia and viscous coefficient variations). The transfer between the speed and electromagnetic torque is given by

$$\frac{\hat{\omega}(s)}{C_{em}} = \frac{K_{stat}}{s\tau + 1} \tag{4.158}$$

where, $K_{stat} = \frac{1}{K_f}$ is the static gain and $\tau = \frac{J}{K_f}$ is the mechanical time constant of the transfer function (4.158). The characteristics of the transfer function (4.158) can vary according to the inertia and the viscous coefficient variations. In the automotive application, these variations depend on certain unpredictable phenomena as: weight, tires quality, road type (sand, clay and mud), meteorological conditions (wind, rain) ...etc.
The MSO gains are functions of mechanical system parameters. Consequently, the tuning and the stability of the mechanical system observer depend on these parameter variations. To evaluate the robustness of the MSO in simulation and in experiments, an arbitrary profile of the mechanical time constant is considered and represented in Figure 4.5. On the obtained results shown in Figure 4.18 and Figure 4.19, the following cases can be noted

- When the nominal mechanical time constant is used, a good rotor speed and position estimations are obtained.
- In the other time intervals, consequent errors can be seen on the rotor position and speed estimation in transient mode which are due to the considered mechanical time constant variation. A static errors appeared on the speed and position estimation which are due to the viscous coefficient variations.

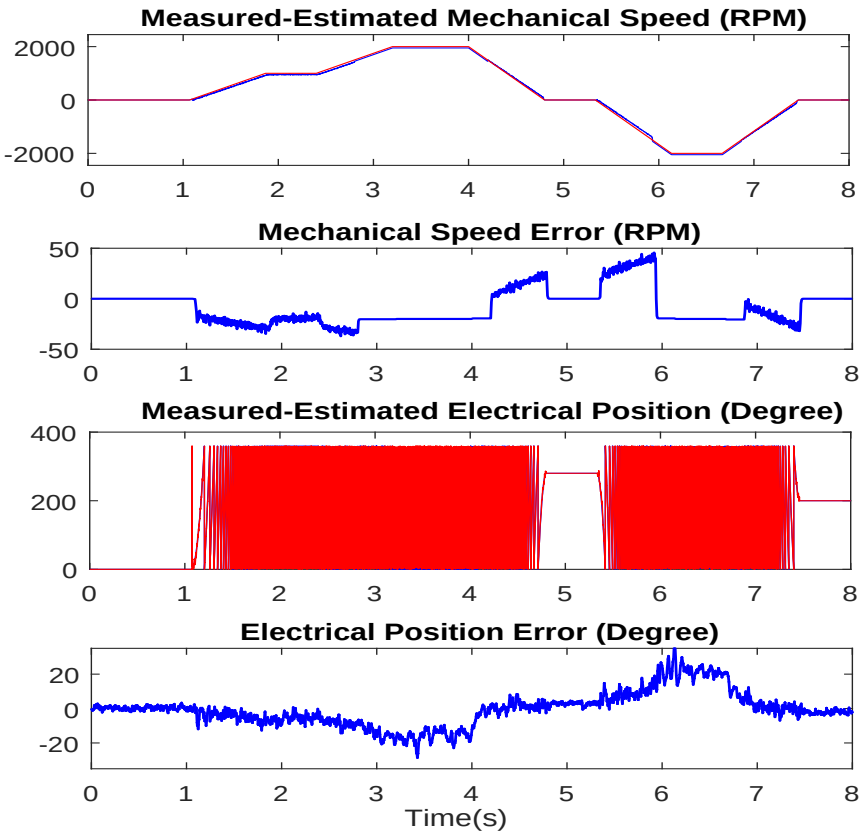

Figure 4.18: MSO simulation results under mechanical time constant variation

Additionally, the MSO gains vary according to the mechanical system parameters (inertia and viscous coefficient) which affects the estimation process. These results underline the sensitivity

of the MSO against mechanical system parameter variations. The previous results are obtained with well known inductance values (without considering I_{cn} profile), once the I_{cn} profile is considered (see Figure 4.4), the MSO diverges except if one adapt the gain I_{cn} as it shown in Figure 4.19. In this case, an important errors can be noticed in both rotor position and speed estimation. These results prove that this method is very sensitive to acceleration effects and parameter (inductances) variations.

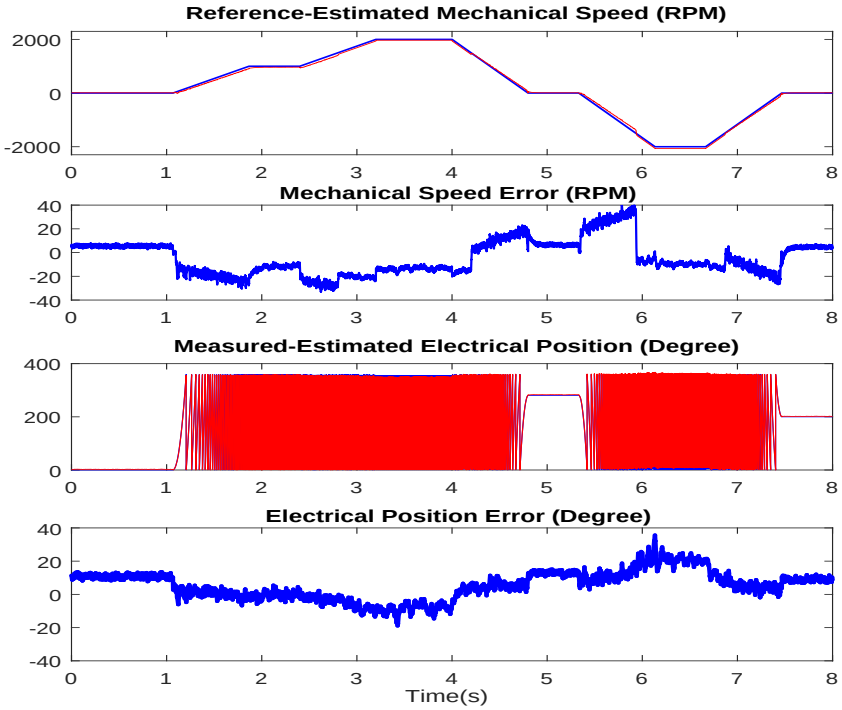

Figure 4.19: MSO experimental results under mechanical time constant variation and I_{cn} adaptation

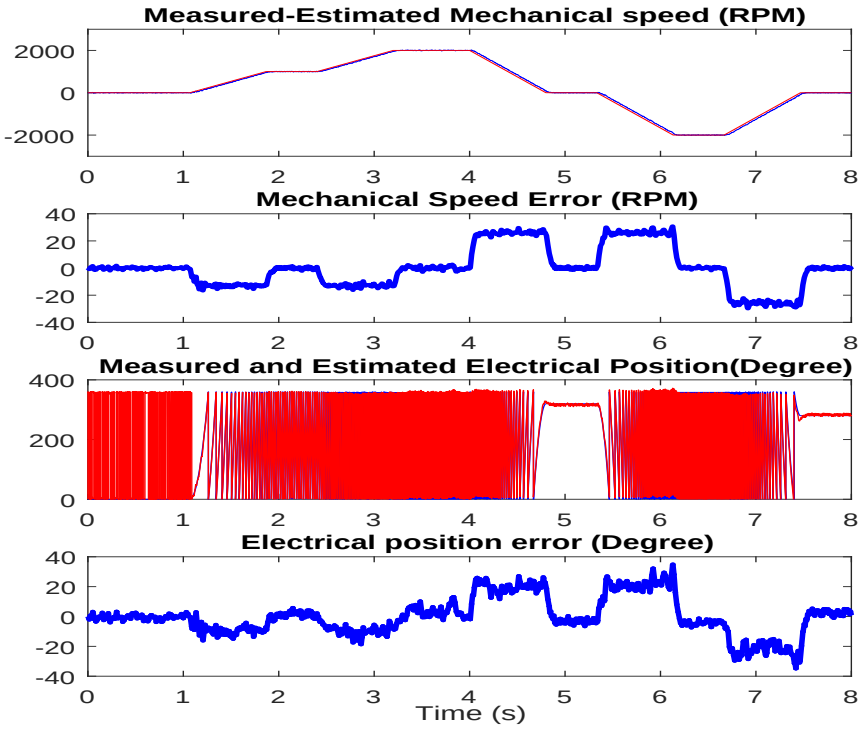

Figure 4.20: PLL simulation results without considering I_{cn} variations

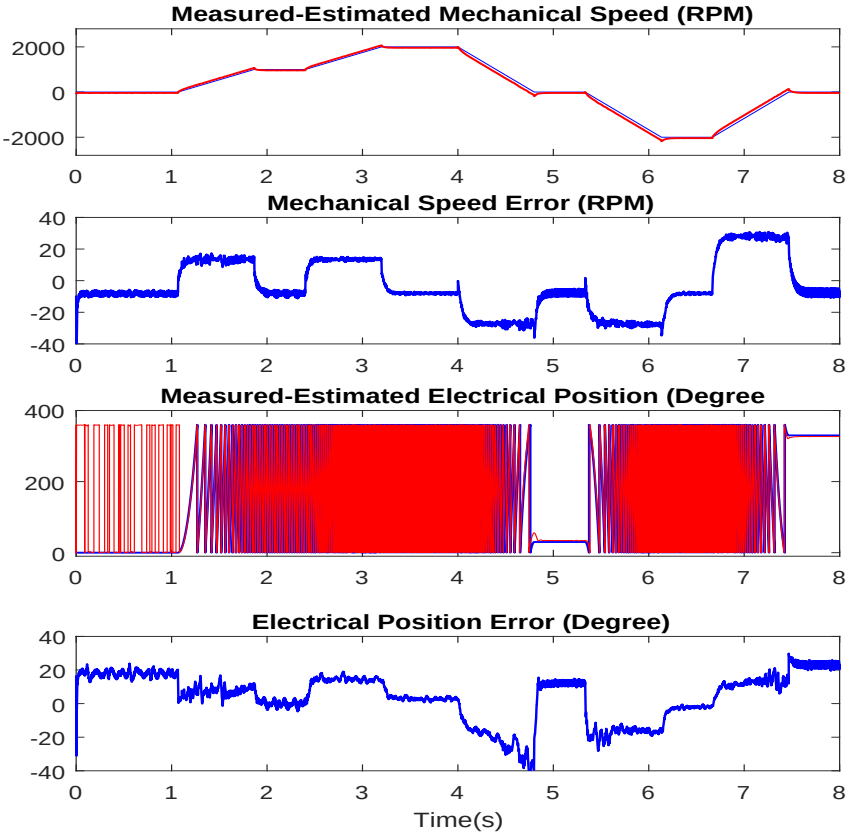

Figure 4.21: PLL experimental results with I_{cn} adaptation

These results confirm that the proposed estimation strategy offers a significant and attractive improvement compared to the previous methods.
The comparative study between the proposed algorithm (A-S-B-S SMO) and the classical tracking algorithms recalled in Section 4.3 is summarized in the Table 4.9.

Table 4.9: Summary of the comparative study between the improved pulsating sine-wave HFVI technique coupled with the A-S-B-S SMO or with the MSO or with the PLL.

Observers / Criterions	A-S-B-S SMO	MSO	PLL
Mechanical parameters	Independent	Dependent	Independent
Electrical parameters	Independent	Dependent	Dependent
Maximal rotor position estimation error (Degree)	2	25	30
Maximal speed estimation error (RPM)	4	45	50
Machine acceleration	Insensitive	Sensitive	Very sensitive
Delays generated by filters, inverter and sampling time	Insensitive	Sensitive	Very sensitive

This comparative study confirms that the tracking algorithm proposed in Section 4.4.3 offers a significant and attractive improvement compared to classical techniques.

4.5 Test, validation and selection of the proposed HFVI techniques

In the previous section, the A-S-B-S SMO is chosen as the best tracking algorithm. In this section, this observer is coupled with classical and improved HFVI techniques (pulsating sine-wave, pulsating square-wave and rotating sine-wive) given in Chapter 3 in order to compare their performances and to choose the best HFVI from the presented techniques.

4.5.1 Validation of the improved pulsating sine-wave HFVI technique

In this section, the effects of the machine parameters, filters, the inverter, sensitivity of current sensors and the chattering effects on self-sensing control performances is accomplished. This effects on position estimation accuracy have been verified by lab experiments. The test has been realized to confirm that the proposed self-sensing strategy is not affected by the presence of filters, the inverter, the sampling time and the chattering phenomena.

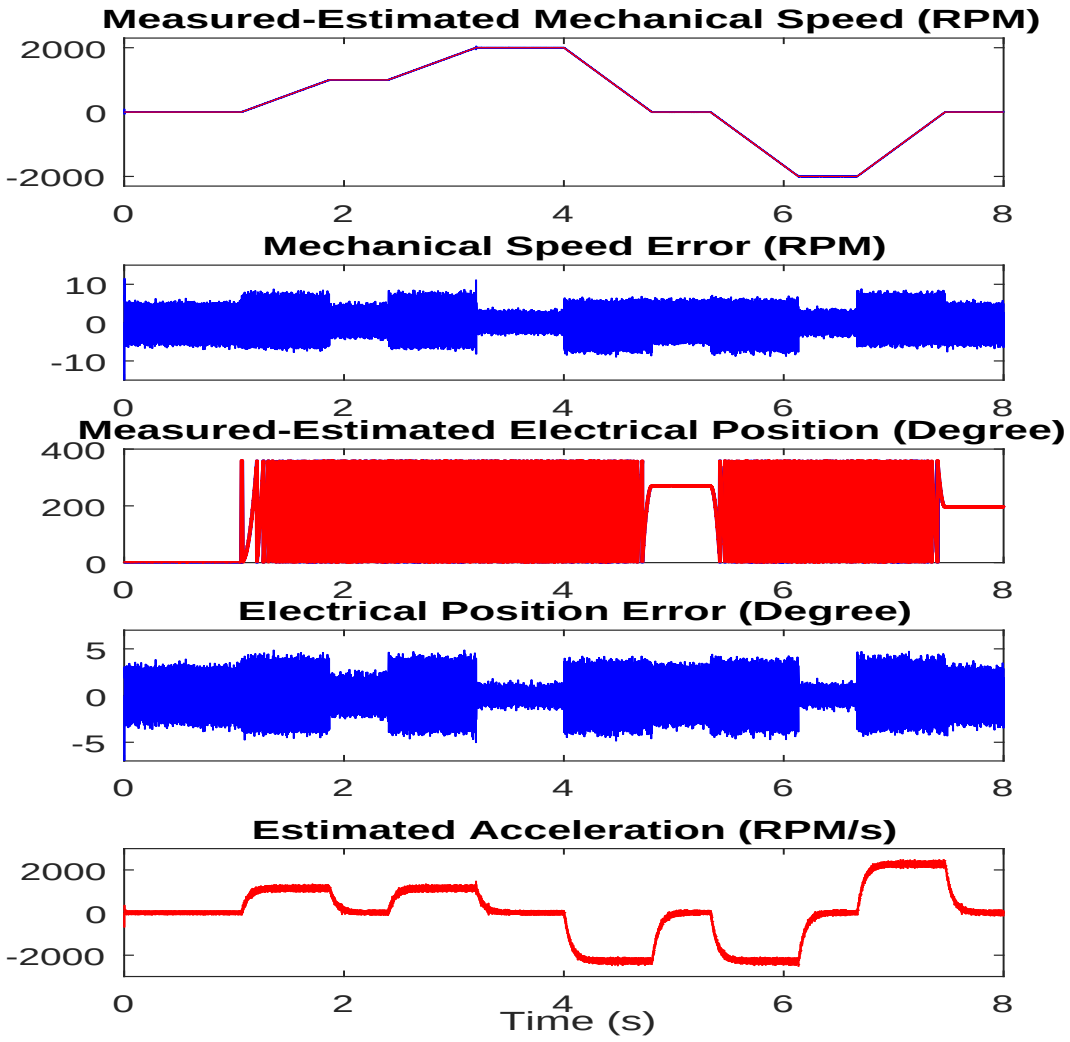

Figure 4.22: Experimental results of the improved pulsating sine-wave HFVI technique coupled with A S-B-S SMO

The experimental results shown in Figure 4.22 and 4.23 are obtained by coupling the

improved pulsating sine-wave voltage injection method with the A-S-B-S SMO. It can be seen from experimental results obtained by the first test (Figure 4.22) that

- Convenient rotor position and speed estimation results are obtained in all speed/torque ranges.
- The rotor position and speed estimation errors are centered around zero.
- The chattering effect is reduced in steady state-range.
- The transient modes still suffering from the chattering phenomena.

In order to reduce again the chattering effect acting on the transient and steady-state modes, 4 order LPFs is introduced allowing to filter out the chattering.
The obtained experimental results shown in Figure 4.23 are achieved by coupling the A-S-B-S SMO with the improved pulsating sine-wave HFVI, the described test is adopted as a solution to improve the position estimation accuracy in critical operation region and reduce the acting of the chattering phenomenas both in transient and steady-state modes.

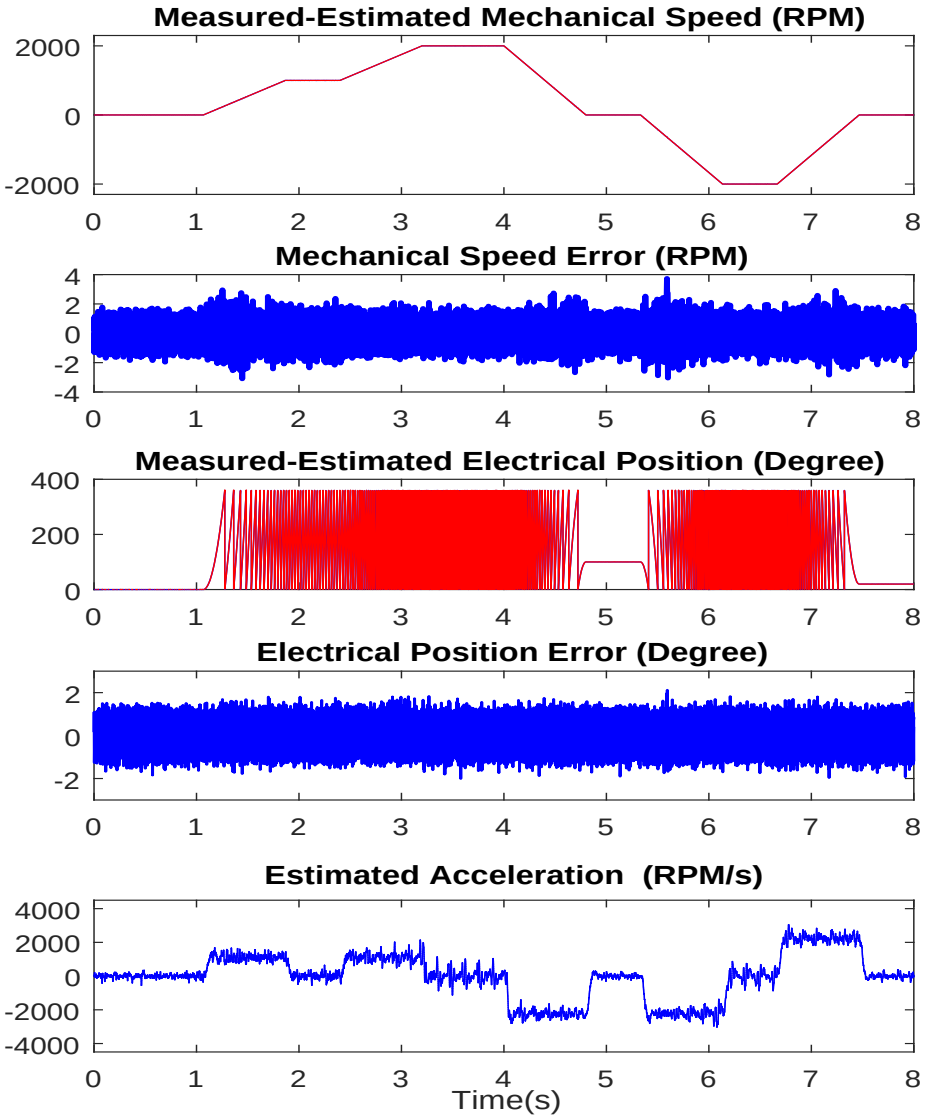

Figure 4.23: Experimental results of improved pulsating sine-wave technique coupled with filtered A-S-B-S SMO

It can be noted from Figure 4.23 that

- A well improved rotor position and speed estimation results are obtained in all speed/torque ranges.
- The electrical position estimation error is very small and centered around zero, the highest noise peak does not exceed a threshold of 1.8 degrees.
- The mechanical speed estimation error is very small centered around zero, the highest noise peak does not exceed a threshold of 4RPM.
- The chattering effect is nearly filtered to reduce again its effects in both transient and steady-state modes.

The filtered A-S-B-S SMO will be now associated to the pulsating square-wave and rotating sine-wave HFVI technique given the two next sections

4.5.2 Validation of the improved pulsating square-wave HFVI technique

This part focuses on the validation of the improved pulsating square-wave topology. The validation consists in coupling the selected A-S-B-S SMO given in Section 4.4.3 with and without the rotating demodulation improvements given in Section 3.2. In this section, the effects of filters and the chattering effects on self-sensing control performances are accomplished. The filters and chattering impacts on position estimation accuracy have been verified by lab experiments.

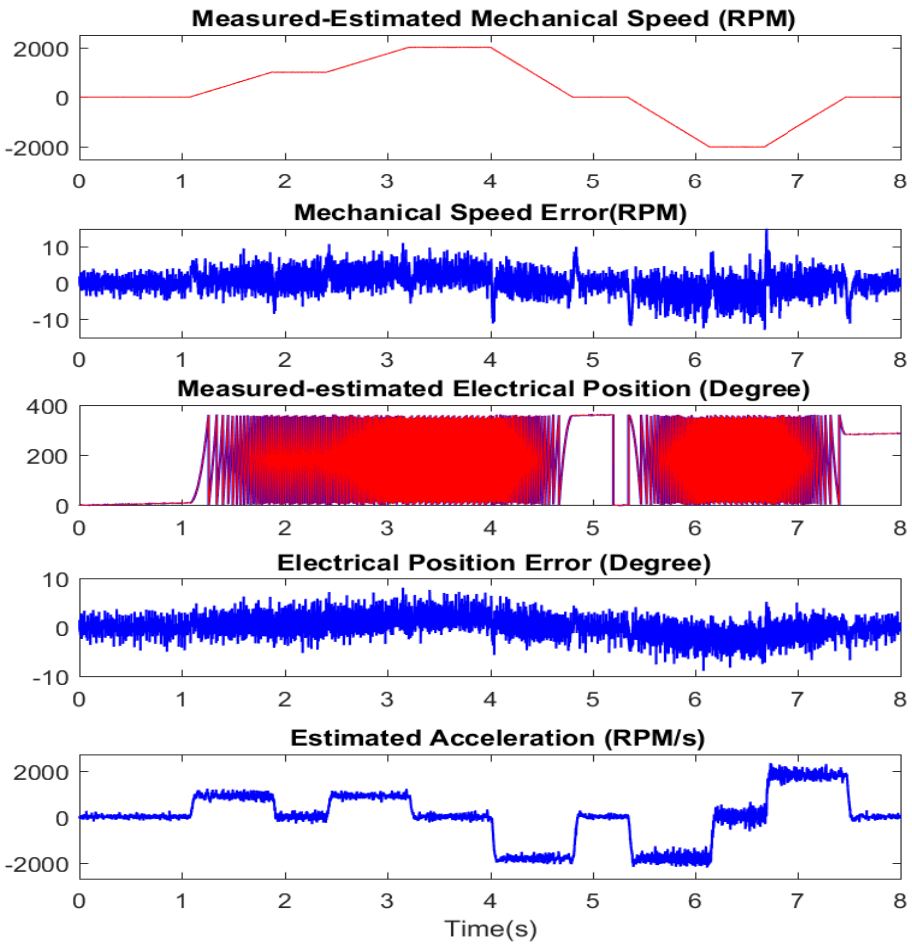

Figure 4.24: Experimental results of classical pulsating square-wave HFVI coupled with the filtered A-S-B-S SMO

To confirm that the observed position error is mainly linked to the filters used and the

chattering effects, two tests have been realized. The experimental result shown in Figure 4.24 is obtained by coupling the classical square wave-sine HFVI technique with filtered A-S-B-S SMO for the objectives detailed in Section 4.4.3. The obtained experimental results show the evolution of following quantities: the measured and the estimated mechanical speeds, the mechanical speed estimation error, the measured and the estimated electrical positions, the electrical position estimation error and the estimated acceleration of the machine.
It can be seen from experimental results obtained by the first test (Figure 4.24) that

- Convenient rotor position and speed estimation results are obtained in all speed/torque ranges even in difficult situations mentioned on the cycle of drive benchmark (Figure 4.3).
- The acceleration is well estimated, this enables to get an enhanced rotor position and speed estimation even in acceleration modes (transients modes).
- The electrical position estimation error is not really centered around zero, a small position shift can be noticed. This position shifts is generated by the filter used. The position estimation error is noisy which is caused by the sign function used (chattering effects), the highest noise peak does not exceed a threshold of 10 degrees.
- The mechanical speed estimation error is not centered around zero, a speed shift can be noticed. this is due to the filter used. The speed error is noisy which is caused by the sign function used (chattering effects), the highest noise peak does not exceed a threshold of 13*RPM*.

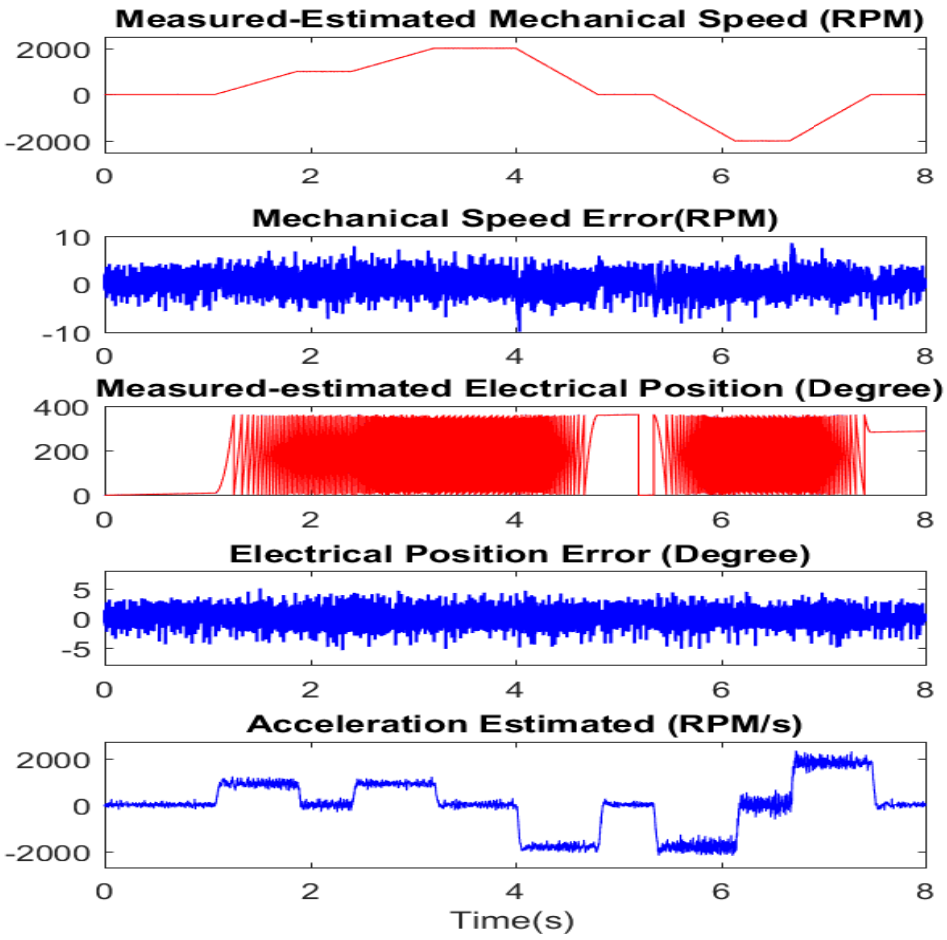

Figure 4.25: Experimental results of the improved pulsating square-wave HFVI technique coupled with the filtered A-S-B-S SMO

The second experimental result shown in Figure 4.25 is realized by coupled the improved square-

wave HFVI technique and the filtered A-S-B-S SMO.

In addition to the advantages of the previous method, the obtained experimental results show that

- A very acceptable rotor position and speed estimation is obtained.
- The electrical position estimation error is centered around zero, the highest noise peak does not exceed a threshold of 6 degrees.
- The mechanical speed estimation error is centered around zero, the highest noise peak does not exceed a threshold of $7RPM$.

As a conclusion, very acceptable rotor position and speed estimation results are obtained at different speed/torque ranges, which confirms the accuracy and the performances of the improved square-wave HFVI technique. This comparative study confirms that the improved self-sensing strategy offers a significant and attractive improvement compared to classical methods.

4.5.3 Validation of the improved rotating sine-wave HFVI technique

In this part, we will focus on the validation of the improved rotating sine-wave topology. The validation consists in coupling the selected A-S-B-S SMO given in Section 4.4.3 with classical and improved rotating sine-wave HFVI technique given in Section 3.4.

To confirm that the observed position error is mainly linked to the filters used, the presence of the inverter, the sampling time and the chattering effects, two tests have been realized. The experimental result shown in Figure 4.26 is realized by coupling the classical rotating wave-sine HFVI technique with filtered A-S-B-S SMO.

It can be seen from The experimental results obtained by the first test (Figure 4.26) that

- convenient rotor position and speed estimation results are obtained in all speed/torque ranges even in difficult situations mentioned on the cycle of drive benchmark (Figure 4.3).
- the acceleration is well estimated, this enables to get an enhanced rotor position and speed estimation even in acceleration modes (transients modes).
- the electrical position estimation error is not really centered around zero, a position shift can be noticed. this position shift is generated by the filter used. The position estimation error is noisy which is caused by the sign function used (chattering effects), the highest noise peak does not exceed a threshold of 12 degrees.
- the mechanical speed estimation error is not centered around zero, a speed shift can be noticed. this is due to the filter used. The speed error is noisy which is caused by the sign function used (chattering effects), the highest noise peak does not exceed a threshold of $15RPM$.

The second experimental result shown in Figure 4.27 is realized by coupled the improved rotating sine-wave and the filtered A-S-B-S SMO.

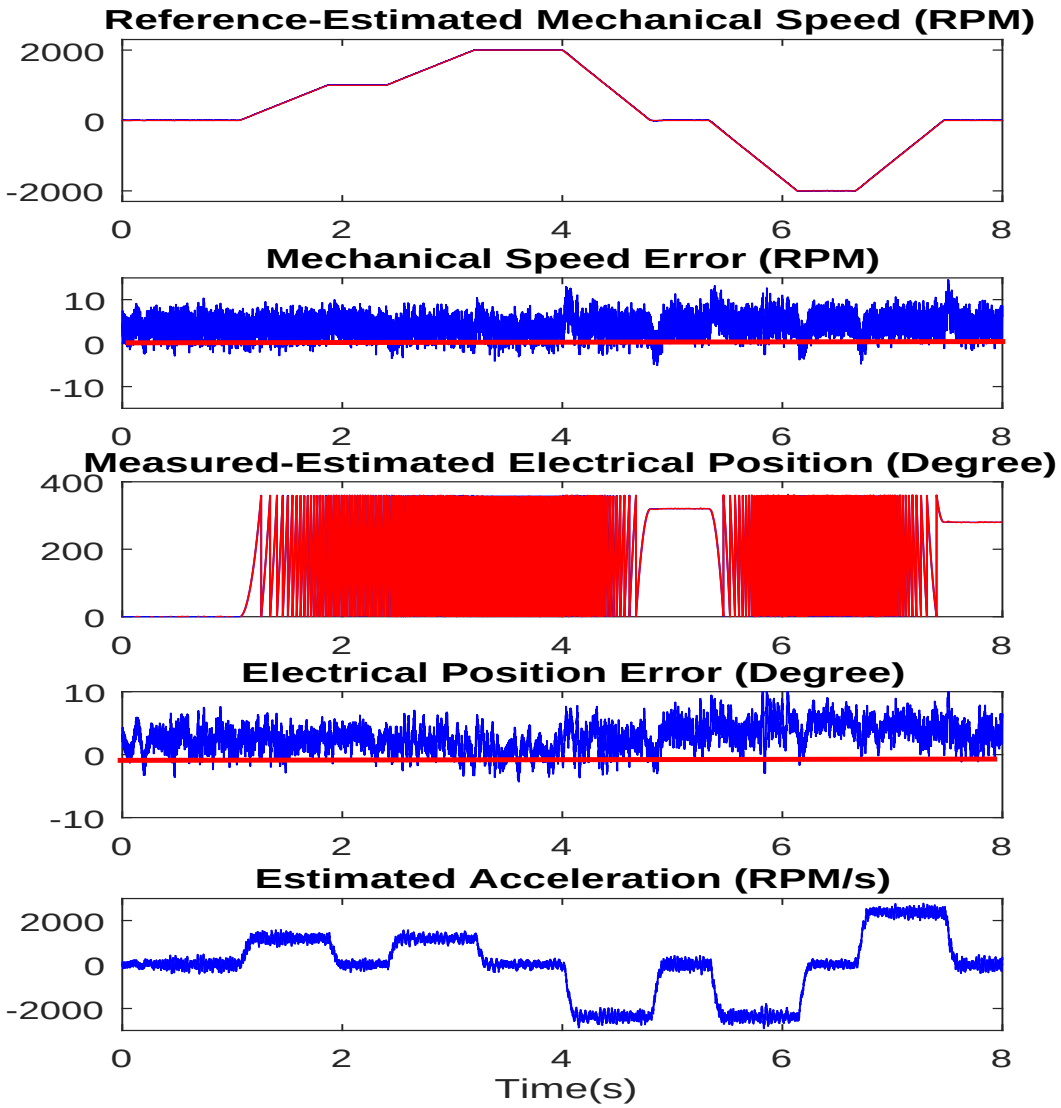

Figure 4.26: Experimental results of classical rotating sine-wave HFVI technique coupled with the filtered A-S-B-S SMO

In addition to the advantages of the previous method, the obtained experimental results show that

- A very acceptable rotor position and speed estimation is obtained.
- The electrical position estimation error is centered around zero, the highest noise peak does not exceed a threshold of 5 degrees.
- The mechanical speed estimation error is centered around zero, the highest noise peak does not exceed a threshold of 7RPM.
- The chattering effect is reduced compared to previous experimental result.

As a conclusion, very acceptable rotor position and speed estimation results are obtained at different speed/torque ranges, which confirms the accuracy and the performances of the technique. These results confirm that the improved estimation strategy offers a significant and attractive improvement compared to the classical technique.

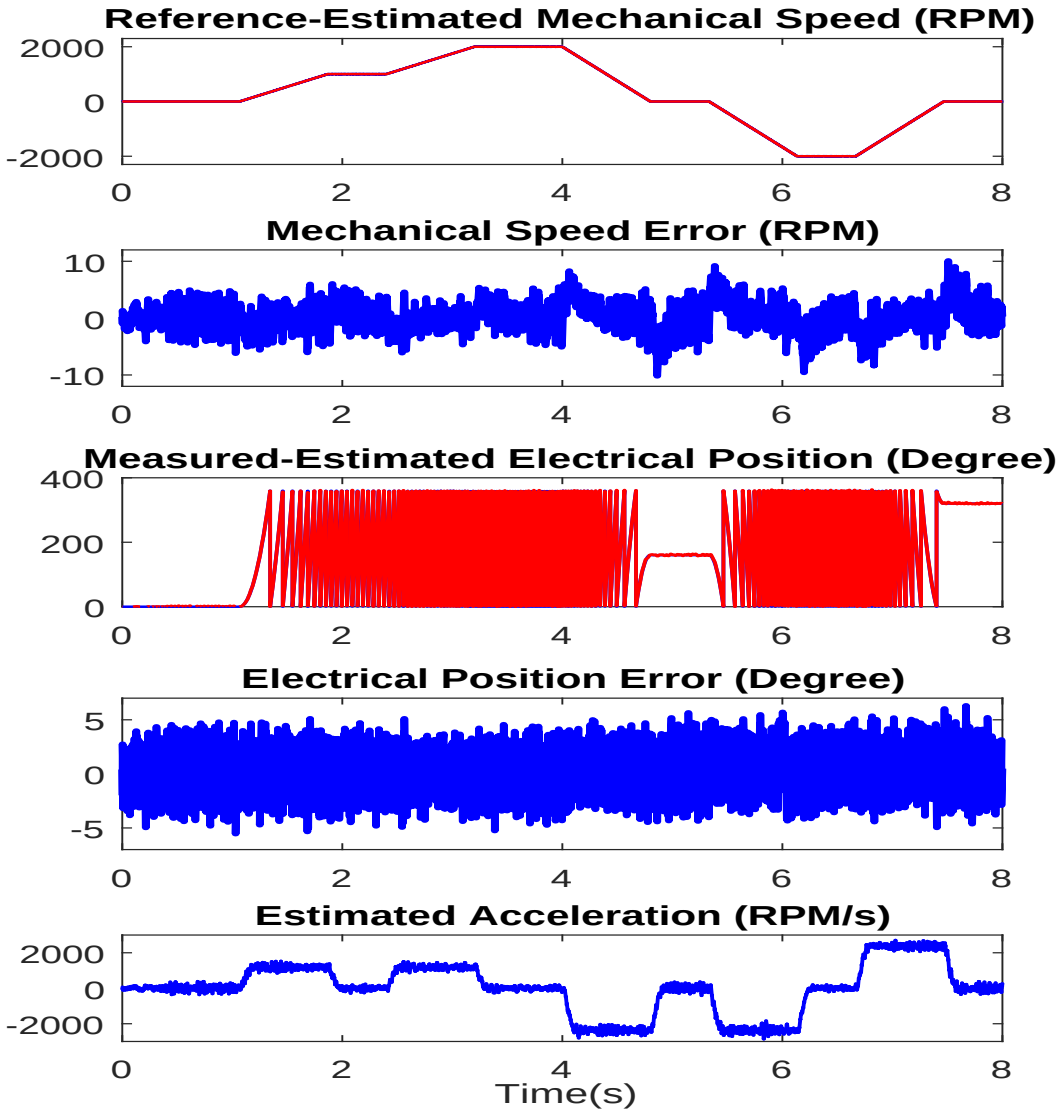

Figure 4.27: Experimental results of improved rotating sine-wave technique coupled with the A-S-B-S SMO

This comparative study confirms that the improved self-sensing strategy offers a significant and attractive improvement compared to classical methods.

4.6 Comparative study of the improved HFVI techniques

In the previous sections, performances and robustness of the developed self-sensing control strategies are evaluated through simulation and experimental tests. Many comparative studies are given in order to evaluate the strategies developed to show the evolutions and the improvements compared to classical techniques. This part focuses on comparative study between the improved pulsating sine-wave, the improved pulsating square-wave and the improved rotating sine-wave HFVI techniques. This comparative study is conducted with respect to the following criteria: rotor position and speed estimation error, sensitivity to electrical and mechanical parameters, delays caused by filters used, noise generated by the HF of the injected signal, acoustic noise and phase shifts generated by sampling time and inverter, the number of used filters and the implementation complexity. Moreover, in automotive applications, torque ripples phenomena is critical. For this reason, the impact of each HF signal injection technique on torque ripples, the number of used filters and the implementation complexity is discussed. For this comparison, the improved HFVI techniques introduced in Chapter 3 are coupled with the A-S-B-S SMO. From the obtained experimental results displayed in Figure 4.23 (for the improved pulsating sine-wave), Figure 4.27 (for the improved rotating sine-wave) and Figure 4.25 (for the improved pulsating square-wave), it can be noticed that

- The rotor position estimation error is centered around zero for all HFVI technique, the highest noise peak doesn't exceed a threshold of 1.8 *degrees* for the improved pulsating sine-wave technique, 4 *degrees* for the improved pulsating square-wave technique and 5 *degrees* for the improved rotating sine-wave technique.
- The mechanical speed estimation error is centered around zero, the highest noise peak doesn't exceed a threshold of 4 *RPM* for the improved pulsating sine-wave HFVI technique, 8 *RPM* for the improved pulsating square-wave HFVI technique and 10 *RPM* for the improved rotating sine-wave HFVI technique.
- The chattering has less effects for the improved pulsating sine-wave method compared to other HFVI techniques, the rotating sine-wave is less influenced by the chattering compared the pulsating square-wave method. This is due to harmonics generated by the too high injected frequency and the injected voltage's form (square-wave).
- The pulsating square-wave HFVI technique generates non negligible acoustic noise and requires sensitive current sensors. However, the pulsating sine-wave and the rotating sine-wave HFVI technique doesn't generate acoustic noise and doesn't require sensitive current sensors.
- The pulsating square-wave HFVI technique doesn't requires any filter, and it is very robust to the delays and phase shift of sampling time and used filters. On the other hand, the pulsating sine-wave HFVI technique requires one LPF filter, while, the rotating sine-wave HFVI technique requires at list one HPF and one LPF. Moreover, these two last HFVI techniques require a robust phase shift estimator in order to compensate all phase shifts generated by the phenomena cited before.
- It is important to analyze the impact of each HFVI technique on torque ripples. It follows, based on numerous simulation and experimental tests on IPMSM that both pulsating sine-wave and pulsating square-wave HFVI technique results are more effective compared to rotating sine-wave HFVI technique. This can be explained by the fact that injection occurs on the estimated d-axis, which results on less ripples on the q-axis, known as the most impactful on the torque value. The pulsating sine-wave HFVI technique generates less torque ripples, On the other hand, the pulsating square-wave HFVI technique generates small harmonics on the electromagnetic torque, however, the rotating sine-wave HFVI technique introduce an important torque ripples.

As a conclusion, very acceptable rotor position and speed estimation results are obtained at different speed/torque ranges for all improved HFVI methods. However, the pulsating sine-wave HFVI technique presents some strengths compared the other techniques. This comparative study, done between the improved pulsating sine-wave, pulsating square-wave and the rotating sine-wave HFVI techniques, is summarized in Table 4.10.

Table 4.10: Summary of the comparative study between the improved pulsating sine-wave, improved pulsating square-wave and the improved rotating sine-wave HFVI techniques.

Techniques / Criterions	Improved pulsating sine-wave HFVI	Improved pulsating square-wave HFVI	Improved rotating sine-wave HFVI
Mechanical parameters	Independent	Independent	Independent
Electrical parameters	Independent	Independent	Independent
Maximal rotor position estimation error (Degree)	1.8	5	8
Maximal speed estimation error (RPM)	2.7	7	6
Machine acceleration	Insensitive	Insensitive	Insensitive
Delays generated by filters inverter and sampling time	Insensitive	Insensitive	Insensitive
Number of filter used	One filter	No filter	Two filters
Torque ripples	Less sensitive	Less sensitive	Sensitive
Noise generated by the HIF	Less sensitive	Sensitive	Less sensitive

4.7 Evaluation of the improved pulsating sine-wave self-sensing technique under 120% and step load torque

From Table 4.10, the improved pulsating sine-wave HFVI technique is selected as a suitable HFVI techniques. This part consist in studying its accuracy under 0% and 120% load torque (greater than the nominal torque). In torque step test, the speed reference is varying, The torque reference signal of the load AC machine is changed by step signal from zero to 1.2 time the nominal value and back to zero. This test is performed at zero speed and at high speed in order to check the robustness and efficiency of the developed strategy in critical hard situation. It can be verify by the experimental results given in Figure 4.28 that

- A very convenient rotor position and speed estimation result is obtained even when in critical situations defined by 120% of the step load torque on both zero and high speed.
- The rotor position and speed estimation errors are very centered around zero.

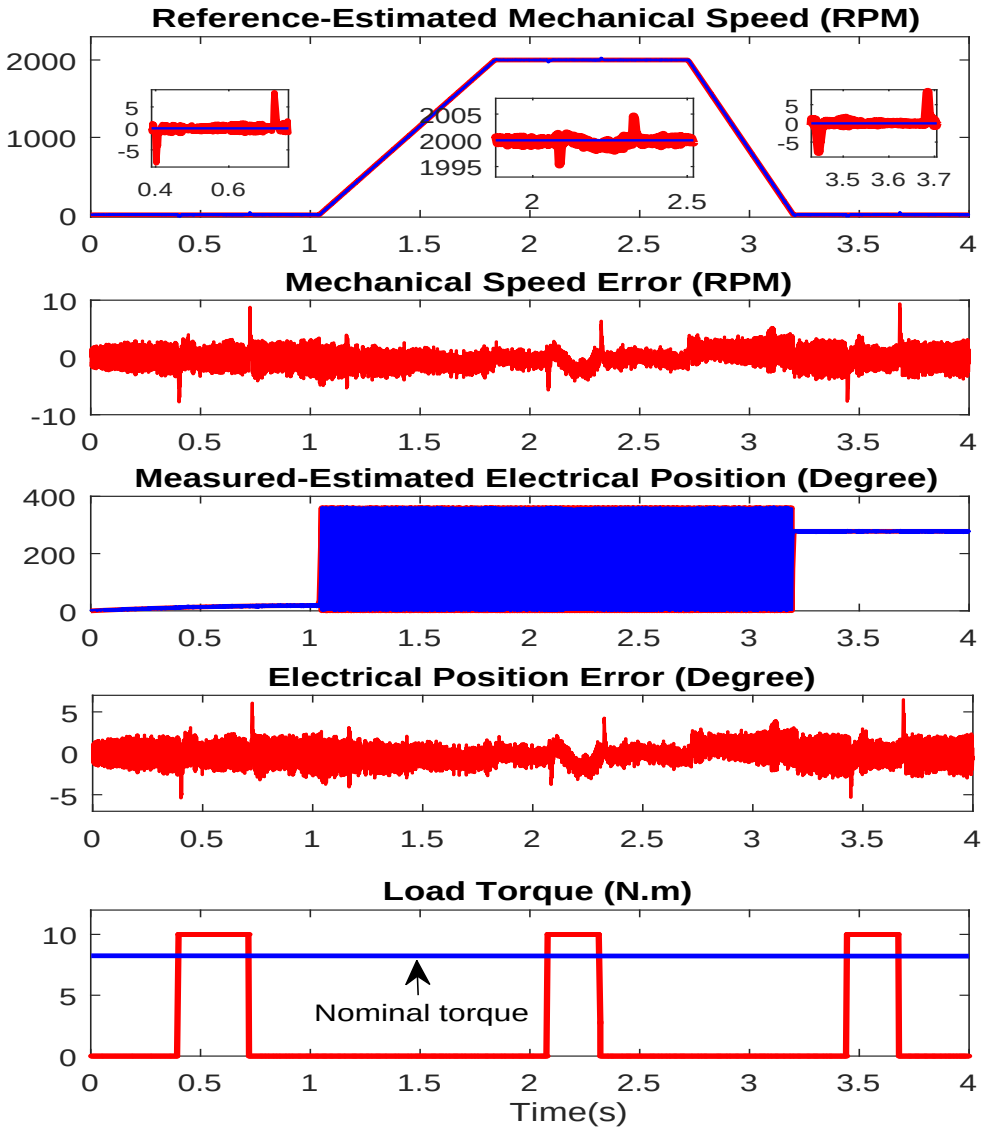

Figure 4.28: Experimental result of the improved pulsating sine-wave HFVI self-sensing strategy coupled with the A-S-B-S SMO under 120% step load torque

4.8 Conclusion

This chapter presented novel approaches for tracking algorithms associated to HFVI techniques in order to estimate the rotor position and speed of IPMSM. These approaches are based only on the sign of the rotor position estimation error instead of the rotor position estimation error used by the classical tracking algorithms. The use of the sign allows to get ride of machine's parameters dependency. The developed approach allows also to remove the LPFs used to extract the rotor position estimation error. As the sign of the rotor position estimation error is only the available measurement, the first order SMO is the natural choice to estimate the rotor position. This chapter proposed many improved alternative solutions: S-B-S SMO which leads to get the observer tuning with a decoupled manner and A-S-B-S SMO which deals with the chattering remaining on the estimated quantities. The stability of the proposed observers are proven in transient and steady state ranges.
The performances of the proposed approach are highlighted in simulation and experimentally with and without considering the improved demodulation (HPF/SFF removals and robust phase

shift estimator) given in Chapter 3. The comparative study between all the proposing tracking algorithms is given to show the main improvements. A second comparative study between the filtered A-S-B-S SMO and principal existing tracking algorithms is given to illustrate the effectiveness and the efficiency of the proposed selected A-S-B-S SMO. A robustness comparative study between the improved HFVI methods is given at the end in terms of:

- Rotor position and speed estimation error,
- Sensitivity to electrical and mechanical parameters, delays caused by filters used, noise generated by the HF of the injected signal,
- Generated torque ripples, acoustic noise and phase shifts caused by sampling time and Inverter.

This study served to select the suitable HFVI technique in terms of above cited criterion.

Finally, a very hard critical test is given to investigate accuracy and effectiveness of the improved pulsating sine-wave HFVI self-sensing strategy under 120% load torque. An improved rotor position and speed estimation result is obtained even when in critical situations defined by 120% of the step load torque on both zero and high speed. The rotor position and speed estimation errors are well centered around zero.

5

Conclusion and open topics

This work thesis is conducted in the framework of the chair between Ranault and Centrale Nantes about performances improvement of electric vehicles. New self-sensing control strategies based HFVI of the synchronous machine for EV/HEV applications are proposed. The main contributions are:
- to reduce the effects of filtering and delays of classical HFVI strategies,
- to make the estimation chain independent of electrical and mechanical machine parameters, and easier to tun,
- to ensure stable and robust motor operation in all speed and torque ranges,

The selected self-sensing control technique has been an important focus of this research work since it is a crucial issue at all speed ranges with different torque values. Indeed, the well-known pulsating sine-wave, rotating sine-wave and pulsating square-wave HF voltage injection methods have been investigated and implemented by paying attention to the demodulation process to extract the position error information and the tracking algorithm used to get the rotor position and speed estimation.
The demodulation process should be properly selected so as to
- reduce the number of filters,
- compensate the induced phase shifts and delays,
- obtain a rotor position error information independent of electrical machine parameters, while the tracking algorithm should:
- be independent of the knowledge of both electrical and mechanical machine's parameters,
- gives an acceptable estimation performance accuracy in both transient and steady state modes with an easier tunning.

The demodulation process combined with the tracking algorithm should ensures convenient rotor position and speed estimation results in all speed/torque ranges even in difficult situations imposed by the cycle of an electric propulsion drive benchmark.

The second chapter began by recalling the state-of-the-art of classical self-sensing HF techniques for IPMSM-based electric drives. The main interests and limitations of each self-sensing method in terms of demodulation process and tracking algorithm are highlighted. This allows to introduce the proposed saliency based methods of chapters 3 and 4 to estimate the rotor and speed of IPMSM.

The third chapter presented the first main contributions of this thesis work from the side of demodulation and signal processing of HF signal injection self-sensing method in order to extract the rotor position information of IPMSM. These contributions allow improving significantly the estimation process and covering an extended operating range of the machine (medium and high speeds operating modes with different torque values). The proposed contributions in this chapter help for reducing the delays sources effects and the effect of filtering, and for getting over the knowledge of electrical and mechanical machine parameters in order to increase the estimation performance on the drive self-sensing control of IPMSM. More precisely, in the context of EV drives, one of the most problems caused by the saliency based method is the carrier recovery at the demodulation side. The drive system can in fact introduce an unknown delay and phase shifts in the HF signals that can hardly be analytically predicted. A wrong phase shift of the demodulation signal with respect to the useful one can in fact lead to poor accuracy of the estimates or, in the worst case, to the impossibility of extracting the rotor position at all. This implies that the actual phase of superimposed high frequency signals has to be known, but this is not true in practical implementations. In fact, the effects of inverter nonlinearity (dead time, T_{on}, T_{off},...), HPF/SFF, sampling time, current sensors and LPFs are considered the main delays and phase shifts sources in the case of the HFVI approach. As clarified, these delays sources reflect uncertainties in the demodulated signal. Then a suitable carrier recovery algorithm is required for a correct demodulation of the HF current components. From this point of view, the main contributions of this chapter are :

- to reduce the filtering effects of HPF/SFF and LPF, in terms of delays, used in the estimation process,
- to estimate the phase shift related to the use of HPF/SFF, inverter effects, sampling time, current sensors sensitivity, and delays generated by the use of LPFs,
- to reclaim a new position estimation error with reduced harmonics and without the knowledge of electrical and mechanical IPMSM parameters.

The forth chapter presented the second main contribution of this work thesis from the side of tracking algorithms associated to HF signal injection self-sensing method in order to estimate the rotor position and speed. To overcome the dependency to machine parameters, the proposed tracking algorithm approach is based only on the sign of the rotor position estimation error instead of the rotor position estimation error used by the classical tracking algorithms. Besides of the parameter insensitivity, the developed approach allows also to remove the LPFs used to extract the rotor position estimation error.

By having only the sign of the rotor position estimation error as a known information, the first order sliding mode observer is the natural solution to estimate the rotor position.

From this point of view, this chapter proposed some improved alternative tracking algorithms based first-order SMO. Among them the S-B-S SMO with constant and adaptive gains. It is well known that the sliding mode observer with constant gains suffers from chattering phenomena. This phenomena can be reduced by using an LPF, but this solution generates delays and increases the cost and the complexity of the implementation. That is why, a S-B-S SMO with adaptive gains was proposed, in order to estimate the rotor position and speed with less chattering and with an easy tuning of the observer. Moreover, the acceleration was estimated to improve the position estimation in transient modes and a complete stability analysis was given to ensure the observer convergence in steady-state, transient and intermediate modes. This A-S-B-S SMO was associated to the classical and improved HFVI techniques. Then, from the results of conducted experimental tests and comparative study, the A-S-B-S SMO coupled with improved pulsating sine-wave HFVI technique was selected as the best solution in terms of accuracy, number of filters, generated torque ripples and delays.

Our next objectives are to:
- Deal with the cross saturation problem.
- Deal with power losses (reduction of torque ripples and acoustic noise) due to the HF signal injection.

Given the wide field research in electrical machines, a lot of development exist from the theatrical or practice point of view. Novel technologies must be integrated and more powerful control strategies must be implemented to answer to the new challenging problems for industrial applications. One of the most interesting prospects of research for AC machine control development could be to increase the applicability of these machines even if fault appears. Fault diagnostics methods can be used. Next, a prospect could be to adapt the control to detected the fault in order to carry on the machine control with limited but safe objectives. A direct application can be the aeronautic areas or variable speed drive.

A

Inverter

Appendix: Inverter

The inverter used in this work is a classic 3-leg inverter such as the switching frequency is set to 10kHz, the dead time is set at 2μs, and the corresponding dc-bus voltage is set to 400V. The bridge inverter is constituted of tree IGBT transistor legs, each one is composed by two transistors and a freewheeling which places just in parallel of these IGBTs, the diode conduct when there is a flowing current, the Figure A.1 illustrate 3-leg inverter which are connected to the stator of PMSM. The studies of the inverter show that the board of controller enable just one transistor and block the others in each leg of the inverter, also, two transistors in the same leg (the highest and the lowest) cannot be enable simultaneously in order to avoid the short circuit phenomena, this controller card permit to modulate the transistor state in function of the desired voltage in the output of the inverter a three-phase voltage source inverter.

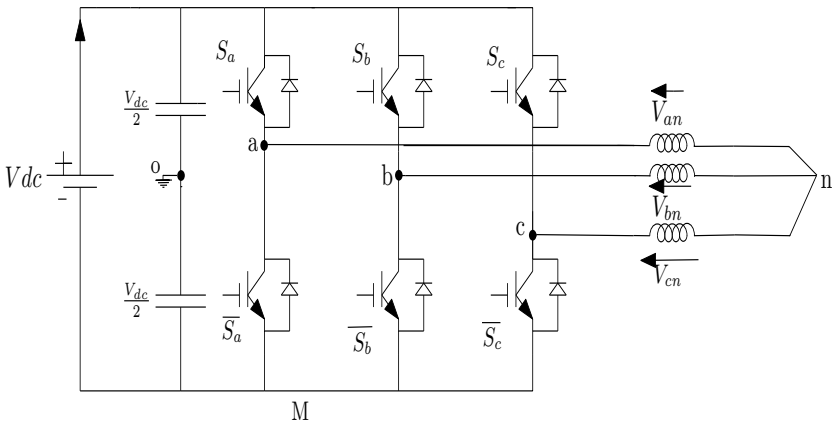

Figure A.1: A three phase bridge inverter

A.1 Classical modeling of the inverter

In this part, the classical model of the inverter is recalled. In order to recall the classical model of the inverter. The following assumptions are regarded:

- The voltage drop of switch (V_{ce}) is neglected.
- The voltage of freewheeling diode (V_d) is neglected.
- The dead time effect is neglected .

Considering the switching pattern for i= 0,1,2,3

$$\begin{cases} S_a = 1 & \text{if } S_a \text{ is turned on} \\ S_a = 0 & \text{if } S_a \text{ is turned off.} \end{cases} \tag{A.1}$$

$$\begin{cases} S_b = 1 & \text{if } S_b \text{ is turned on} \\ S_b = 0 & \text{if } S_b \text{ is turned off.} \end{cases} \tag{A.2}$$

$$\begin{cases} S_c = 1 & \text{if } S_c \text{ is turned on} \\ S_c = 0 & \text{if } S_c \text{ is turned off.} \end{cases} \tag{A.3}$$

Base on previous assumptions, the actual phase to center voltage are given as follows

$$\begin{cases} V_{ao} = \frac{V_{dc}}{2} & \text{if } S_a = 1 \\ V_{ao} = \frac{-V_{dc}}{2} & \text{if } S_a = 0 \end{cases} \tag{A.4}$$

$$\begin{cases} V_{bo} = \frac{V_{dc}}{2} & \text{if } S_b = 1 \\ V_{bo} = \frac{-V_{dc}}{2} & \text{if } S_b = 0 \end{cases} \tag{A.5}$$

$$\begin{cases} V_{co} = \frac{V_{dc}}{2} & \text{if } S_c = 1 \\ V_{co} = \frac{-V_{dc}}{2} & \text{if } S_c = 0. \end{cases} \tag{A.6}$$

Based on Equations (A.6), (A.5) and (A.4), the phase-to-center voltages can be written as follows

$$V_{io} = V_{dc}(S_i - \frac{1}{2}) \tag{A.7}$$

where, i=a,b,c.
The three phase-to-center voltage can be written as

$$\begin{cases} V_{ao} = V_{dc}(S_a - \frac{1}{2}) \\ V_{bo} = V_{dc}(S_b - \frac{1}{2}) \\ V_{co} = V_{dc}(S_c - \frac{1}{2}). \end{cases} \tag{A.8}$$

Using the Equation (A.8), the phase-to-phase voltages expression are given as follows

$$\begin{cases} V_{ab} = V_{ao} - V_{bo} \\ V_{bc} = V_{ao} - V_{bo} \\ V_{ca} = V_{co} - V_{ao}. \end{cases} \tag{A.9}$$

By replacing the expressions of V_{ao}, V_{bo} and V_{co} (given by (A.8)) in (A.9), phase-to-phase voltages are obtained

$$\begin{bmatrix} V_{ab} \\ V_{bc} \\ V_{ca} \end{bmatrix} = V_{dc} \begin{pmatrix} 1 & -1 & 0 \\ 0 & 1 & -1 \\ -1 & 0 & 1 \end{pmatrix} \begin{pmatrix} S_a \\ S_b \\ S_c \end{pmatrix} \tag{A.10}$$

To obtain the phase neutral voltages of this inverter, the following equations are considered

$$\begin{cases} V_{ao} = V_{an} + V_{no} \\ V_{bo} = V_{bn} + V_{no} \\ V_{co} = V_{cn} + V_{no} \end{cases} \tag{A.11}$$

Assuming that the system is balanced, the following expressions can be written

$$i_{an} + i_{bn} + i_{cn} = 0 \tag{A.12}$$

and

$$V_{an} + V_{bn} + V_{cn} = 0. \tag{A.13}$$

Based on (A.11) and (A.13), the expression of V_{no} is written as

$$V_{no} = \frac{1}{3}(V_{ao} + V_{bo} + V_{co}). \tag{A.14}$$

By replacing (A.14) in (A.11), the following equation is obtained

$$\begin{cases} V_{an} = V_{ao} - \frac{1}{3}(V_{ao} + V_{bo} + V_{co}) \\ V_{bn} = V_{bo} - \frac{1}{3}(V_{ao} + V_{bo} + V_{co}) \\ V_{cn} = V_{co} - \frac{1}{3}(V_{ao} + V_{bo} + V_{co}). \end{cases} \tag{A.15}$$

Replacing the V_{ao},V_{bo} and V_{co} in (A.15), the phase neutral voltages expression are given

$$\begin{bmatrix} V_{an} \\ V_{bn} \\ V_{cn} \end{bmatrix} = \frac{V_{dc}}{3} \begin{pmatrix} 2 & -1 & -1 \\ -1 & 2 & -1 \\ -1 & -1 & 2 \end{pmatrix} \begin{pmatrix} S_a \\ S_b \\ S_c \end{pmatrix}. \tag{A.16}$$

A.2 Voltage distortion analysis for the compensation strategy

There are several causes to distort the output voltage in voltage-fed PWM inverter. the commonly distortion caused by the dead time that is inevitable to prevent it.
During the dead time (T_d), both the power devices in the same leg cease to conduct , the load current continues to crossing an anti-parallel diode (freewheel) during the dead time even if the two trigger signals are weak [55] [202]. If the current flows to load (see Figure. A.2), the lower diode will conduct. Otherwise (see Figure. A.3) the upper diode will conduct.
In this part, the analysis of the voltage distortion is discussed with consideration of the dead time effect and voltage drop of the power devices [55] [203], in order to discuss this distortion, voltage drops of the power devices, turn-on/off delay time are also considered.

A.2.1 When the current flows to the load

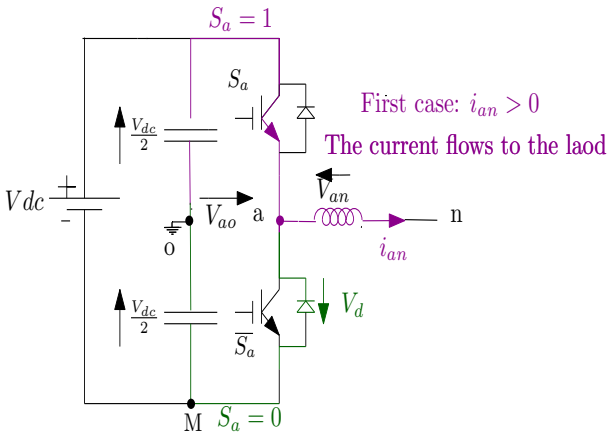

Figure A.2: The behavior of devices of inverter when the current flows to the load

In addition to dead time effect, there exist the voltage drops of the power devices (V_{ce} and V_d) that distort the output voltage. If the current flows to the load ($i_{an} > 0$) (see Figure. A.2), the actual phase to center voltage is

$$\begin{cases} V_{ao} = \frac{V_{dc}}{2} - V_{ce} & \text{if} \quad S_a = 1 \\ V_{ao} = \frac{-V_{dc}}{2} - V_d & \text{if} \quad S_a = 0. \end{cases} \tag{A.17}$$

A.2.2 When the current flows from the load

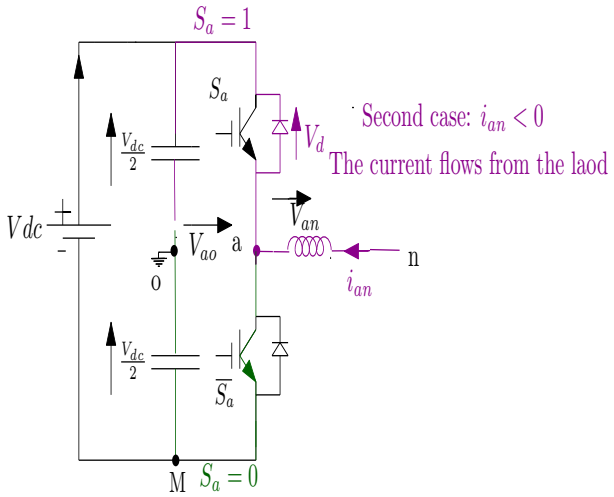

Figure A.3: The behavior of devices of inverter when the current flows from the load

If the current flows from the load ($i_{an} < 0$) (see Figure. A.3), the phase-to-center voltage is

$$\begin{cases} V_{ao} = \frac{V_{dc}}{2} + V_d & \text{if} \quad S_a = 1 \\ V_{ao} = \frac{-V_{dc}}{2} + V_{ce} & \text{if} \quad S_a = 0. \end{cases} \tag{A.18}$$

Based on the previous two Equations (A.17) (A.18) and by considering the voltage drop of the power devices switching state and the current direction, phase-to-center voltages can be written as follows

$$V_{io} = (V_{dc} - V_{ce} + V_d)(S_i - \frac{1}{2}) - \frac{1}{2}(V_{ce} + V_d)sign(i_{jn}) \tag{A.19}$$

where, $j = a, b, c$.

The three phase-to-center voltage can be written as

$$\begin{cases} V_{ao} = (V_{dc} - V_{ce} + V_d)(S_a - \frac{1}{2}) - \frac{1}{2}(V_{ce} + V_d)sign(i_{an}) \\ V_{bo} = (V_{dc} - V_{ce} + V_d)(S_b - \frac{1}{2}) - \frac{1}{2}(V_{ce} + V_d)sign(i_{bn}) \\ V_{co} = (V_{dc} - V_{ce} + V_d)(S_c - \frac{1}{2}) - \frac{1}{2}(V_{ce} + V_d)sign(i_{cn}). \end{cases} \tag{A.20}$$

Generally, both the voltages drops of the freewheeling and the active switching linearly increase with increasing of the current at the normal region, its can be modeled as

$$V_{ce} = V_{ce0} + r_{ce}|i_{an}| \tag{A.21}$$

where
- V_{ce0} threshold voltage of the active switch.
- r_{ce} on-state slope resistance of the active switch.

$$V_d = V_{d0} + r_d|i_{an}| \tag{A.22}$$

where
- V_{d0} threshold voltage of the freewheeling diode.
- r_d on-state slope resistance of the freewheeling diode.

The Equation (A.20) phase to center voltage can be written as

$$\begin{cases} V_{ao} = (V_{dc} - V_{ce} + V_d)(S_a - \frac{1}{2}) - \frac{1}{2}sign(i_{an})(V_{ce0} + V_{d0}) - \frac{1}{2}(r_{ce} + r_d)(i_{an}) \\ V_{bo} = (V_{dc} - V_{ce} + V_d)(S_b - \frac{1}{2}) - \frac{1}{2}sign(i_{bn})(V_{ce0} + V_{d0}) - \frac{1}{2}(r_{ce} + r_d)(i_{bn}) \\ V_{co} = (V_{dc} - V_{ce} + V_d)(S_c - \frac{1}{2}) - \frac{1}{2}sign(i_{cn})(V_{ce0} + V_{d0}) - \frac{1}{2}(r_{ce} + r_d)(i_{cn}). \end{cases} \tag{A.23}$$

By replacing the expressions of V_{ao} V_{bo} V_{co} given in (A.23) in the previous Equation (A.9), the phase-to-phase voltages are obtained

$$\begin{bmatrix} V_{ab} \\ V_{bc} \\ V_{ca} \end{bmatrix} = (V_{dc} - V_{ce} + V_d) \begin{pmatrix} 1 & -1 & 0 \\ 0 & 1 & -1 \\ -1 & 0 & 1 \end{pmatrix} \begin{pmatrix} S_a \\ S_b \\ S_c \end{pmatrix} - \frac{(V_{ce0} + V_{d0})}{2} \begin{pmatrix} 1 & -1 & 0 \\ 0 & 1 & -1 \\ -1 & 0 & 1 \end{pmatrix} \begin{pmatrix} sign(i_{an}) \\ sign(i_{bn}) \\ sign(i_{cn}) \end{pmatrix} - \frac{(r_d + r_{ce})}{2} \begin{pmatrix} i_{an} \\ i_{bn} \\ i_{cn} \end{pmatrix}. \tag{A.24}$$

To obtain the phase neutral voltages of this inverter, Equations (A.11), (A.12), (A.13) and (A.14) are considered.
Replacing the V_{ao},V_{bo}, V_{co} given in (A.23), the phase neutral voltages expression are given as follows

$$\begin{bmatrix} V_{an} \\ V_{bn} \\ V_{cn} \end{bmatrix} = \frac{(V_{dc} - V_{ce} + V_d)}{3} \begin{pmatrix} 2 & -1 & -1 \\ -1 & 2 & -1 \\ -1 & -1 & 2 \end{pmatrix} \begin{pmatrix} S_a \\ S_b \\ S_c \end{pmatrix} - \frac{(V_{ce0} + V_{d0})}{6} \begin{pmatrix} 2 & -1 & -1 \\ -1 & 2 & -1 \\ -1 & -1 & 2 \end{pmatrix} \begin{pmatrix} sign(i_{an}) \\ sign(i_{bn}) \\ sign(i_{cn}) \end{pmatrix} - \frac{(r_{ce} - r_d)}{2} \begin{pmatrix} i_{an} \\ i_{bn} \\ i_{cn} \end{pmatrix}. \tag{A.25}$$

Bibliography

[1] A. Messali, M. A. Hamida, M. Ghanes, and M. Koteich, "Enhanced square wave signal injection for self-sensing ac machines with improved transient performances," in *IET Electric Power Applications*, Correction phase. 5, 53

[2] A. Messali, M. Aassad Hamida, M. Ghanes, and M. Koteich, "A novel high frequency signal injection strategy for self-sensing control of electric ac machine drives," in *IECON 2018 - 44th Annual Conference of the IEEE Industrial Electronics Society*, Oct 2018, pp. 343–348. 5, 52, 53, 79, 91

[3] A. Messali, M. A. Hamida, M. Ghanes, and M. Koteich, "Robust phase-shift estimator for self-sensing control of pm synchronous machines," in *IEEE International Conference on Sensorless Control for Electrical Drives (SLED), Torino, Italy*, Sep 2019. 5, 59

[4] A. Messali, M. A. Hamida, M. Ghanes, and M. Koteich, "A rotor position, speed and acceleration estimation for salient-pole ac machines at all speed and torque ranges," in *IEEE International Conference on Power Electronics and Drive Systems (PEDS 2019), Toulouse, France*, Jul 2019. 5, 59

[5] A. Messali, M. Ghanes, M. A. Hamida, and M. Koteich, "A resilient adaptive sliding mode observer for self-sensing ac machine drives based on an improved hf injection technique," in *IFAC Control Engineering Practice*, Accepted. 5, 6, 59, 100

[6] A. Messali, M. A. Hamida, M. Ghanes, and M. Koteich, "Rotating hf signal injection method improvement based on robust phase-shift estimator for self-sensing control of ipmsm," in *IEEE International Conference on Diagnostics for Electric Machines, Power Electronics and Drives (SDEMPED), Toulouse, France*, Aug 2019. 5, 71

[7] A. Messali, M. Ghanes, M. Koteich, and M. A. Hamida, "A robust observer of rotor position and speed for ipmsm hfi sensorless drives," in *2018 IEEE 9th International Symposium on Sensorless Control for Electrical Drives (SLED)*, Sept 2018, pp. 90–95. 6, 52, 79, 91

[8] A. Messali, M. Ghanes, and M. Koteich, "Procédé de commande des machines électriques triphasées sans capteur de position," Patent, 2019. 6, 91

[9] A. Messali, M. Ghanes, M. A. Hamida, and M. Koteich, "An estimation procedure based on less filtering and robust tracking for a self-sensing control of pole salient ac machine," in *IEEE Transactions on Industrial Electronics (Correction phase)*, Sep. 2019, pp. 90–95. 6, 95

[10] A. Messali, M. Ghanes, and M. Koteich, "Procédé d'estimation de la position, vitesse et accélération d'une machine électrique tournante triphasée," Patent, 2019. 6, 95, 100

[11] A. Messali, M. Ghanes, M. A. Hamida, and M. Koteich, "Robust adaptive sliding mode observer for self-sensing ipmsm control based on optimized hf injection method," in *Nonlinear Control Systems - 11th IFAC Symposium on Nonlinear Control Systems (NOLCOS), Vienna, Austria*, Sep. 2019. 6, 100

[12] L. Situ, "Electric vehicle development: The past, present future," in *2009 3rd International Conference on Power Electronics Systems and Applications (PESA)*, May 2009, pp. 1–3. 9, 15, 16, 18

[13] C. C. Chan, "An overview of electric vehicle technology," *Proceedings of the IEEE*, vol. 81, no. 9, pp. 1202–1213, Sep. 1993. 9, 17

[14] V. Mester, "Global Optimal Design of Electric Drive Trains Components," Theses, Ecole Centrale de Lille, May 2007. 9, 18

[15] C. Philipps-Bertin and L. Poupon, "De l'acceptabilité à l'adoption du ve: le rôle des émotions dans le processus," 2017. 15, 16, 17, 18, 19

[16] G. A. Covic, J. T. Boys, M. Budhia, and C.-Y. Huang, "Electric vehicles–personal transportation for the future," *World Electric Vehicle Journal*, vol. 4, no. 4, pp. 693–704, 2010. 16

[17] K. Itani, "Récupération dénergie pour système intégré moteur roue, application au véhicule électrique," Ph.D. dissertation, Université Paris-Saclay, 2017. 16

[18] A.-F. Garçon, "La voiture électrique dans la nature (1890_1900). approche micro-historique d'un échec technique," *Cahiers François Viète*, no. 5, pp. 17–43, 2003. 16

[19] A.-F. GARÇON, "La voiture électrique dans la nature (1890-1900)," *Cahiers François Viète*, vol. 5, pp. 17–43, 2003. 16, 17

[20] C. C. Chan, "The state of the art of electric, hybrid, and fuel cell vehicles," *Proceedings of the IEEE*, vol. 95, no. 4, pp. 704–718, 2007. 16

[21] A. Foucquier and Y. Thomas, *Histoire de la voiture électrique et de ses constituants*. ISTE Group, 2017. 16, 17

[22] J.-L. Loubet, D. Larroque, and P. Griset, *Electricité électronique: un siècle de développement automobile*. ETAI, 2003. 16

[23] S. D'Agostino, "The electric car," *IEEE Potentials*, vol. 12, no. 1, pp. 28–32, Feb 1993. 16

[24] M. Callon, "L'état face à l'innovation technique: le cas du véhicule électrique," *Revue de science politique*, pp. 426–447, 1979. 16

[25] H. Shareef, M. M. Islam, and A. Mohamed, "A review of the stage-of-the-art charging technologies, placement methodologies, and impacts of electric vehicles," *Renewable and Sustainable Energy Reviews*, vol. 64, pp. 403–420, 2016. 16

[26] G.-A. Nazri and G. Pistoia, *Lithium batteries: science and technology*. Springer Science & Business Media, 2008. 17

[27] T. Horiba, K. Hironaka, T. Matsumura, T. Kai, M. Koseki, and Y. Muranaka, "Manganese-based lithium batteries for hybrid electric vehicle applications," *Journal of Power Sources*, vol. 119, pp. 893–896, 2003. 17

[28] A. G. Boulanger, A. C. Chu, S. Maxx, and D. L. Waltz, "Vehicle electrification: Status and issues," *Proceedings of the IEEE*, vol. 99, no. 6, pp. 1116–1138, 2011. 18

[29] O. Wyman, "Future of ice: why accelerating r&d spend is critical for future competitiveness & to reach 50g co2/km," in *2015 ICE research needs workshop, ERTRAC Workshop, 2 June 2015, Brussels*, 2015. 18

[30] C. Thiel, A. Perujo, and A. Mercier, "Cost and co2 aspects of future vehicle options in europe under new energy policy scenarios," *Energy policy*, vol. 38, no. 11, pp. 7142–7151, 2010. 18

[31] A. Tiwari and O. P. Jaga, "Component selection for an electric vehicle: A review," in *2017 International Conference on Computation of Power, Energy Information and Commuincation (ICCPEIC)*, March 2017, pp. 492–499. 19

[32] I. Boldea, "Control issues in adjustable speed drives," *IEEE Industrial Electronics Magazine*, vol. 2, no. 3, pp. 32–50, Sep. 2008. 19

[33] M. Pacas, "Sensorless drives in industrial applications," *IEEE Industrial Electronics Magazine*, vol. 5, no. 2, pp. 16–23, June 2011. 19

[34] F. Betin, G. Capolino, D. Casadei, B. Kawkabani, R. I. Bojoi, L. Harnefors, E. Levi, L. Parsa, and B. Fahimi, "Trends in electrical machines control: Samples for classical, sensorless, and fault-tolerant techniques," *IEEE Industrial Electronics Magazine*, vol. 8, no. 2, pp. 43–55, June 2014. 19

[35] E. Yesilbag and L. T. Ergene, "Field oriented control of permanent magnet synchronous motors used in washers," in *2014 16th International Power Electronics and Motion Control Conference and Exposition*, Sep. 2014, pp. 1259–1264. 19

[36] M. M. Bech, J. K. Pedersen, and F. Blaabjerg, "Field-oriented control of an induction motor using random pulsewidth modulation," *IEEE Transactions on Industry Applications*, vol. 37, no. 6, pp. 1777–1785, Nov 2001. 19

[37] V. Lesic, M. Vasak, M. Gulin, N. Peric, G. Joksimovic, and T. M. Wolbank, "Field-oriented control of an induction machine with winding asymmetries," in *2012 15th International Power Electronics and Motion Control Conference (EPE/PEMC)*, Sep. 2012, pp. LS7b–1.2–1–LS7b–1.2–7. 19

[38] H. Chai, P. Yan, and L. Guo, "Feedback linearization design for permanent magnet synchronous motor with disturbance observer," in *Proceedings of the 32nd Chinese Control Conference*, July 2013, pp. 2739–2744. 19

[39] Li Fang, Wang Yushun, and Wang Ruiqi, "Simulation of speed-control system for pmsm based on sliding mode control," in *Proceedings 2013 International Conference on Mechatronic Sciences, Electric Engineering and Computer (MEC)*, Dec 2013, pp. 52–56. 19

[40] W. Lin, C. Hong, M. Lee, C. Huang, C. Huang, and B. Wu, "Fuzzy sliding mode-based control for pmsg maximum wind energy capture with compensated pitch angle," in *2010 International Symposium on Computer, Communication, Control and Automation (3CA)*, vol. 2, May 2010, pp. 397–400. 19

[41] M. Karabacak and H. I. Eskikurt, "Speed and current regulation of a permanent magnet synchronous motor via nonlinear and adaptive backstepping control," *Mathematical and Computer Modelling*, vol. 53, no. 9, pp. 2015 – 2030, 2011. 19

[42] H. Xue and Y. Wang, "Passivity-based control of synchronous motors," *2012 3rd IEEE PES Innovative Smart Grid Technologies Europe (ISGT Europe)*, pp. 1–5, 2009. 19

[43] D. Bao, Y. Wang, X. Pan, X. Wang, and K. Li, "Improved sensorless control method combining smo and mras for surface pmsm drives," in *2017 IEEE Industry Applications Society Annual Meeting*, Oct 2017, pp. 1–5. 19, 30, 32

[44] W. Zhao, S. Jiao, Q. Chen, D. Xu, and J. Ji, "Sensorless control of a linear permanent-magnet motor based on an improved disturbance observer," *IEEE Transactions on Industrial Electronics*, vol. 65, no. 12, pp. 9291–9300, Dec 2018. 19, 30, 32

[45] Y. Duan, "A comparison of saliency based sensorless control techniques for a pm machine," Ph.D. dissertation, University of Nottingham, 2012. 19, 30, 31, 33, 47, 48, 79

[46] R. Ueda, H. Takata, S. Nakagaki, and S. Takata, "On the estimation of transient state of power system by discrete nonlinear observer," *IEEE Transactions on Power Apparatus and Systems*, vol. 94, no. 6, pp. 2135–2140, Nov 1975. 19, 30, 32

[47] C. Lascu, I. Boldea, and F. Blaabjerg, "Comparative study of adaptive and inherently sensorless observers for variable-speed induction-motor drives," *IEEE Transactions on Industrial Electronics*, vol. 53, no. 1, pp. 57–65, Feb 2006. 19, 30, 32

[48] F. Blaschke, "The principle of field orientation as applied to the new trans vector closed-loop control system for rotating-field machine," *Book*, pp. 217–220, 1972. 23, 26, 30

[49] F. Blaschke, J. van der Burgt, and A. Vandenput, "Sensorless direct field orientation at zero flux frequency," in *IAS '96. Conference Record of the 1996 IEEE Industry Applications Conference Thirty-First IAS Annual Meeting*, vol. 1, Oct 1996, pp. 189–196 vol.1. 23, 30

[50] Q. Gao, G. M. Asher, M. Sumner, and P. Makys, "Position estimation of ac machines over a wide frequency range based on space vector pwm excitation," *IEEE Transactions on Industry Applications*, vol. 43, no. 4, pp. 1001–1011, July 2007. 23, 48

[51] Y. Hua, "Sensorless control of surface mounted permanent magnet machine using fundamental pwm excitation," Ph.D. dissertation, University of Nottingham, 2009. 23, 24, 26, 47, 79

[52] M. Linke, R. Kennel, and J. Holtz, "Sensorless position control of permanent magnet synchronous machines without limitation at zero speed," in *IEEE 2002 28th Annual Conference of the Industrial Electronics Society. IECON 02*, vol. 1, Nov 2002, pp. 674–679 vol.1. 24

[53] J. Holtz, "Sensorless control of induction machineswith or without signal injection?" *IEEE Transactions on Industrial Electronics*, vol. 53, no. 1, pp. 7–30, Feb 2006. 24

[54] P. Vas, *Vector control of AC machines*. Oxford [England] : Clarendon Press ; New York : Oxford University Press, 1990. 24, 25, 26, 30

[55] A. K. Jebai, "Sensorless control of synchronous permanent magnet motors by signal injection," Theses, Ecole Nationale Supérieure des Mines de Paris, Mar. 2013. 25, 129

[56] A. B. Proca, A. Keyhani, A. El-Antably, Wenzhe Lu, and Min Dai, "Analytical model for permanent magnet motors with surface mounted magnets," *IEEE Transactions on Energy Conversion*, vol. 18, no. 3, pp. 386–391, Sep. 2003. 25

[57] T. M. Jahns, G. B. Kliman, and T. W. Neumann, "Interior permanent-magnet synchronous motors for adjustable-speed drives," *IEEE Transactions on Industry Applications*, vol. IA-22, no. 4, pp. 738–747, July 1986. 25

[58] B. Bose, "Power electronics and ac drives, prentices," *Inc. Englewood Cliffs*, 1986. 25

[59] S.-K. Sul, *Control of Electric Machine Drive Systems*. Wiley-IEEE Press, 2011. 25, 35, 41, 42, 51

[60] A. Glumineau and J. Morales, *Sensorless AC Electric Motor Control, Book*. Springer, 2015. 25

[61] A. M. Trzynadlowski, *The Field Orientation Principle in Control of Induction Motors*. University of Nevada, Reno, 1994. 25, 26, 30

[62] L. Gong, "Carrier signal injection based sensorless control of permanent magnet brushless ac machines," Ph.D. dissertation, University of Sheffield, 2012. 25

[63] G. Kron, "Steady-state equivalent circuits of synchronous and induction machines," *Transactions of the American Institute of Electrical Engineers*, vol. 67, no. 1, pp. 175–181, Jan 1948. 25, 26

[64] M. Koteich, "Modélisation et observabilité des machines électriques en vue de la commande sans capteur mécanique," Ph.D. dissertation, 2016. 26, 32

[65] S. Medjmadj, D. Diallo, M. Mostefai, C. Delpha, and A. Arias, "Pmsm drive position estimation: Contribution to the high-frequency injection voltage selection issue," *IEEE Transactions on Energy Conversion*, vol. 30, no. 1, pp. 349–358, March 2015. 26, 36

[66] R. H. Park, "Two-reaction theory of synchronous machines generalized method of analysis-part i," *Transactions of the American Institute of Electrical Engineers*, vol. 48, no. 3, pp. 716–727, July 1929. 26, 27

[67] R. H. Park, "Two-reaction theory of synchronous machines-ii," *Transactions of the American Institute of Electrical Engineers*, vol. 52, no. 2, pp. 352–354, June 1933. 26, 27

[68] C. Concordia, "Two-reaction theory or synchronous machines with any balanced terminal impedance," *Transactions of the American Institute of Electrical Engineers*, vol. 56, no. 9, pp. 1124–1127, Sep. 1937. 26, 27

[69] H. C. Stanley, "An analysis of the induction machine," *Transactions of the American Institute of Electrical Engineers*, vol. 57, no. 12, pp. 751–757, Dec 1938. 26

[70] G. Kron, "Classification of the reference frames of a synchronous machine," *Transactions of the American Institute of Electrical Engineers*, vol. 69, no. 2, pp. 720–727, Jan 1950. 26

[71] G. Xie, K. Lu, S. K. Dwivedi, J. R. Rosholm, and F. Blaabjerg, "Minimum-voltage vector injection method for sensorless control of pmsm for low-speed operations," *IEEE Transactions on Power Electronics*, vol. 31, no. 2, pp. 1785–1794, Feb 2016. 29, 33

[72] G. Wang, L. Yang, G. Zhang, X. Zhang, and D. Xu, "Comparative investigation of pseudorandom high-frequency signal injection schemes for sensorless ipmsm drives," *IEEE Transactions on Power Electronics*, vol. 32, no. 3, pp. 2123–2132, March 2017. 29

[73] T. Yoon, H. Sim, J. Lee, and K. Lee, "A simplified method to estimate the rotor position using the high frequency voltage signal injection," in *2014 IEEE Applied Power Electronics Conference and Exposition - APEC 2014*, March 2014, pp. 2453–2458. 29

[74] F. Blaschke, J. van der Burgt, and A. Vandenput, "Sensorless direct field orientation at zero flux frequency," in *IAS '96. Conference Record of the 1996 IEEE Industry Applications Conference Thirty-First IAS Annual Meeting*, vol. 1, Oct 1996, pp. 189–196 vol.1. 30

[75] K. Sahri, M. Pietrzak-David, M. Fadel, and A. Kheloui, "Sensorless tolerant fault control for dual permanent magnet synchronous motor drive with global fpga emulator," in *2018 20th European Conference on Power Electronics and Applications (EPE'18 ECCE Europe)*, Sep. 2018, pp. P.1–P.8. 30

[76] M. Fadel and A. LLOR, "Comparison of different solutions in predictive control for two pmsm in parallel," *IFAC Proceedings Volumes*, vol. 47, no. 3, pp. 11 962 – 11 967, 2014, 19th IFAC World Congress. 30

[77] F. Morel, X. Lin-Shi, J. Retif, B. Allard, and C. Buttay, "A comparative study of predictive current control schemes for a permanent-magnet synchronous machine drive," *IEEE Transactions on Industrial Electronics*, vol. 56, no. 7, pp. 2715–2728, July 2009. 30

[78] R. Bojoi, M. Lazzari, F. Profumo, and A. Tenconi, "Digital field-oriented control for dual three-phase induction motor drives," *IEEE Transactions on Industry Applications*, vol. 39, no. 3, pp. 752–760, May 2003. 30

[79] C. Ilas, A. Bettini, L. Ferraris, G. Griva, and F. Profumo, "Comparison of different schemes without shaft sensors for field oriented control drives," in *Proceedings of IECON'94 - 20th*

Annual Conference of IEEE Industrial Electronics, vol. 3, Sep. 1994, pp. 1579–1588 vol.3. 30

[80] H. Kubota, K. Matsuse, and T. Nakano, "Dsp-based speed adaptive flux observer of induction motor," *IEEE Transactions on Industry Applications*, vol. 29, no. 2, pp. 344–348, March 1993. 31, 32

[81] S. Sangwongwanich, S. Suwankawin, S. Po-ngam, and S. Koonlaboon, "A unified speed estimation design framework for sensorless ac motor drives based on positive-real property," in *2007 Power Conversion Conference - Nagoya*, April 2007, pp. 1111–1118. 31, 32

[82] F. Briz, M. W. Degner, P. Garcia, and R. D. Lorenz, "Comparison of saliency-based sensorless control techniques for ac machines," *IEEE Transactions on Industry Applications*, vol. 40, no. 4, pp. 1107–1115, July 2004. 31, 33

[83] H. Tajima, G. Guidi, and H. Umida, "Consideration about problems and solutions of speed estimation method and parameter tuning for speed sensorless vector control of induction motor drives," in *Conference Record of the 2000 IEEE Industry Applications Conference. Thirty-Fifth IAS Annual Meeting and World Conference on Industrial Applications of Electrical Energy (Cat. No.00CH37129)*, vol. 3, Oct 2000, pp. 1787–1793 vol.3. 31, 33

[84] W. Zine, Z. Makni, E. Monmasson, L. Idkhajine, and B. Condamin, "Interests and limits of machine learning-based neural networks for rotor position estimation in ev traction drives," *IEEE Transactions on Industrial Informatics*, vol. 14, no. 5, pp. 1942–1951, May 2018. 31, 49

[85] G. Lefebvre, "Commande de machine asynchrone sans capteur de vitesse : Application traction ferroviaire," Ph.D. dissertation, Lyon, INSA, 2016. 31, 32

[86] M. Koteich, A. Maloum, G. Duc, and G. Sandou, "Discussion on ac drive observability analysis," *IEEE Transactions on Industrial Electronics*, vol. 62, no. 11, pp. 7224–7225, Nov 2015. 32

[87] M. Hinkkanen, "Analysis and design of full-order flux observers for sensorless induction motors," *IEEE Transactions on Industrial Electronics*, vol. 51, no. 5, pp. 1033–1040, Oct 2004. 32

[88] M. A. Hamida, J. De Leon-Morales, and A. Messali, "Observer design for nonlinear interconnected systems: experimental tests for self-sensing control of synchronous machine," *The International Journal of Advanced Manufacturing Technology*, pp. 1041–1054, Aug 2019. 32

[89] M. Fadel, "Load torque observer of permanent magnet synchronous motor," 2010. 32

[90] A. Zgorski, X. Lin-Shi, and J. Gauthier, "Sensorless position control for surface permanent magnet synchronous motors at zero speed and acceleration," *IFAC Proceedings Volumes*, vol. 46, no. 11, pp. 122 – 127, 2013, 11th IFAC Workshop on Adaptation and Learning in Control and Signal Processing. 32, 33

[91] G. Lefebvre, X. Lin-Shi, M. Nadri, J.-Y. Gauthier, and A. Hijazi, "Observability measurement and control strategy for induction machine sensorless drive in traction applications," *IFAC-PapersOnLine*, vol. 50, no. 1, pp. 15 773 – 15 779, 2017, 20th IFAC World Congress. 32

[92] G. Faten and S. Lassaâd, "Speed sensorless ifoc of pmsm based on adaptive luenberger observer," *International Journal of Electrical and Electronics Engineering*, vol. 2, no. 1, pp. 7–13, 2009. 32

[93] A. Hijazi, L. Sidhom, A. Zgorski, and X. Lin-Shi, "On Speed Estimation of Permanent Magnet Synchronous Motor Using Adaptive Robust Position Observer and Differentiator," in *IFAC*, ser. 11th IFAC International Workshop on Adaptation and Learning in Control and Signal Processing, F. Giri and V. Van Assche, Eds., vol. 11, no. 1, Giri, Fouad and Fadili, Jalal and Duclos, Daniel. Caen, France: International Federation of Automatic Control, Jul. 2013, pp. 116–121. 32

[94] F. E. M. El Fadili, A. Giri and G. Besançon, "Sensorless induction machine observation with nonlinear magnetic characteristic," *International Journal of Adaptive Control and Signal Processing*, vol. 28, no. 2, pp. 149–168, 2014. 32

[95] A. Ticlea and G. Besançon, "Observer scheme for state and parameter estimation in asynchronous motors with application to speed control," *European Journal of Control*, vol. 12, no. 4, pp. 400 – 412, 2006. 32

[96] G. Besançon and A. Ticlea, "Simultaneous state and parameter estimation in asynchronous motors under sensorless speed control," in *2003 European Control Conference (ECC)*, Sep. 2003, pp. 2788–2793. 32

[97] M. A. Hamida, J. De Leon, A. Glumineau, and R. Boisliveau, "An adaptive interconnected observer for sensorless control of pm synchronous motors with online parameter identification," *IEEE Transactions on Industrial Electronics*, vol. 60, no. 2, pp. 739–748, Feb 2013. 32

[98] D. Liang, J. Li, and R. Qu, "Sensorless control of permanent magnet synchronous machine based on second-order sliding-mode observer with online resistance estimation," *IEEE Transactions on Industry Applications*, vol. 53, no. 4, pp. 3672–3682, July 2017. 32

[99] D. Zaltni and M. Ghanes, "Observability analysis and improved zero-speed position observer design of synchronous motor with experimental results," *Asian J. Control*, vol. 15, no. 4, pp. 957–970, Jul. 2013. 32

[100] A. I. Ticlea, "Techniques d'immersion pour l'estimation non linre : application aux systs de puissance," Ph.D. dissertation, 2006. [Online]. Available: http://www.theses.fr/2006INPG0101 32

[101] Y. Wang, L. Zhou, S. A. Bortoff, A. Satake, and S. Furutani, "High gain observer for speed-sensorless motor drives: Algorithm and experiments," in *2016 IEEE International Conference on Advanced Intelligent Mechatronics (AIM)*, July 2016, pp. 1127–1132. 32

[102] S. A. A. Rizvi and A. Y. Memon, "Robust output feedback control of pmsm using cascaded sliding mode and high gain observers," *IECON 2014 - 40th Annual Conference of the IEEE Industrial Electronics Society*, pp. 274–280, 2014. 32

[103] M. A. Hamida, A. Glumineau, and J. De Leon, "High order sliding mode controller and observer for sensorless ipm sycnronous motor," in *4th International Conference on Power Engineering, Energy and Electrical Drives*, May 2013, pp. 955–960. 32

[104] M. Ghanes and G. Zheng, "On sensorless induction motor drives: Sliding-mode observer and output feedback controller," *IEEE Transactions on Industrial Electronics*, vol. 56, no. 9, pp. 3404–3413, Sep. 2009. 32

[105] E. Zerdali and M. Barut, "The comparisons of optimized extended kalman filters for speed-sensorless control of induction motors," *IEEE Transactions on Industrial Electronics*, vol. 64, no. 6, pp. 4340–4351, June 2017. 32

[106] M. Habibullah and D. D. C. Lu, "A speed-sensorless fs-ptc of induction motors using extended kalman filters," *IEEE Transactions on Industrial Electronics*, vol. 62, no. 11, pp. 6765–6778, Nov 2015. 32

[107] S. Caux and M. Fadel, *Observation of the Rotor Position to Control the Synchronous Machine without Mechanical Sensor*. John Wiley & Sons, Ltd, 2013, ch. 8, pp. 405–459. 32

[108] S. Kaux and M. Fadel, "Kalman filter and redundant observer comparison for sensorless pmsm velocity control," in *Proceedings of the IEEE International Symposium on Industrial Electronics, 2005. ISIE 2005.*, vol. 3, June 2005, pp. 887–892 vol. 3. 32

[109] Zhiqian Chen, M. Tomita, S. Ichikawa, S. Doki, and S. Okuma, "Sensorless control of interior permanent magnet synchronous motor by estimation of an extended electromotive force," in *Conference Record of the 2000 IEEE Industry Applications Conference. Thirty-Fifth IAS Annual Meeting and World Conference on Industrial Applications of Electrical Energy (Cat. No.00CH37129)*, vol. 3, Oct 2000, pp. 1814–1819 vol.3. 32

[110] T. Takeshita, M. Ichikawa, J. Y. Lee, and N. Matsui, "Back emf estimation-based sensorless salient-pole brushless dc motor drives," 1997. 32

[111] M. Koteich, A. Maloum, G. Duc, and G. Sandou, "Permanent magnet synchronous drives observability analysis for motion-sensorless control," in *2015 IEEE Symposium on Sensorless Control for Electrical Drives (SLED)*, June 2015, pp. 1–8. 32

[112] Zhiqian Chen, M. Tomita, S. Doki, and S. Okuma, "An extended electromotive force model for sensorless control of interior permanent-magnet synchronous motors," *IEEE Transactions on Industrial Electronics*, vol. 50, no. 2, pp. 288–295, April 2003. 32

[113] M. Naidu and B. K. Bose, "Rotor position estimation scheme of a permanent magnet synchronous machine for high performance variable speed drive," in *Conference Record of the 1992 IEEE Industry Applications Society Annual Meeting*, Oct 1992, pp. 48–53 vol.1. 32

[114] Y. Li, Z. Q. Zhu, D. Howe, and C. M. Bingham, "Improved rotor position estimation in extended back-emf based sensorless pm brushless ac drives with magnetic saliency," in *2007 IEEE International Electric Machines Drives Conference*, vol. 1, May 2007, pp. 214–219. 32

[115] M. Koteich, "Flux estimation algorithms for electric drives: A comparative study," in *2016 3rd International Conference on Renewable Energies for Developing Countries (REDEC)*, July 2016, pp. 1–6. 32

[116] A. K. Jebai, "Commande sans capteur des moteurs synchrones á aimants permanents par injection de signaux," Ph.D. dissertation, Paris, ENMP 2013, 2013. 33

[117] F. Malrait, A. K. Jebai, P. Martin, and P. Rouchon, "Sensorless position estimation and control of permanent-magnet synchronous motors using a saturation model," *International Journal of Control*, vol. 89, no. 3, pp. 535–549, Aug. 2015. 33

[118] P. Martin, P. Combes, F. Malrait, and P. Rouchon, "Obtaining the current-flux relations of the saturated PMSM by signal injection," in *IECON 2017 - 43rd Annual Conference of the IEEE Industrial Electronics Society*, Beijing, China, Oct. 2017. 33

[119] P. Combes, A. K. Jebai, F. Malrait, P. Martin, and P. Rouchon, "Adding virtual measurements by signal injection," in *2016 American Control Conference (ACC)*, July 2016, pp. 999–1005. 33

[120] P. L. Jansen and R. D. Lorenz, "Transducerless position and velocity estimation in induction and salient ac machines," *IEEE Transactions on Industry Applications*, vol. 31, no. 2, pp. 240–247, March 1995. 33, 79

[121] P. Jansen, M. Corley, and R. Lorenz, "Flux, position, and velocity estimation in ac machines at zero and low speed via tracking of high frequency saliencies," *EPE Journal*, vol. 9, no. 1-2, pp. 45–50, 1999. 33, 36, 51, 79

[122] P. L. Jansen, "The integration of state estimation, control, and design for induction machines." *EPE Journal*, 1995. 33, 35, 36, 51, 79

[123] M. Schroedl, "Sensorless control of ac machines at low speed and standstill based on the "inform" method," in *IAS '96. Conference Record of the 1996 IEEE Industry Applications Conference Thirty-First IAS Annual Meeting*, vol. 1, Oct 1996, pp. 270–277 vol.1. 33, 79

[124] Ji-Hoon Jang, Seung-Ki Sul, Jung-Ik Ha, K. Ide, and M. Sawamura, "Sensorless drive of smpm motor by high frequency signal injection," in *APEC. Seventeenth Annual IEEE Applied Power Electronics Conference and Exposition (Cat. No.02CH37335)*, vol. 1, March 2002, pp. 279–285 vol.1. 33, 37, 51, 79

[125] P. L. Xu and Z. Q. Zhu, "Carrier signal injection-based sensorless control for permanent-magnet synchronous machine drives considering machine parameter asymmetry," *IEEE Transactions on Industrial Electronics*, vol. 63, no. 5, pp. 2813–2824, May 2016. 33, 37, 51, 79

[126] M. J. Corley and R. D. Lorenz, "Rotor position and velocity estimation for a salient-pole permanent magnet synchronous machine at standstill and high speeds," *IEEE Transactions on Industry Applications*, vol. 34, no. 4, pp. 784–789, July 1998. 33, 37, 79

[127] D. Raca, P. Garcia, D. Reigosa, F. Briz, and R. Lorenz, "A comparative analysis of pulsating vs. rotating vector carrier signal injection-based sensorless control," in *2008 Twenty-Third Annual IEEE Applied Power Electronics Conference and Exposition*, Feb 2008, pp. 879–885. 33, 37, 51, 79

[128] R. Leidhold and P. Mutschler, "Improved method for higher dynamics in sensorless position detection," in *2008 34th Annual Conference of IEEE Industrial Electronics*. IEEE, 2008, pp. 1240–1245. 33, 43

[129] N.-C. Park and S.-H. Kim, "Simple sensorless algorithm for interior permanent magnet synchronous motors based on high-frequency voltage injection method," *IET Electric Power Applications*, vol. 8, pp. 68–75(7), February 2014. 33, 43, 46

[130] Y.-D. Yoon, S. Sul, S. Morimoto, and K. Ide, "High-bandwidth sensorless algorithm for ac machines based on square-wave-type voltage injection," *IEEE Transactions on Industry Applications*, vol. 47, no. 3, pp. 1361–1370, 5 2011. 33, 43, 51, 53, 56

[131] S. Kim and S. Sul, "High performance position sensorless control using rotating voltage signal injection in ipmsm," in *Proceedings of the 2011 14th European Conference on Power Electronics and Applications*, Aug 2011, pp. 1–10. 33, 43, 51, 56

[132] J. Juliet and J. Holtz, "Sensorless acquisition of the rotor position angle for induction motors with arbitrary stator windings," in *Conference Record of the 2004 IEEE Industry Applications Conference, 2004. 39th IAS Annual Meeting.*, vol. 2, Oct 2004, pp. 1321–1328 vol.2. 33

[133] M. A. Jabbar, M. A. Hoque, and M. A. Rahman, "Sensorless permanent magnet synchronous motor drives," in *CCECE '97. Canadian Conference on Electrical and Computer Engineering. Engineering Innovation: Voyage of Discovery. Conference Proceedings*, vol. 2, May 1997, pp. 878–883 vol.2. 33, 47

[134] L. A. S. Ribeiro, M. W. Degner, F. Briz, and R. D. Lorenz, "Comparison of carrier signal voltage and current injection for the estimation of flux angle or rotor position," in *Conference Record of 1998 IEEE Industry Applications Conference. Thirty-Third IAS Annual Meeting (Cat. No.98CH36242)*, vol. 1, Oct 1998, pp. 452–459 vol.1. 33

[135] D. Raca, P. Garcia, D. Reigosa, F. Briz, and R. D. Lorenz, "Carrier signal selection for sensorless control of pm synchronous machines at zero and very low speeds," in *2008 IEEE Industry Applications Society Annual Meeting*, Oct 2008, pp. 1–8. 33, 37

[136] M. Koteich, A. Messali, and S. Daurelle, "Self-sensing control of the externally-excited synchronous machine for electric vehicle traction application," in *2017 IEEE International Symposium on Sensorless Control for Electrical Drives (SLED)*, Sept 2017, pp. 91–96. 35

[137] Z. Chen, M. Tomita, S. Doki, and S. Okuma, "An extended electromotive force model for sensorless control of interior permanent-magnet synchronous motors," *IEEE Transactions on Industrial Electronics*, no. 2, Apr. 2003. 35

[138] P. Brandstetter and T. Krecek, "Sensorless control of permanent magnet synchronous motor using voltage signal injection," *Elektronika ir Elektrotechnika*, vol. 19, no. 6, pp. 19–24, 2006. 35, 83, 90

[139] M. W. Degner and R. D. Lorenz, "Position estimation in induction machines utilizing rotor bar slot harmonics and carrier-frequency signal injection," *IEEE Transactions on Industry Applications*, vol. 36, no. 3, pp. 736–742, May 2000. 36

[140] J. Holtz and J. Juliet, "Sensorless acquisition of the rotor position angle of induction motors with arbitrary stator windings," *IEEE Transactions on Industry Applications*, vol. 41, no. 6, pp. 1675–1682, Nov 2005. 37, 48

[141] X. Luo, Q. Tang, A. Shen, and Q. Zhang, "Pmsm sensorless control by injecting hf pulsating carrier signal into estimated fixed-frequency rotating reference frame," *IEEE Transactions on Industrial Electronics*, vol. 63, no. 4, pp. 2294–2303, April 2016. 40, 60, 70, 72

[142] S. C. Yang and Y. L. Hsu, "Full speed region sensorless drive of permanent-magnet machine combining saliency-based and back-emf-based drive," *IEEE Transactions on Industrial Electronics*, vol. 64, no. 2, pp. 1092–1101, Feb 2017. 40, 46, 60, 72

[143] Jung-Ik Ha and Seung-Ki Sul, "Sensorless field-orientation control of an induction machine by high-frequency signal injection," *IEEE Transactions on Industry Applications*, vol. 35, no. 1, pp. 45–51, Jan 1999. 41

[144] W. Hammel and R. M. Kennel, "Position sensorless control of pmsm by synchronous injection and demodulation of alternating carrier voltage," in *2010 First Symposium on Sensorless Control for Electrical Drives*, July 2010, pp. 56–63. 43

[145] Y. Yoon, S. Sul, S. Morimoto, and K. Ide, "High bandwidth sensorless algorithm for ac machines based on square-wave type voltage injection," in *2009 IEEE Energy Conversion Congress and Exposition*, Sep. 2009, pp. 2123–2130. 43

[146] S. Bolognani, S. Calligaro, R. Petrella, and M. Tursini, "Sensorless control of ipm motors in the low-speed range and at standstill by hf injection and dft processing," *IEEE Transactions on Industry Applications*, vol. 47, no. 1, pp. 96–104, Jan 2011. 43, 52

[147] H. Zhang, W. Liu, Z. Chen, G. Luo, J. Liu, and D. Zhao, "Rotor position estimation of pmsm using square-wave voltage injection with asymmetric space vector modulation," in *2017 IEEE Applied Power Electronics Conference and Exposition (APEC)*, March 2017, pp. 2723–2729. 46, 53, 56, 58

[148] Y. Yoon and S. Sul, "Sensorless control for induction machines based on square-wave voltage injection," *IEEE Transactions on Power Electronics*, vol. 29, no. 7, pp. 3637–3645, July 2014. 46, 53, 58

[149] E. Robeischl and M. Schroedl, "Optimized inform-measurement sequence for sensorless pm synchronous motor drives with respect to minimum current distortion," in *Conference Record of the 2002 IEEE Industry Applications Conference. 37th IAS Annual Meeting (Cat. No.02CH37344)*, vol. 1, Oct 2002, pp. 92–98 vol.1. 47, 48

[150] M. Schroedl, "Sensorless control of ac machines at low speed and standstill based on the "inform" method," in *IAS '96. Conference Record of the 1996 IEEE Industry Applications Conference Thirty-First IAS Annual Meeting*, vol. 1, Oct 1996, pp. 270–277 vol.1. 47

[151] M. Schroedl, D. Hennerbichler, and T. M. Wolbank, "Induction motor drive for electric vehicles without speed- and position sensors," in *1993 Fifth European Conference on Power Electronics and Applications*, Sep. 1993, pp. 271–275 vol.5. 47

[152] E. Robeischl and M. Schroedl, "Direct axis current utilization for intelligent sensorless permanent magnet synchronous drives," in *Conference Record of the 2001 IEEE Industry Applications Conference. 36th IAS Annual Meeting (Cat. No.01CH37248)*, vol. 1, Sep. 2001, pp. 475–481 vol.1. 48

[153] T. M. Wolbank, H. Giuliani, R. Woehrnschimmel, and J. L. Machl, "Sensorless control of induction machines by combining fundamental wave models with transient excitation technique," in *IEEE International Conference on Electric Machines and Drives, 2005.*, May 2005, pp. 1379–1384. 48

[154] M. A. Vogelsberger, S. Grubic, T. G. Habetler, and T. M. Wolbank, "Using pwm-induced transient excitation and advanced signal processing for zero-speed sensorless control of ac machines," *IEEE Transactions on Industrial Electronics*, vol. 57, no. 1, pp. 365–374, Jan 2010. 48

[155] R. Leidhold, "Position sensorless control of pm synchronous motors based on zero-sequence carrier injection," *IEEE Transactions on Industrial Electronics*, vol. 58, no. 12, pp. 5371–5379, Dec 2011. 48

[156] S. Bolognani, S. Calligaro, R. Petrella, and M. Sterpellone, "Sensorless control for ipmsm using pwm excitation: Analytical developments and implementation issues," in *2011 Symposium on Sensorless Control for Electrical Drives*, Sep. 2011, pp. 64–73. 48

[157] J. Talla and J. Stehlik, "Fpga based neural network position and speed estimator for switched reluctance motor drive," in *WSEAS International Conference. Proceedings. Mathematics and Computers in Science and Engineering*, no. 7. World Scientific and Engineering Academy and Society, 2008. 49, 79

[158] M. Majdi and F. Rashidi, "Sensorless speed and position control of induction motor servo drives using mlp neural network and sliding mode controller," in *Proceedings of the 4th WSEAS International Conference on Non-linear Analysis, Non-linear Systems and Chaos*, ser. NOLASC'05. Stevens Point, Wisconsin, USA: World Scientific and Engineering Academy and Society (WSEAS), 2005, pp. 94–102. 49

[159] A. Mishra, H. S. Dhalival, S. Singh, and A. K. Mishra, "Auto levelling of heavy load articulation platform using induction motor with sensorless control," in *2012 IEEE Students' Conference on Electrical, Electronics and Computer Science*, March 2012, pp. 1–4. 49, 79

[160] M. Larrea, E. Irigoyen, V. G, and F. Artaza, "Nonlinear system control based on neural networks with adaptive predictive strategy," in *2010 IEEE 15th Conference on Emerging Technologies Factory Automation (ETFA 2010)*, Sep. 2010, pp. 1–7. 49, 79

[161] Z. Ibrahim and E. Levi, "A comparative analysis of fuzzy logic and pi speed control in high-performance ac drives using experimental approach," *IEEE Transactions on Industry Applications*, vol. 38, no. 5, pp. 1210–1218, Sep. 2002. 49, 79

[162] H. Chaoui and P. Sicard, "Adaptive fuzzy logic control of permanent magnet synchronous machines with nonlinear friction," *IEEE Transactions on Industrial Electronics*, vol. 59, no. 2, pp. 1123–1133, Feb 2012. 49, 79

[163] A. A. Silva, A. M. Bazzi, and S. Gupta, "Fault diagnosis in electric drives using machine learning approaches," in *2013 International Electric Machines Drives Conference*, May 2013, pp. 722–726. 49, 79

[164] T. D. Batzel and K. Y. Lee, "A diagonally recurrent neural network approach to sensorless operation of the permanent magnet synchronous motor," in *2000 Power Engineering Society Summer Meeting (Cat. No.00CH37134)*, vol. 4, July 2000, pp. 2441–2445 vol. 4. 49, 79

[165] R. D. Lorenz and K. V. Patten, "High resolution velocity estimation for all digital, ac servo drives," in *Conference Record of the 1988 IEEE IAS Annual Meeting*, Oct 1988, pp. 363–368 vol.1. 51, 87

[166] J. Holtz, "Acquisition of position error and magnet polarity for sensorless control of pm synchronous machines," *IEEE Transactions on Industry Applications*, vol. 44, no. 4, pp. 1172–1180, July 2008. 51

[167] A. K. Jebai, F. Malrait, P. Martin, and P. Rouchon, "Sensorless position estimation and control of permanent-magnet synchronous motors using a saturation model," *International Journal of Control*, vol. 89, no. 3, pp. 535–549, 2016. 51

[168] M. Roetzer, U. Vollmer, and R. Kennel, "Demodulation approach for slowly sampled sensorless field-oriented control systems enabling multiple-frequency injections," in *2016 IEEE Industry Applications Society Annual Meeting*, Oct 2016, pp. 1–9. 51

[169] Y. C. Kwon and S. K. Sul, "Reduction of injection voltage in signal injection sensorless drives using a capacitor-integrated inverter," *IEEE Transactions on Power Electronics*, vol. 32, no. 8, pp. 6261–6274, Aug 2017. 51

[170] A. Yousefi-T, P. Pescetto, G. Pellegrino, and I. Boldea, "Combined active flux and high-frequency injection methods for sensorless direct-flux vector control of synchronous reluctance machines," *IEEE Transactions on Power Electronics*, vol. 33, no. 3, pp. 2447–2457, March 2018. 51

[171] G. Wang, H. Zhou, N. Zhao, C. Li, and D. Xu, "Sensorless control of ipmsm drives using a pseudo-random phase-switching fixed-frequency signal injection scheme," *IEEE Transactions on Industrial Electronics*, vol. 65, no. 10, pp. 7660–7671, Oct 2018. 51

[172] J. Wei, H. Xue, B. Zhou, Z. Zhang, and C. Gerada, "An integrated method for three-phase ac excitation and high-frequency voltage signal injection for sensorless starting of aircraft starter/generator," *IEEE Transactions on Industrial Electronics*, pp. 1–1, 2018. 51

[173] D. Mingardi, M. Morandin, S. Bolognani, and N. Bianchi, "On the proprieties of the differential cross-saturation inductance in synchronous machines," *IEEE Transactions on Industry Applications*, vol. 53, no. 2, pp. 991–1000, March 2017. 51, 58

[174] F. Parasiliti, R. Petrella, and M. Tursini, "Sensorless speed control of salient rotor pm synchronous motor based on high frequency signal injection and kalman filter," in *IEEE 2nd International Power and Energy Conference*, 2002. 52, 63, 68

[175] S. Bolognani, S. Calligaro, R. Petrella, and M. Tursini, "Sensorless control of ipm motors in the low-speed range and at stand-still by hf-injection and dft processing," in *2009 IEEE International Electric Machines and Drives Conference*, May 2009, pp. 1557–1564. 52, 63, 68

[176] S. Kim, J. Ha, and S. Sul, "Pwm switching frequency signal injection sensorless method in ipmsm," *IEEE Transactions on Industry Applications*, vol. 48, no. 5, pp. 1576–1587, Sep. 2012. 53

[177] P. Wang, Y. W. Wong, Z. Man, Z. Cao, and J. Zheng, "Sign propagation: The art behind the methodology of sliding observers," in *2017 11th Asian Control Conference (ASCC)*, Dec 2017, pp. 78–83. 58, 65, 71, 74, 76, 91

[178] D. Raca, M. C. Harke, and R. D. Lorenz, "Robust magnet polarity estimation for initialization of pm synchronous machines with near zero saliency," in *Conference Record of the 2006 IEEE Industry Applications Conference Forty-First IAS Annual Meeting*, vol. 1, Oct 2006, pp. 481–487. 58

[179] O. Wallmark, L. Harnefors, and O. Carlson, "An improved speed and position estimator for salient permanent-magnet synchronous motors," *IEEE Transactions on Industrial Electronics*, vol. 52, no. 1, pp. 255–262, Feb 2005. 63, 83, 84, 85, 86, 90

[180] O. Mansouri-Toudert, H. Zeroug, F. Auger, and A. Chibah, "Improved rotor position estimation of salient-pole pmsm using high frequency carrier signal injection," in *2013 IEEE International Conference on Mechatronics (ICM)*, Feb 2013, pp. 761–767. 70

[181] T. C. Lin, L. M. Gong, J. M. Liu, and Z. Q. Zhu, "Investigation of saliency in a switched-flux permanent-magnet machine using high-frequency signal injection," *IEEE Transactions on Industrial Electronics*, vol. 61, no. 9, pp. 5094–5104, Sept 2014. 70

[182] S. Shinnaka, "A new speed-varying ellipse voltage injection method for sensorless drive of permanent-magnet synchronous motors with pole saliency," *IEEE Transactions on Industry Applications*, vol. 44, no. 3, pp. 777–788, May 2008. 80, 83, 84, 90

[183] K. B. Lee, J. Y. Yoo, J. H. Song, and I. Choy, "Improvement of low speed operation of electric machine with an inertia identification using roelo," *IEE Proceedings - Electric Power Applications*, vol. 151, no. 1, pp. 116–120, Jan 2004. 80, 83, 87, 88, 90

[184] L. Wang and R. D. Lorenz, "Rotor position estimation for permanent magnet synchronous motor using saliency-tracking self-sensing method," in *Conference Record of the 2000 IEEE Industry Applications Conference. Thirty-Fifth IAS Annual Meeting and World Conference on Industrial Applications of Electrical Energy*, vol. 1, 2000, pp. 445–450 vol.1. 83, 87, 90

[185] Heui-Wook Kim and Seung-Ki Sul, "A new motor speed estimator using kalman filter in low-speed range," *IEEE Transactions on Industrial Electronics*, vol. 43, no. 4, pp. 498–504, Aug 1996. 83, 87, 90

[186] L. Harnefors and H. P. Nee, "A general algorithm for speed and position estimation of ac motors," *IEEE Transactions on Industrial Electronics*, vol. 47, no. 1, pp. 77–83, Feb 2000. 84

[187] M. H. Bierhoff, "A general pll-type algorithm for speed sensorless control of electrical drives," *IEEE Transactions on Industrial Electronics*, vol. 64, no. 12, pp. 9253–9260, Dec 2017. 84

[188] P. Kanjiya, V. Khadkikar, and M. S. E. Moursi, "Obtaining performance of type-3 phase-locked loop without compromising the benefits of type-2 control system," *IEEE Transactions on Power Electronics*, vol. 33, no. 2, pp. 1788–1796, Feb 2018. 84

[189] Choong-Hyuk Yim, In-Joong Ha, and Myoung-Sam Ko, "A resolver-to-digital conversion method for fast tracking," *IEEE Transactions on Industrial Electronics*, vol. 39, no. 5, pp. 369–378, Oct 1992. 87

[190] C. Verrelli, P. Tomei, E. Lorenzani, G. Migliazza, and F. Immovilli, "Nonlinear tracking control for sensorless permanent magnet synchronous motors with uncertainties," *Control Engineering Practice*, vol. 60, pp. 157 – 170, 2017. 91

[191] J. . E. Slotine, J. K. Hedrick, and E. A. Misawa, "On sliding observers for nonlinear systems," in *1986 American Control Conference*, June 1986, pp. 1794–1800. 91

[192] C. L. Baratieri and H. Pinheiro, "New variable gain super-twisting sliding mode observer for sensorless vector control of nonsinusoidal back-emf pmsm," *Control Engineering Practice*, vol. 52, pp. 59 – 69, 2016. 91

[193] G. Bartolini, A. Ferrara, and E. Punta, "Multi-input second-order sliding-mode hybrid control of constrained manipulators," *Dynamics and Control*, vol. 10, no. 3, pp. 277–296, Jul 2000. 91

[194] Jun Hu, Dongqi Zhu, Yongdong Li, and Jingde Gao, "Application of sliding observer to sensorless permanent magnet synchronous motor drive system," in *Proceedings of 1994 Power Electronics Specialist Conference - PESC'94*, vol. 1, June 1994, pp. 532–536 vol.1. 91

[195] Z. Xu and M. F. Rahman, "An adaptive sliding stator flux observer for a direct-torque-controlled ipm synchronous motor drive," *IEEE Transactions on Industrial Electronics*, vol. 54, no. 5, pp. 2398–2406, Oct 2007. 91

[196] A. Popescu, G. Besançon, and A. Voda, "A new robust observer approach for unknown input and state estimation," in *2018 European Control Conference (ECC)*, June 2018. 91

[197] V. Utkin, "Variable structure systems with sliding modes," *IEEE Transactions on Automatic Control*, vol. 22, no. 2, pp. 212–222, April 1977. 91

[198] Z. Xu and M. F. Rahman, "Comparison of a sliding observer and a kalman filter for direct-torque-controlled ipm synchronous motor drives," *IEEE Transactions on Industrial Electronics*, vol. 59, no. 11, pp. 4179–4188, Nov 2012. 91

[199] J. P. Barbot, T. Boukhobza, and M. Djemai, "Sliding mode observer for triangular input form," in *Proceedings of 35th IEEE Conference on Decision and Control*, vol. 2, Dec 1996, pp. 1489–1490 vol.2. 95

[200] T. Boukhobza, "Observateurs a modes glissants pour des formes d'observabilite et contribution aux techniques de commandes par ordres superieurs," Ph.D. dissertation, Paris 11, 1997. 95

[201] W. Perruquetti, *Sliding Mode Control in Engineering*, J. P. Barbot, Ed. New York, NY, USA: Marcel Dekker, Inc., 2002. 100

[202] Jong-Woo Choi and Seung-Ki Sul, "Inverter output voltage synthesis using novel dead time compensation," *IEEE Transactions on Power Electronics*, vol. 11, no. 2, pp. 221–227, March 1996. 129

[203] N. Teske, G. M. Asher, K. J. Bradley, and M. Summer, "Analysis and suppression of inverter clamping saliency in sensorless position controlled induction machine drives," in *Conference Record of the 2001 IEEE Industry Applications Conference. 36th IAS Annual Meeting*, vol. 4, Sep. 2001, pp. 2629–2636 vol.4. 129

Titre : Contribution à l'estimation de position des machines synchrones par injection des signaux à haute fréquence : Application à la propulsion des véhicules électriques/hybrides

Mots clés : Contrôle sans capteurs mécaniques, moteurs synchrones à aimants permanents, techniques d'injection de signaux haute fréquence, observateurs par modes glissants d'ordre 1 (étapes par étapes et adaptatifs), EV/HEV.

Résumé : Cette thèse s'inscrit dans le cadre de la chaire Renault/Centrale Nantes sur l'amélioration des performances des véhicules électriques (EV/HEV). Elle est dédiée à la problématique de l'estimation de la position/vitesse des moteurs synchrones à aimants permanents (MSAP) sans capteur mécanique, en utilisant les techniques d'injection de signaux haute fréquence (HF) sur toute la plage de vitesse des MSAP.

Dans ce cadre, plusieurs contributions ont été proposées dans les parties de démodulation/traitement du signal et d'algorithmes de poursuite des techniques d'injection HF, afin d'améliorer l'estimation de la position/vitesse des MSAP par rapport aux méthodes existantes.

Dans la partie démodulation/traitement du signal des techniques d'injection HF, les contributions ont consisté à proposer des solutions originales permettant de réduire les effets de filtrage dans la chaine d'estimation et de rendre cette dernière indépendante des paramètres (électriques) de la machine.

Dans la partie poursuite, les contributions portent essentiellement sur l'exploitation de la fonction signe de l'erreur de position (à la place de l'erreur de position) comme information de mesure, pour estimer la position, la vitesse et l'accélération des MSAP sans capteurs mécaniques avec des observateurs par modes glissants d'ordre 1 (classiques, étapes par étapes et adaptatifs).

Les contributions proposées dans les deux parties ont pour avantages d'une part, de robustifier la chaine d'estimation en la rendant indépendante des paramètres électriques et mécaniques. Et d'autre part, d'améliorer la précision et les performances de la chaine d'estimation, et par conséquent du contrôle des MSAP sans capteurs mécaniques, dans les phases transitoires et en régimes permanents avec une méthode de réglage aisée.
Les méthodes d'estimation développées ont été testées en simulation et en expérimentation sur un banc d'essai de machines électriques. Les résultats obtenus ont permis de mettre en évidence les performances de ces méthodes en terme de suivi de trajectoire et de robustesse sur toute la plage de fonctionnement des MSAP sans capteurs mécaniques.

Title : Contribution to Rotor Position and Speed Estimation for Synchronous Machine Drive Using High Frequency Voltage Injection: Application to EV/HEV Powertrains

Keywords : : Self-sensing control, permanent magnet synchronous motors, high frequency (HF) signal injection techniques, first-order sliding mode observers (step-by-step and adaptive), EV/HEV.

Abstract: This thesis is part of the Renault / Centrale Nantes Chair on improving the performance of electric vehicles (EV / HEV). It is dedicated to the problem of estimating the position / speed of self-sensing permanent magnet synchronous motors (PMSM) without mechanical sensors, using high frequency (HF) signal injection techniques over the full speed range of PMSM. In this context, several contributions have been proposed in the demodulation / signal processing and tracking algorithms parts of HF injection techniques, in order to improve the estimation of the position / speed of the MSAP compared to the existing methods.
In the demodulation / signal processing part of the HF injection techniques, the contributions consisted of proposing original solutions making it possible to reduce the filtering effects in the estimation chain and to make the latter independent of the electrical machine parameters.

In the tracking part, the contributions mainly concern the use of the function sign of the position error (instead of the position error) as measurement information, to estimate the position, the speed and the acceleration of self-sensing PMSM with first-order sliding mode observers (conventional, step-by-step and adaptive).
The contributions proposed in both parts have the advantages of robustifying the estimation chain by making it independent of electrical and mechanical parameters on the one hand. On the other hand, they allow improving the accuracy and performance of the estimation chain, and therefore the control of self-sensing PMSM, in transient and steady-state phases with an easy tuning method.
The estimation methods developed were tested in simulation and experimentation on a test bench of electrical machines. The results obtained made it possible to highlight the performances of these methods in terms of trajectory tracking and robustness over the entire operating range of PMSM self-sensing control.